Cosmic rays at the knee
Results and implications

«ETTORE MAJORANA» FOUNDATION AND CENTRE FOR SCIENTIFIC CULTURE

INTERNATIONAL SCHOOL OF COSMIC-RAY ASTROPHYSICS
«MAURICE M. SHAPIRO»

22nd Course: "From cosmic particles to gravitational waves: now and to come"
30 July – 7 August 2022

PRESIDENT AND DIRECTOR OF THE CENTRE: PROFESSOR A. ZICHICHI

DIRECTORS OF THE COURSE: PROFESSORS J.P. WEFEL, T. STANEV, J.R. HÖRANDEL

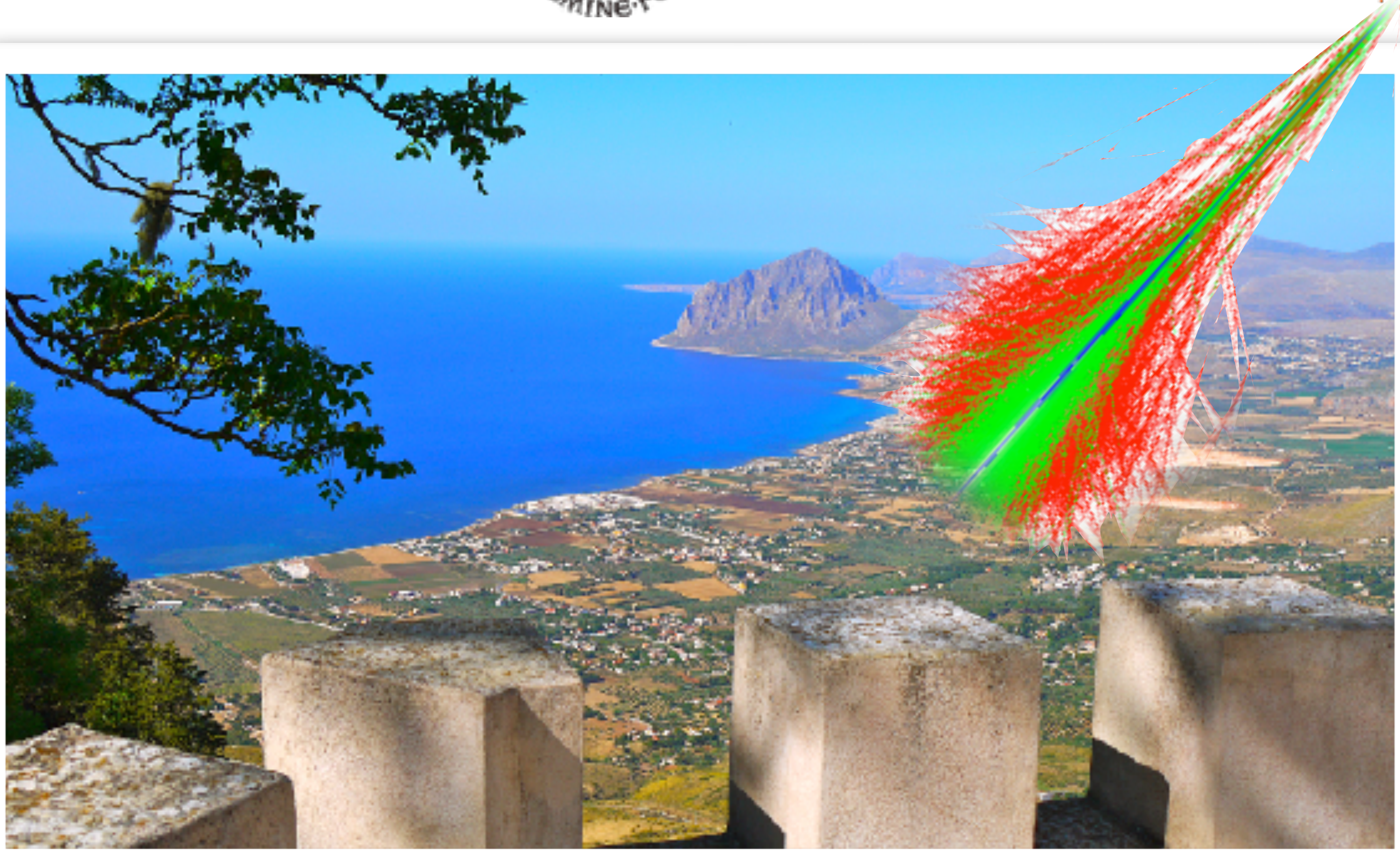

Jörg R. Hörandel **RU Nijmegen, Nikhef, VU Brussel** **http://particle.astro.ru.nl**

Cosmic rays at the knee
Results and implications

energy density

$$\rho_E = \frac{4\pi}{c} \int \frac{E}{\beta} \frac{dN}{dE} dE \approx 1 \ \frac{\text{eV}}{\text{cm}^3}$$

for comparison:

$$\rho_B = \frac{B^2}{2\mu_0} \approx 0.25 \ \text{eV/cm}^3$$

$$\rho_{SL} \approx 0.3 \ \text{eV/cm}^3$$

$$\rho_{IR} \approx 0.4 \ \text{eV/cm}^3$$

$$\rho_{3K} \approx 0.25 \ \text{eV/cm}^3$$

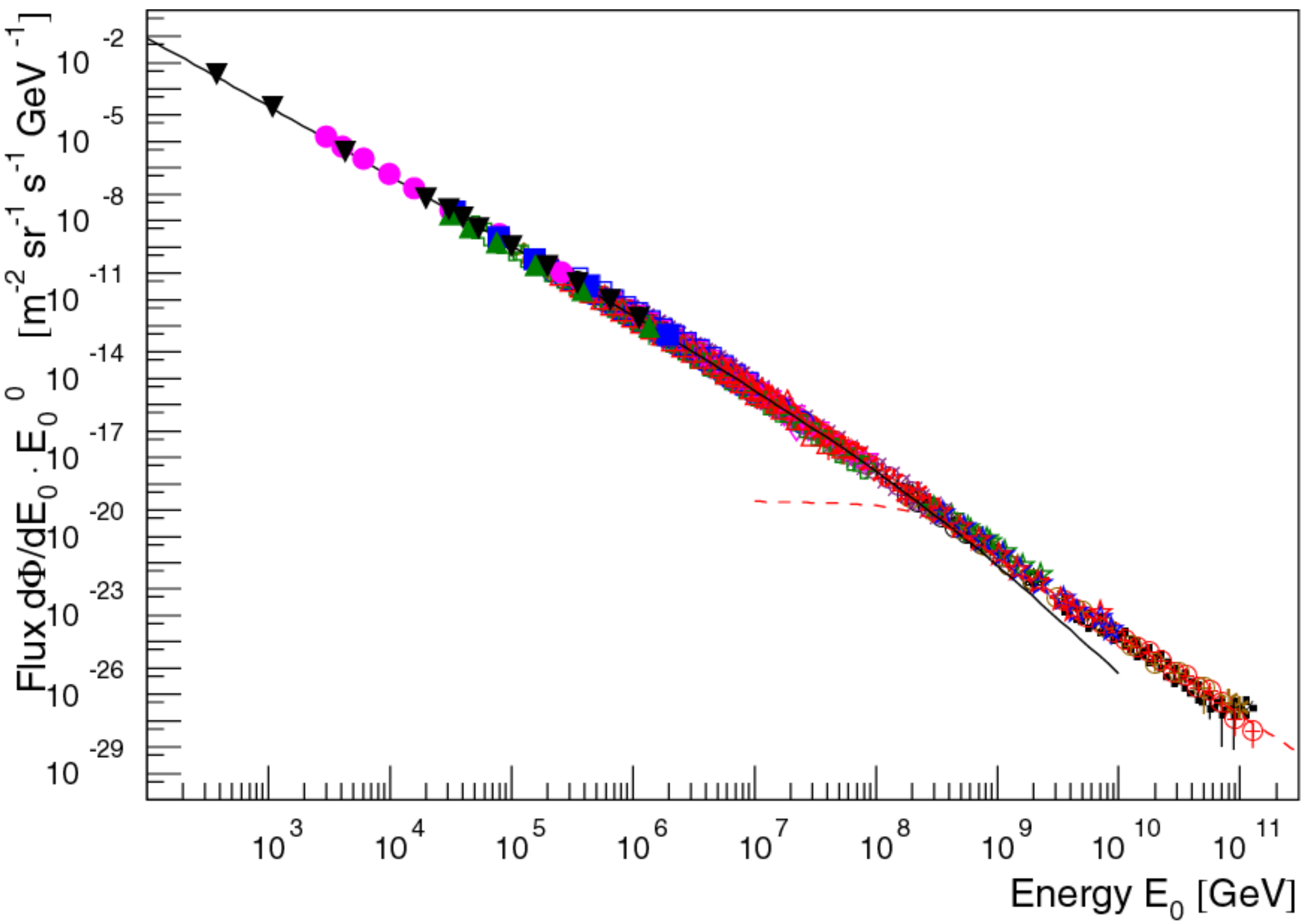

Cosmic rays at the knee
Results and implications

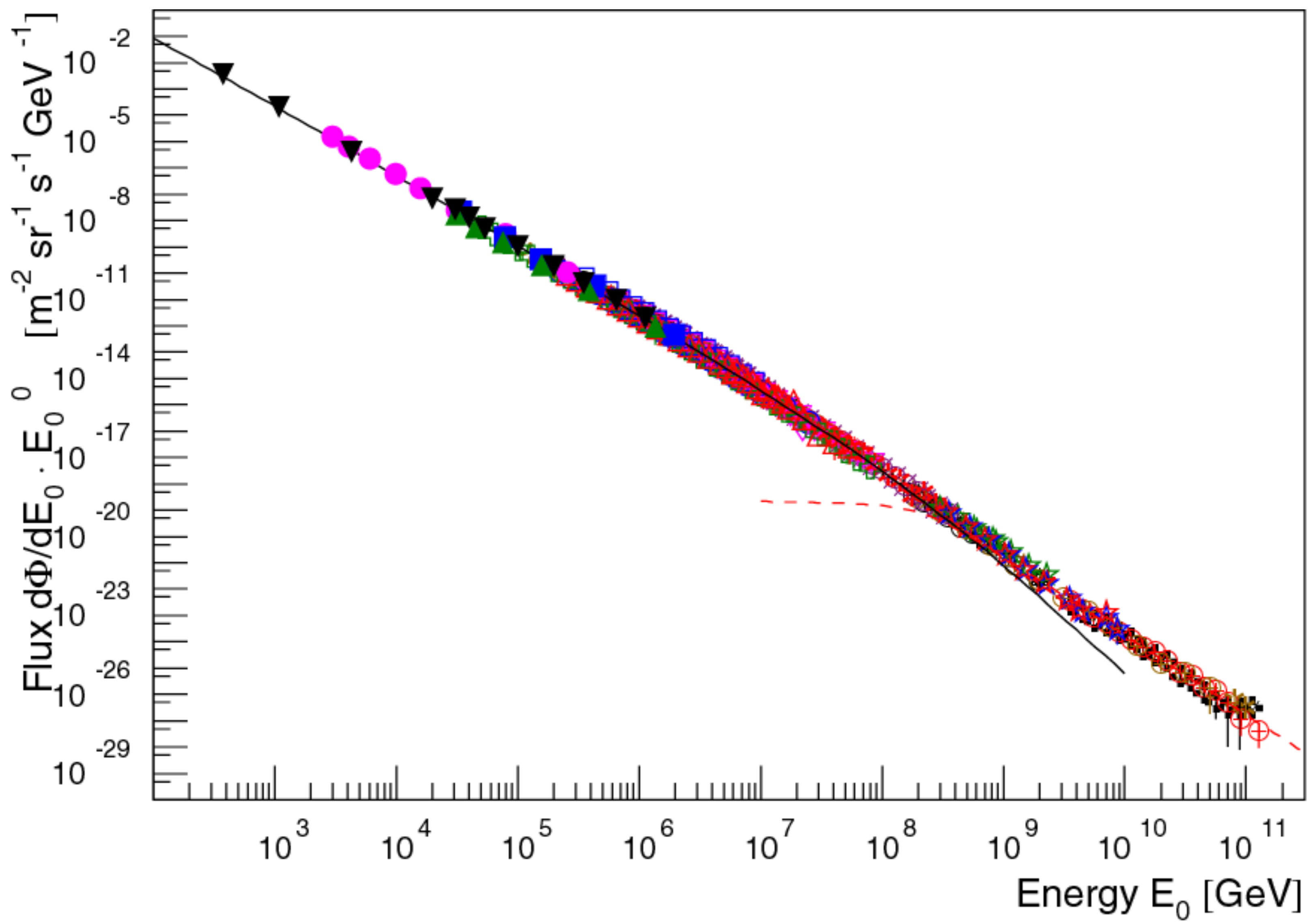

Jörg R. Hörandel RU Nijmegen, Nikhef, VU Brussel http://particle.astro.ru.nl

Cosmic rays at the knee
Results and implications

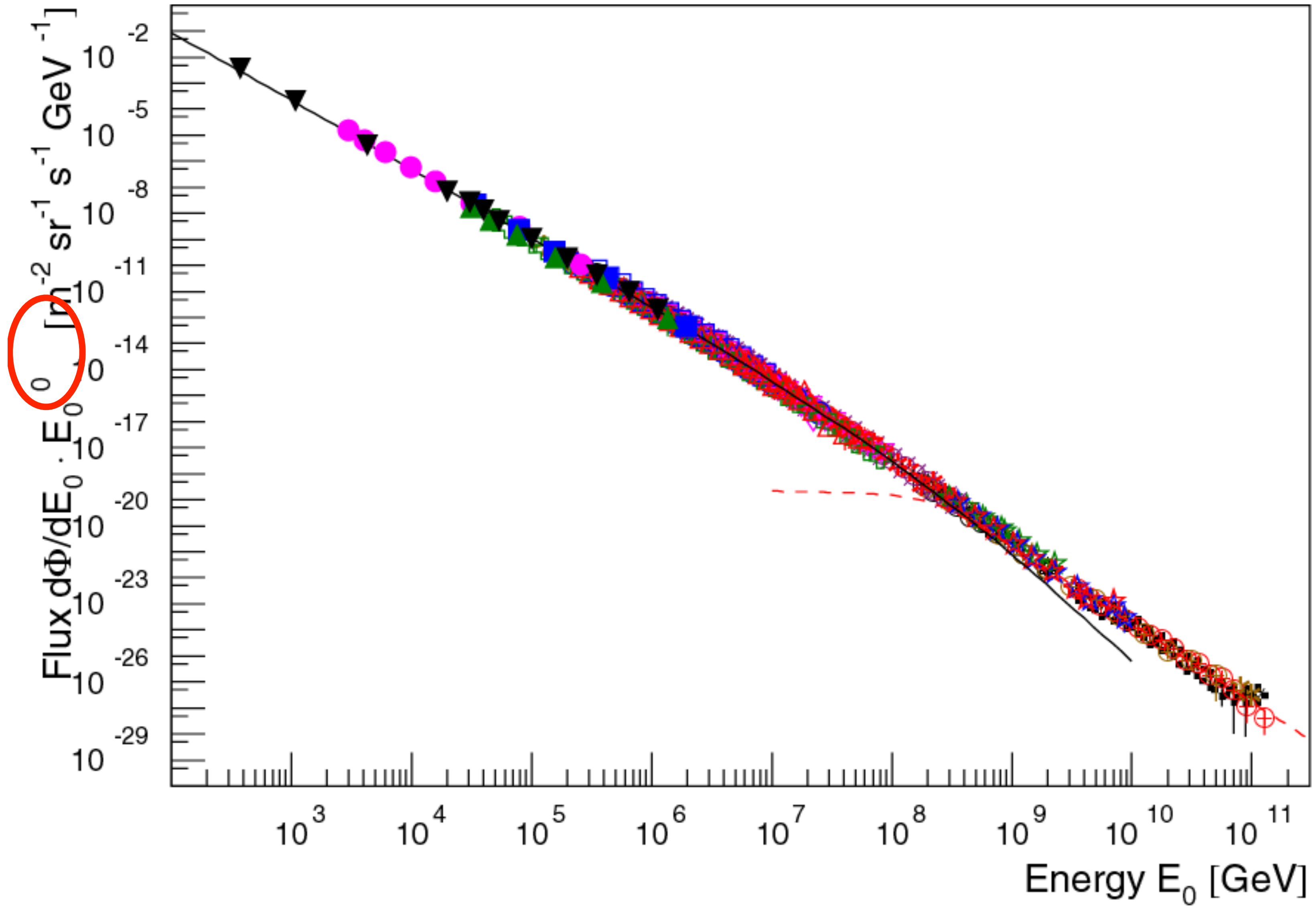

Jörg R. Hörandel RU Nijmegen, Nikhef, VU Brussel http://particle.astro.ru.nl

Cosmic rays at the knee

Results and implications

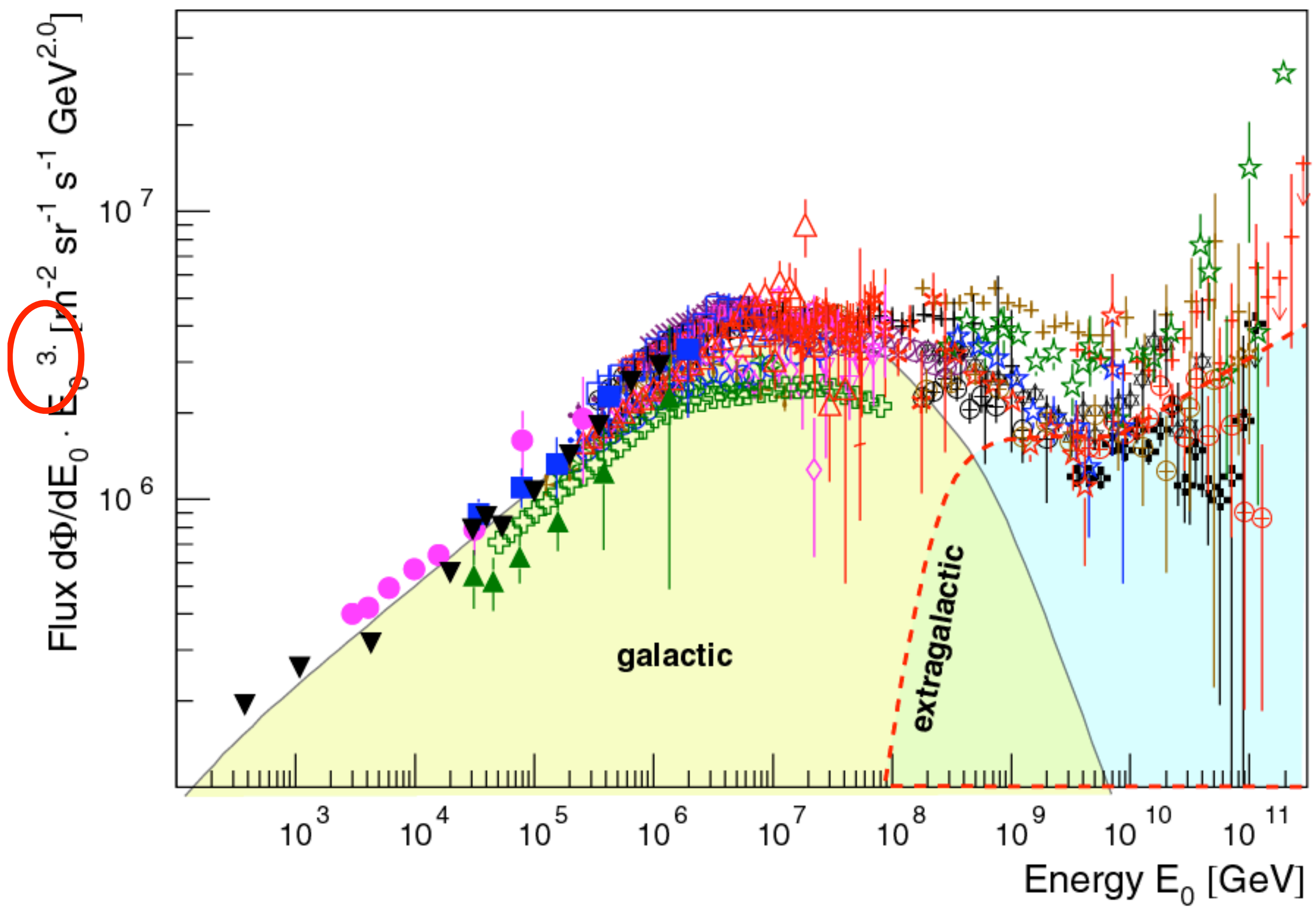

Cosmic rays at the knee

Results and implications

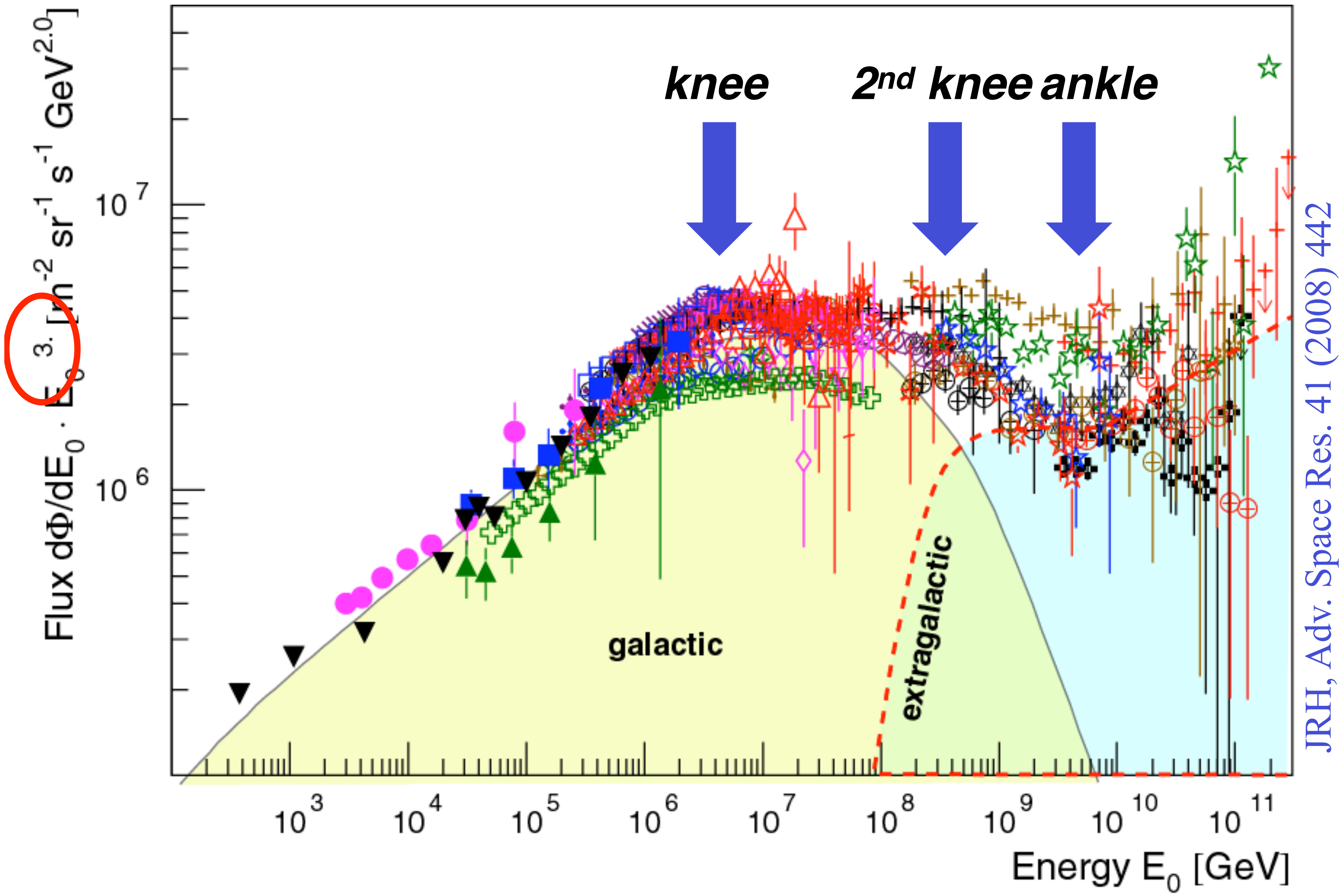

Jörg R. Hörandel RU Nijmegen, Nikhef, VU Brussel http://particle.astro.ru.nl

Cosmic rays at the knee
Results and implications

Solar flares

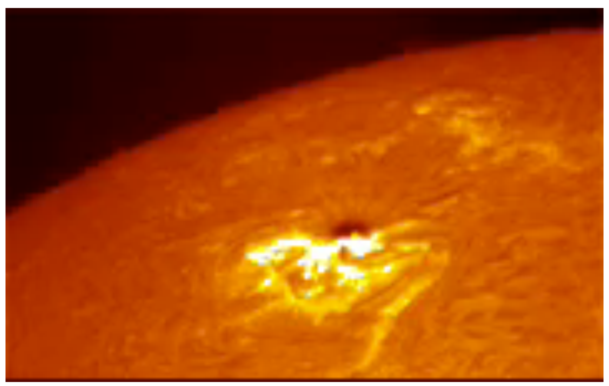
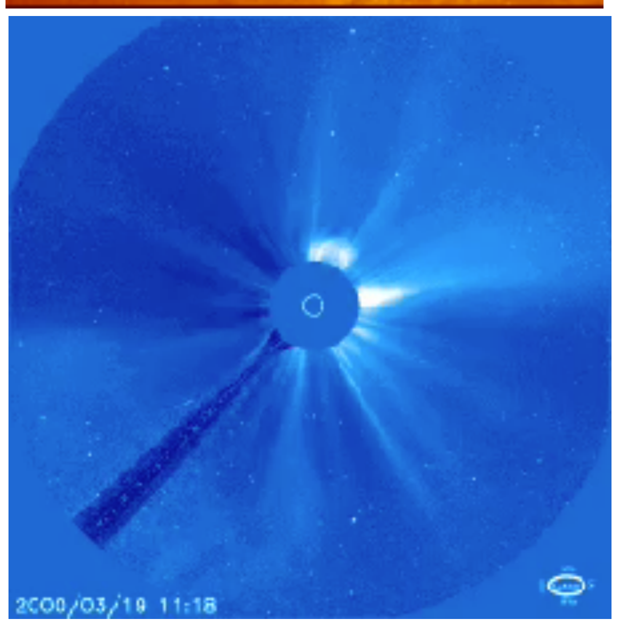


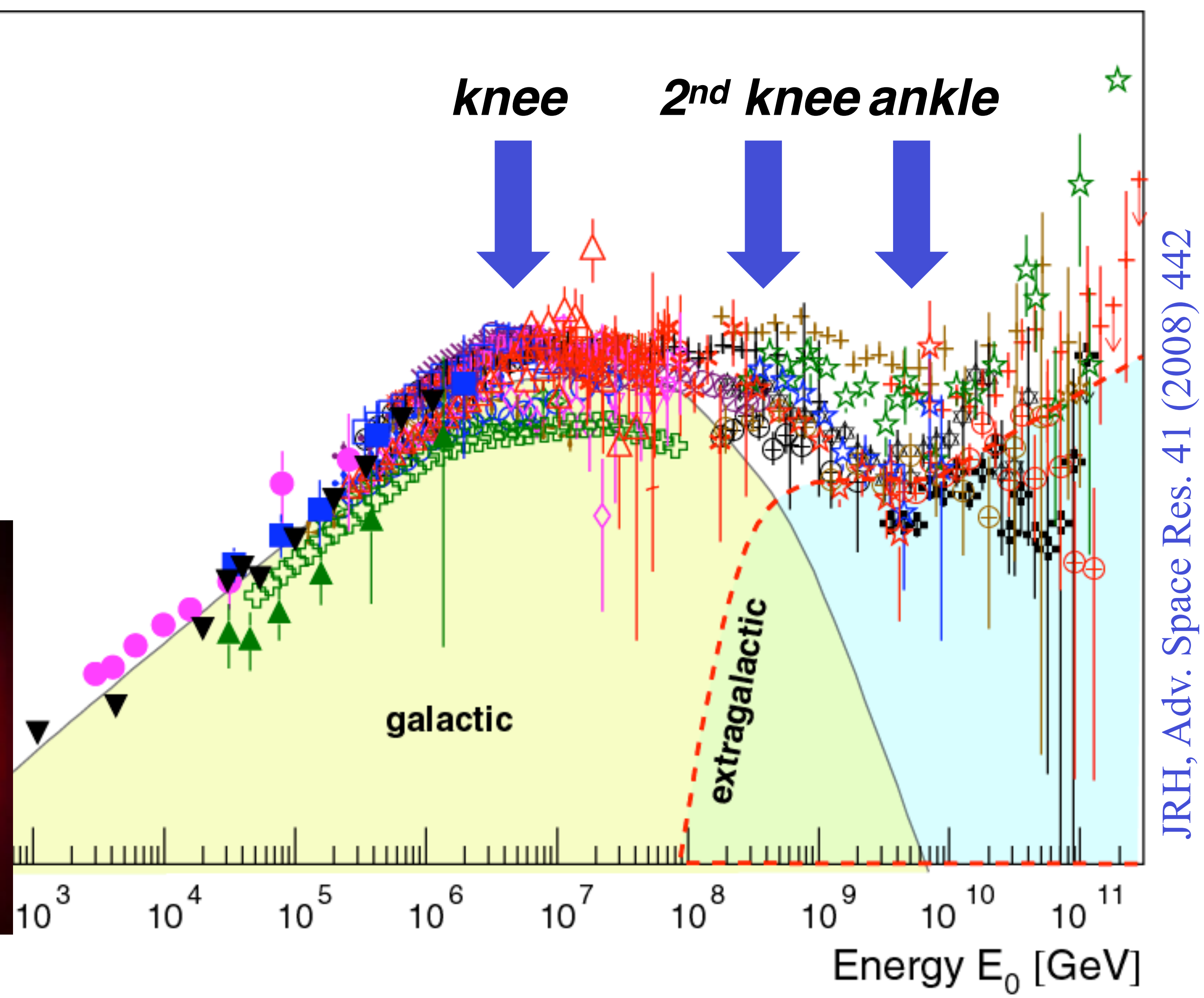

Cosmic rays at the knee

Results and implications

Solar flares

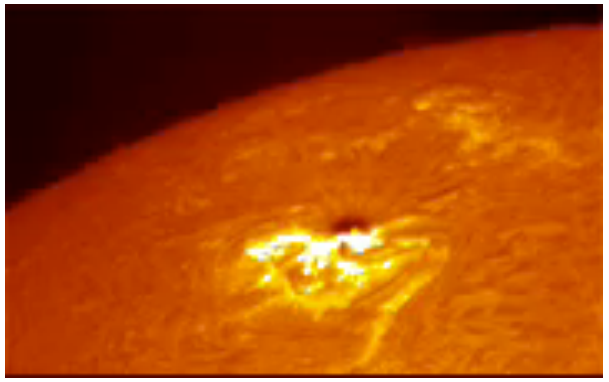

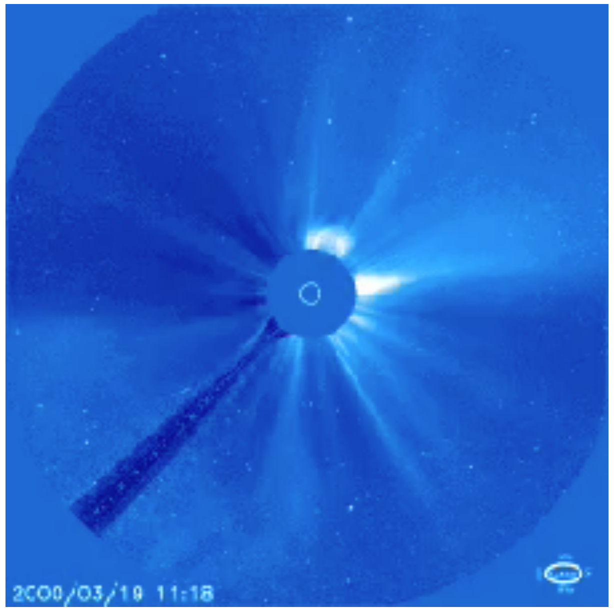

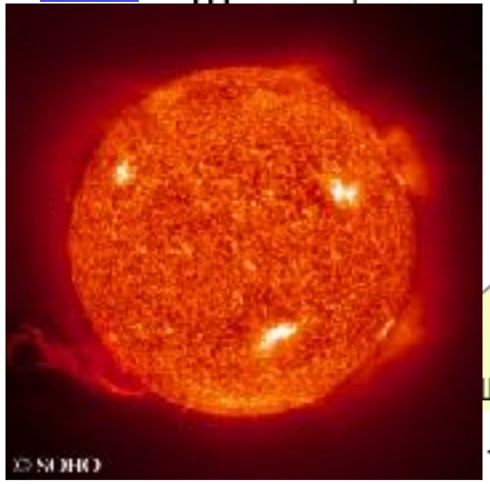

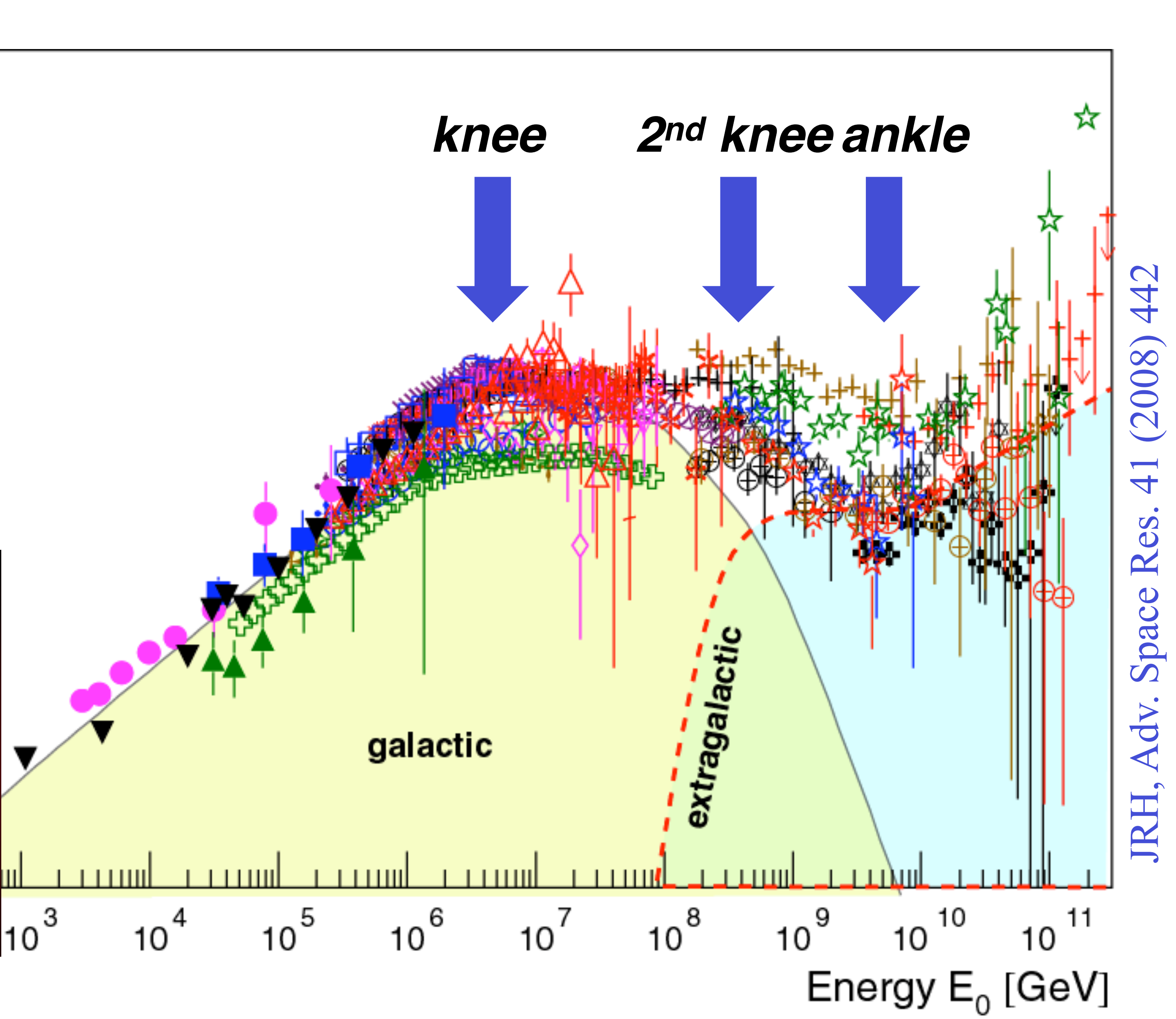

Cosmic rays at the knee
Results and implications

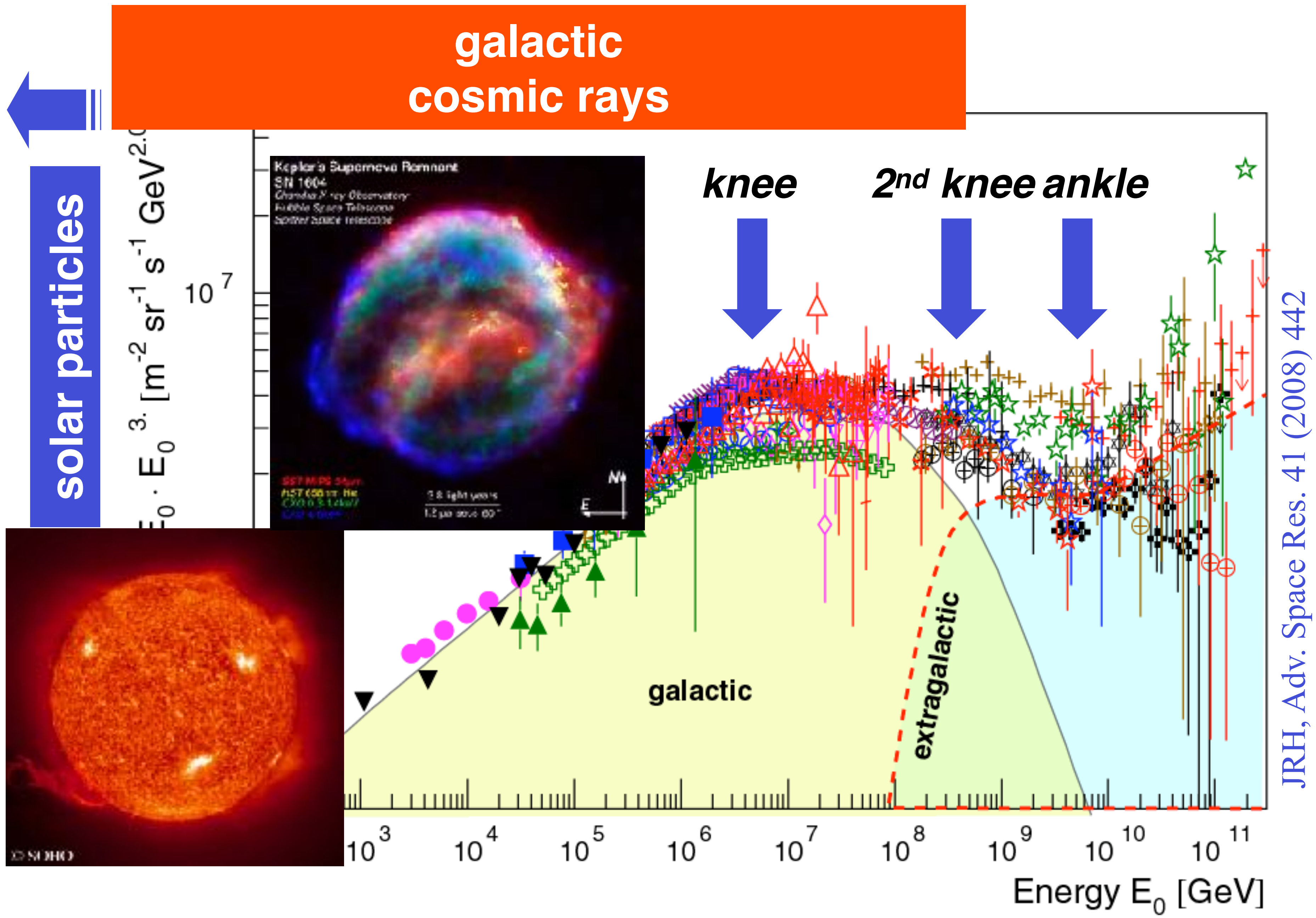

Jörg R. Hörandel RU Nijmegen, Nikhef, VU Brussel http://particle.astro.ru.nl

Cosmic rays at the knee
Results and implications

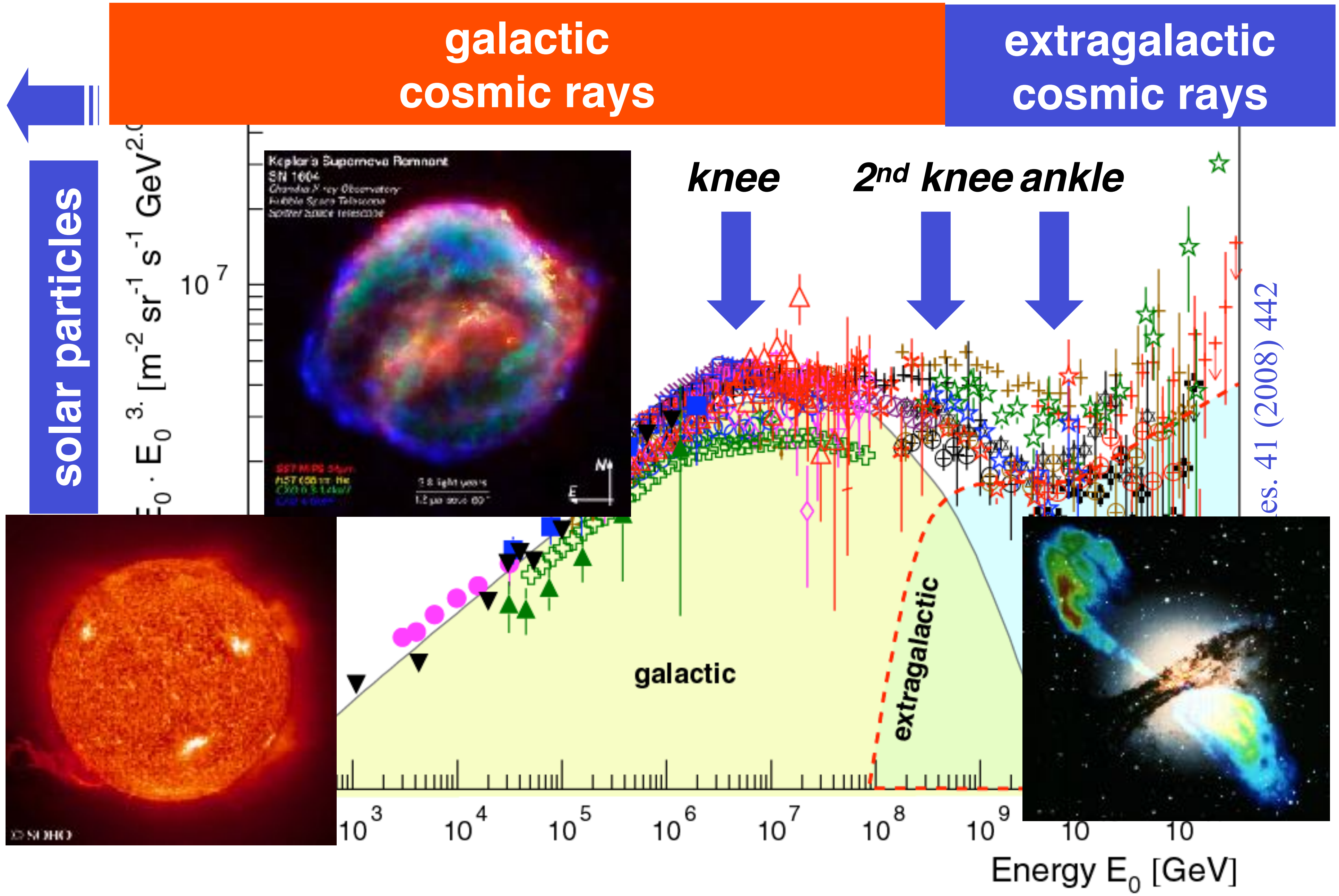

Jörg R. Hörandel RU Nijmegen, Nikhef, VU Brussel http://particle.astro.ru.nl

Cosmic rays at the knee

Results and implications

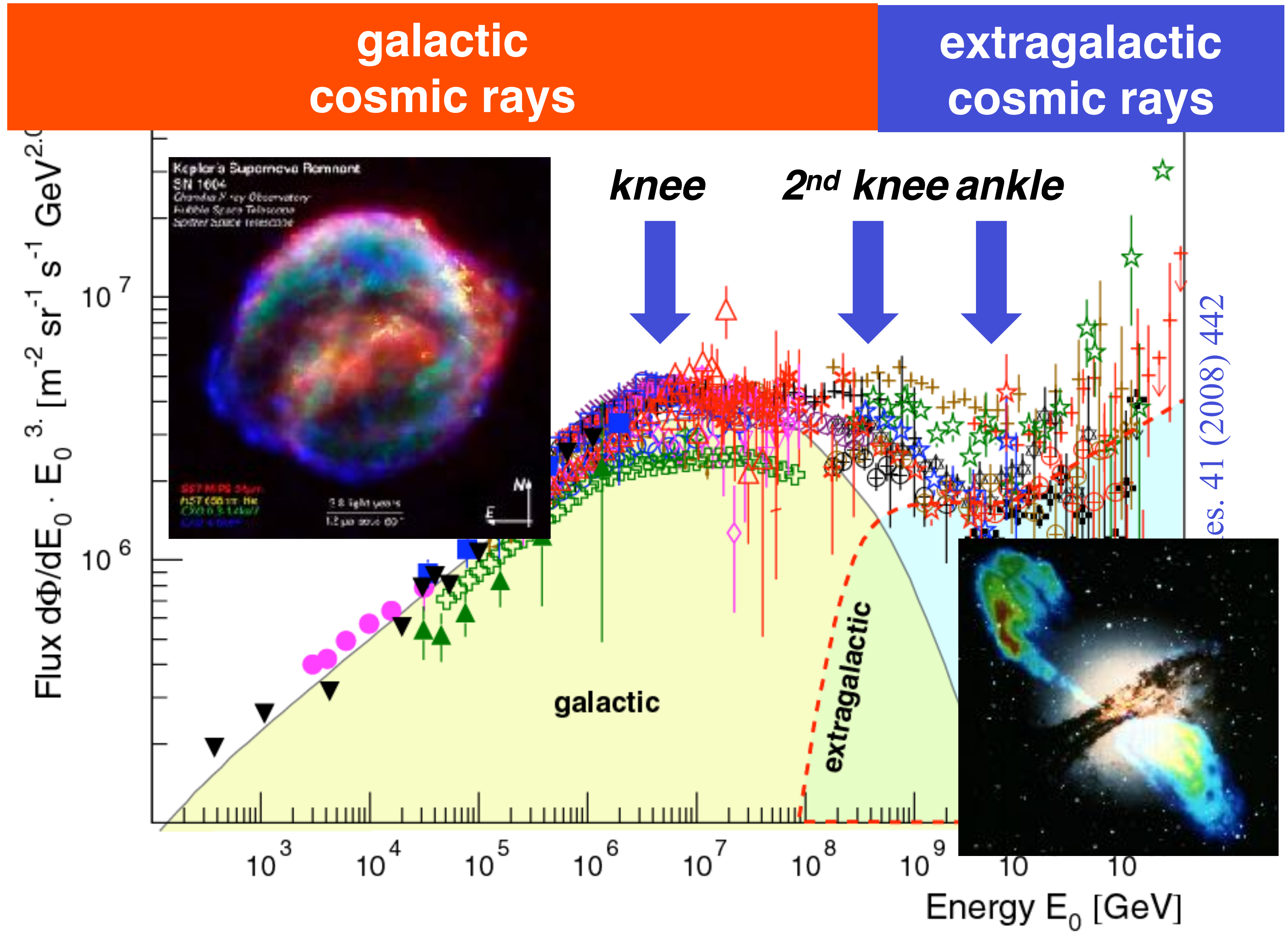

Jörg R. Hörandel RU Nijmegen, Nikhef, VU Brussel http://particle.astro.ru.nl

Cosmic rays at the knee

Results and implications

Radius of particle in magnetic field

$$r = \frac{p}{ZeB} \qquad r[\mathrm{pc}] = 1.08 \cdot \frac{E\ [\mathrm{PeV}]}{B\ [\mu\mathrm{G}]}$$

galactic cosmic rays	extragalactic cosmic rays

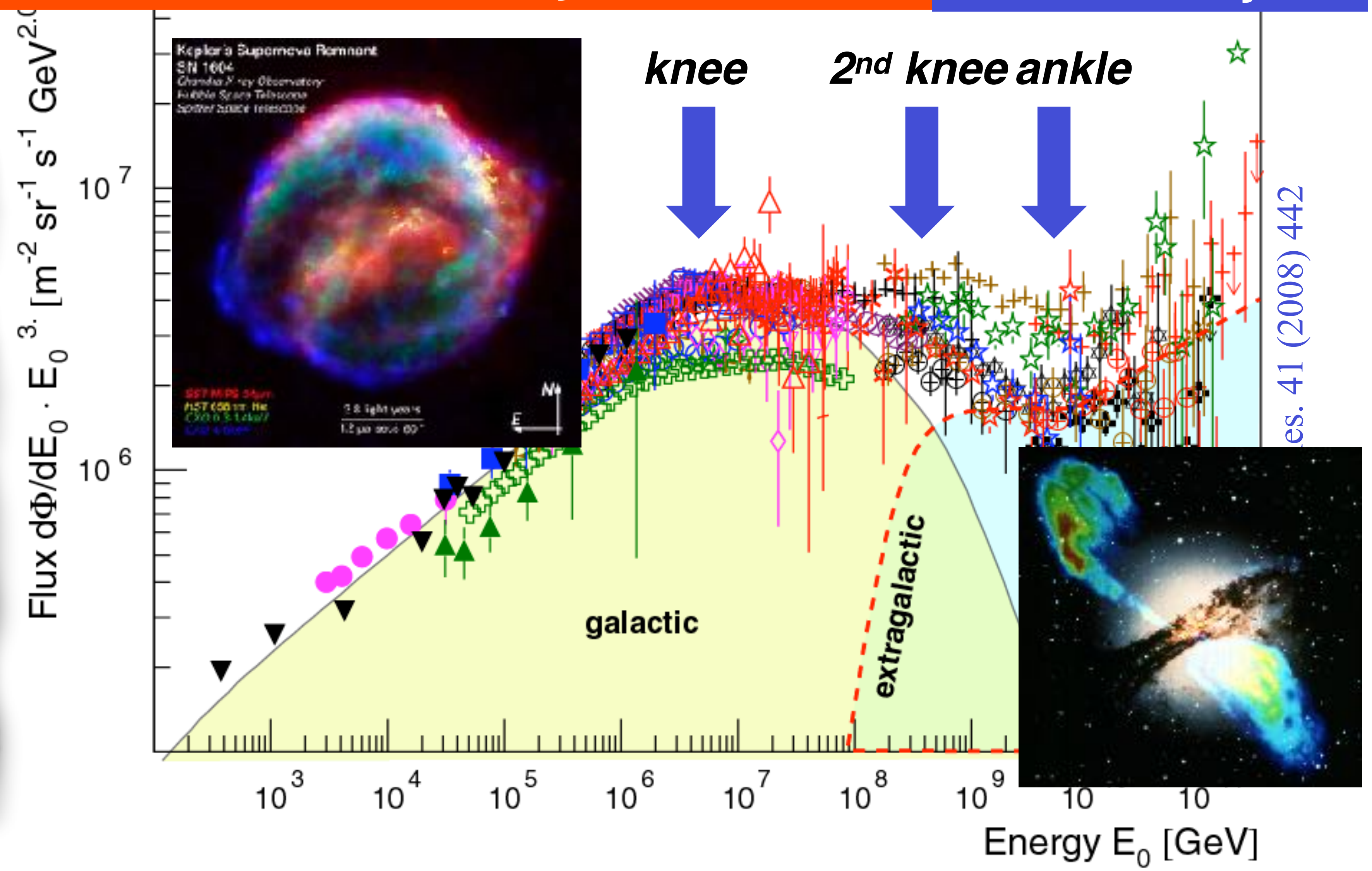

r= 0.04 pc 3.6 pc 360 pc 36 kpc

Jörg R. Hörandel RU Nijmegen, Nikhef, VU Brussel http://particle.astro.ru.nl

Cosmic rays at the knee

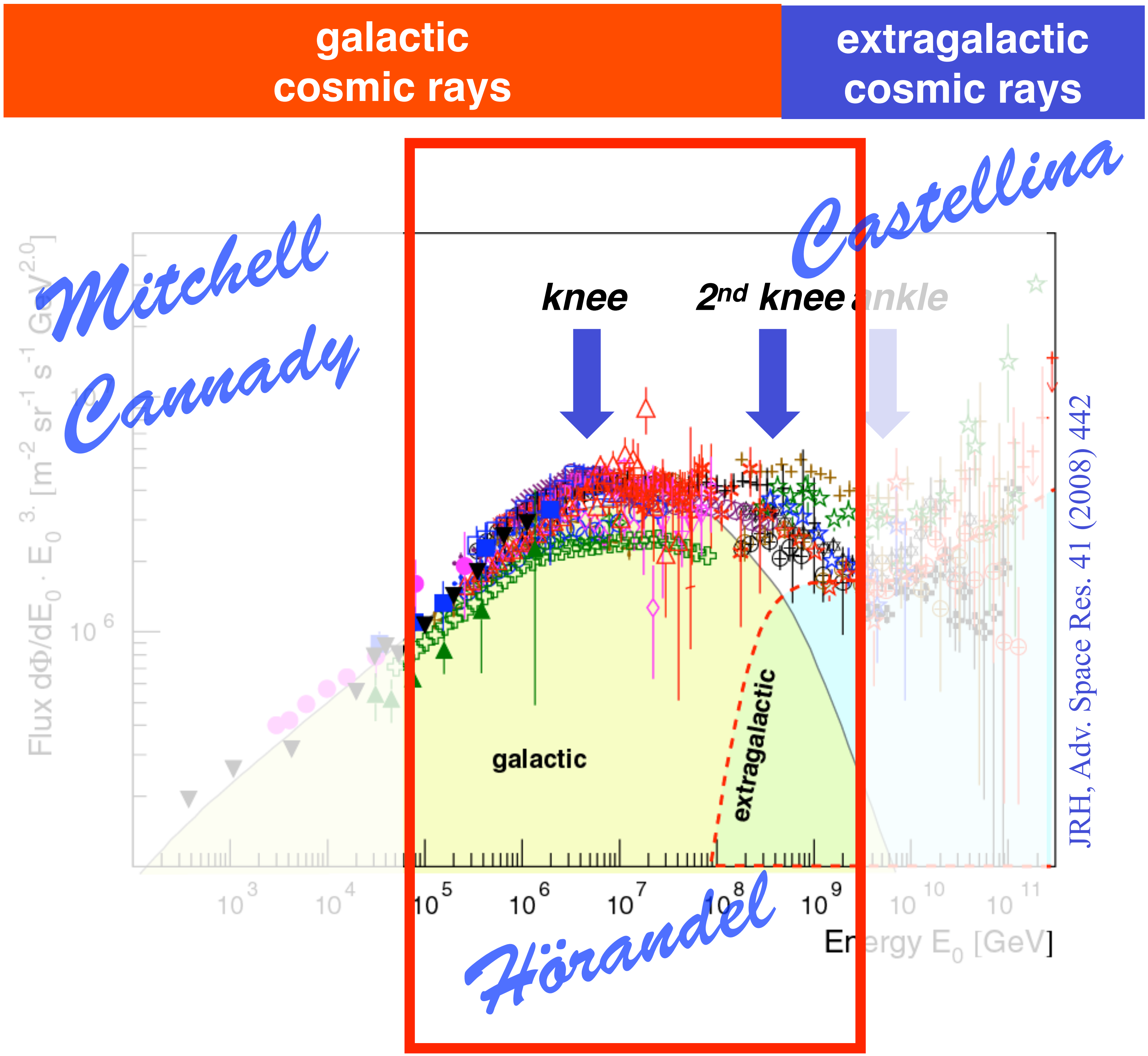

Cosmic rays at the knee

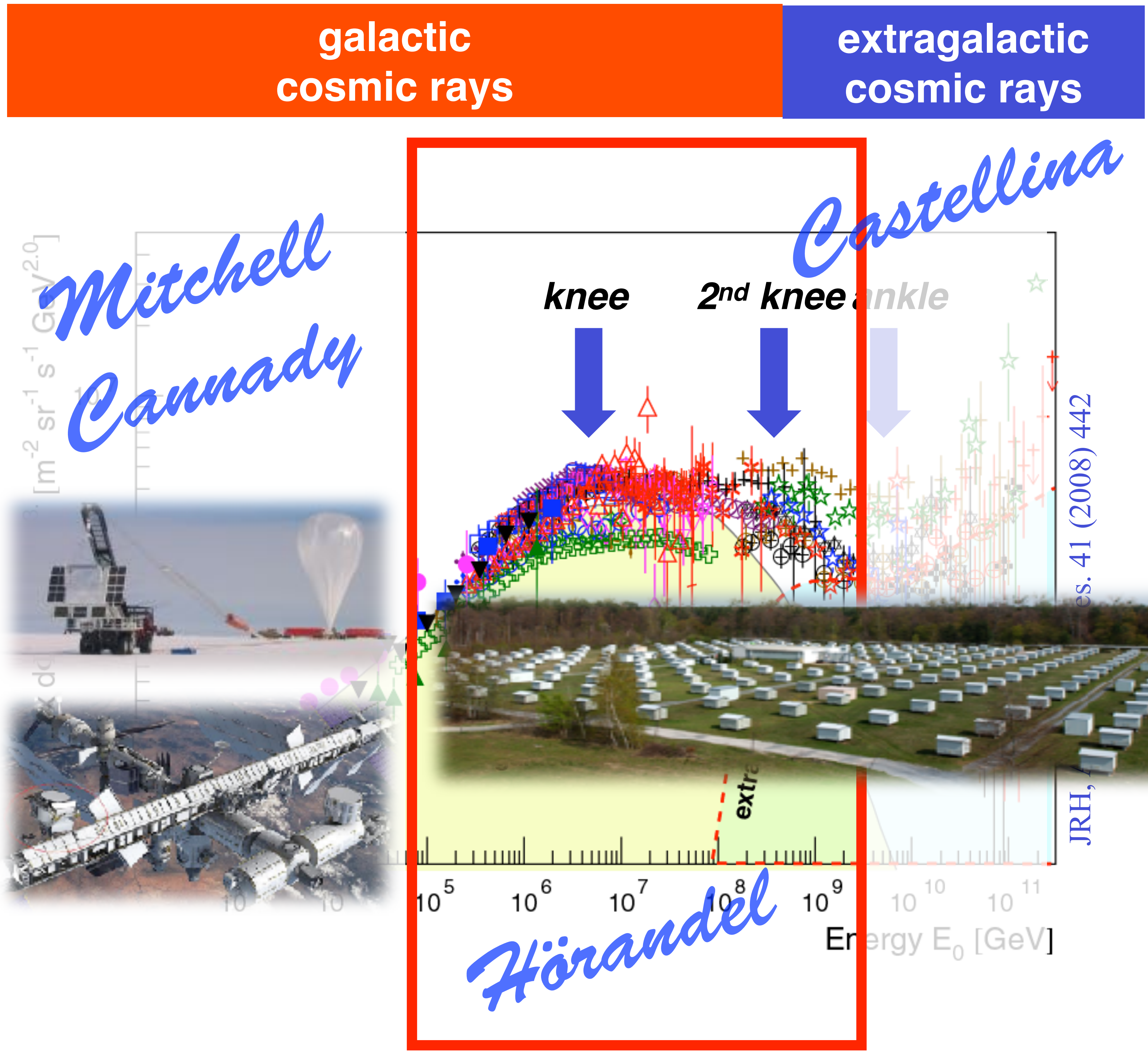

Cosmic rays at the knee

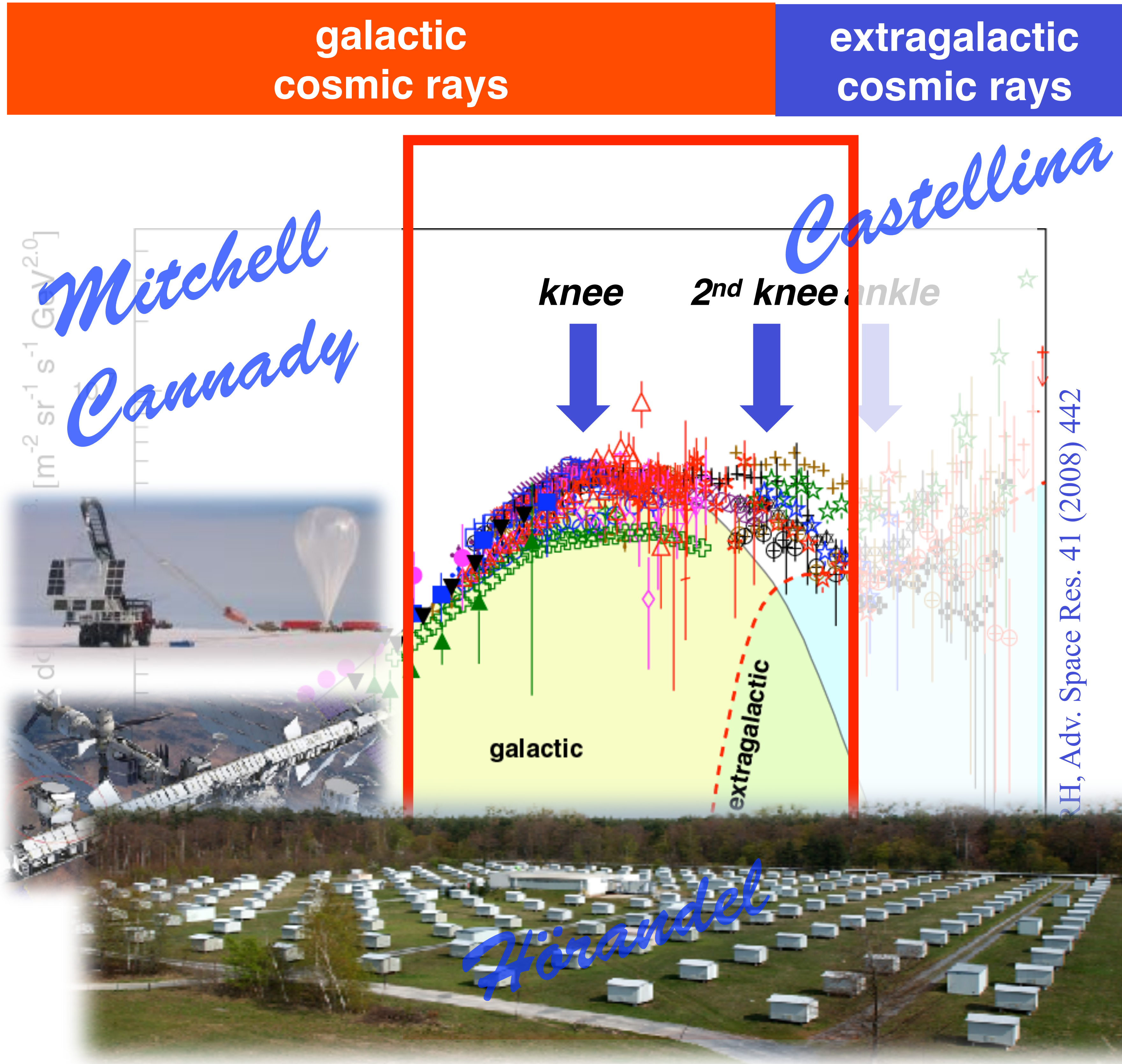

Extensive Air Showers

electromagnetic hadronic muonic

shower component

~ 98% < 1% ~2%

Extensive Air Showers

p

electromagnetic hadronic muonic

shower component

~ 98% < 1% ~2%

Extensive Air Showers

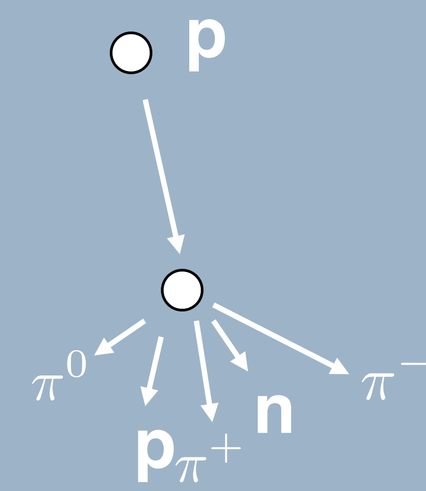

electromagnetic hadronic muonic

shower component

~ 98% < 1% ~2%

Extensive Air Showers

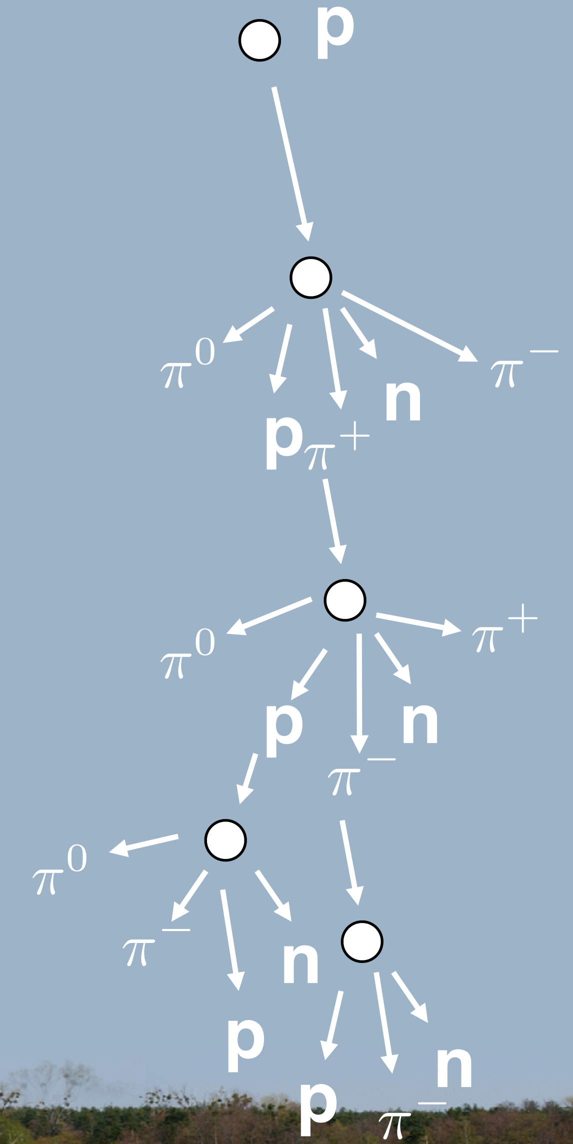

electromagnetic hadronic muonic

shower component

~ 98% < 1% ~2%

Extensive Air Showers

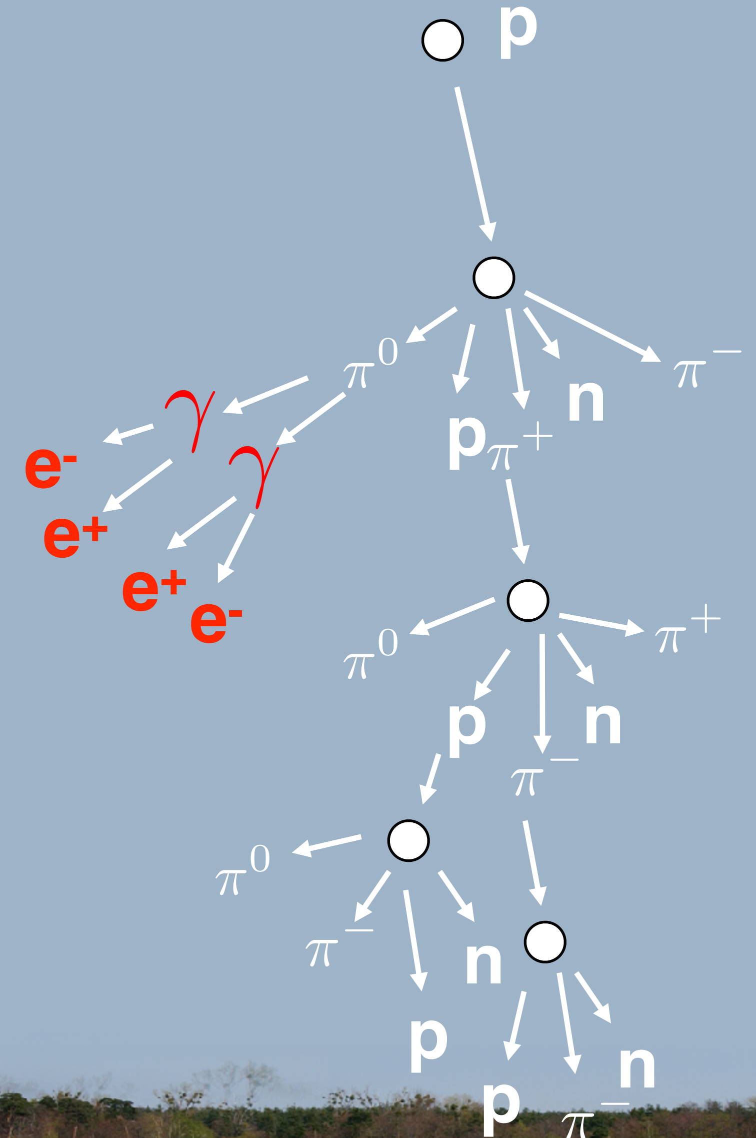

electromagnetic **hadronic** **muonic**

shower component

~ 98% **< 1%** **~2%**

Extensive Air Showers

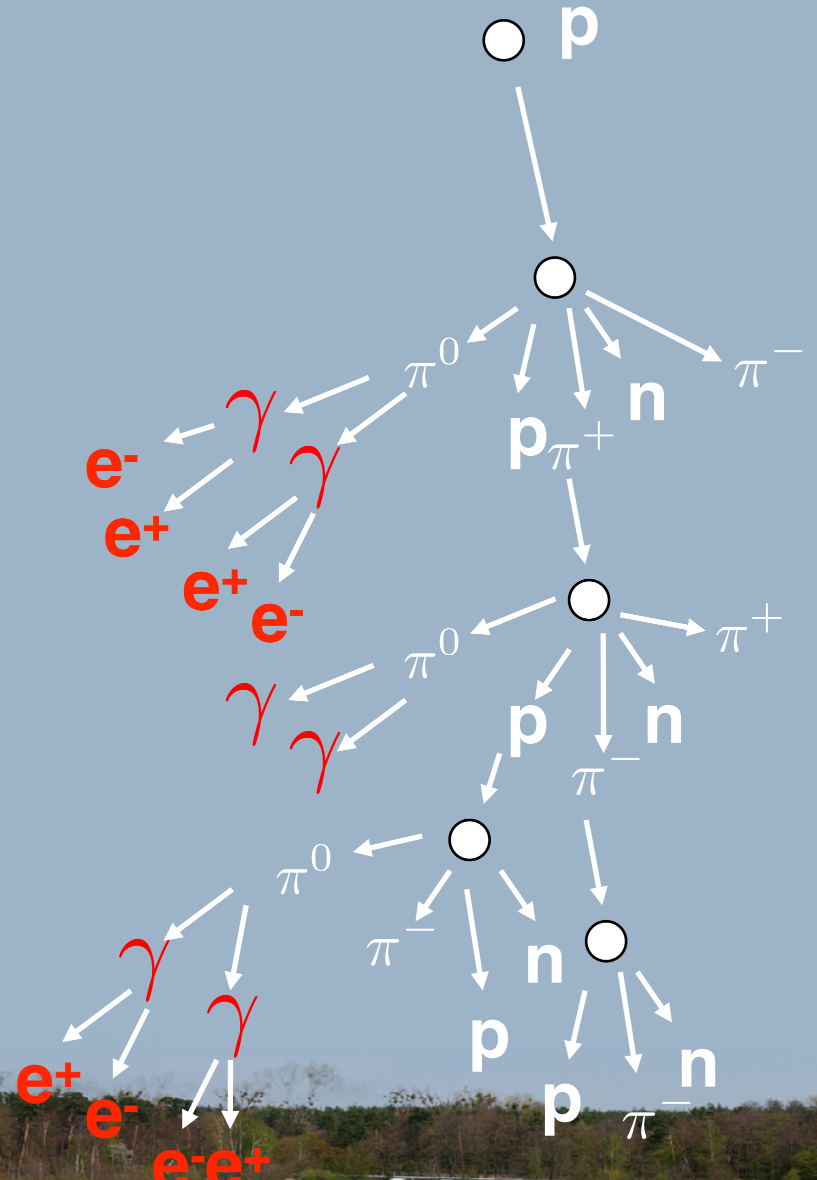

electromagnetic hadronic muonic

shower component

~ 98% < 1% ~2%

Extensive Air Showers

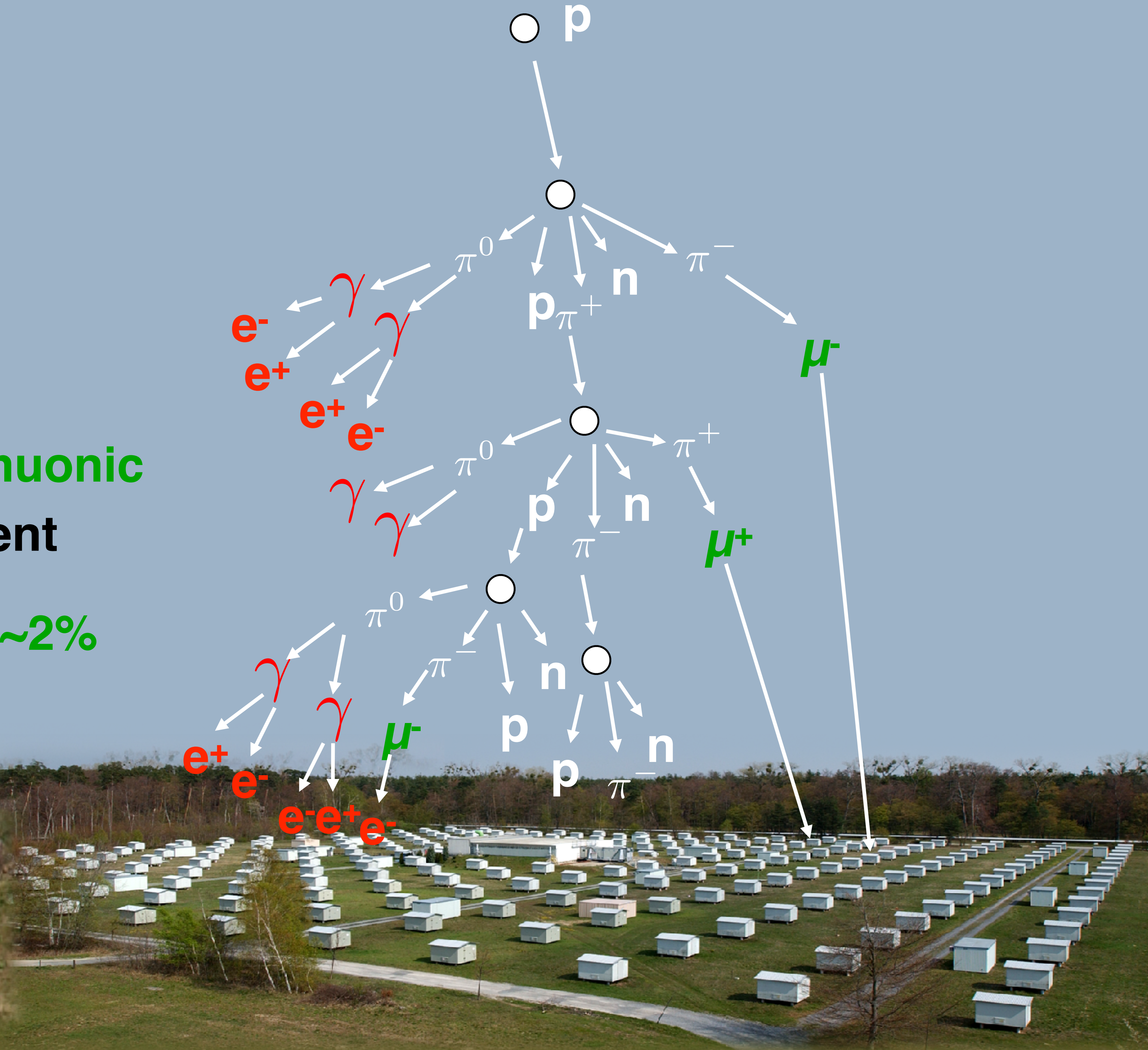

electromagnetic	hadronic	muonic
shower component		
~ 98%	< 1%	~2%

A Matthews Heitler Model – mass resolution in EAS measurements

depth of shower maximum

$$X^{A}_{max} = X^{p}_{max} - X_0 \ln A$$

radiation length X_0=36.7 g/cm²

electron-muon ratio

$$\lg(N_e/N_\mu) = C - 0.065 \ln A.$$

J. Matthews, Astropart. Phys. 22 (2005) 387 JRH, Mod. Phys. Lett. A 22 (2007) 1533 JRH, Nucl. Instr. and Meth. A 588 (2008) 181

A Matthews Heitler Model – mass resolution in EAS measurements

depth of shower maximum

$$X^A_{max} = X^p_{max} - X_0 \ln A$$

radiation length X_0=36.7 g/cm²

typical uncertainty

$$\Delta X_{max} \approx 20 \text{ g/cm}^2$$

electron-muon ratio

$$\lg(N_\mathrm{e}/N_\mathrm{\mu}) = C - 0.065 \ln A.$$

$$\Delta \frac{N_e}{N_\mu} \approx 16\% - 20\%$$

J. Matthews, Astropart. Phys. 22 (2005) 387

JRH, Mod. Phys. Lett. A 22 (2007) 1533

JRH, Nucl. Instr. and Meth. A 588 (2008) 181

A Matthews Heitler Model – mass resolution in EAS measurements

depth of shower maximum

$$X^{A}_{max} = X^{p}_{max} - X_0 \ln A$$

radiation length X_0=36.7 g/cm²

typical uncertainty

$$\Delta X_{max} \approx 20 \text{ g/cm}^2$$

expected mass resolution

$$\Rightarrow \Delta \ln A \approx 0.8 - 1$$

electron-muon ratio

$$\lg(N_e/N_\mu) = C - 0.065 \ln A.$$

$$\Delta \frac{N_e}{N_\mu} \approx 16\% - 20\%$$

$\Rightarrow$ **4 to 5 mass groups**
p, He, CNO, (Si), Fe

J. Matthews, Astropart. Phys. 22 (2005) 387 — JRH, Mod. Phys. Lett. A 22 (2007) 1533 — JRH, Nucl. Instr. and Meth. A 588 (2008) 181

The KASCADE Array

200 m

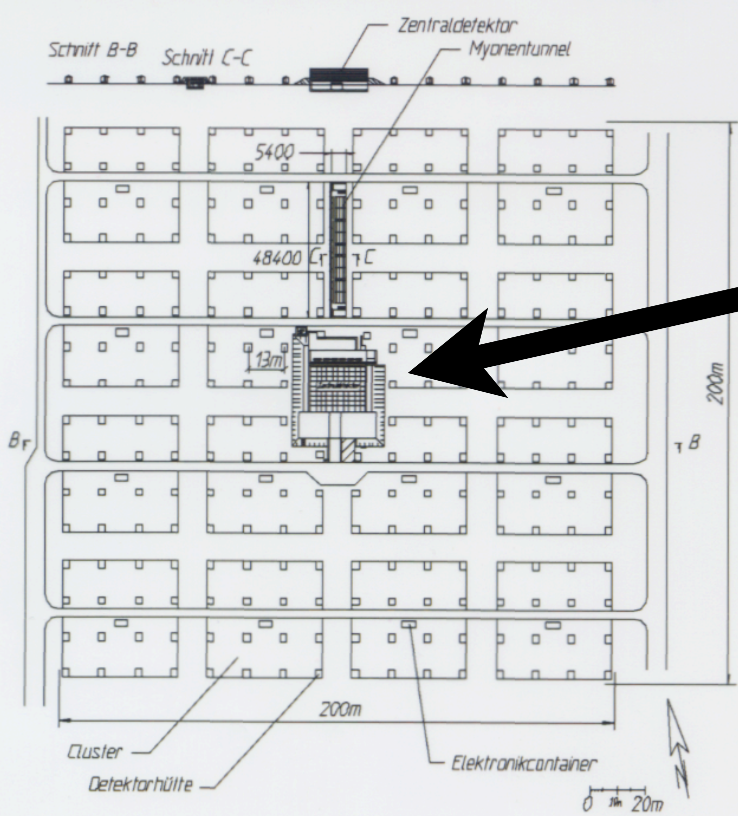

200 m

❑ Array

252 stations with

❑ e/γ detectors: 4 cm liquid scintillator (≈ 3.1 m^2)

❑ muon detectors: 3 cm plastic scintillator (≈ 3.2 m^2)

shield 10 cm Pb + 4 cm Fe ➜ 20 X_0

➠ E_μ > 300 MeV

→ measurement of particle densities and arrival times

JRH 06/96

The KASCADE Central Detector

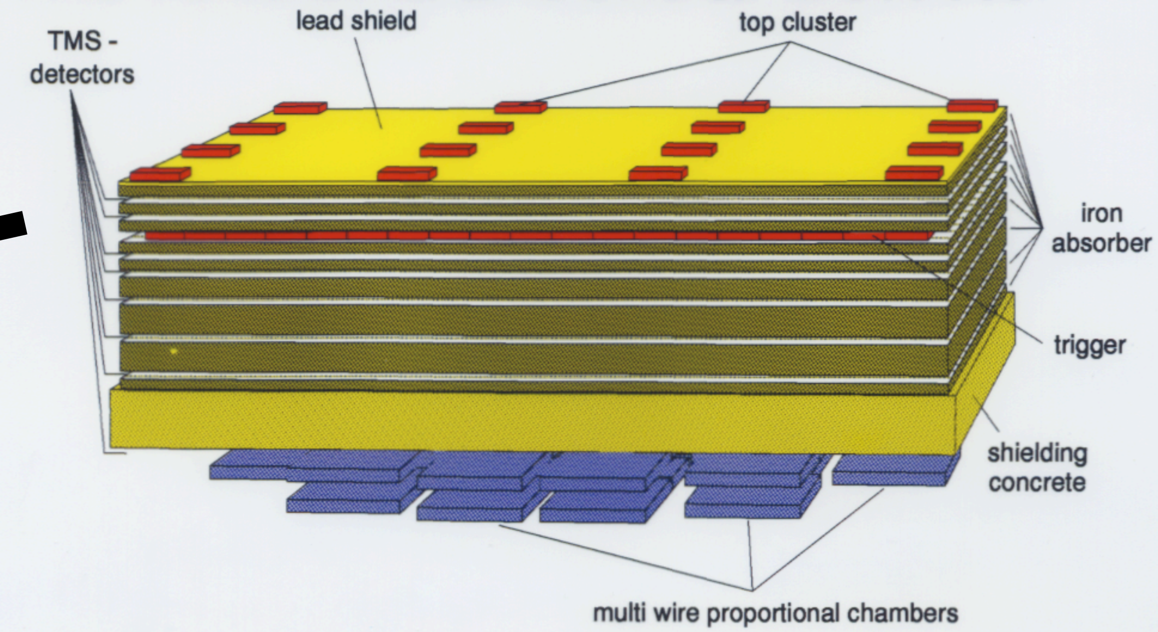

4 different detector systems:

❑ Top array 32 × 0.45 m^2 scintillation counters (14 m^2)

❑ Trigger layer 456 × 0.45 m^2 scintillation counters (206 m^2)

❑ 32 Multiwire proportional chambers (2 × 150 m^2) E_μ > 2 GeV

❑ Iron sampling calorimeter (16 × 20 m^2)

8 active layers → 10 000 liquid ionisation chambers

40 000 electronic channels

separation of individual hadrons by a fine segmentation

depth ≈ 11 λ_I ➜ hadrons up to 10 TeV 95% contained

JRH 06/96

KArlsruhe Shower Core and Array DEtector

Simultaneous measurement of
electromagnetic,
muonic,
hadronic
shower components

T. Antoni et al, Nucl. Instr. & Meth. A 513 (2004) 490

KArlsruhe Shower Core and Array DEtector

Simultaneous measurement of
electromagnetic,
muonic,
hadronic
shower components

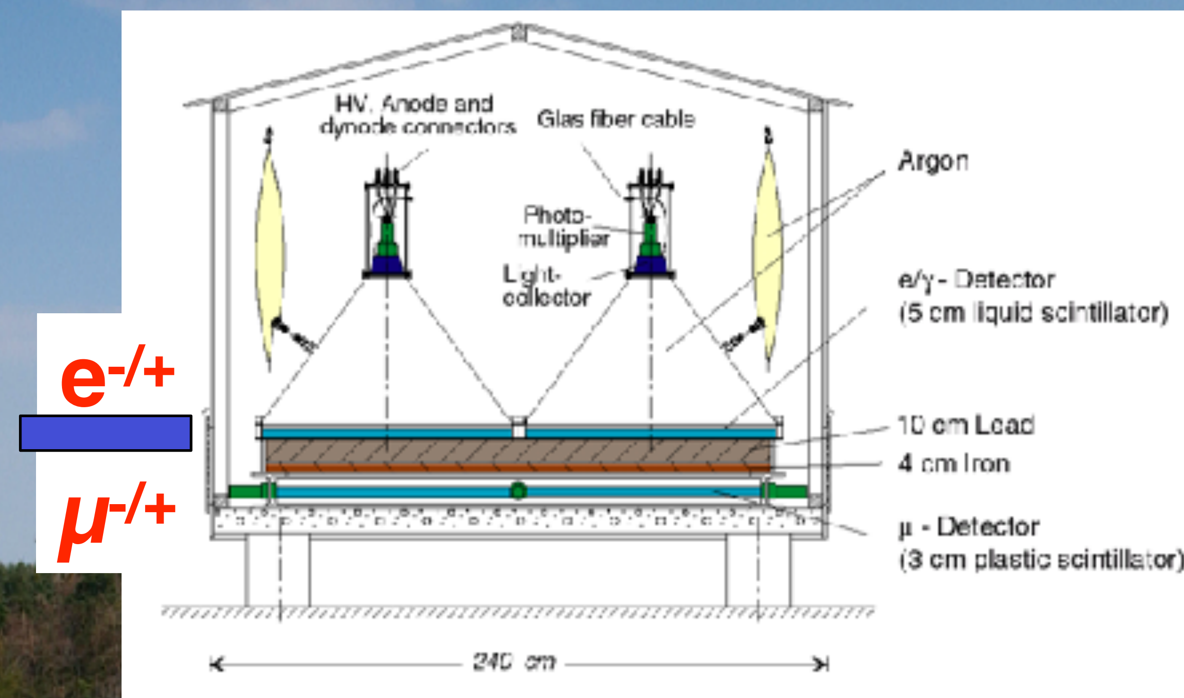

T. Antoni et al, Nucl. Instr. & Meth. A 513 (2004) 490

Event reconstruction in the scintillator array

electromagnetic component

shower core	$\Delta r = 2.5 - 5.5$ m
shower direction	$\Delta\alpha = 0.5° - 1.2°$
shower size	$\Delta N_e/N_e = 6 - 12$ %

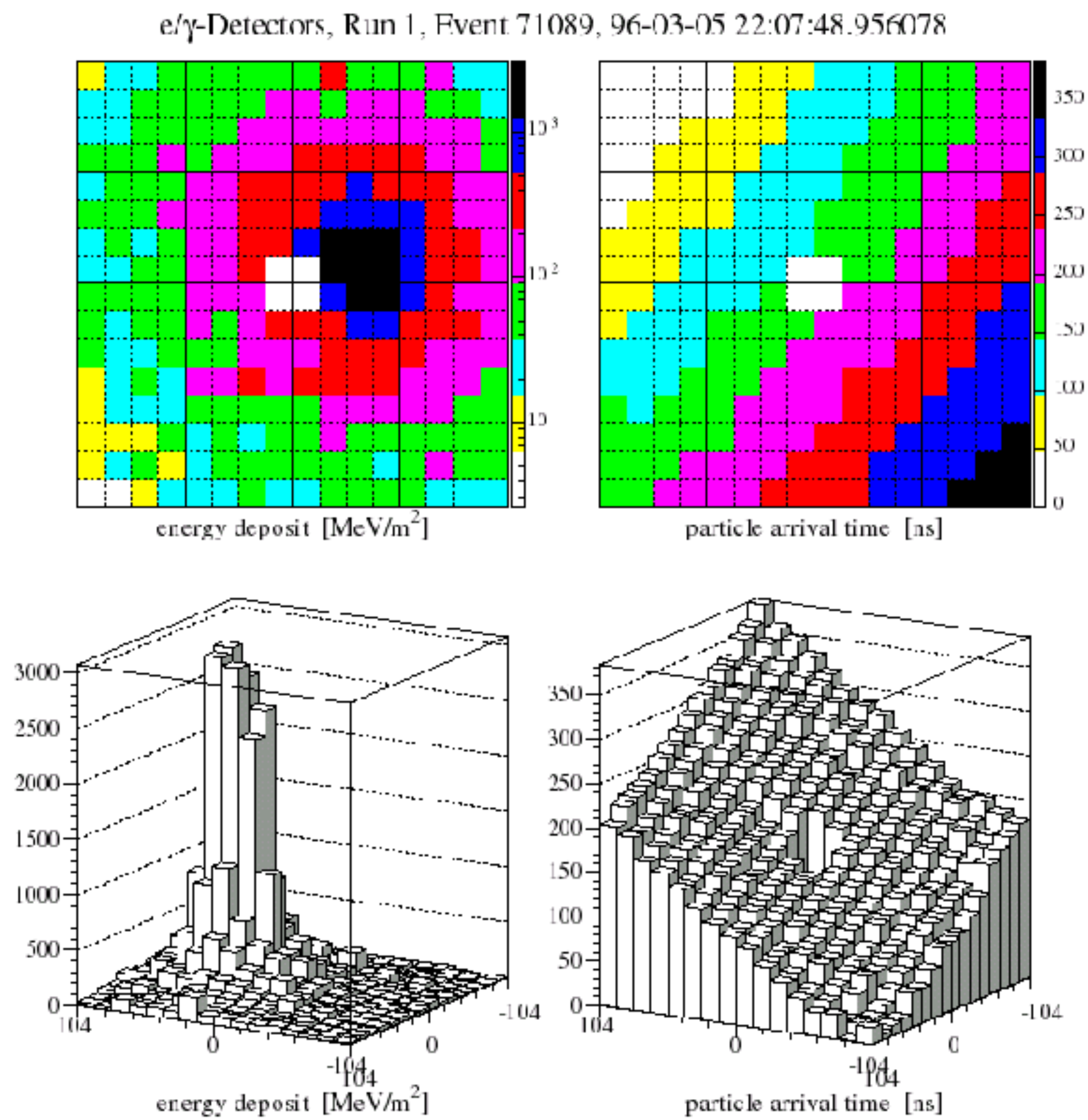

KASCADE GRANDE Array

37 detector stations

370 m² e/γ: scintillation counter

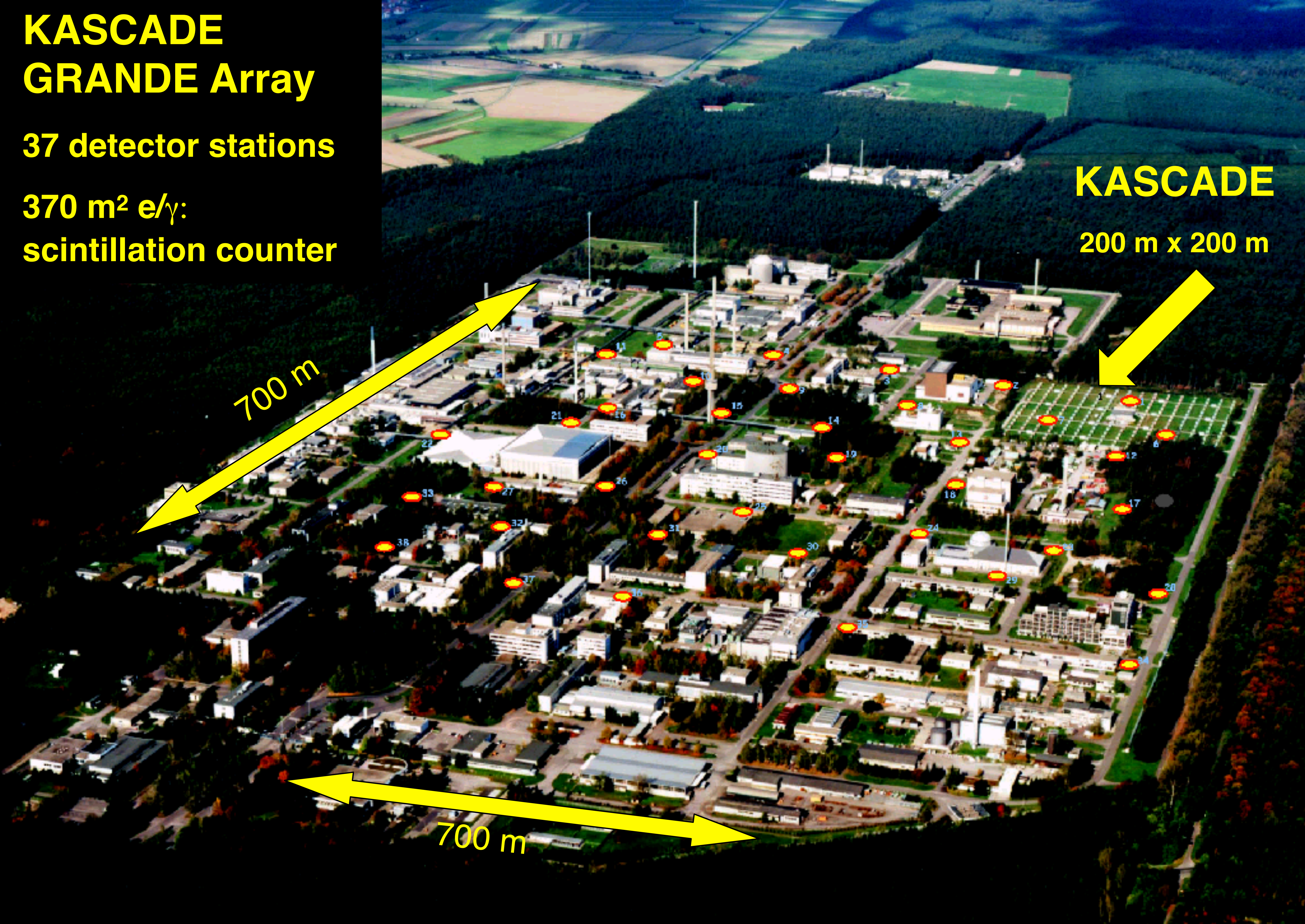

G. Navarra et al., Nucl Instr & Meth A 518 (2004) 207

KASCADE GRANDE Array

37 detector stations

370 m² e/γ: scintillation counter

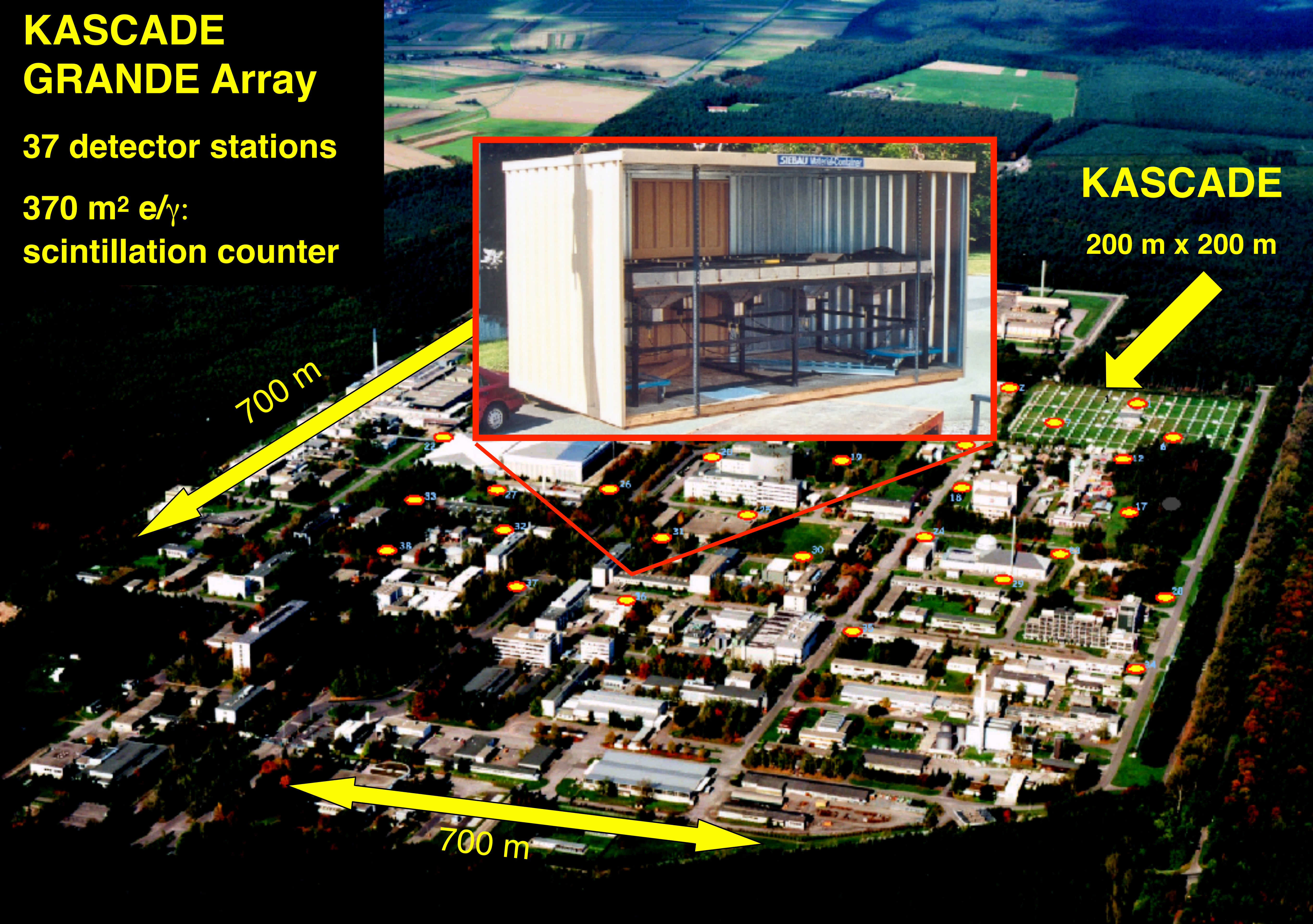

G. Navarra et al., Nucl Instr & Meth A 518 (2004) 207

KASCADE-Grande – Lateral distributions

Electromagnetic component

Muons

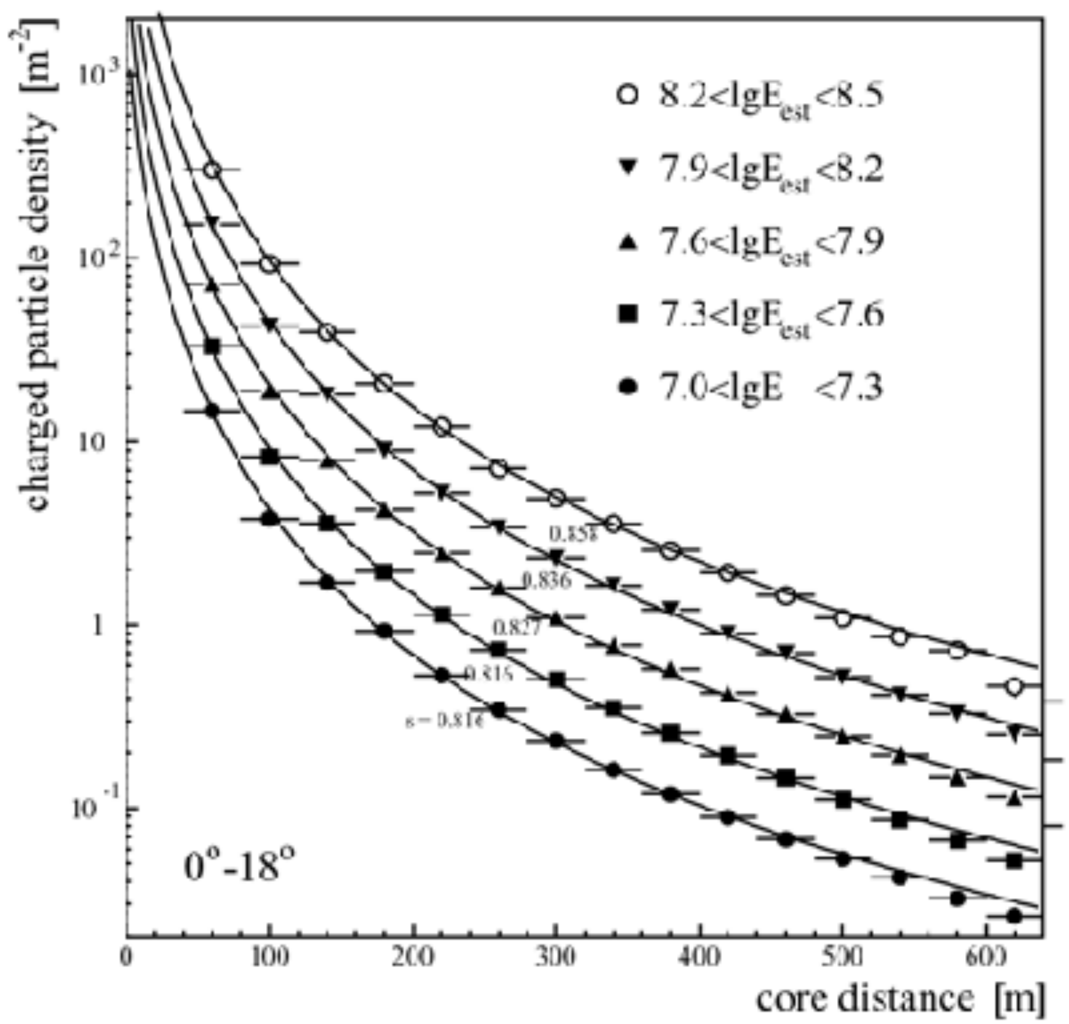

R. Glasstetter et al., Proc. 29th ICRC, Pune 6 (2005) 293

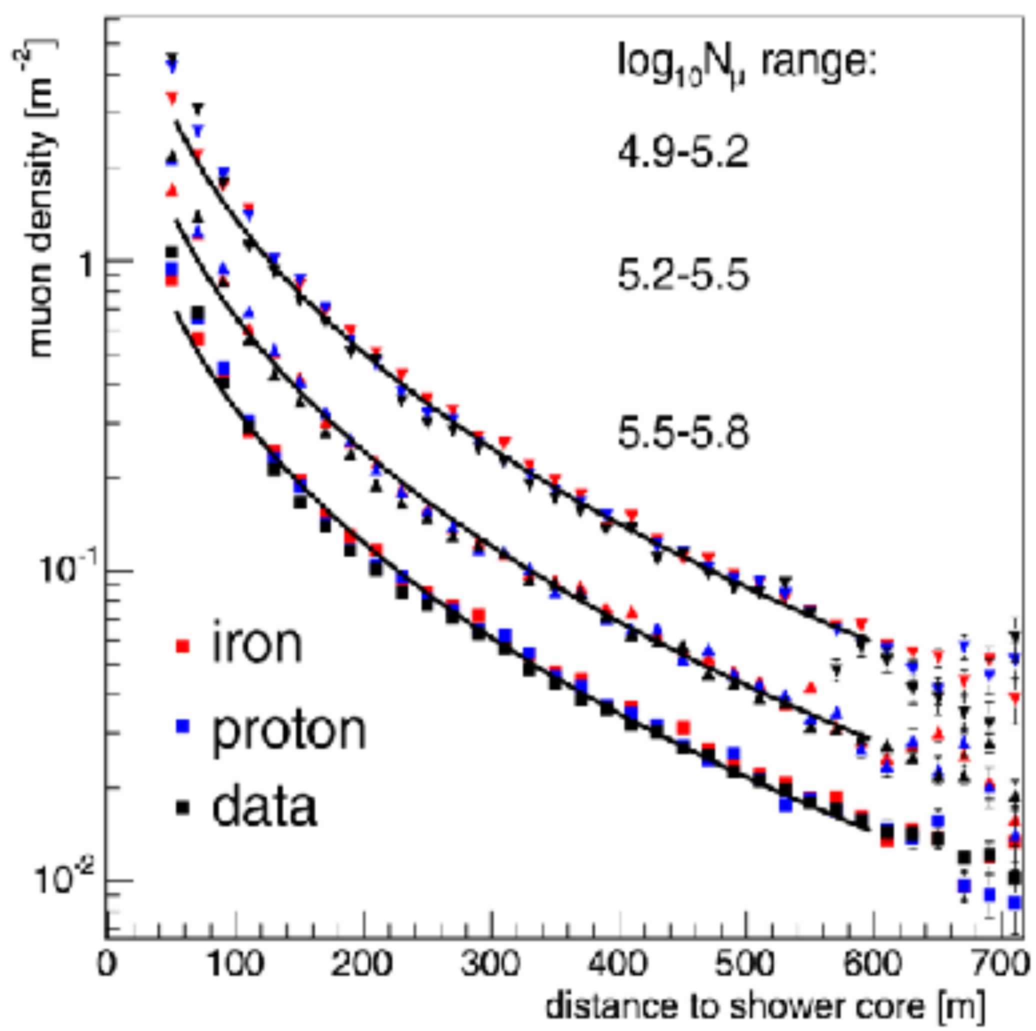

J. v. Buren et al., Proc. 29th ICRC, Pune 6 (2005) 301

KASCADE-Grande – Lateral distributions

Electromagnetic component

Muons

NKG function

$$\rho(r,s,N_e) = \frac{N_e}{r_M^2} \frac{\Gamma(4.5-s)}{2\pi\Gamma(s)\Gamma(4.5-2s)} \left(\frac{r}{r_M}\right)^{s-2} \left(1+\frac{r}{r_M}\right)^{s-4.5}$$

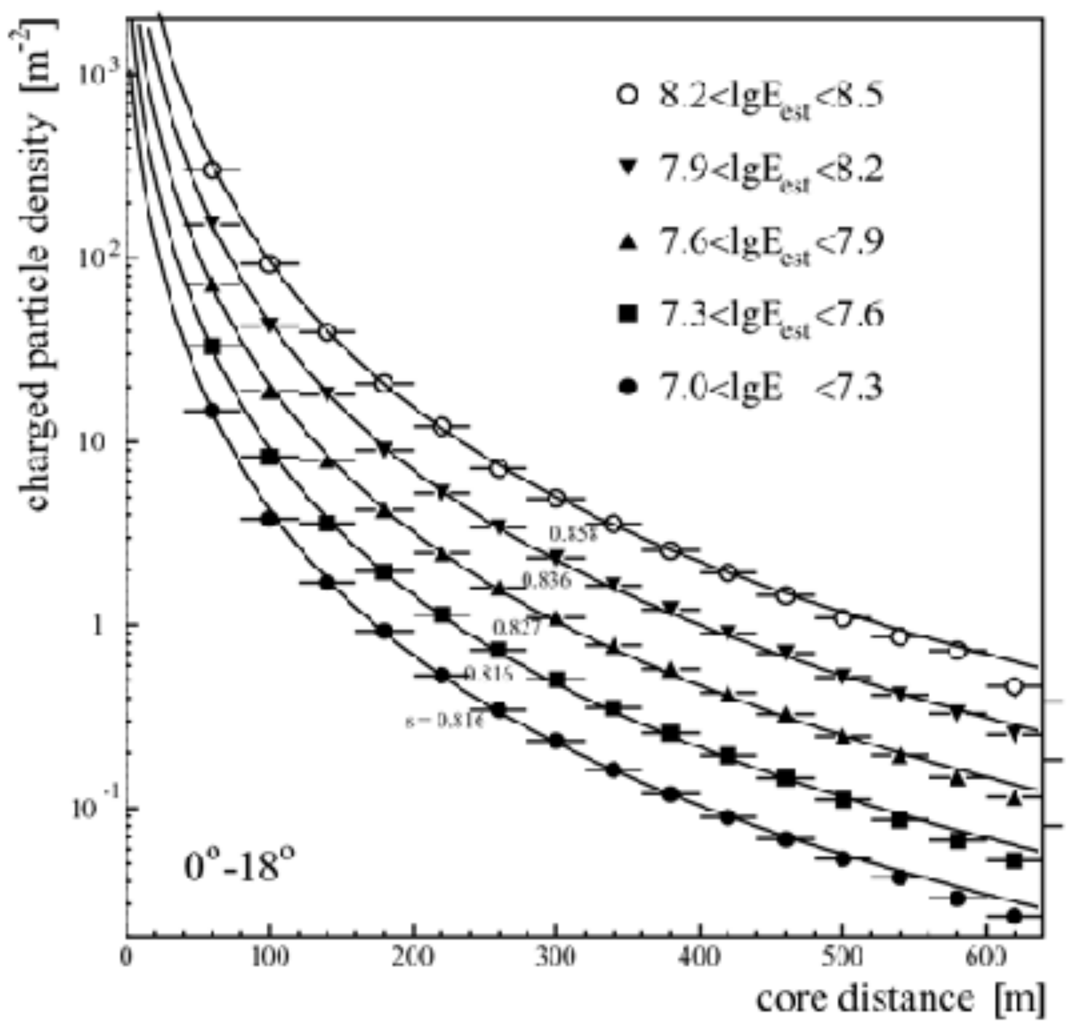

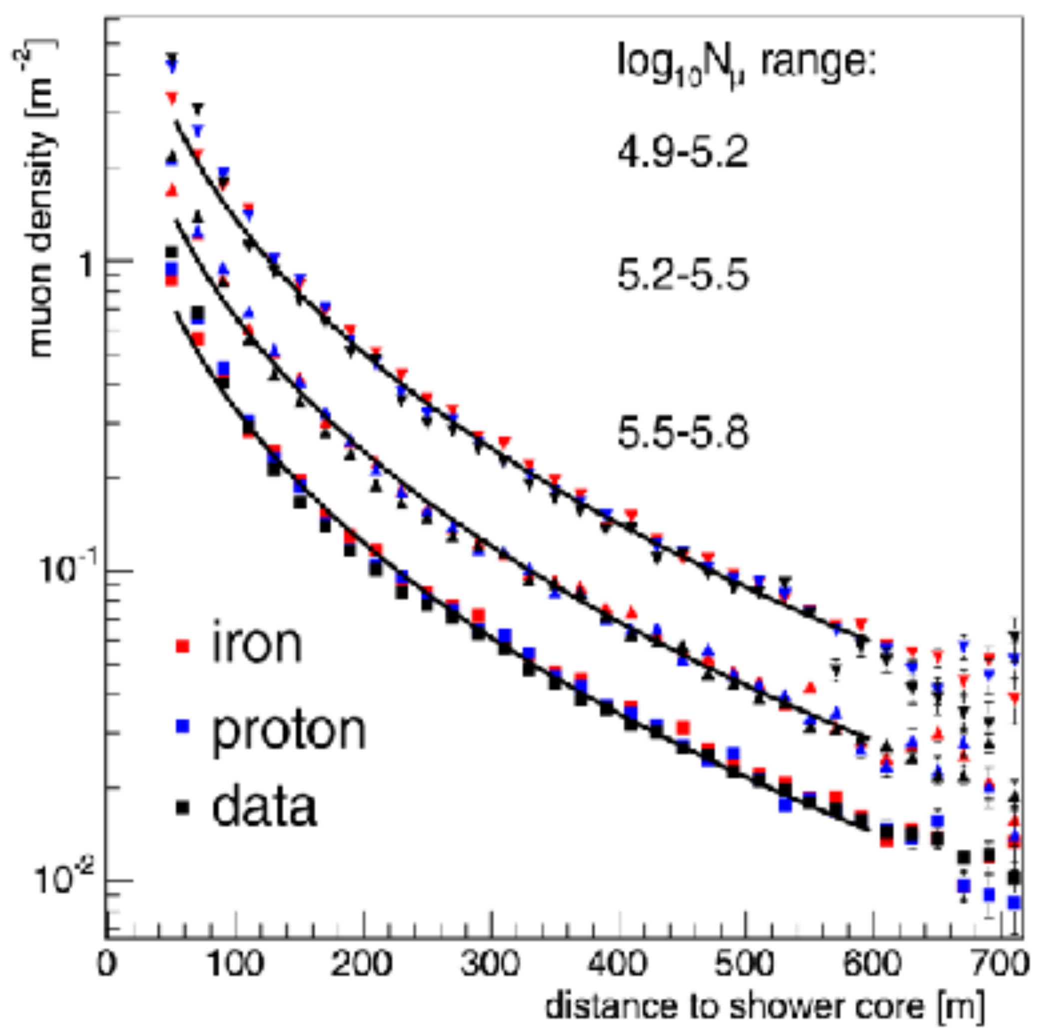

R. Glasstetter et al., Proc. 29th ICRC, Pune 6 (2005) 293

J. v. Buren et al., Proc. 29th ICRC, Pune 6 (2005) 301

KASCADE-Grande – Lateral distributions

Electron

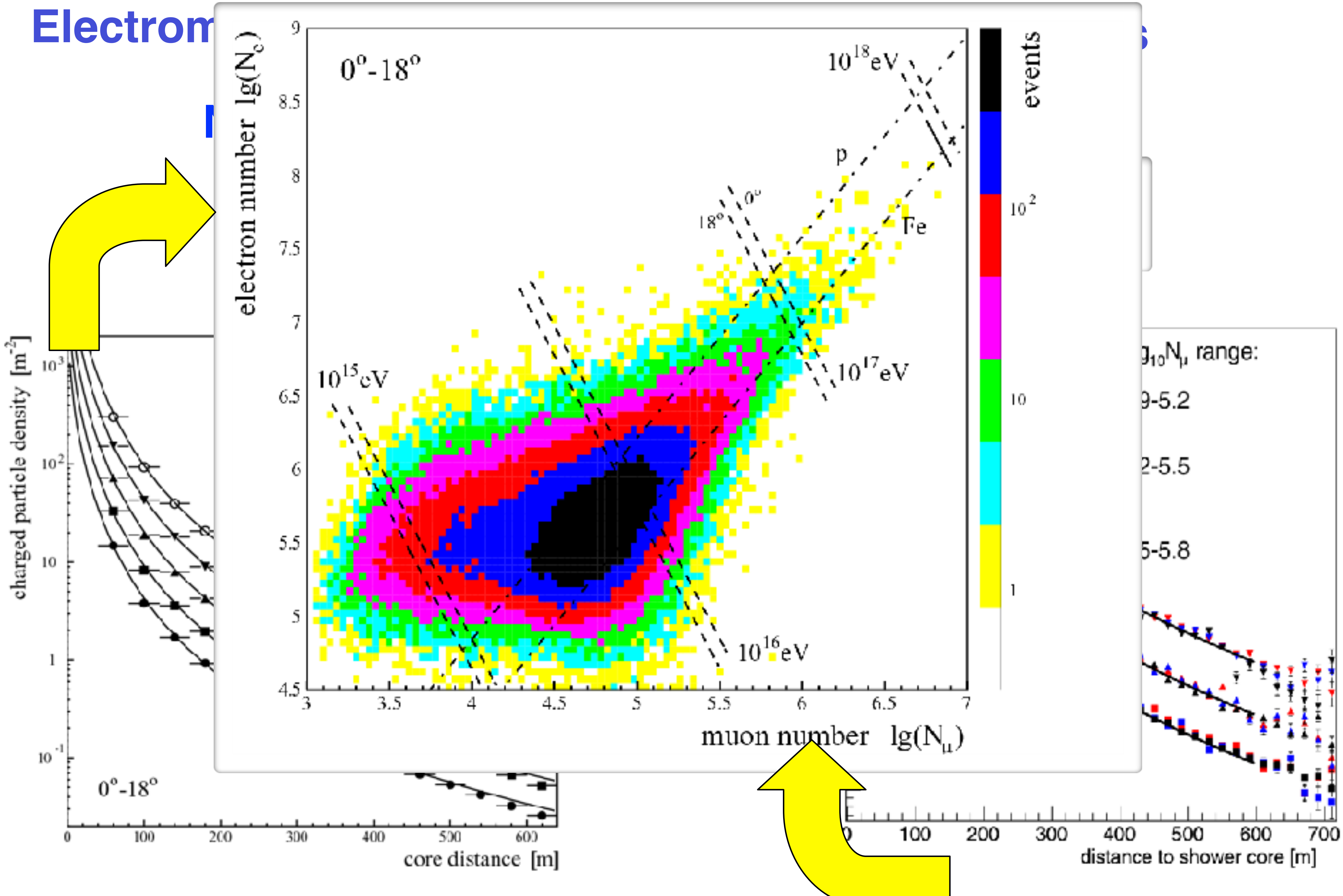

R. Glasstetter et al., Proc. 29th ICRC, Pune 6 (2005) 293

J. v. Buren et al., Proc. 29th ICRC, Pune 6 (2005) 301

KASCADE: Energy spectra for elemental groups

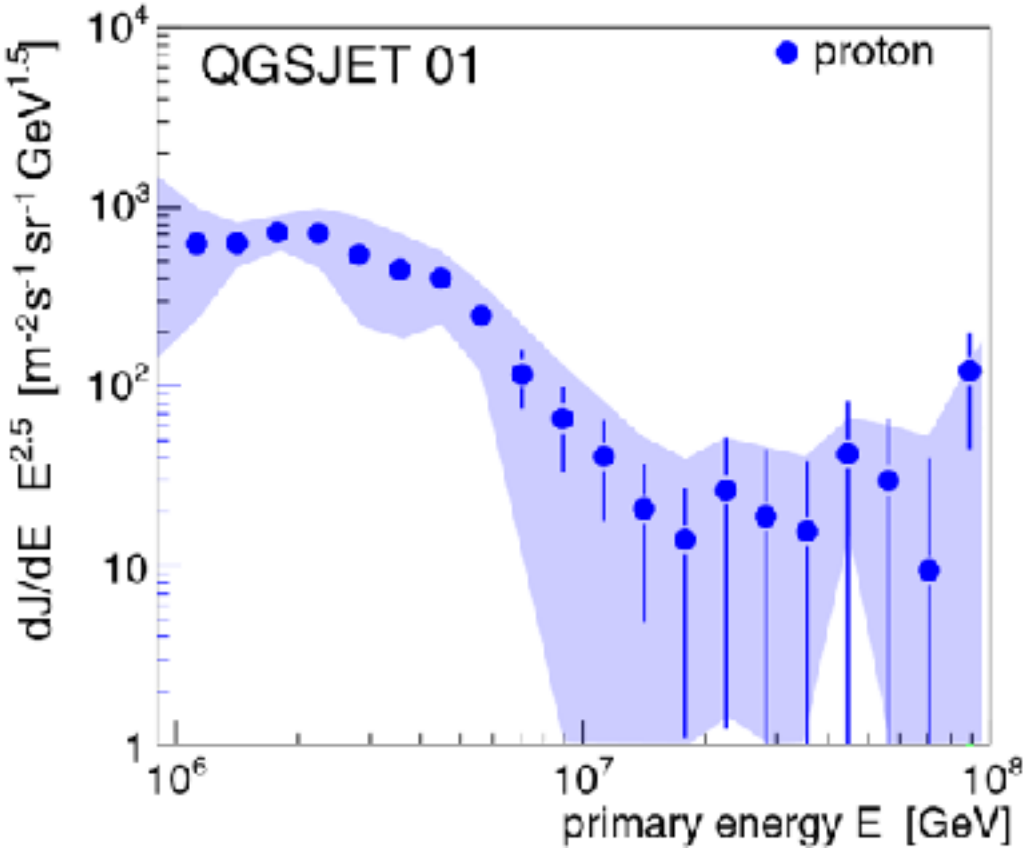

T. Antoni et al., Astropart. Phys. 24 (2005) 1

KASCADE: Energy spectra for elemental groups

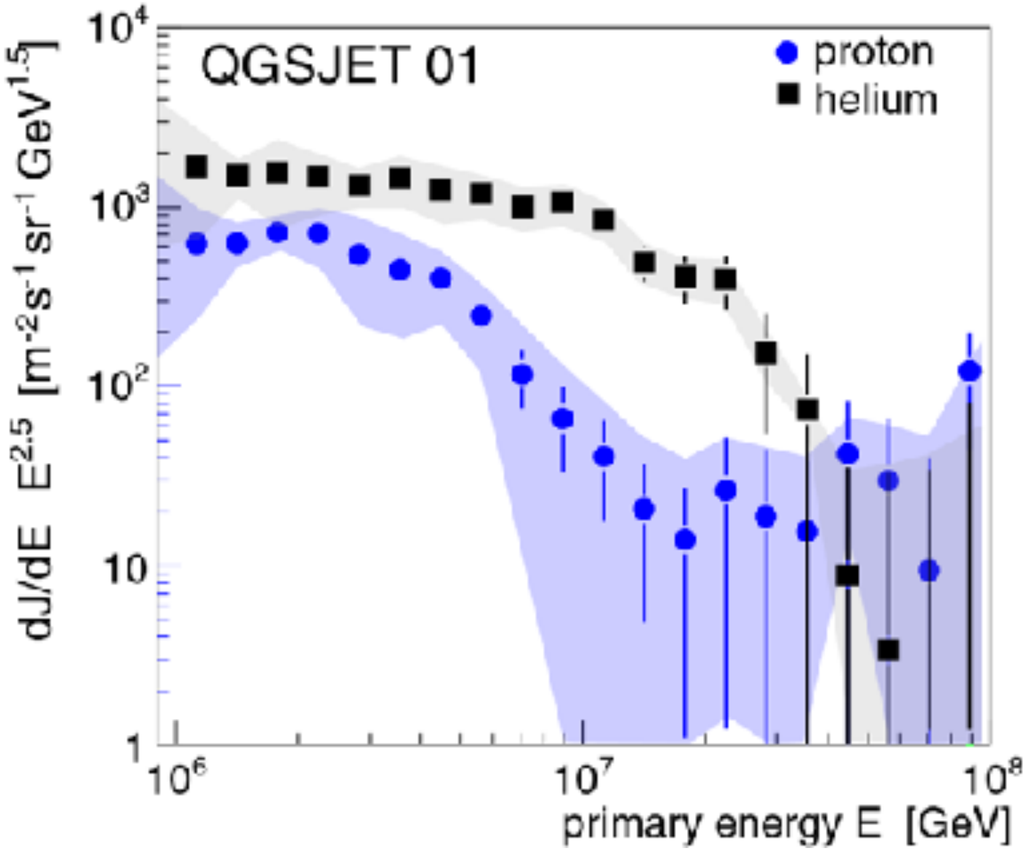

T. Antoni et al., Astropart. Phys. 24 (2005) 1

KASCADE: Energy spectra for elemental groups

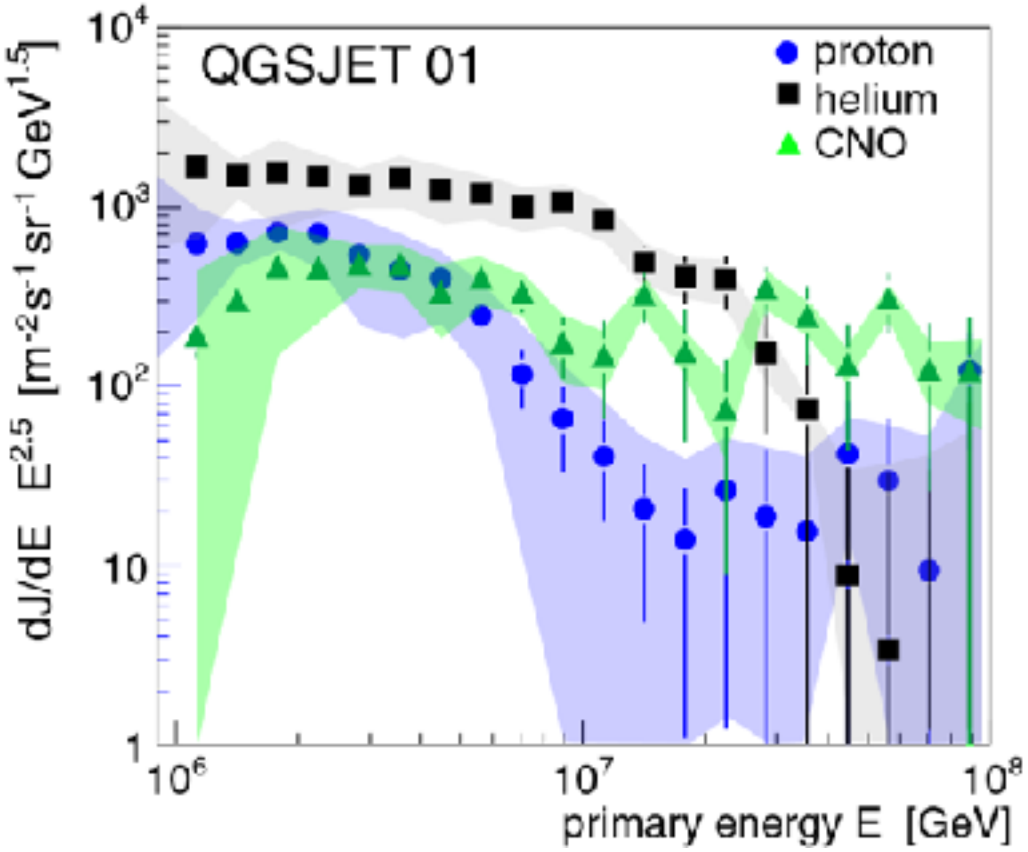

T. Antoni et al., Astropart. Phys. 24 (2005) 1

KASCADE: Energy spectra for elemental groups

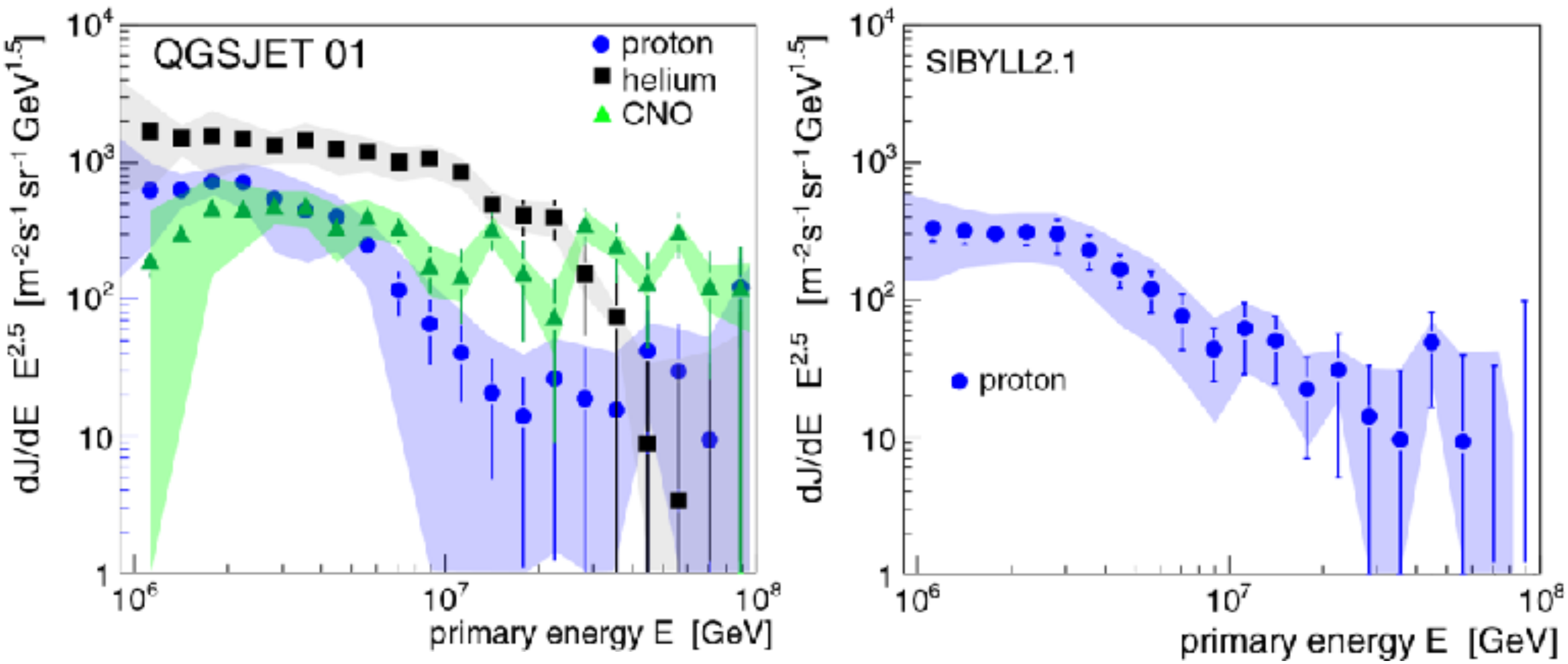

T. Antoni et al., Astropart. Phys. 24 (2005) 1

KASCADE: Energy spectra for elemental groups

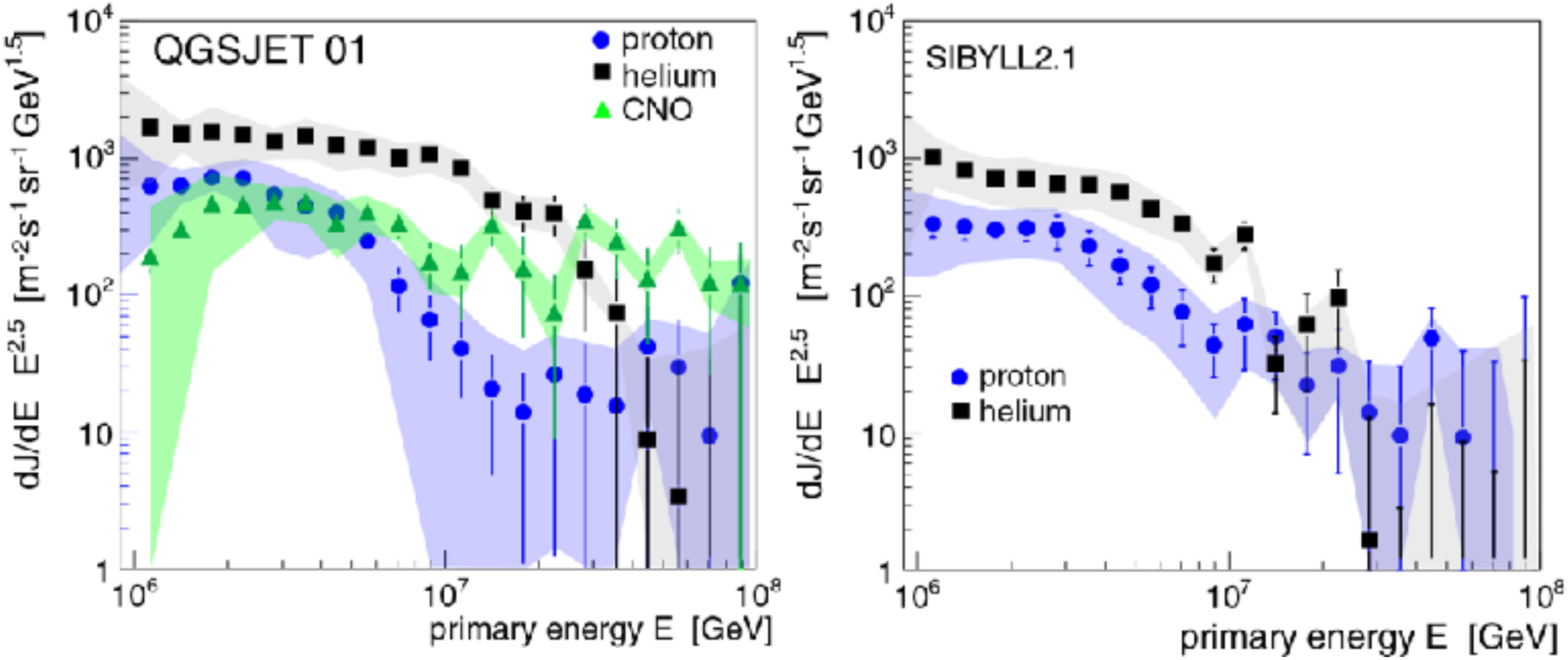

T. Antoni et al., Astropart. Phys. 24 (2005) 1

KASCADE: Energy spectra for elemental groups

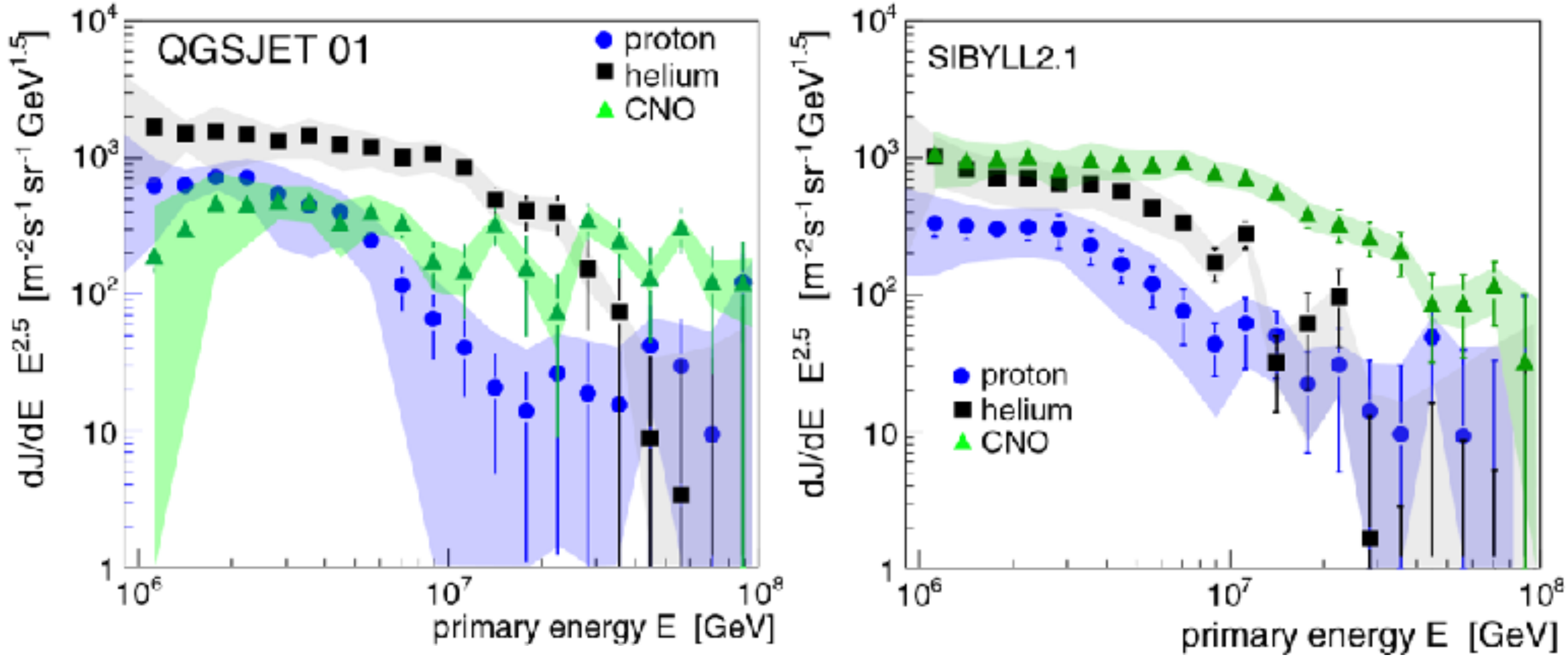

T. Antoni et al., Astropart. Phys. 24 (2005) 1

KASCADE: Energy spectra for elemental groups

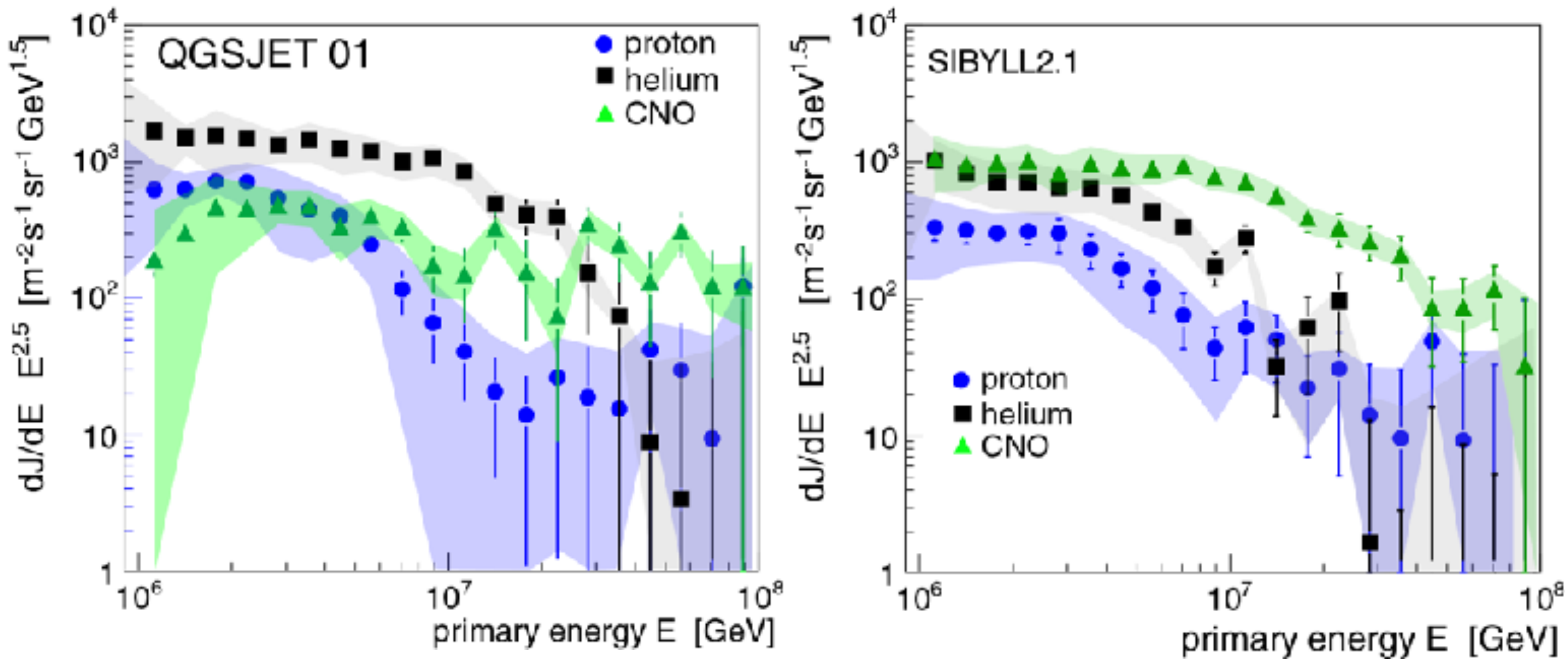

Knee caused by cut-off for light elements

Astrophysical interpretation limited by description of interactions in the atmosphere

T. Antoni et al., Astropart. Phys. 24 (2005) 1

KASCADE: Energy spectra for elemental groups

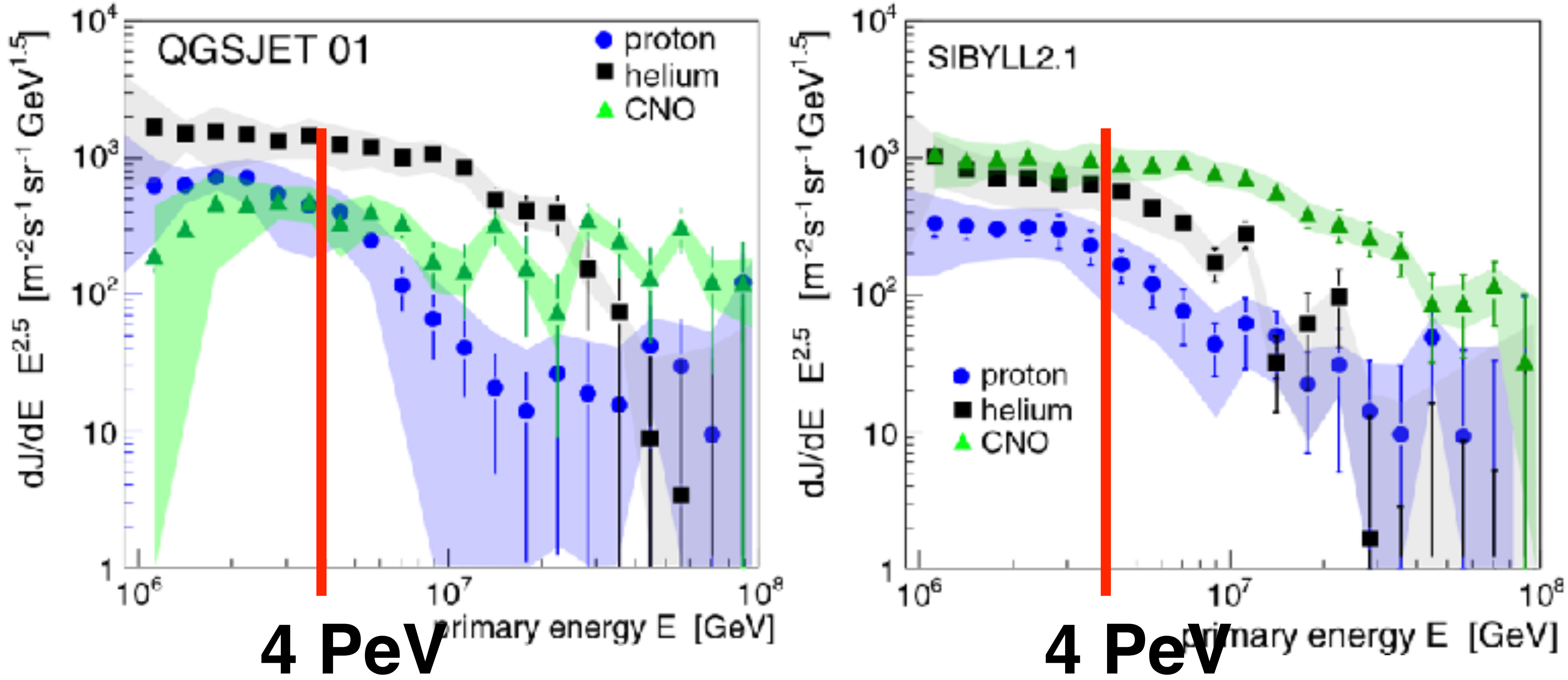

➡ **Knee caused by cut-off for light elements**

Astrophysical interpretation limited by description of interactions in the atmosphere

T. Antoni et al., Astropart. Phys. 24 (2005) 1

KASCADE: Energy spectra for elemental groups

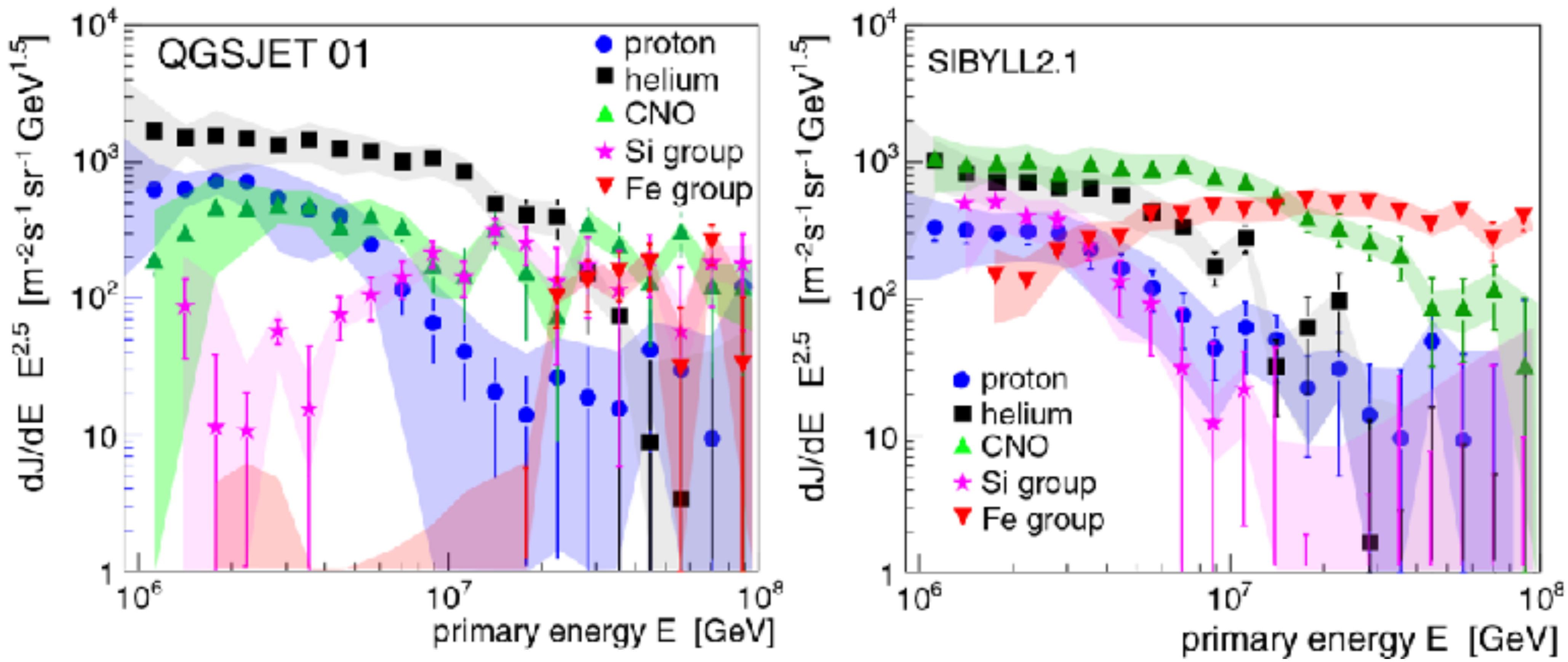

Knee caused by cut-off for light elements

Astrophysical interpretation limited by description of interactions in the atmosphere

T. Antoni et al., Astropart. Phys. 24 (2005) 1

Test of hadronic interaction models

QGSJET 01

N_e-N_μ analysis

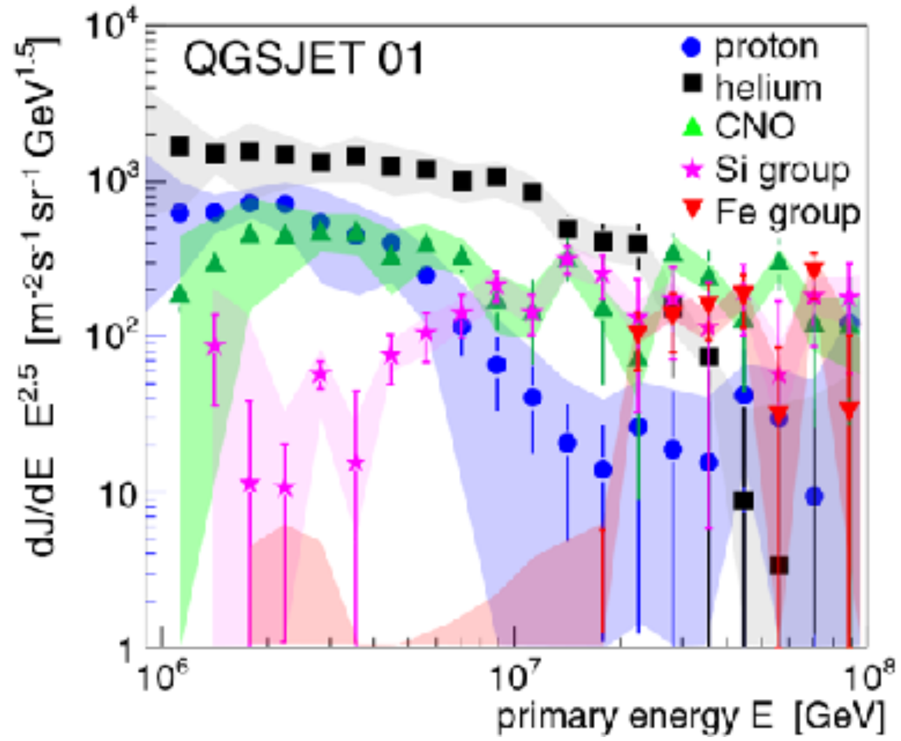

χ^2 distribution

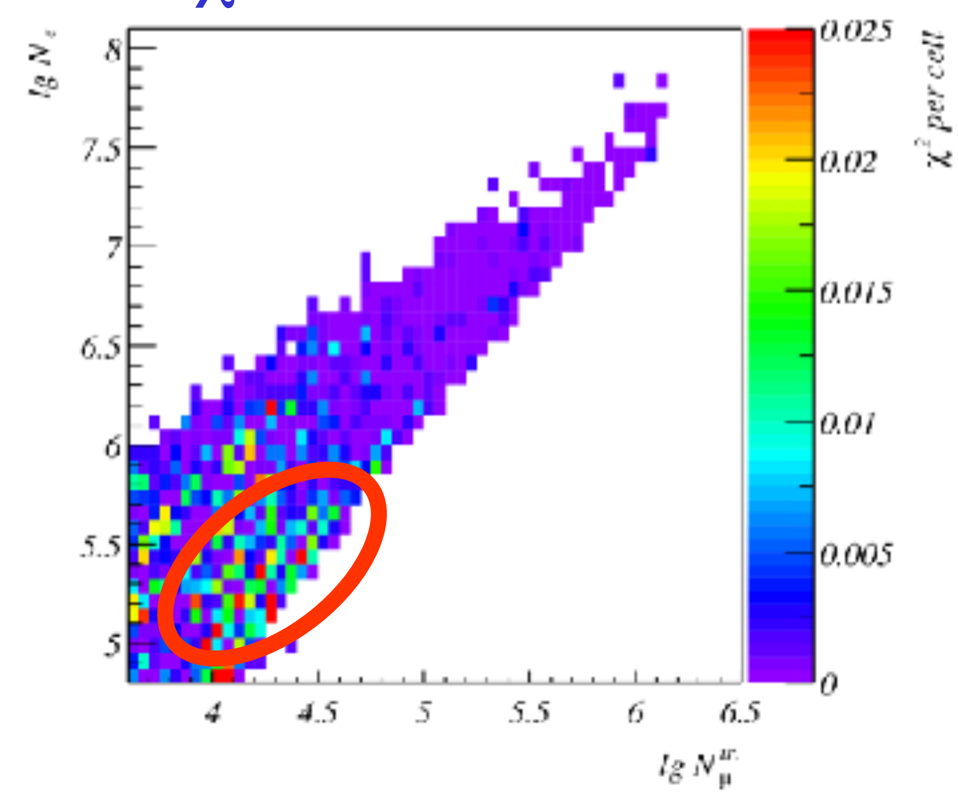

J. Milke et al, Proc. 29th Int. Cosmic Ray Conference Pune 6 (2005) 125

Test of hadronic interaction models

QGSJET 01

Number of hadrons vs. number of muons

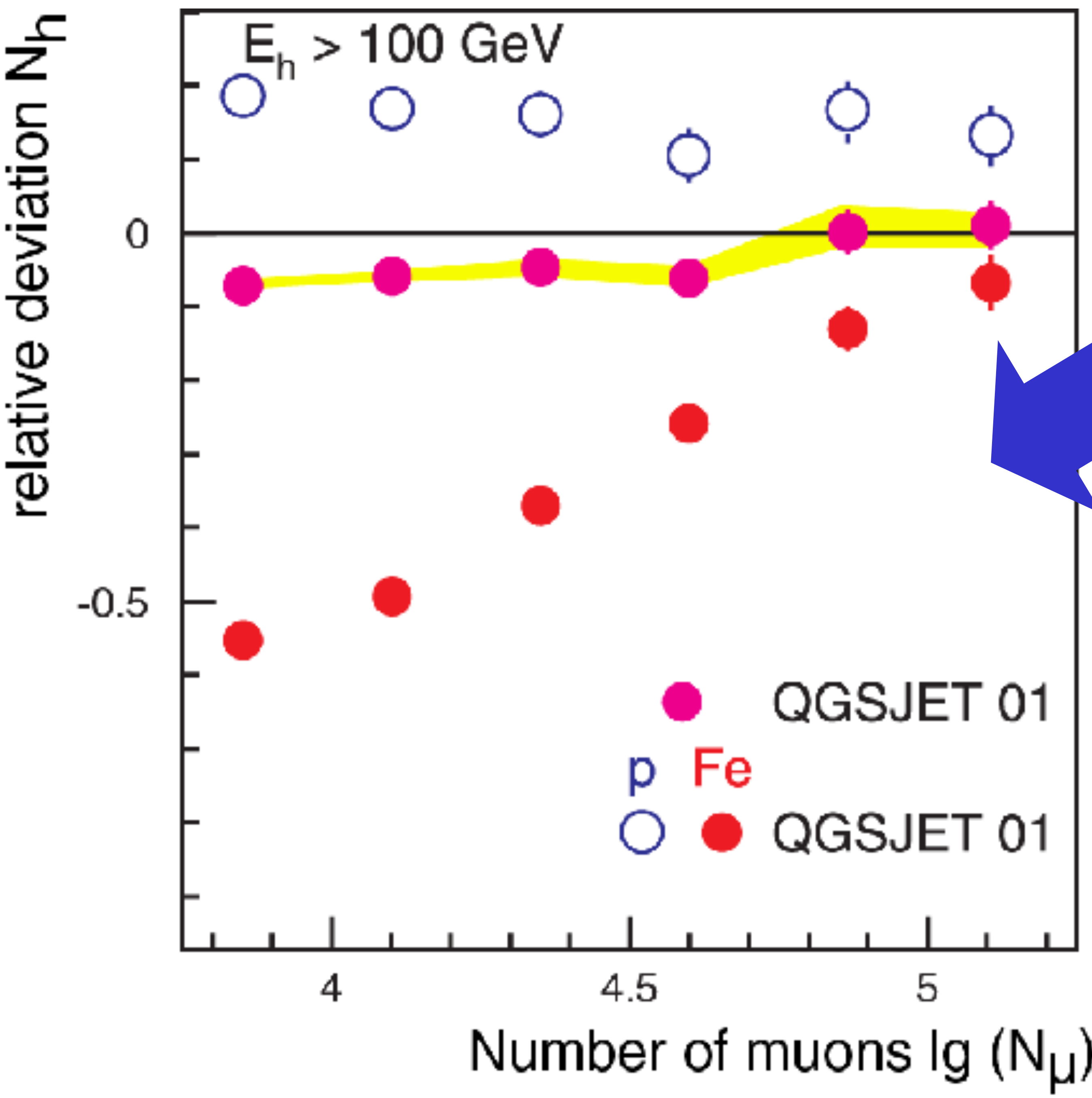

inconsistencies on 10% level

N_e-N_μ analysis

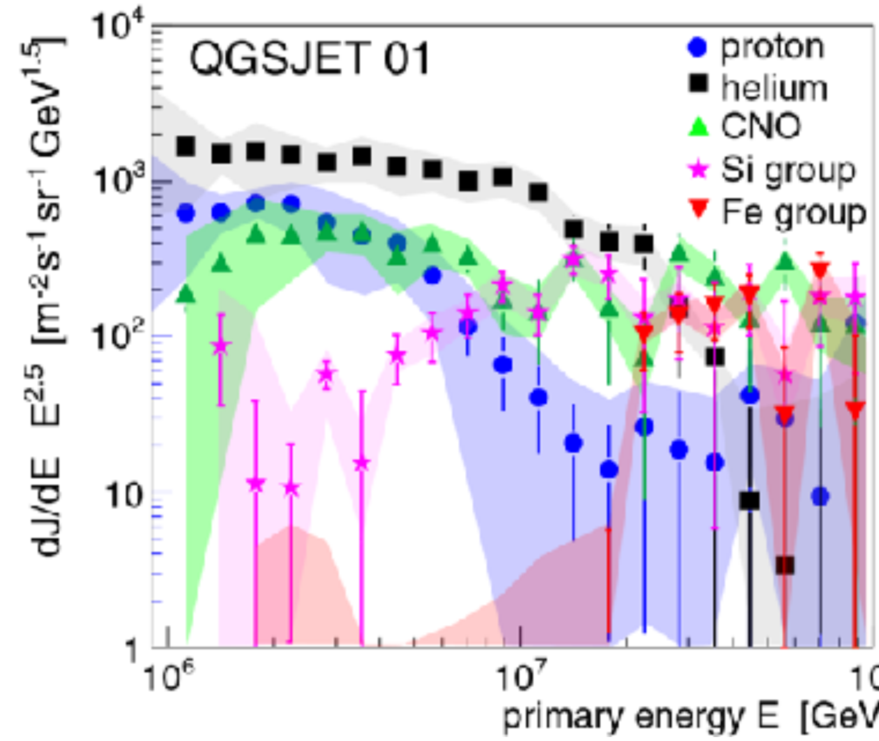

χ^2 distribution

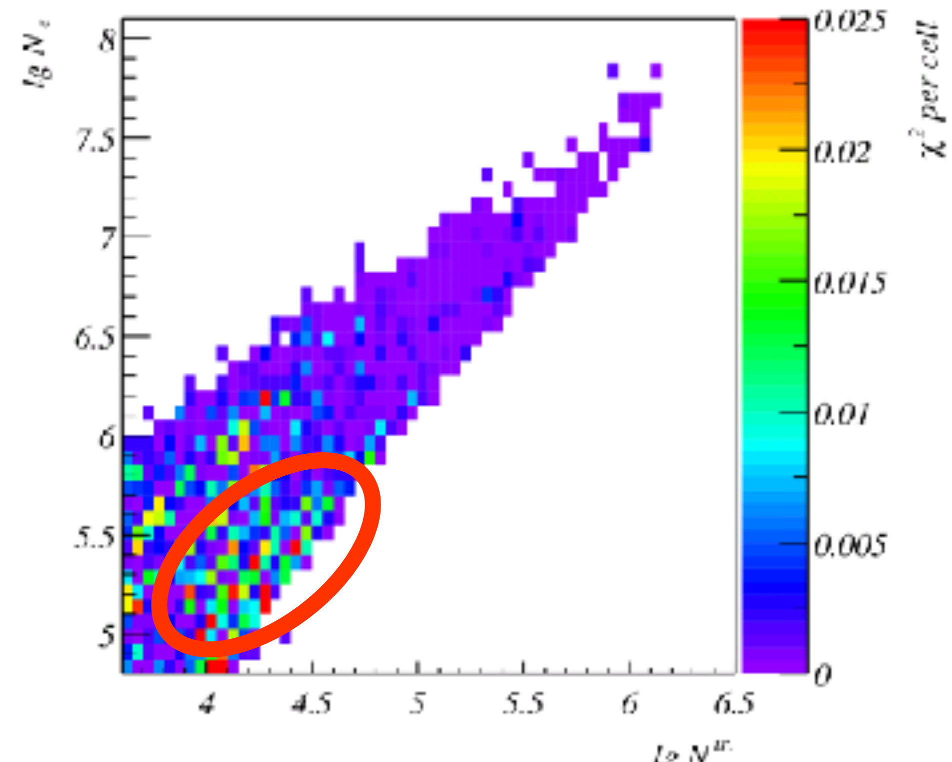

J. Milke et al, Proc. 29th Int. Cosmic Ray Conference Pune 6 (2005) 125

Test of hadronic interaction models

QGSJET 01

Number of hadrons vs. number of muons

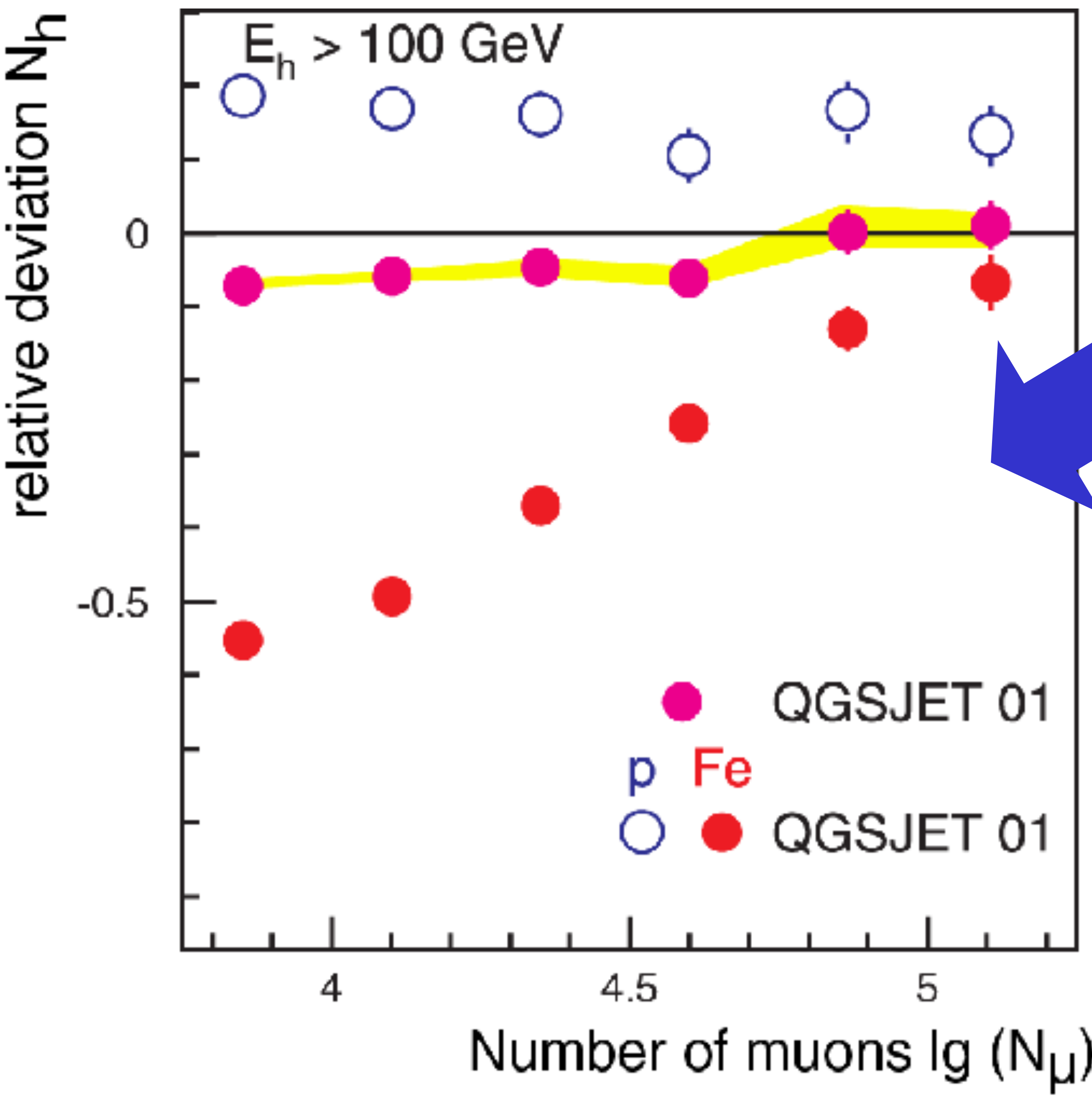

inconsistencies on 10% level

N_e-N_μ analysis

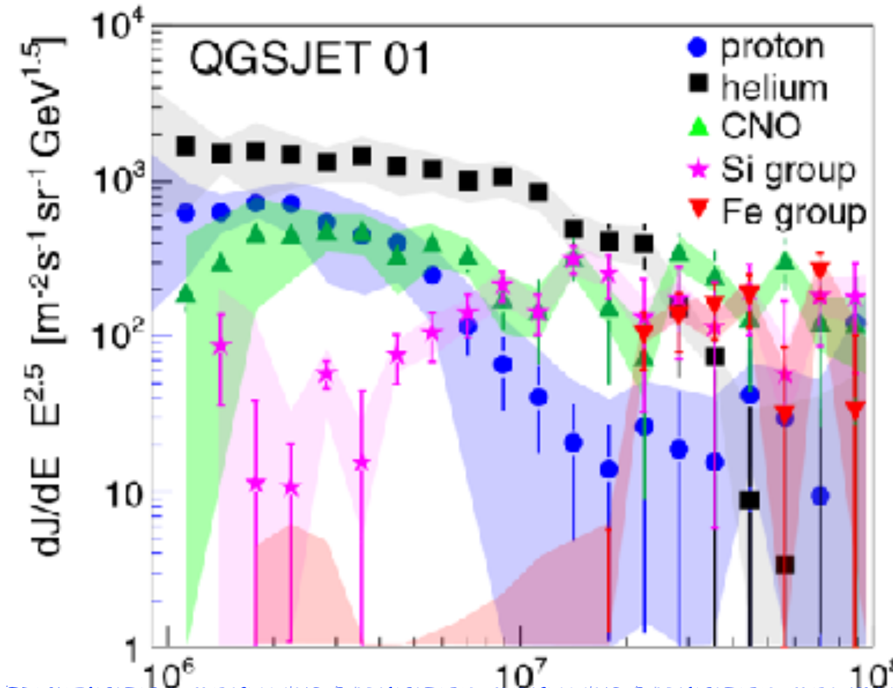

in literature:
ideas that knee is caused by new interactions in atmosphere —> energy is carried away by „invisible channels“

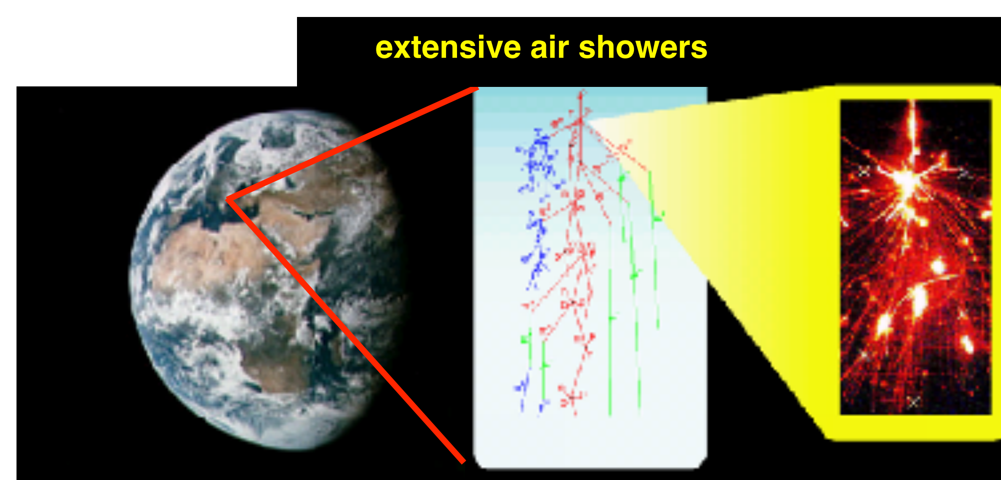

Test of hadronic interaction models

QGSJET 01

Number of hadrons vs. number of muons

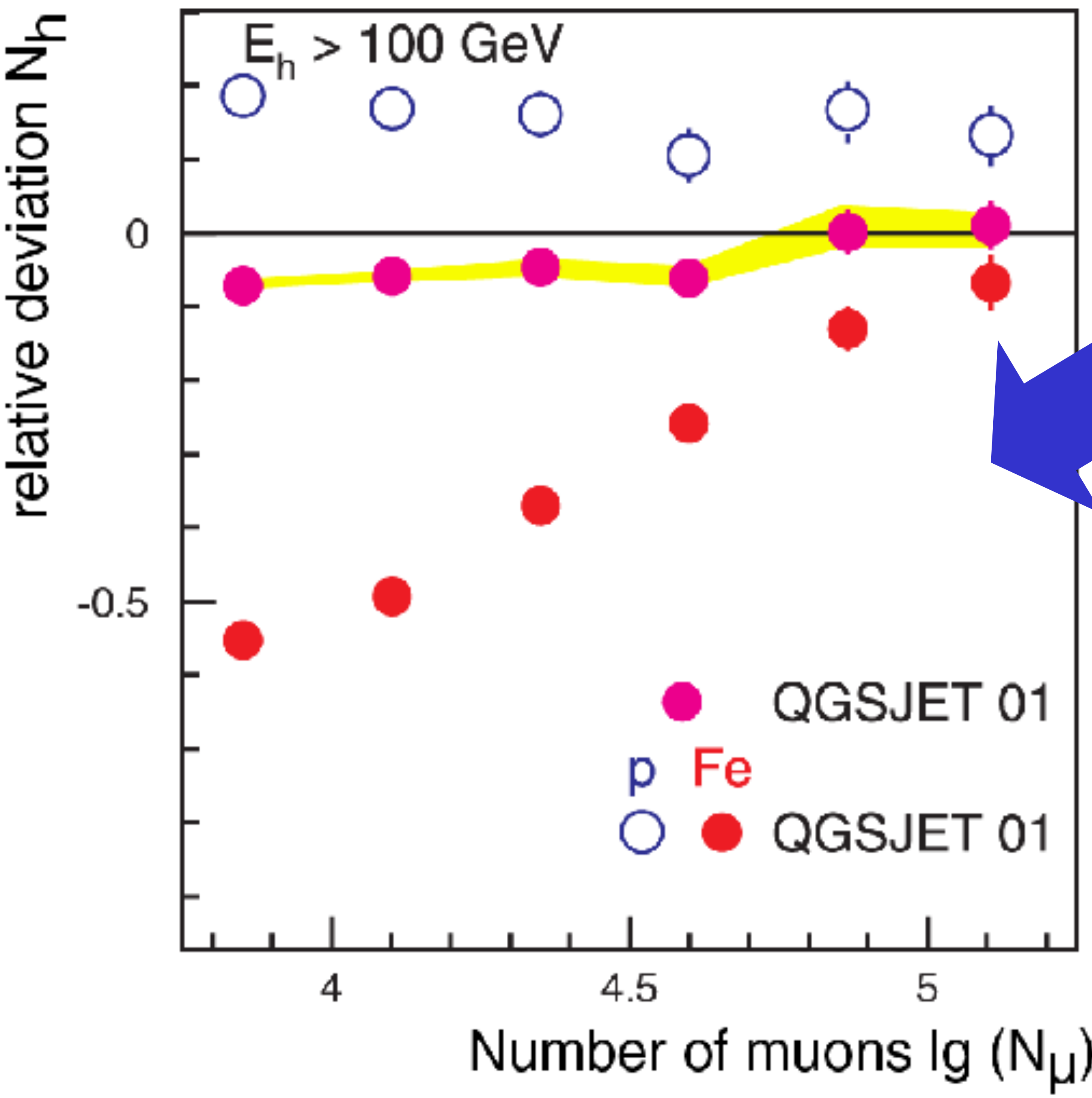

inconsistencies on 10% level

N_e-N_μ analysis

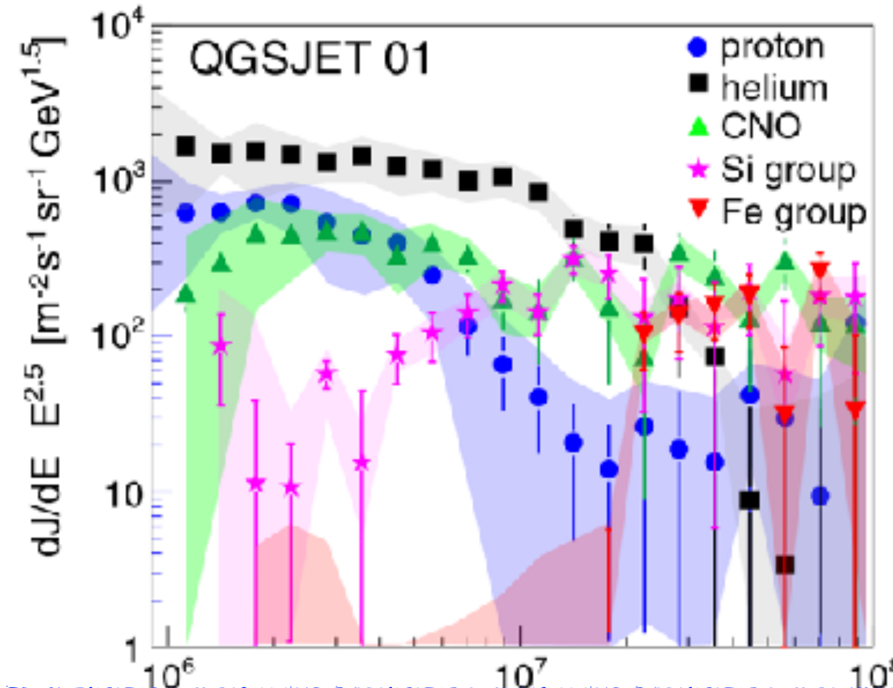

~~*in literature:*~~
~~**ideas that knee is caused by new interactions in atmosphere —> energy is carried away by „invisible channels"**~~

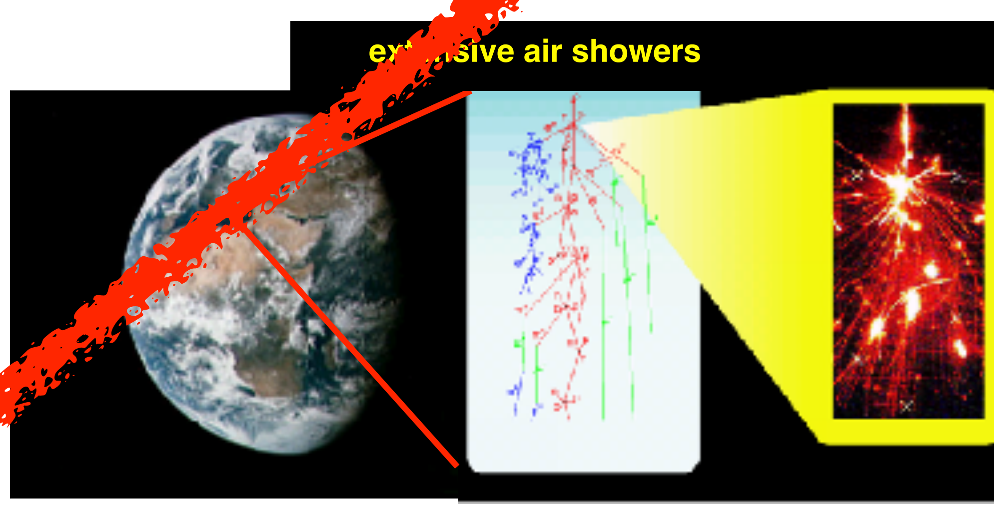

J. Milke et al, Proc. 29th Int. Cosmic Ray Conference Pune 6 (2005) 125

ELSEVIER

Nuclear Physics B (Proc. Suppl.) 75A (1999) 238–240

NUCLEAR PHYSICS B
PROCEEDINGS
SUPPLEMENTS

Electron, muon and hadron size spectra of EAS in the "knee" region

R. Glasstetter[a] and J.R. Hörandel[a] for the KASCADE Collaboration*

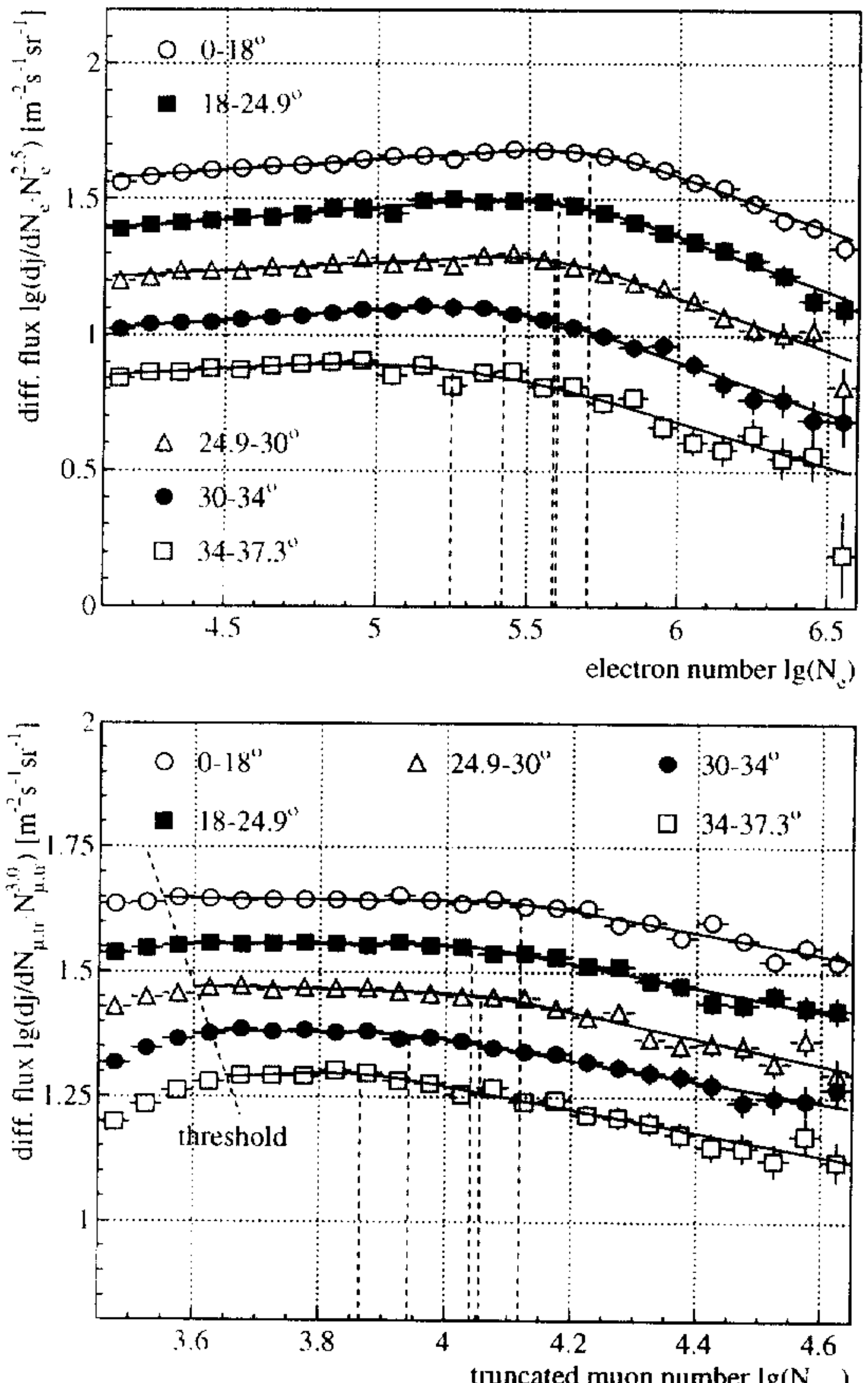

Figure 1. Electromagnetic (top) and muonic (bottom) shower size spectra for different zenith angle bins.

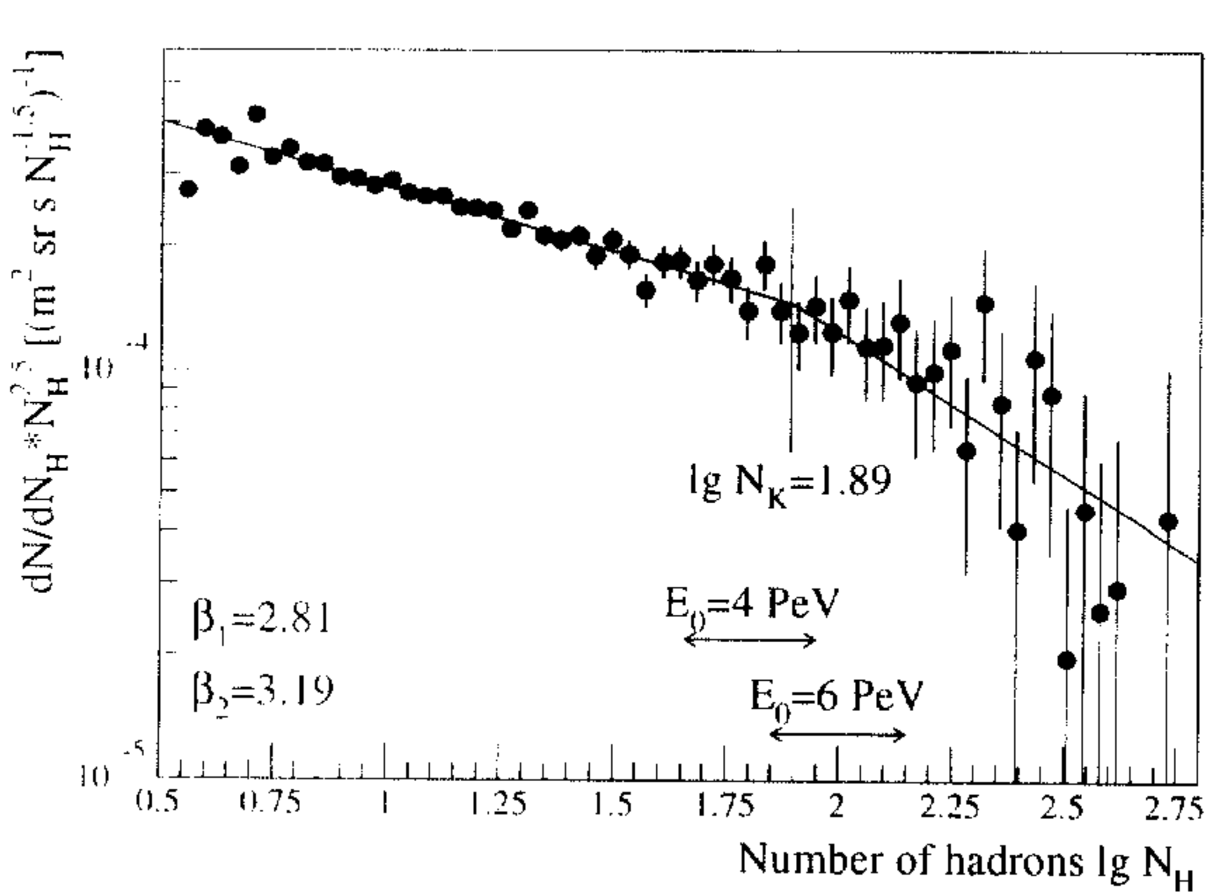

Figure 3. Hadronic shower size spectrum.

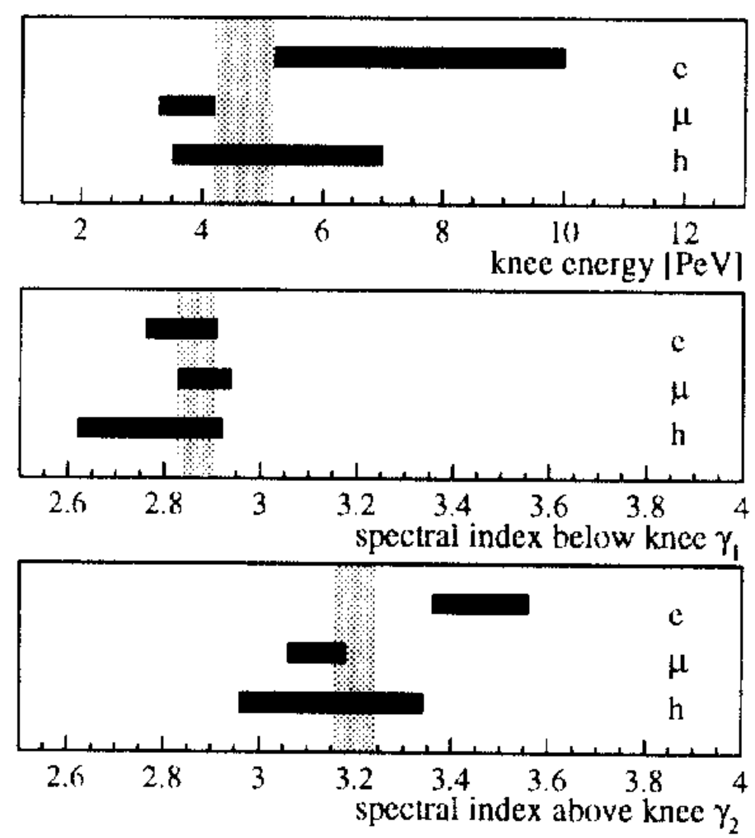

Figure 4. Knee position and spectral indices.

knee observed in all components, electromagnetic, muonic, and hadronic!

KASCADE-Grande

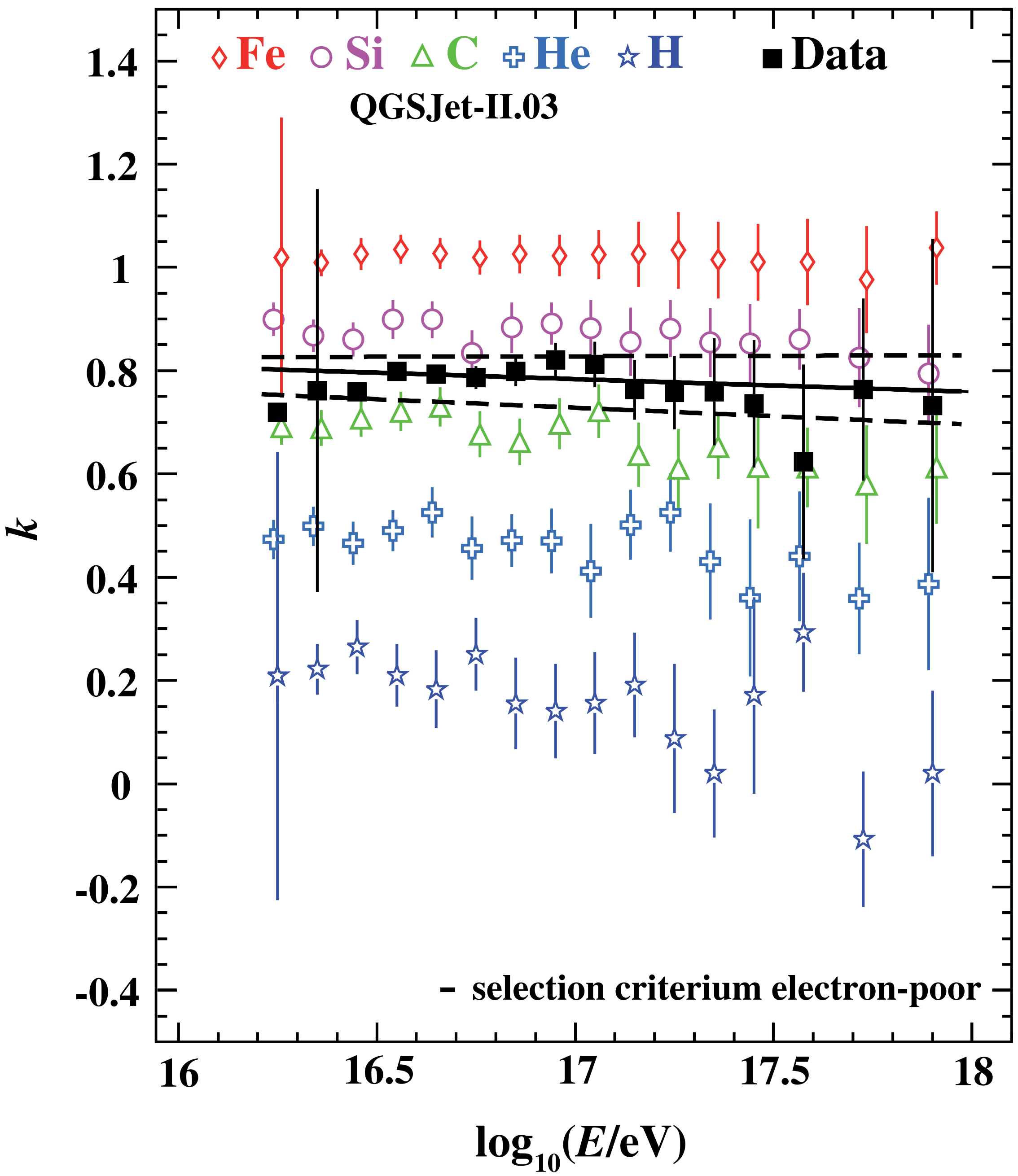

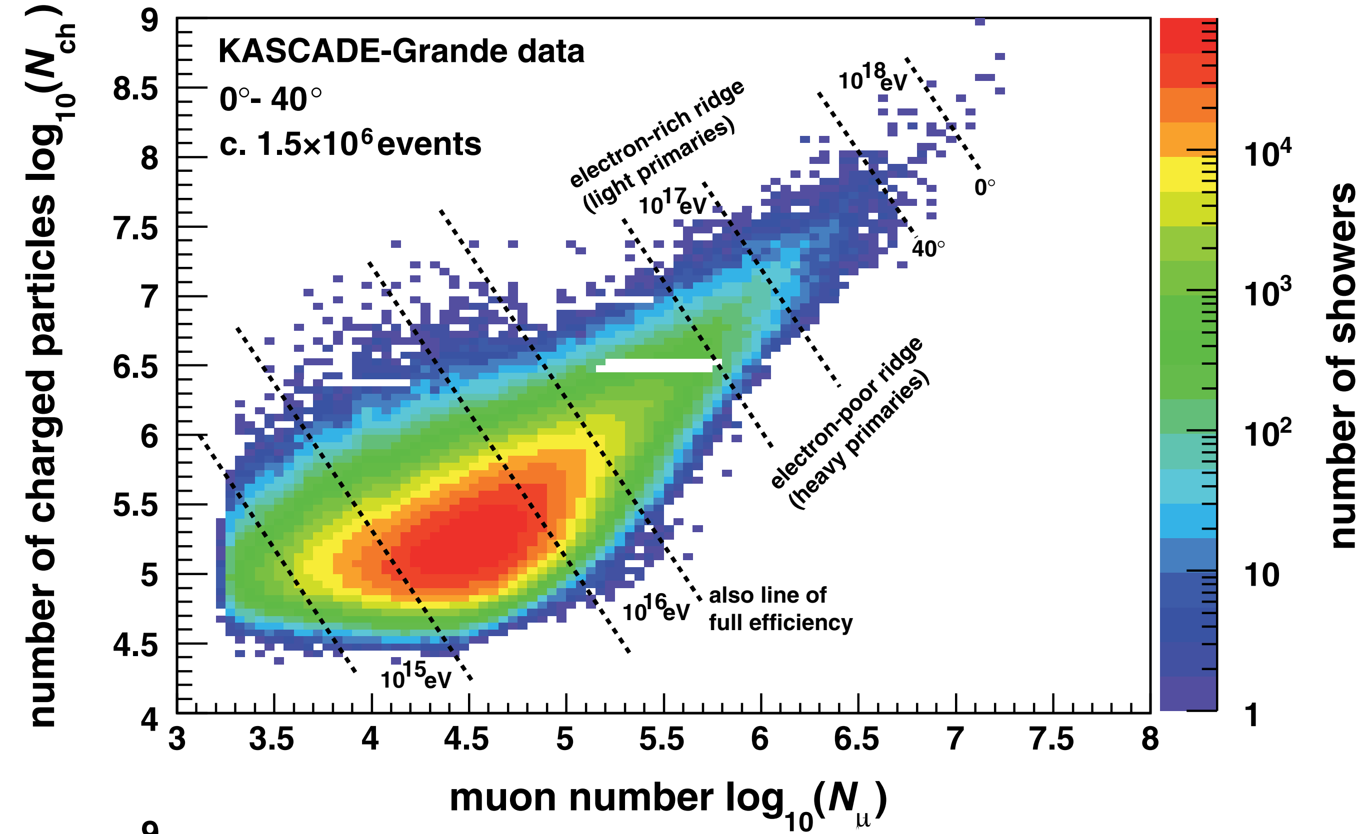

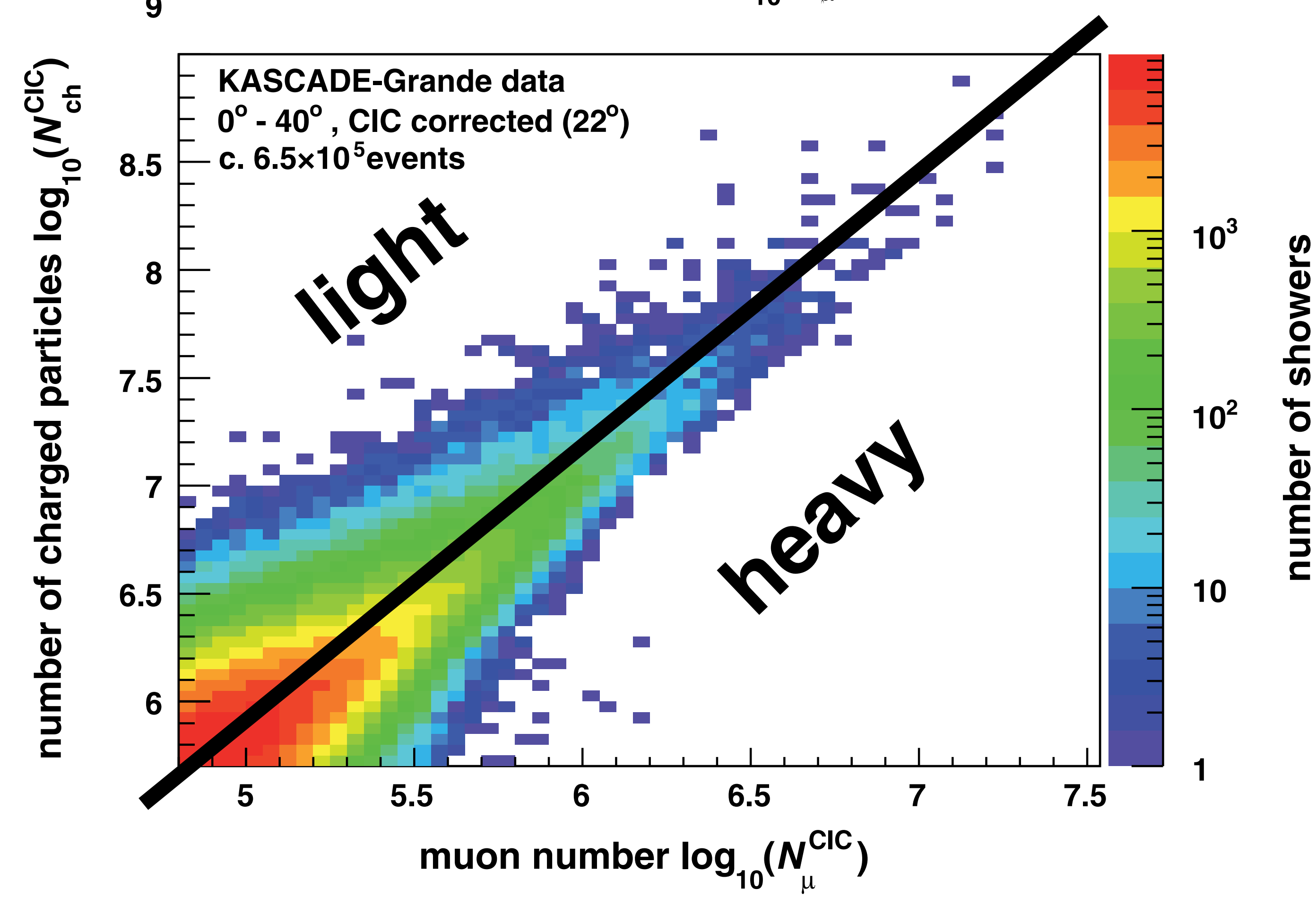

$$k = \frac{\log_{10}(N_{\rm ch}/N_\mu) - \log_{10}(N_{\rm ch}/N_\mu)_{\rm H}}{\log_{10}(N_{\rm ch}/N_\mu)_{\rm Fe} - \log_{10}(N_{\rm ch}/N_\mu)_{\rm H}},$$

W.D. Apel et al., PRL 107 (2011) 171104

KASCADE-Grande

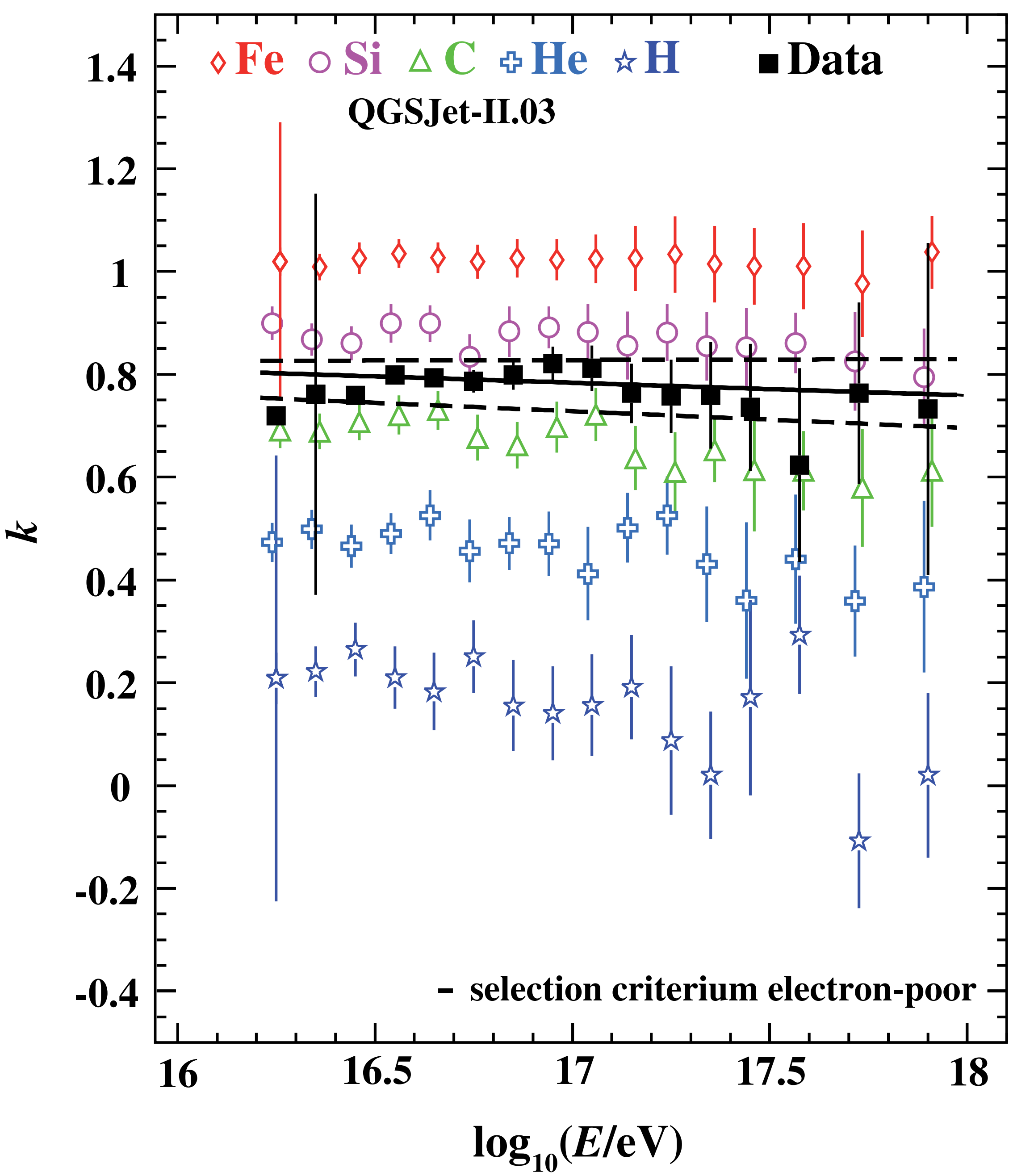

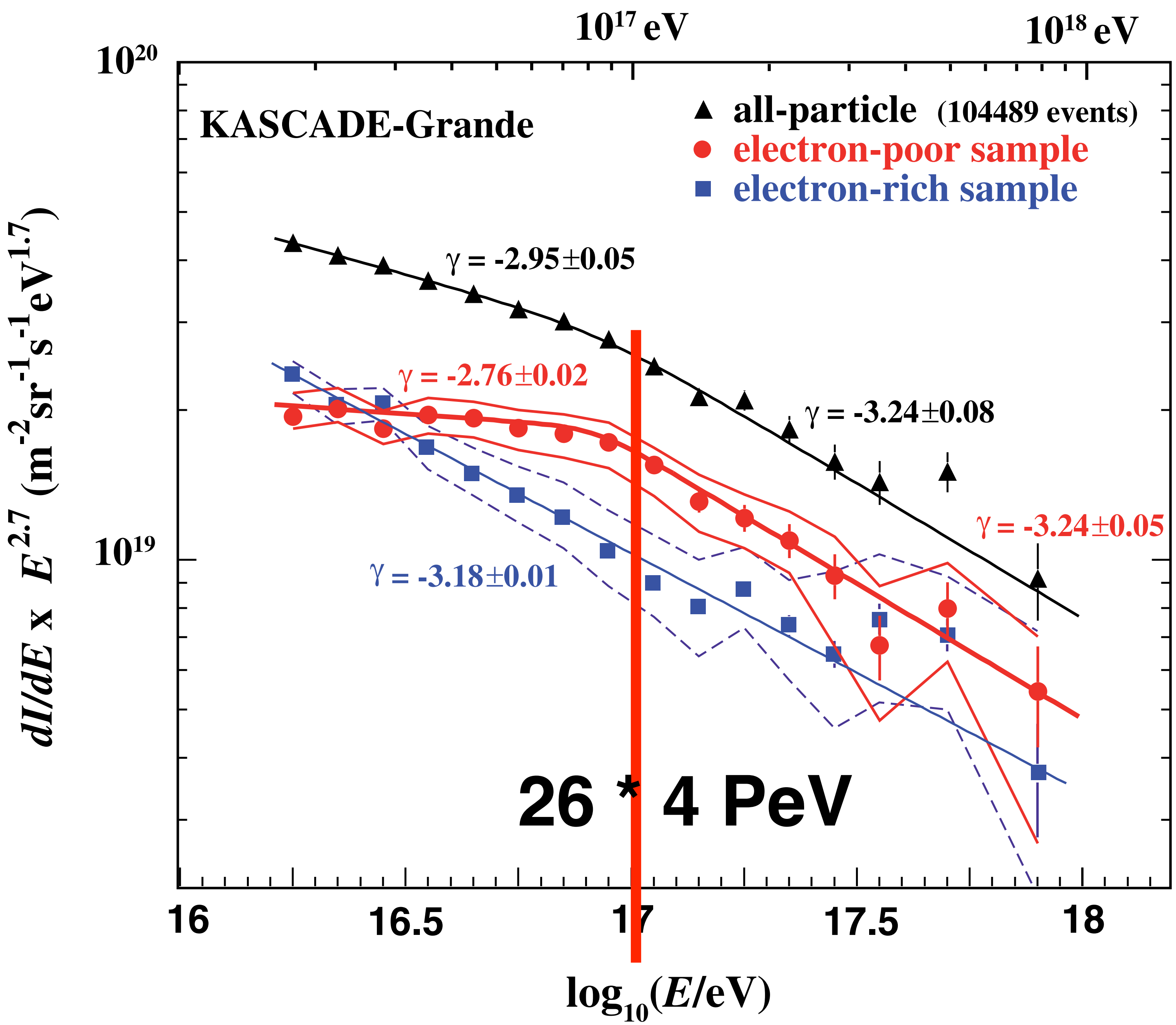

$$k = \frac{\log_{10}(N_{\mathrm{ch}}/N_\mu) - \log_{10}(N_{\mathrm{ch}}/N_\mu)_{\mathrm{H}}}{\log_{10}(N_{\mathrm{ch}}/N_\mu)_{\mathrm{Fe}} - \log_{10}(N_{\mathrm{ch}}/N_\mu)_{\mathrm{H}}},$$

W.D. Apel et al., PRL 107 (2011) 171104

KASCADE-Grande

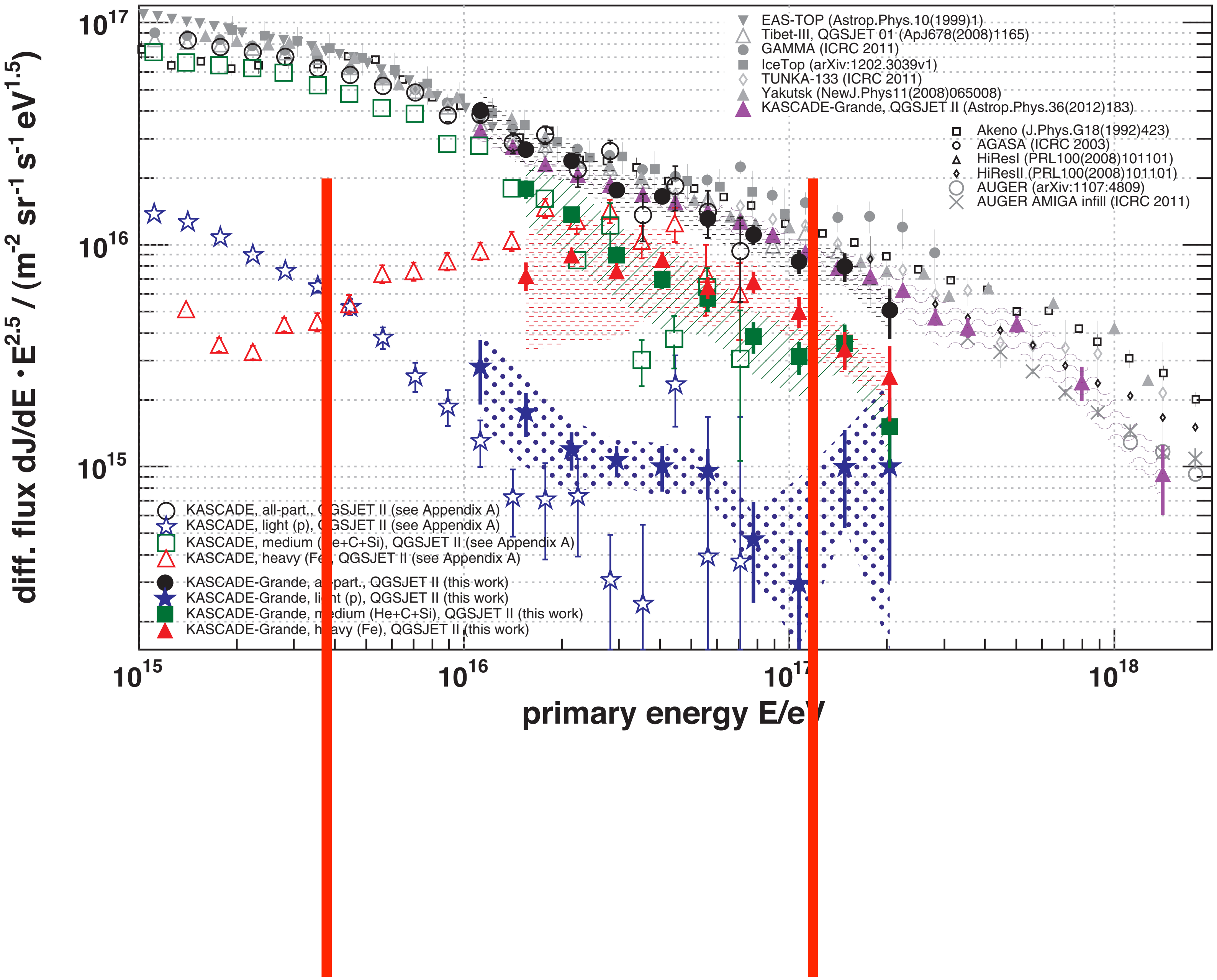

knee 4 PeV **26 * 4 PeV**

W.D. Apel et al., Astropart. Phys 47 (2013) 54

KASCADE-Grande

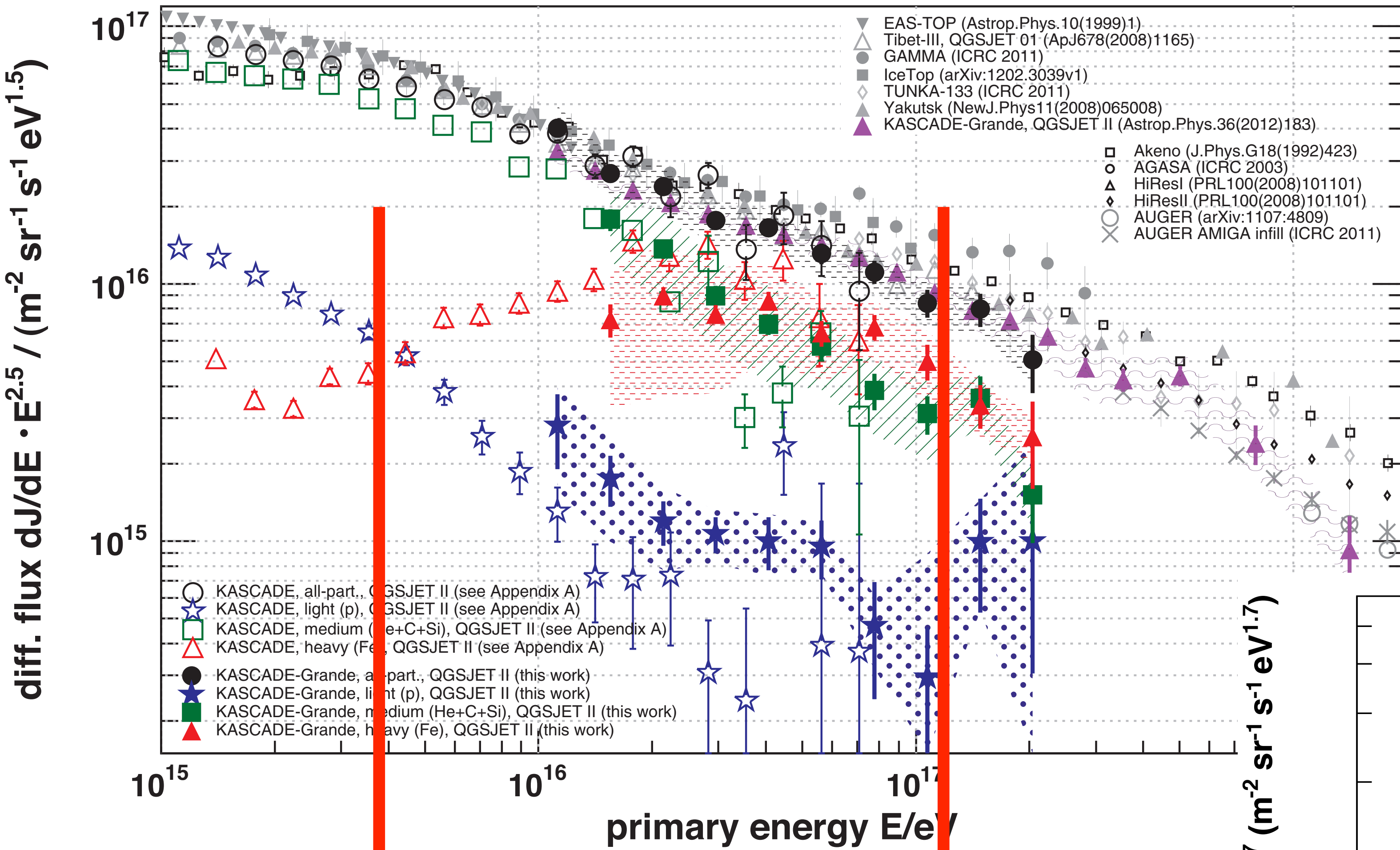

knee 4 PeV   26 * 4 PeV

26 * 4 PeV

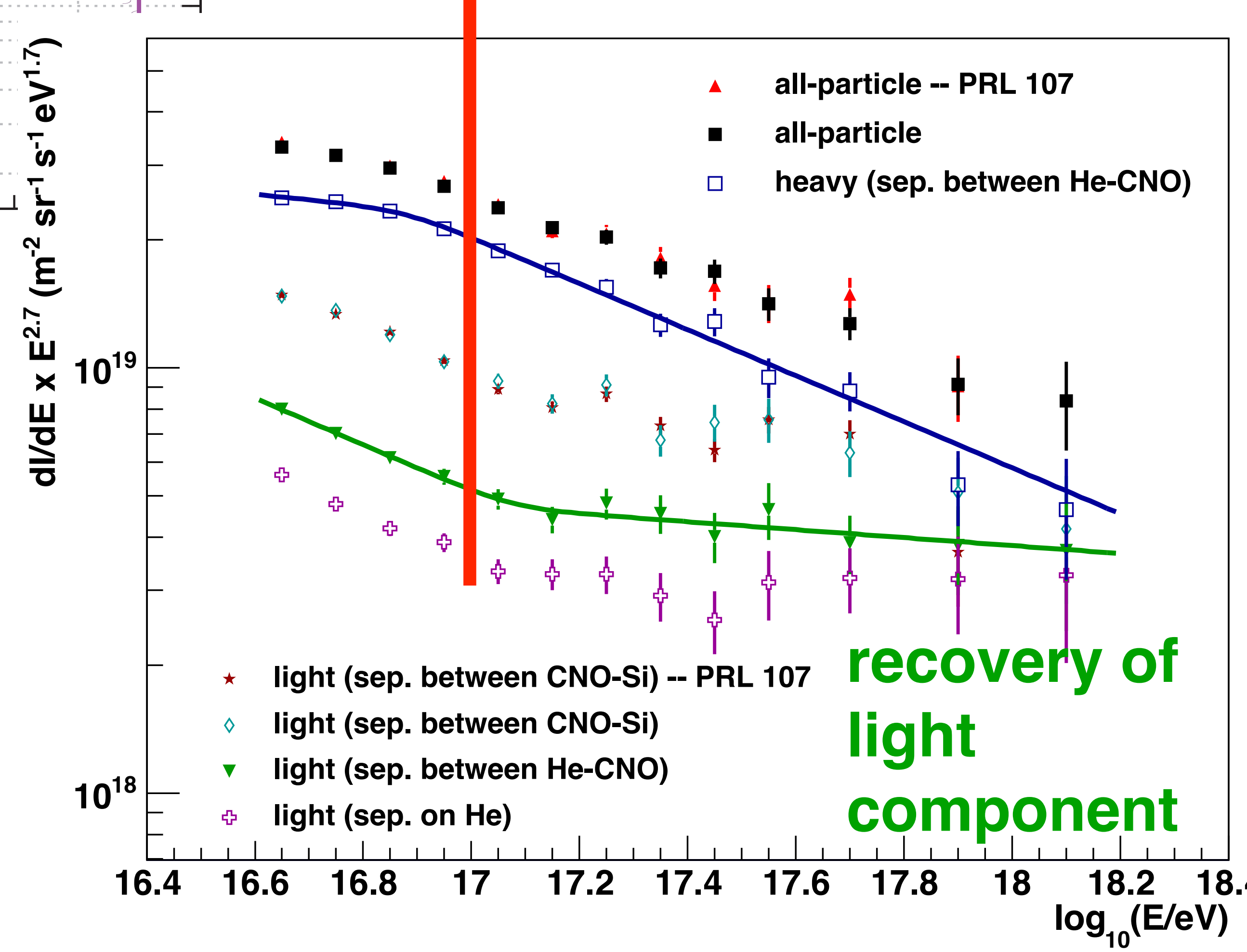

W.D. Apel et al., Astropart. Phys 47 (2013) 54

W.D. Apel et al., PRD 87 (2013) 081101

Ice Cube - Ice Top

e/m (+μ)

IceTop

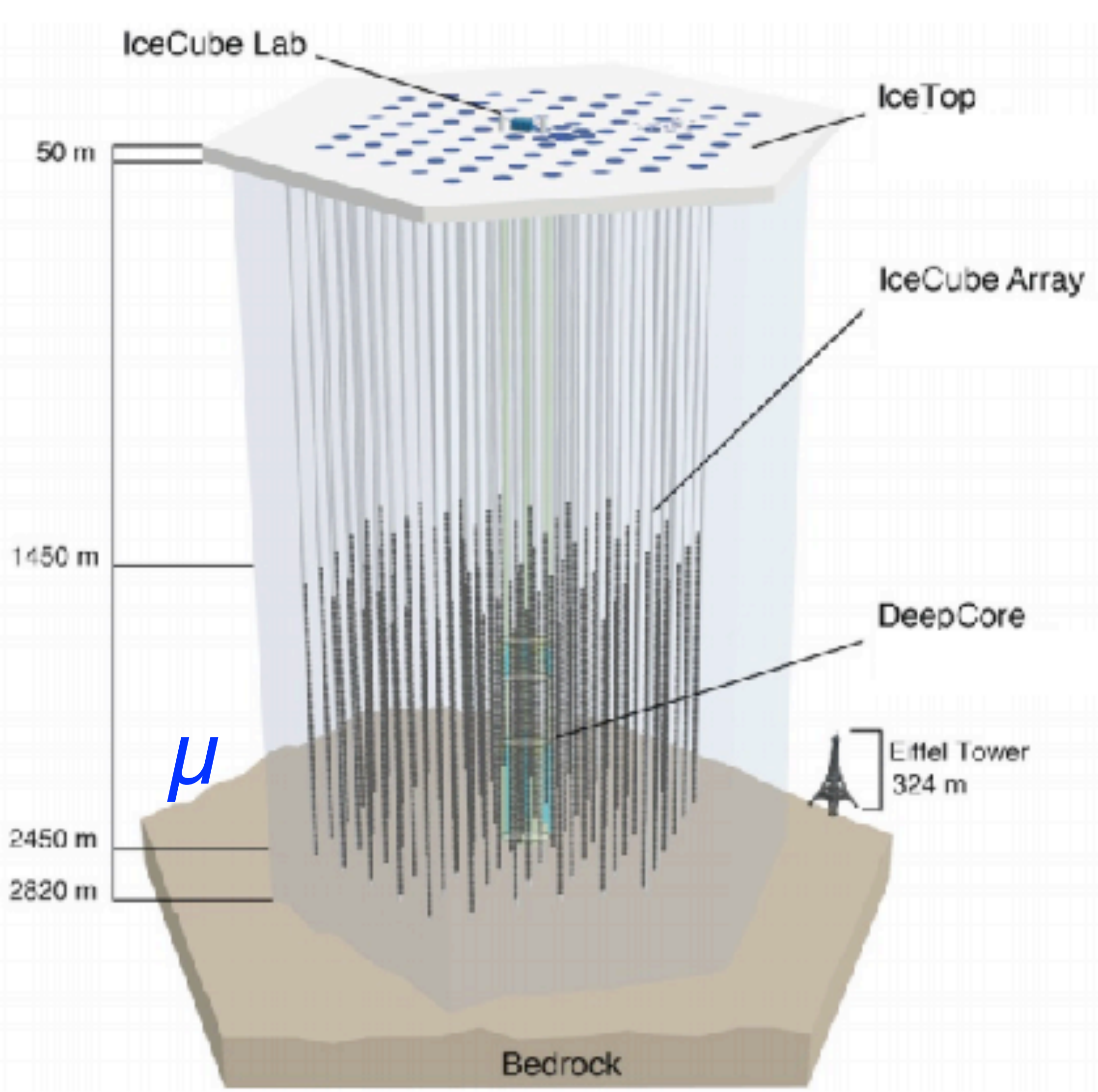

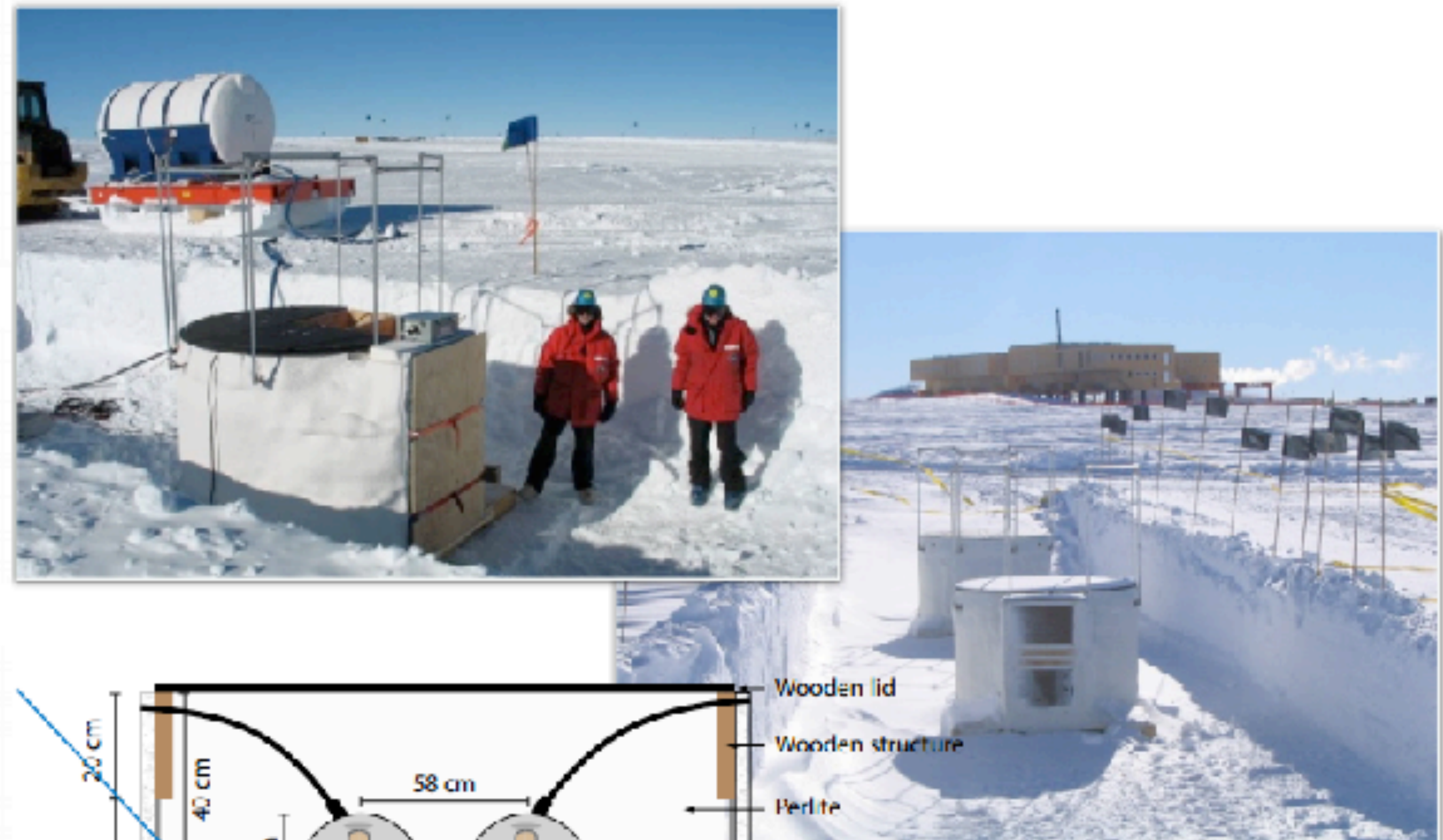

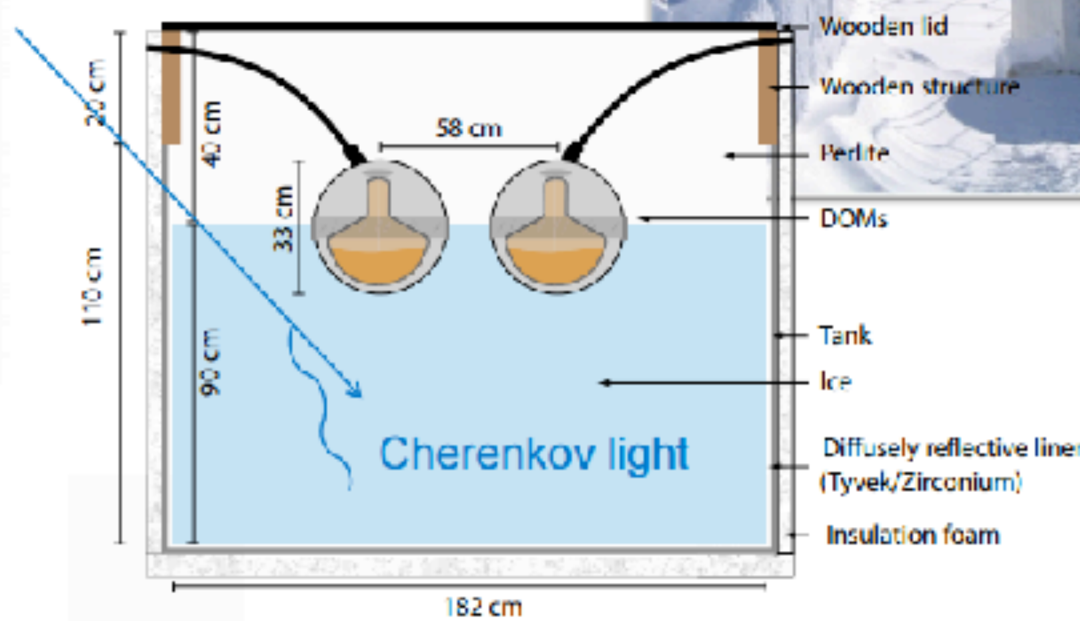

Ice Cube - Ice Top

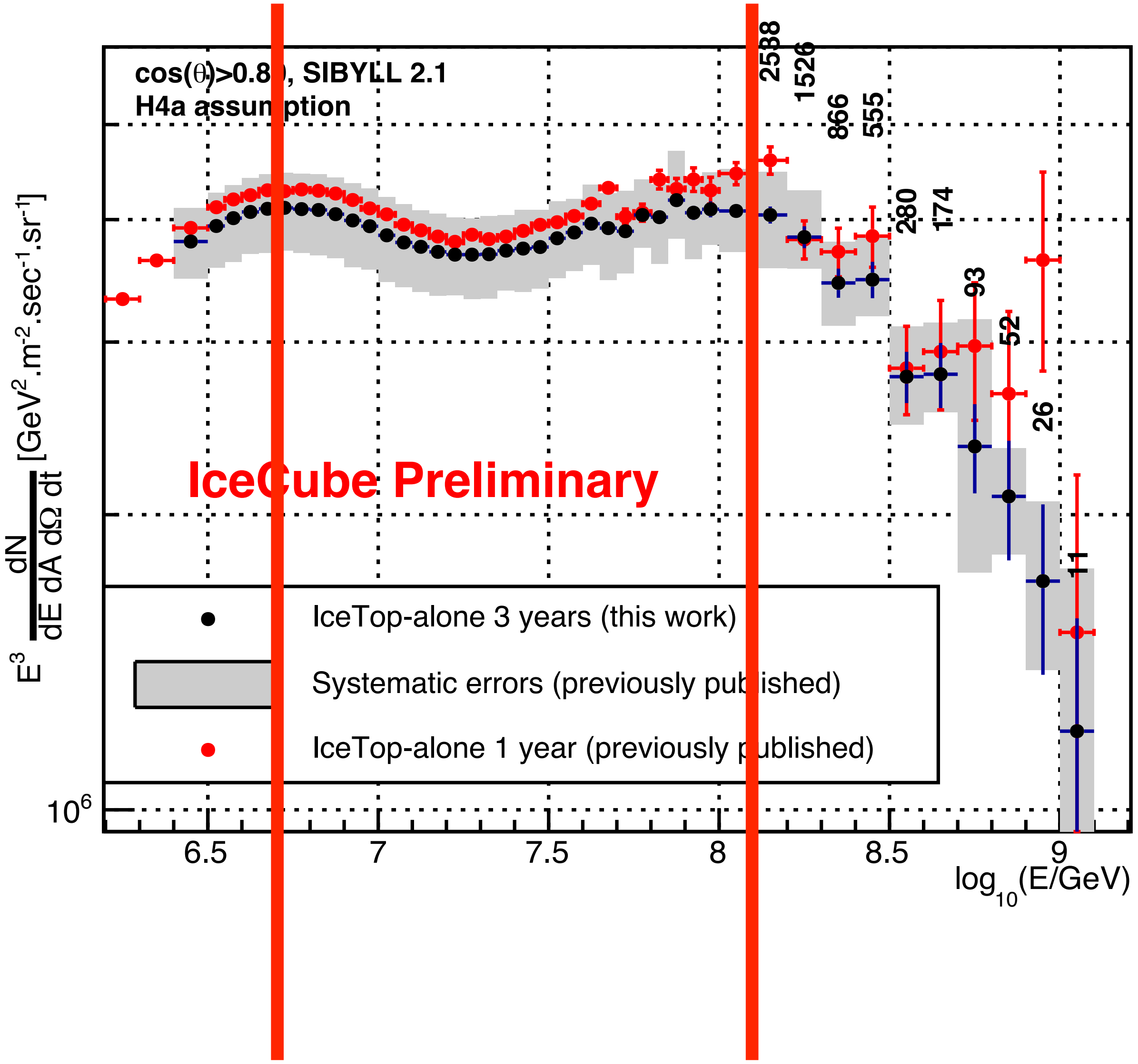

Ice Top only

K. Rawlins J Phys Conf. Ser. 718 (2016) 052033

Ice Cube - Ice Top

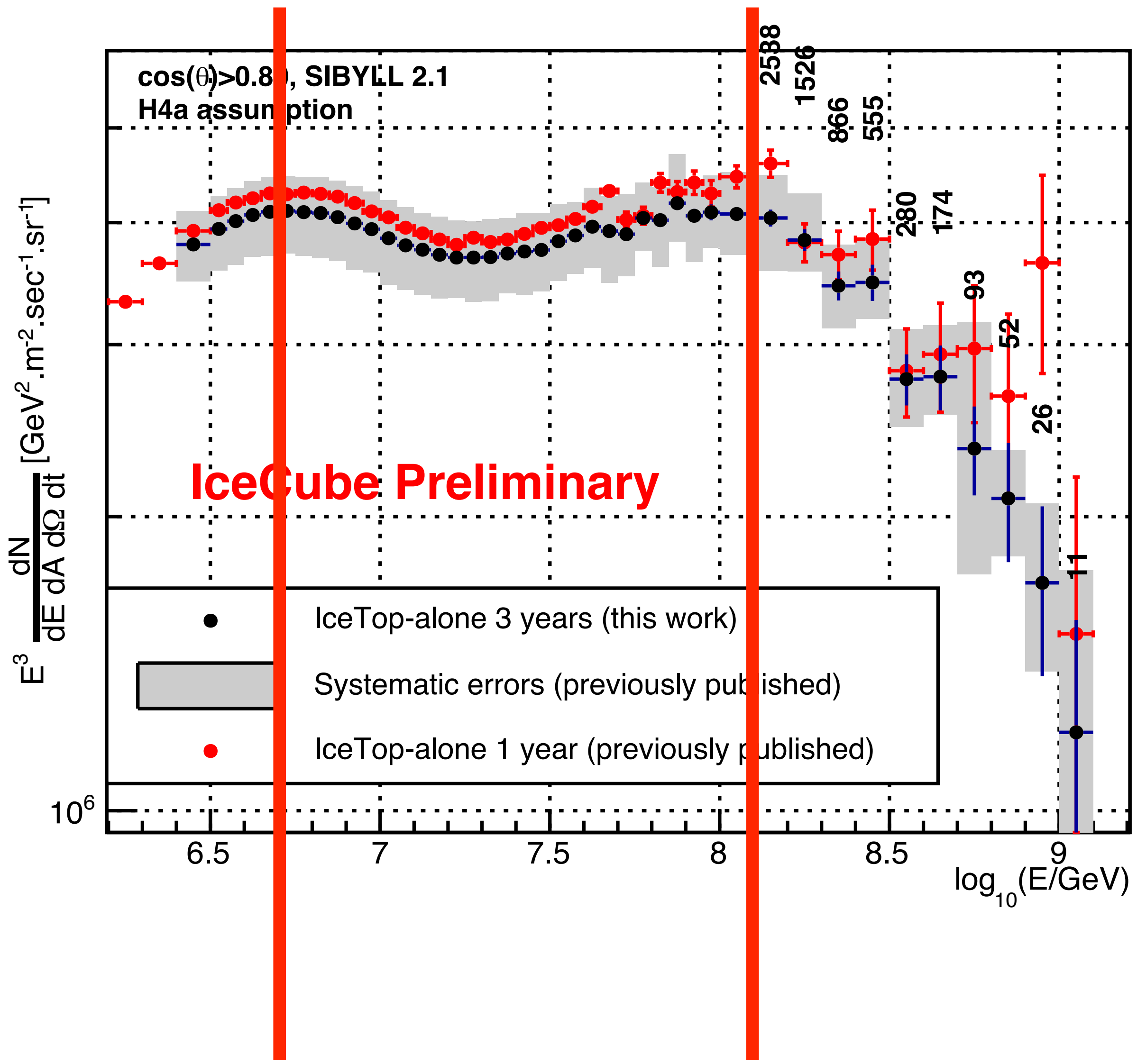

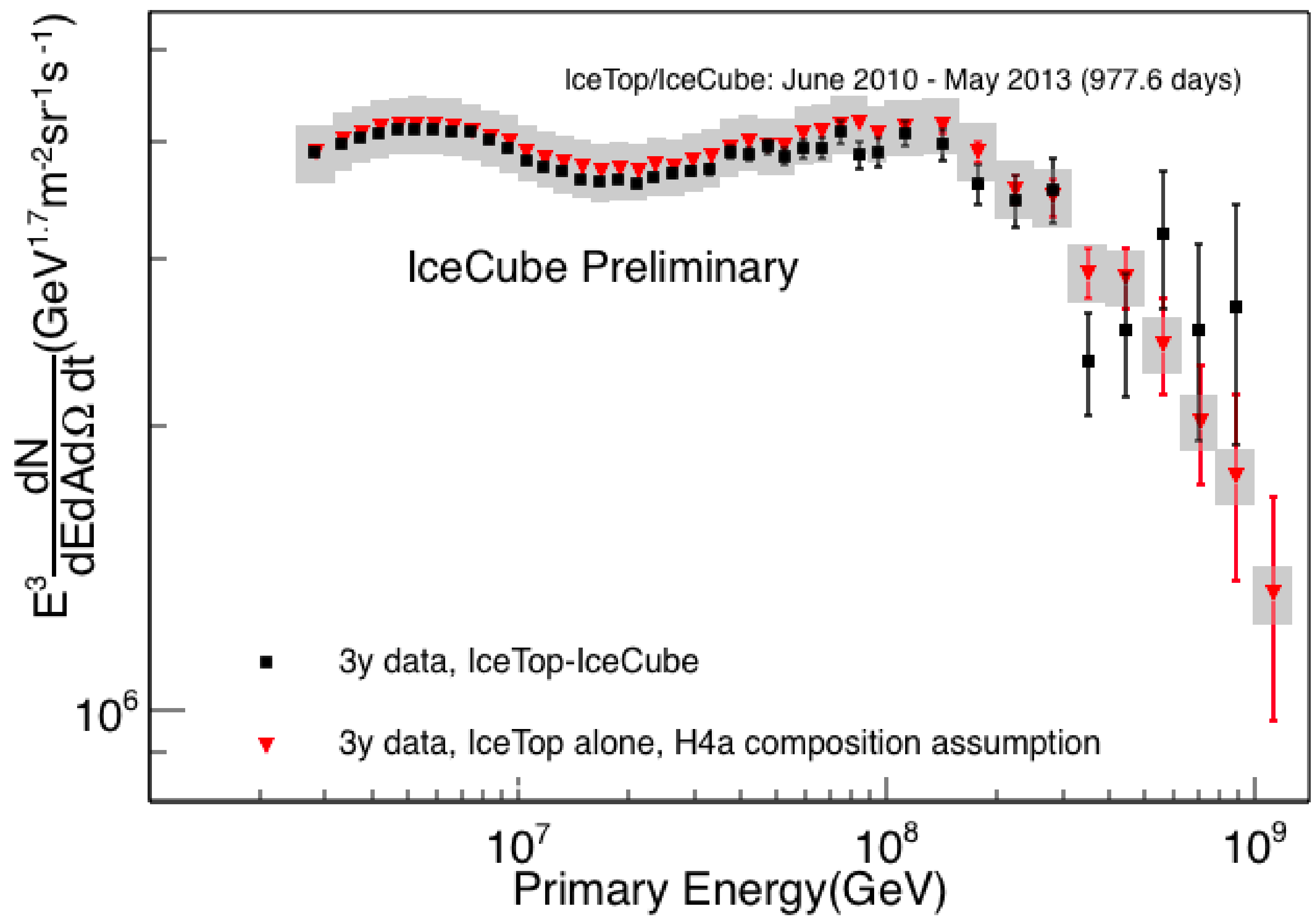

5 PeV **26*5 PeV**

Ice Top only **combined**

K. Rawlins J Phys Conf. Ser. 718 (2016) 052033

Ice Cube - Ice Top

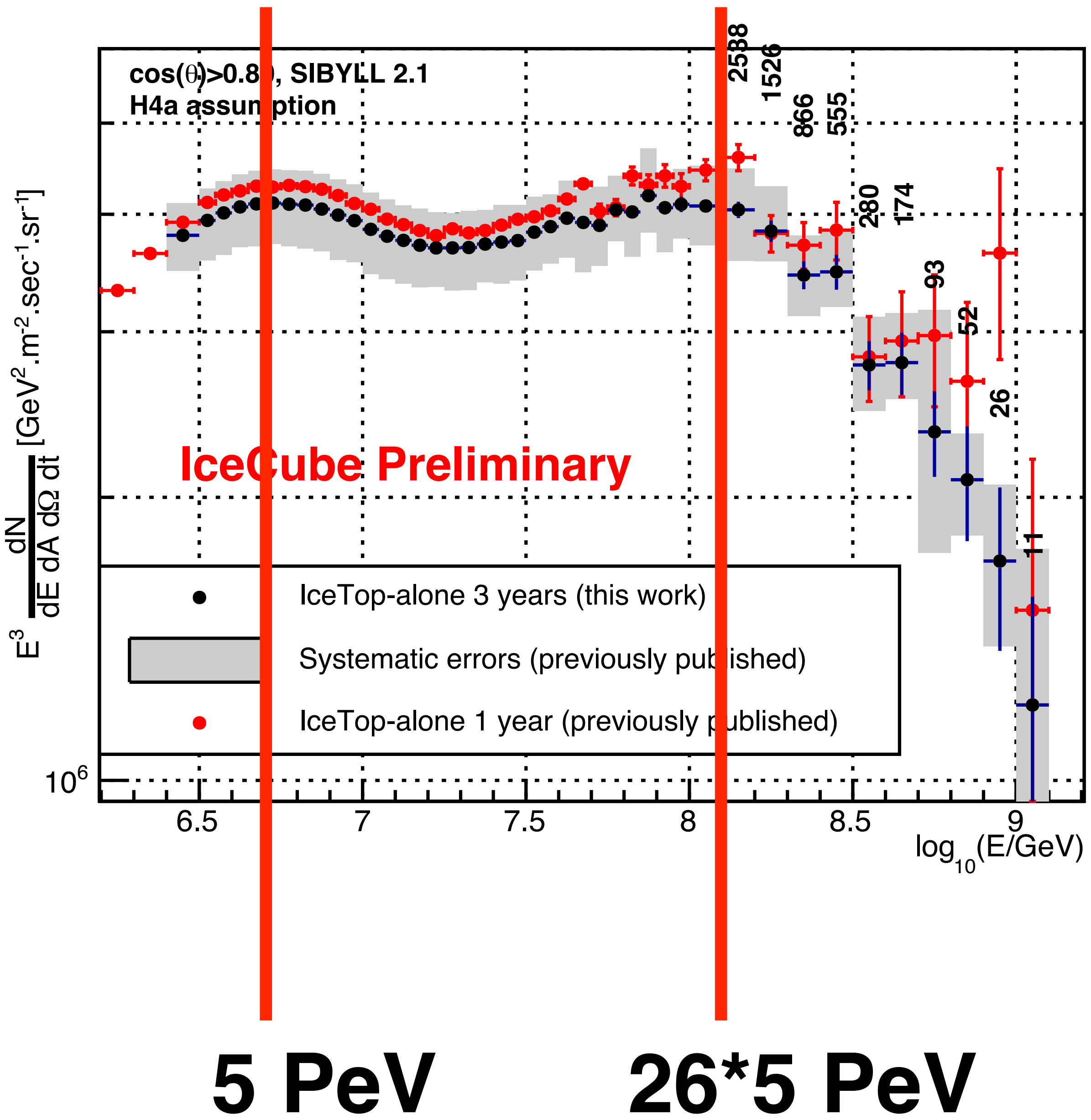

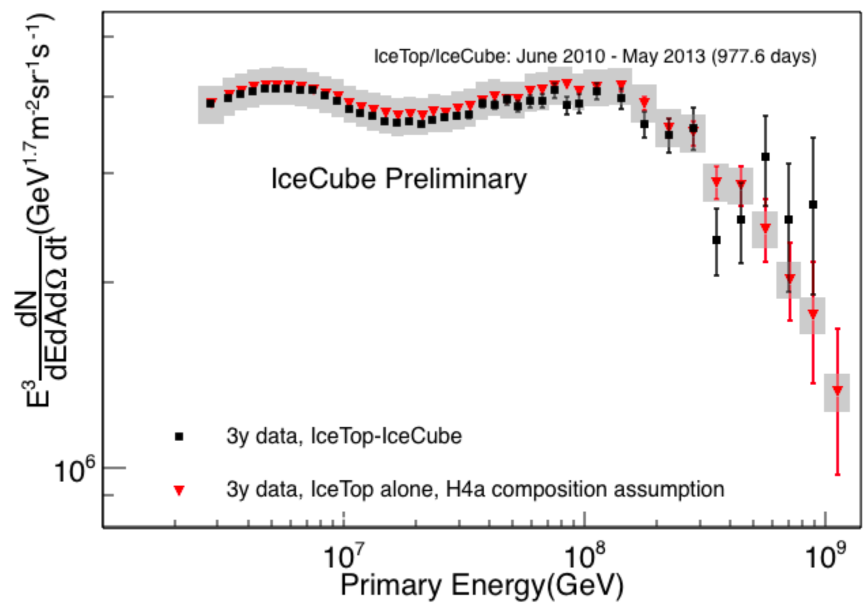

Ice Top only

combined

K. Rawlins J Phys Conf. Ser. 718 (2016) 052033

Ice Cube - Ice Top

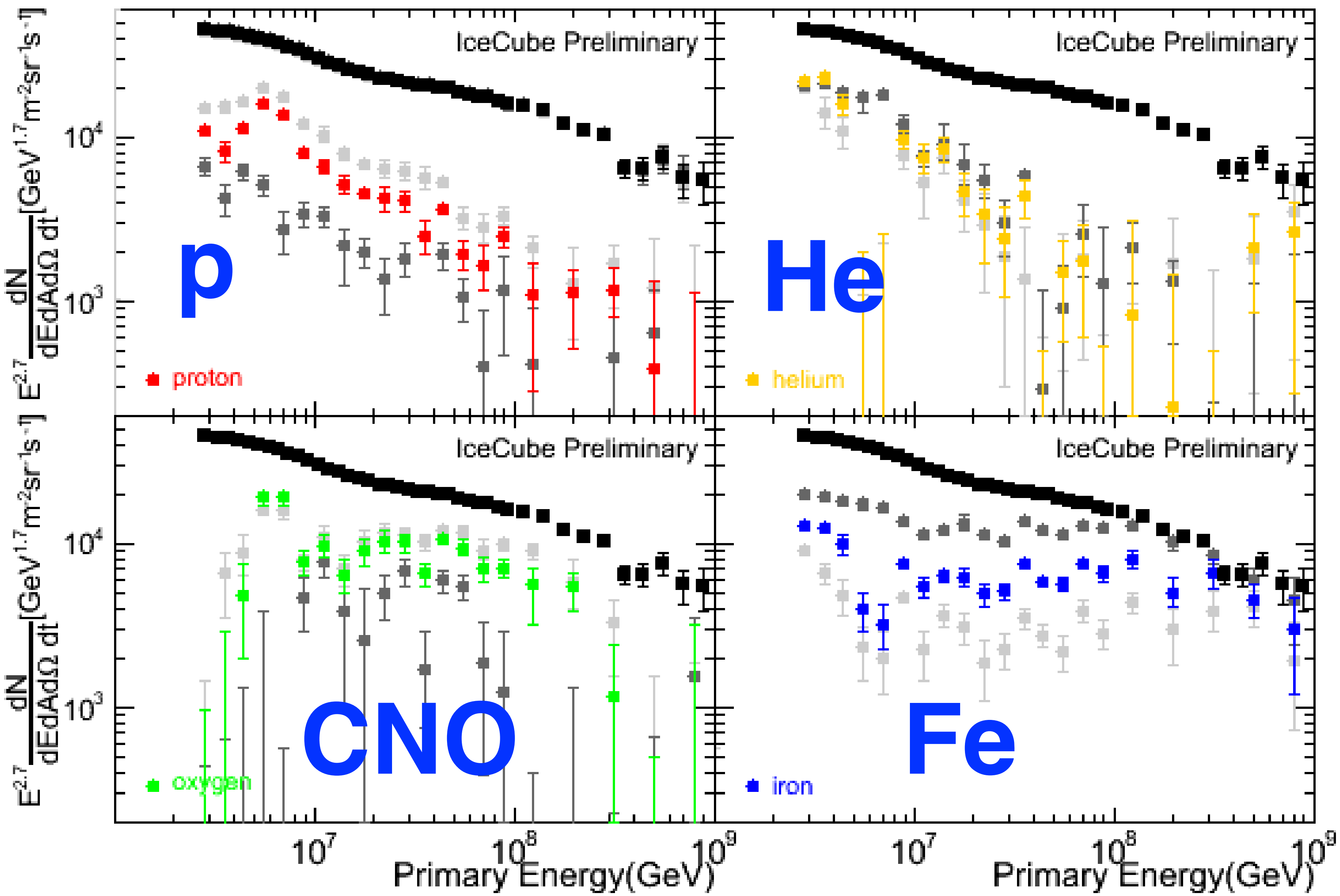

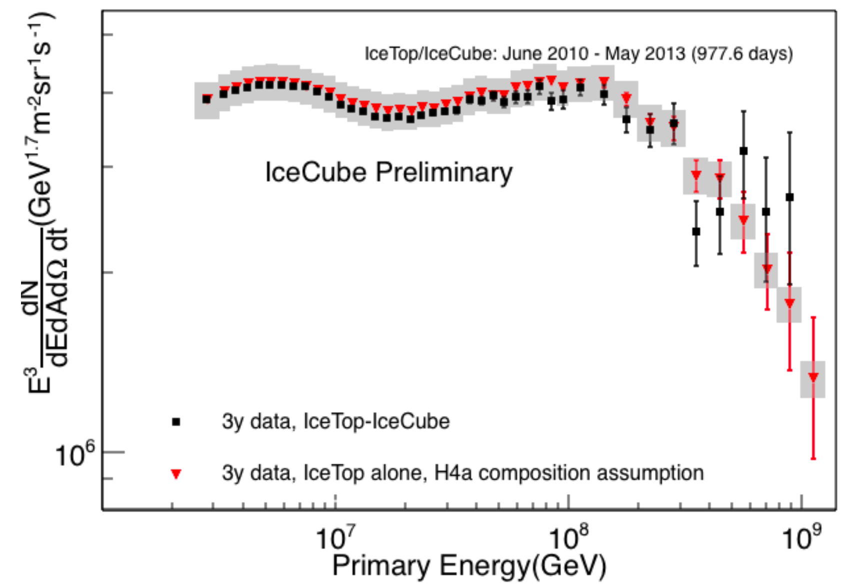

K. Rawlins J Phys Conf. Ser. 718 (2016) 052033

Cosmic-ray energy spectrum

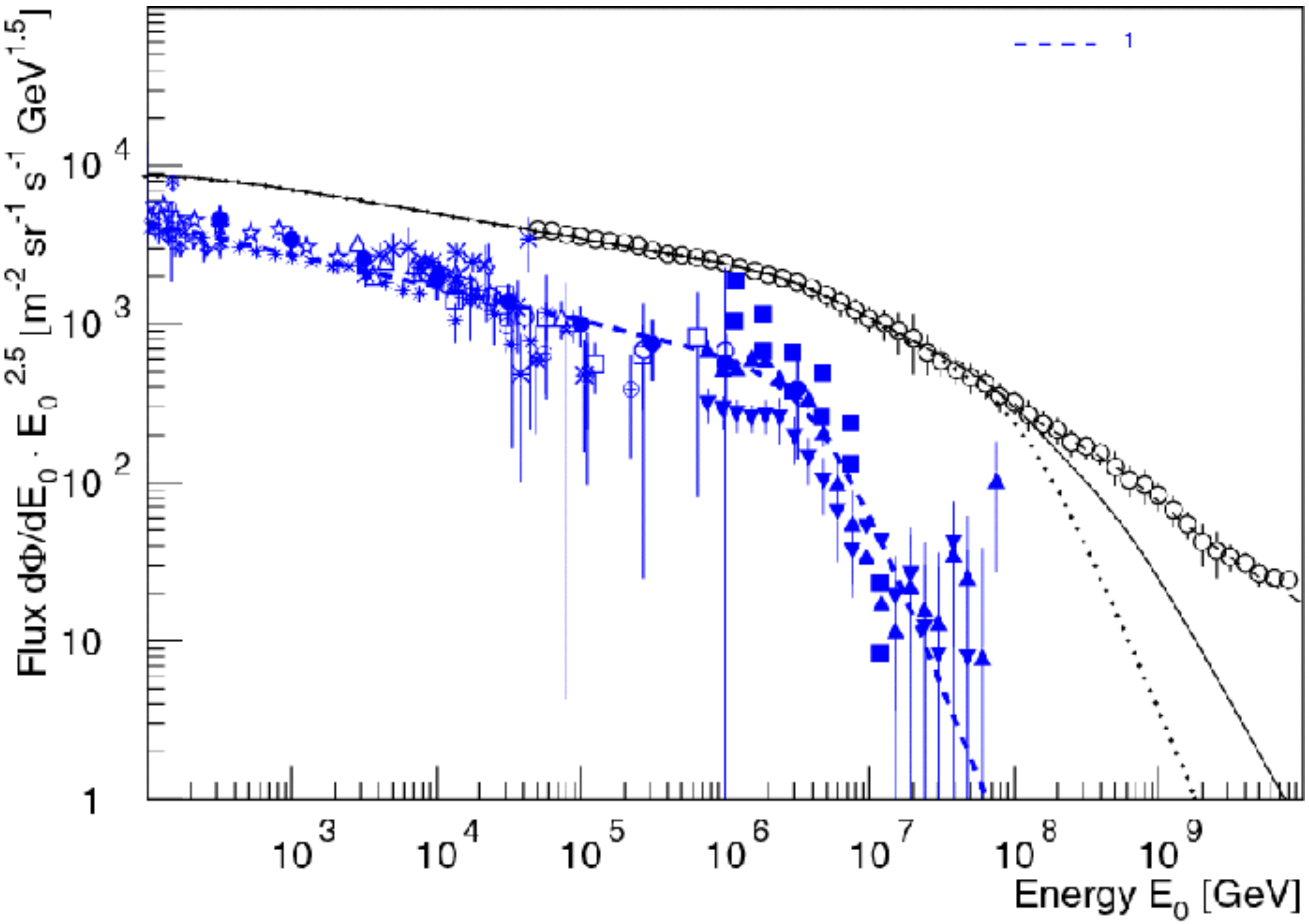

JRH, Astropart. Phys. 19 (2003) 193

Cosmic-ray energy spectrum

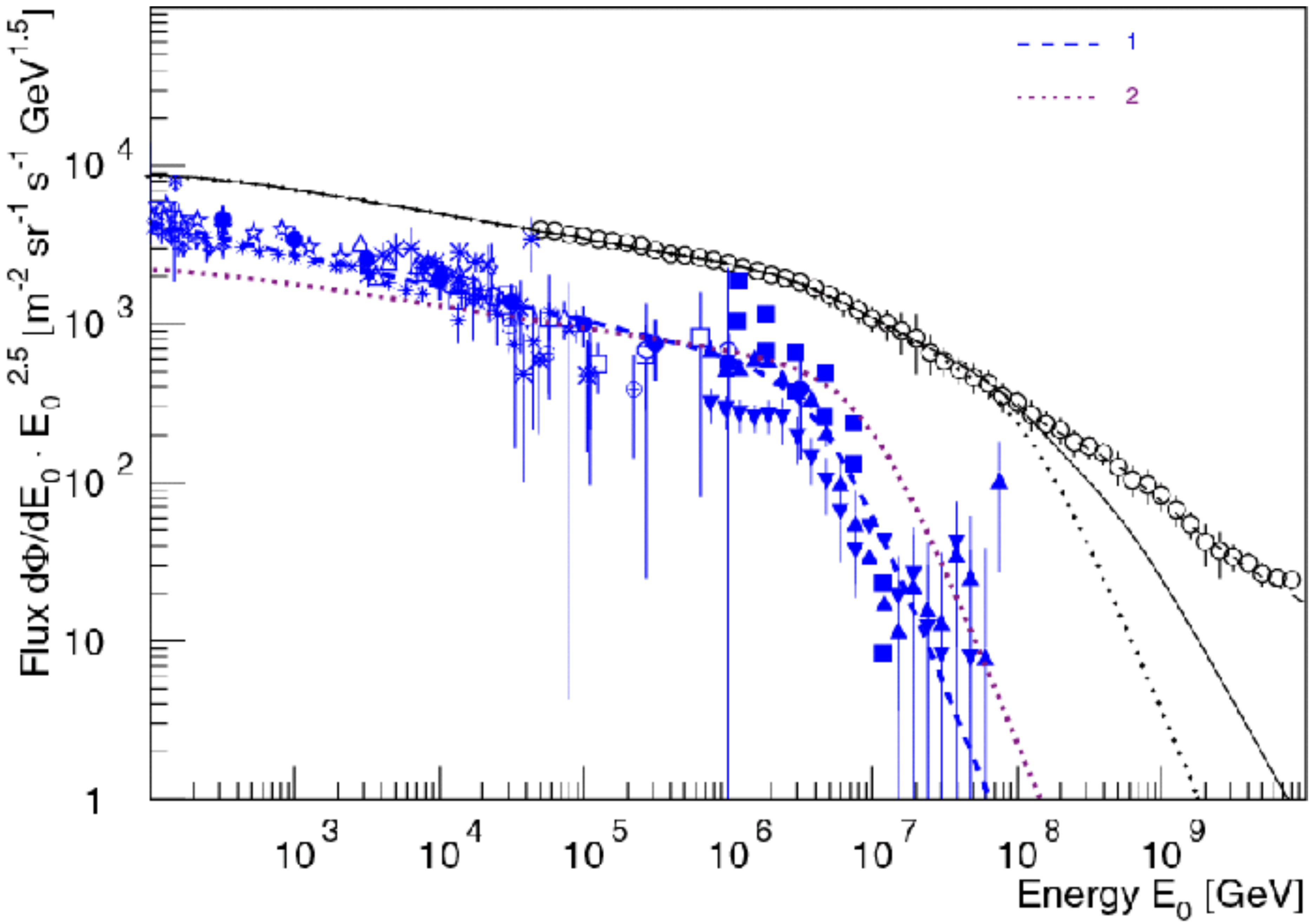

JRH, Astropart. Phys. 19 (2003) 193

Cosmic-ray energy spectrum

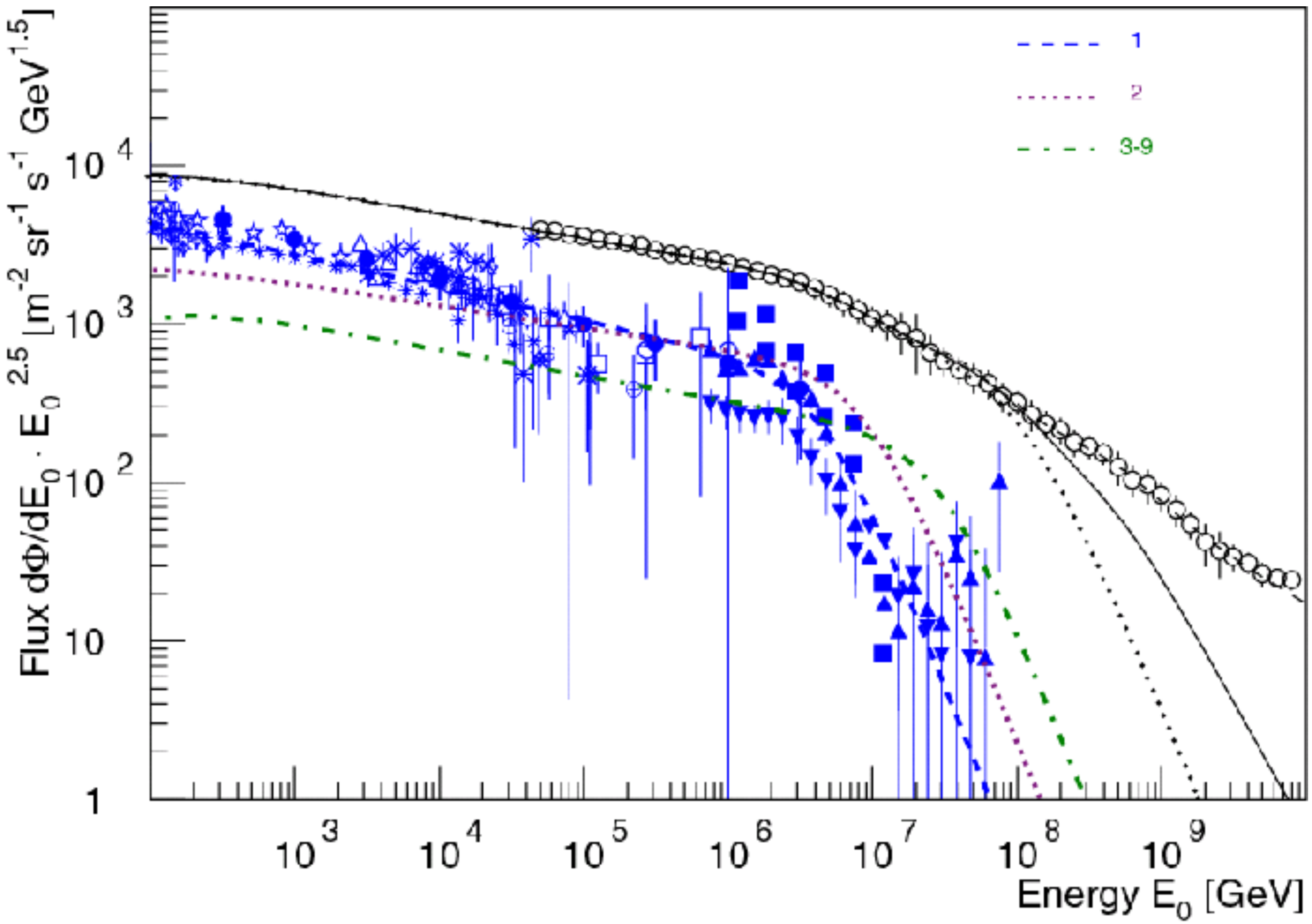

JRH, Astropart. Phys. 19 (2003) 193

Cosmic-ray energy spectrum

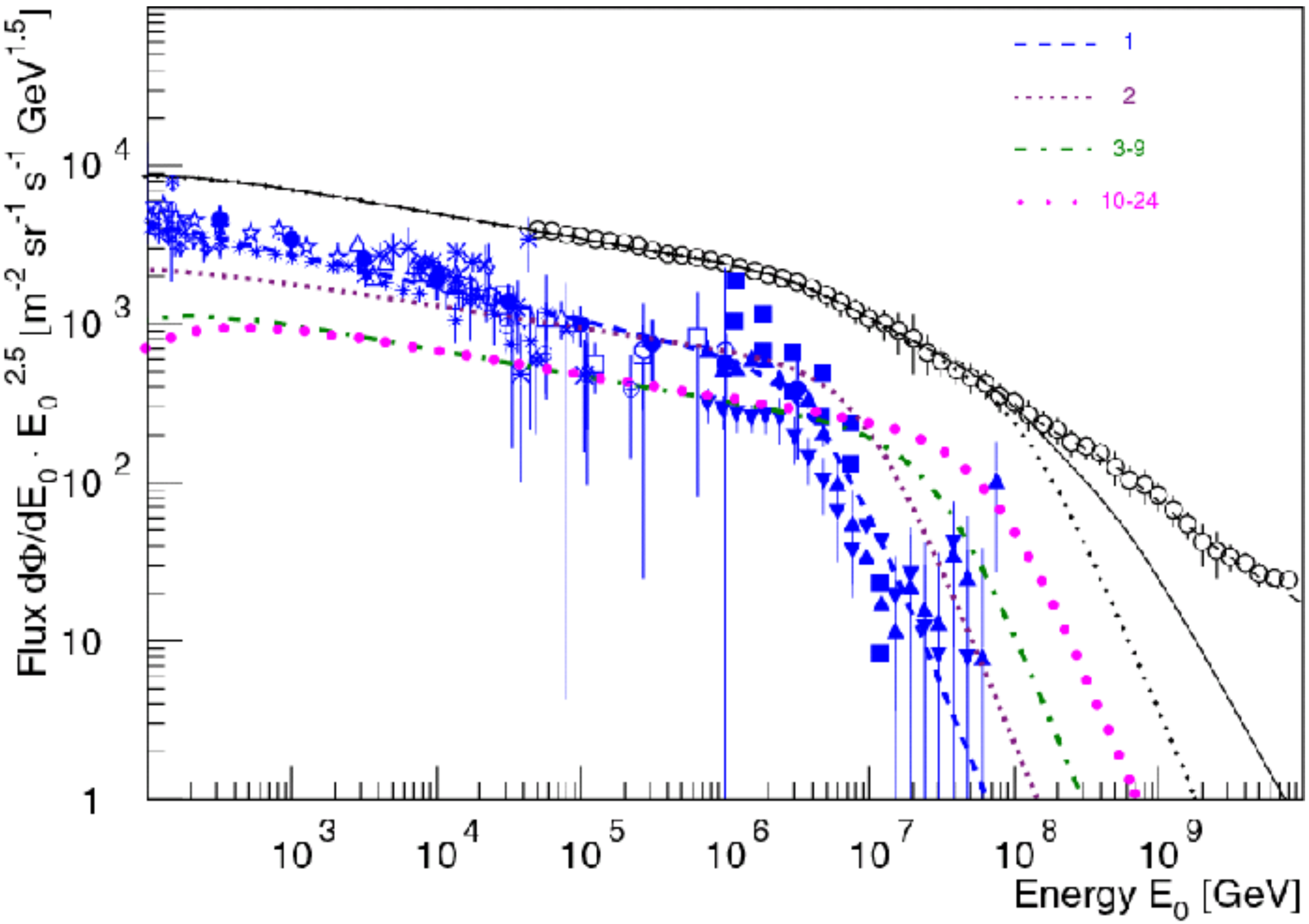

JRH, Astropart. Phys. 19 (2003) 193

Cosmic-ray energy spectrum

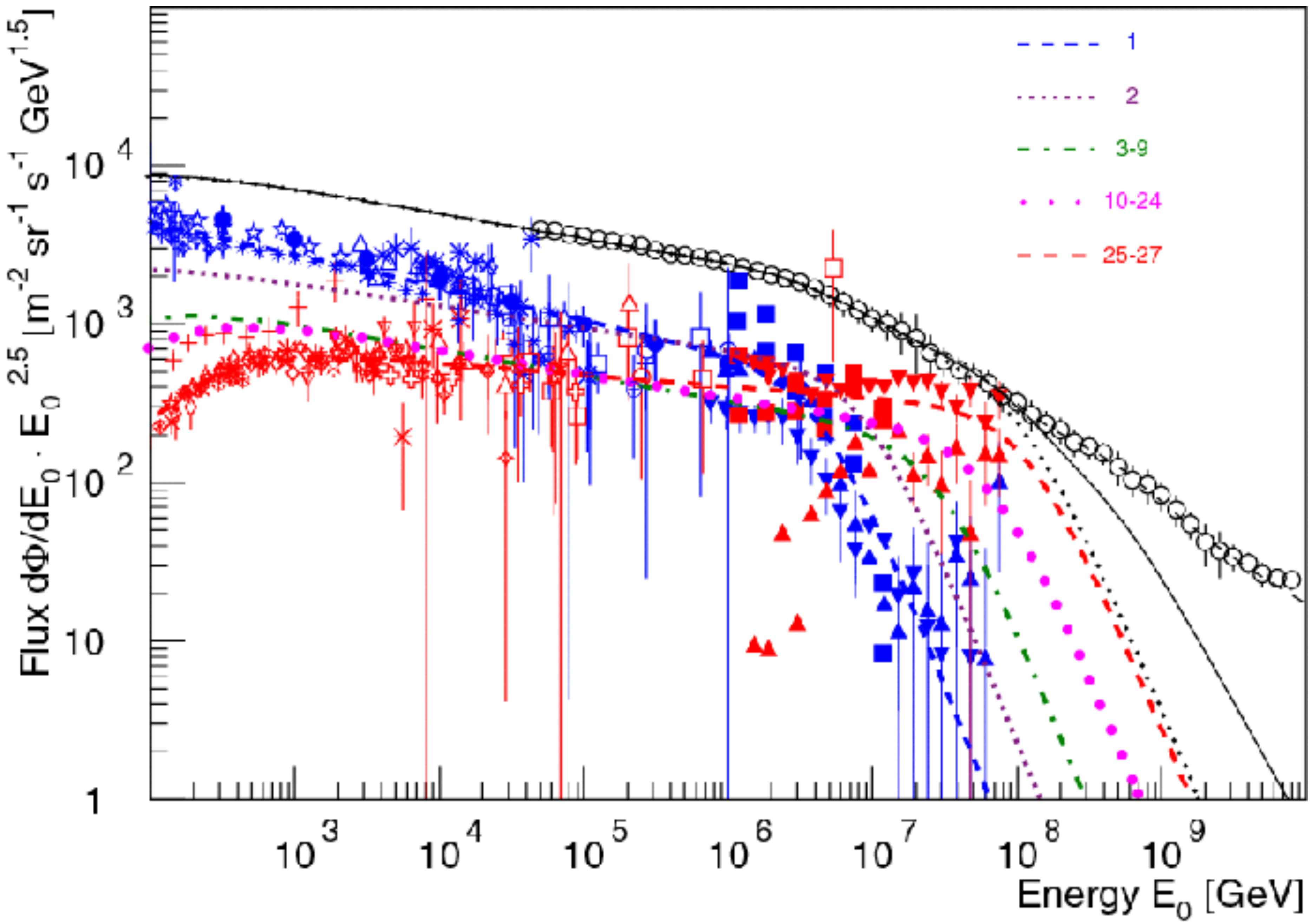

JRH, Astropart. Phys. 19 (2003) 193

Cosmic-ray energy spectrum

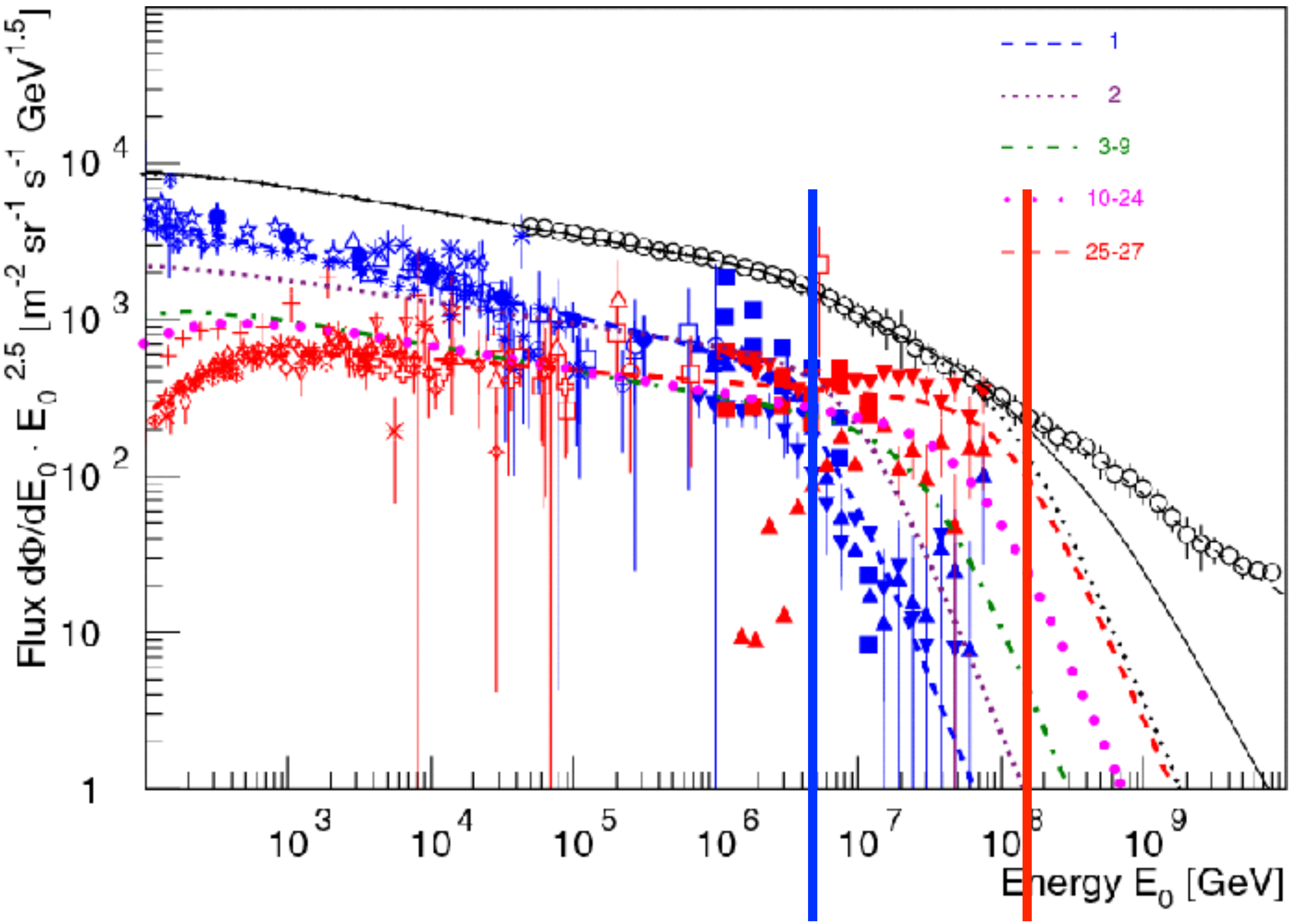

JRH, Astropart. Phys. 19 (2003) 193

Cosmic-ray energy spectrum

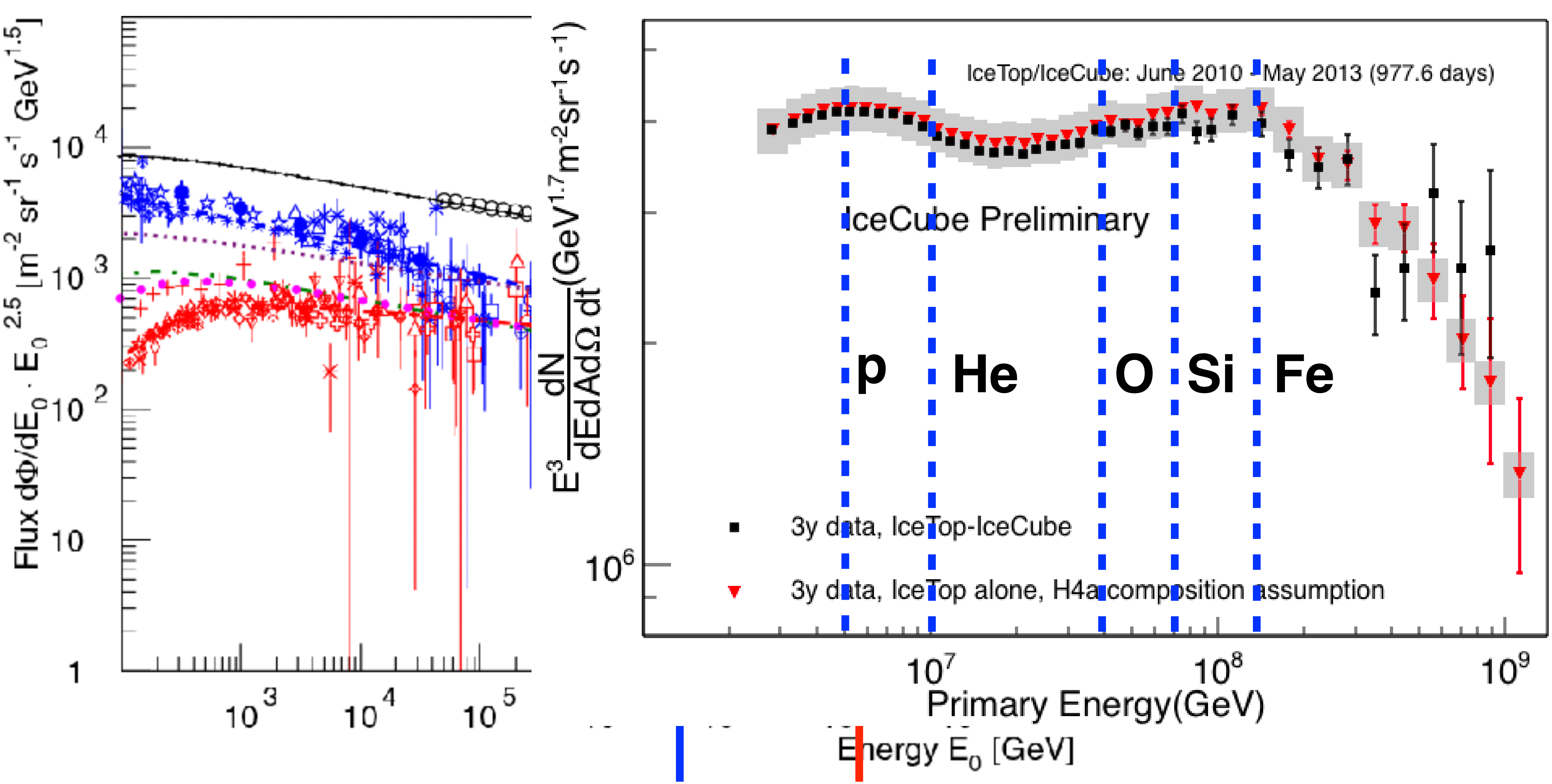

JRH, Astropart. Phys. 19 (2003) 193

TALE (TA low-energy extension)

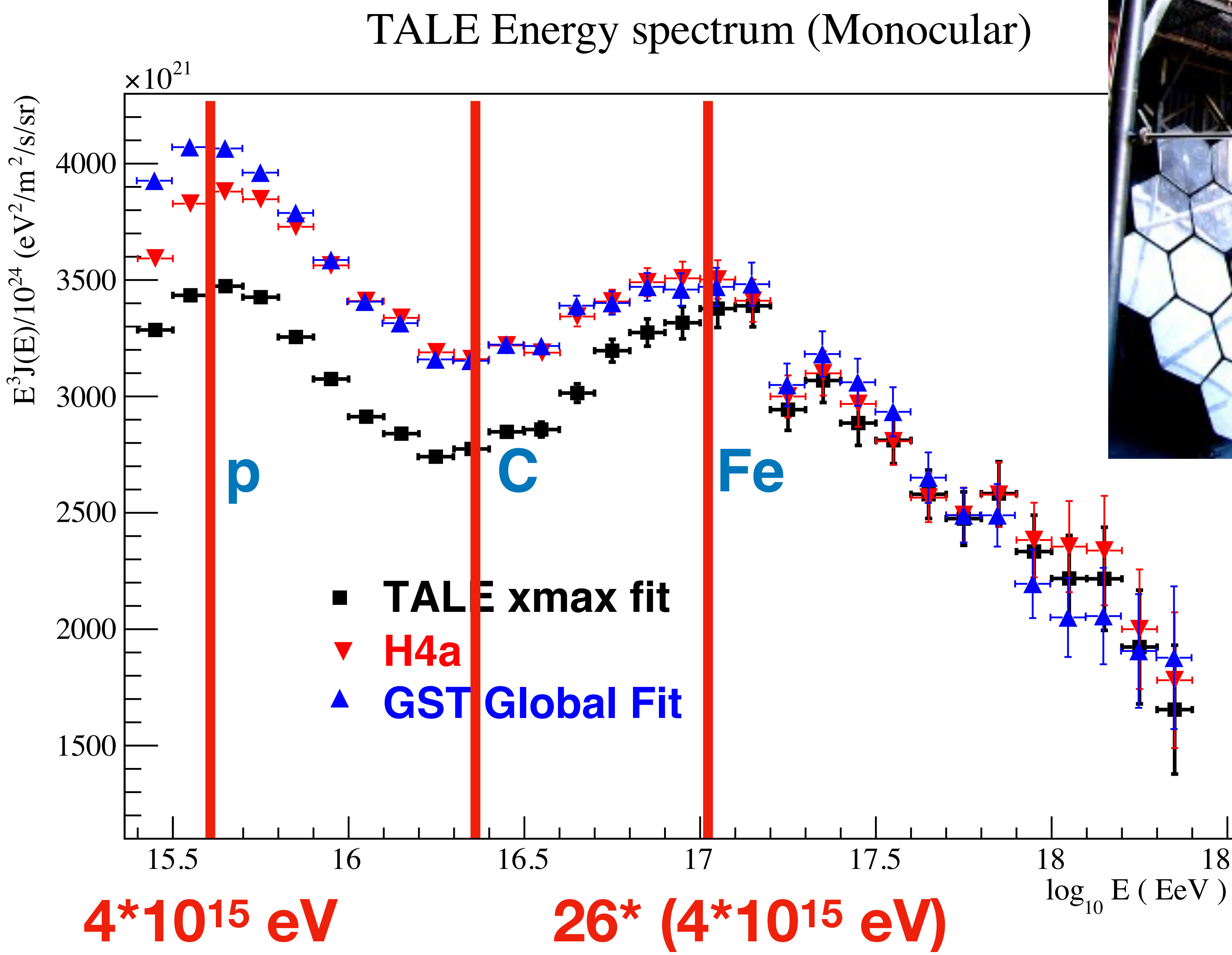

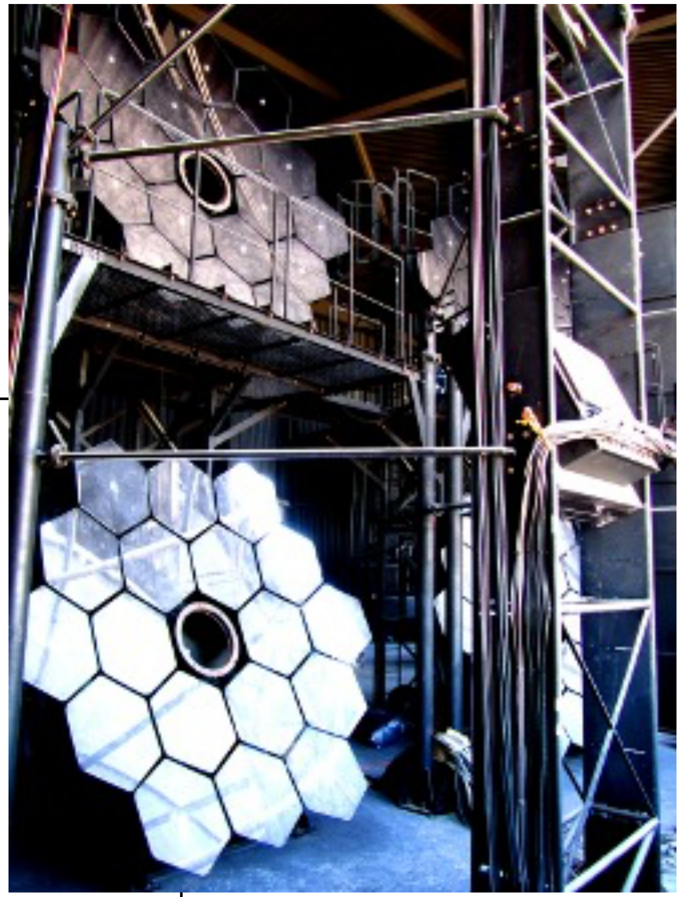

Figure 3: TALE Cosmic rays energy spectrum measured with TALE. The result is based on a QGSJet II-3 hadronic model assumption. A mixed primary composition given by the H4a, and "global fit" models, as well as a TALE derived mix was used in the calculations.

PoS(ICRC2017)534

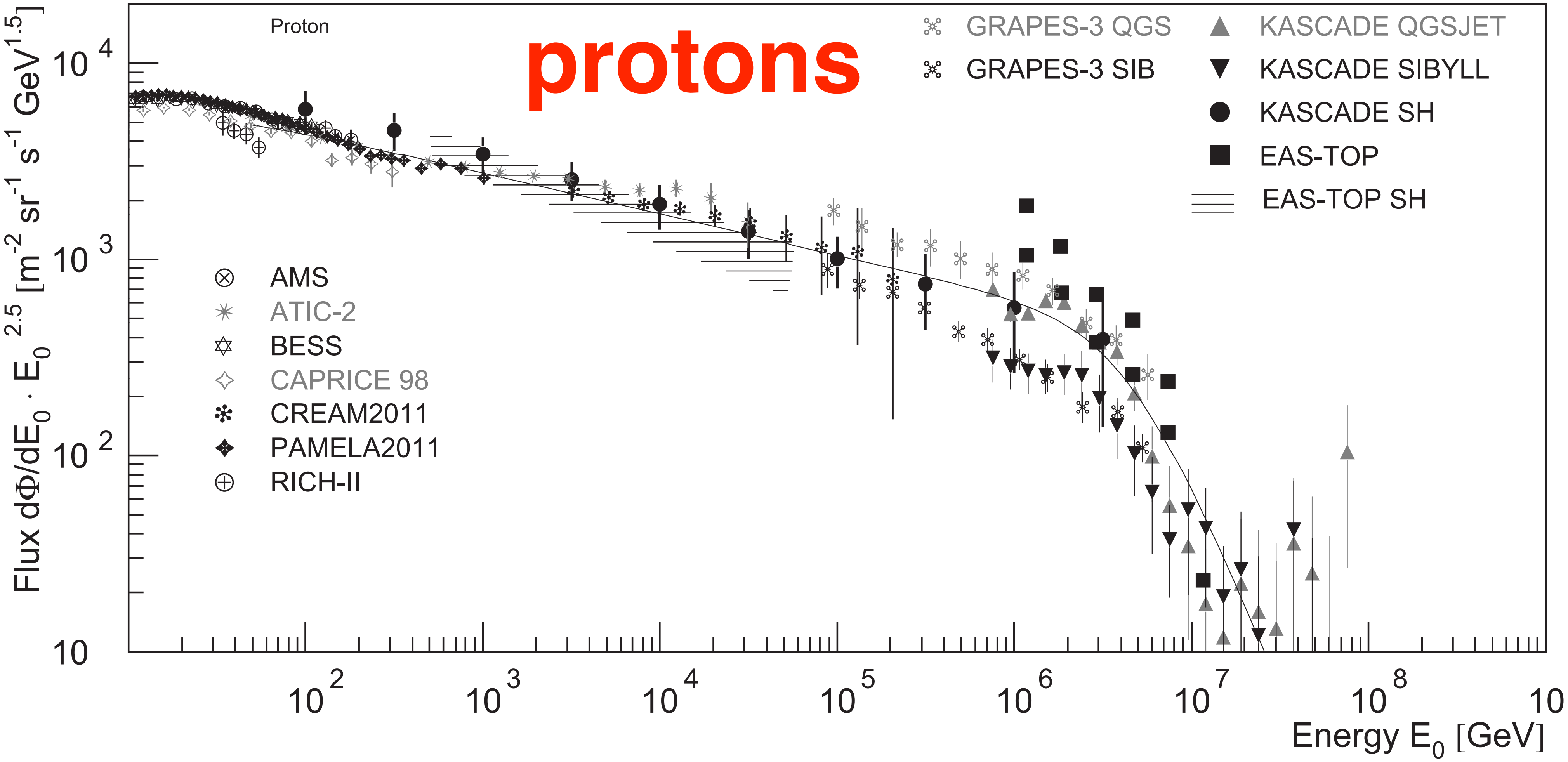

JRH, AIP Conf. Proc. 1516 (2013) 185

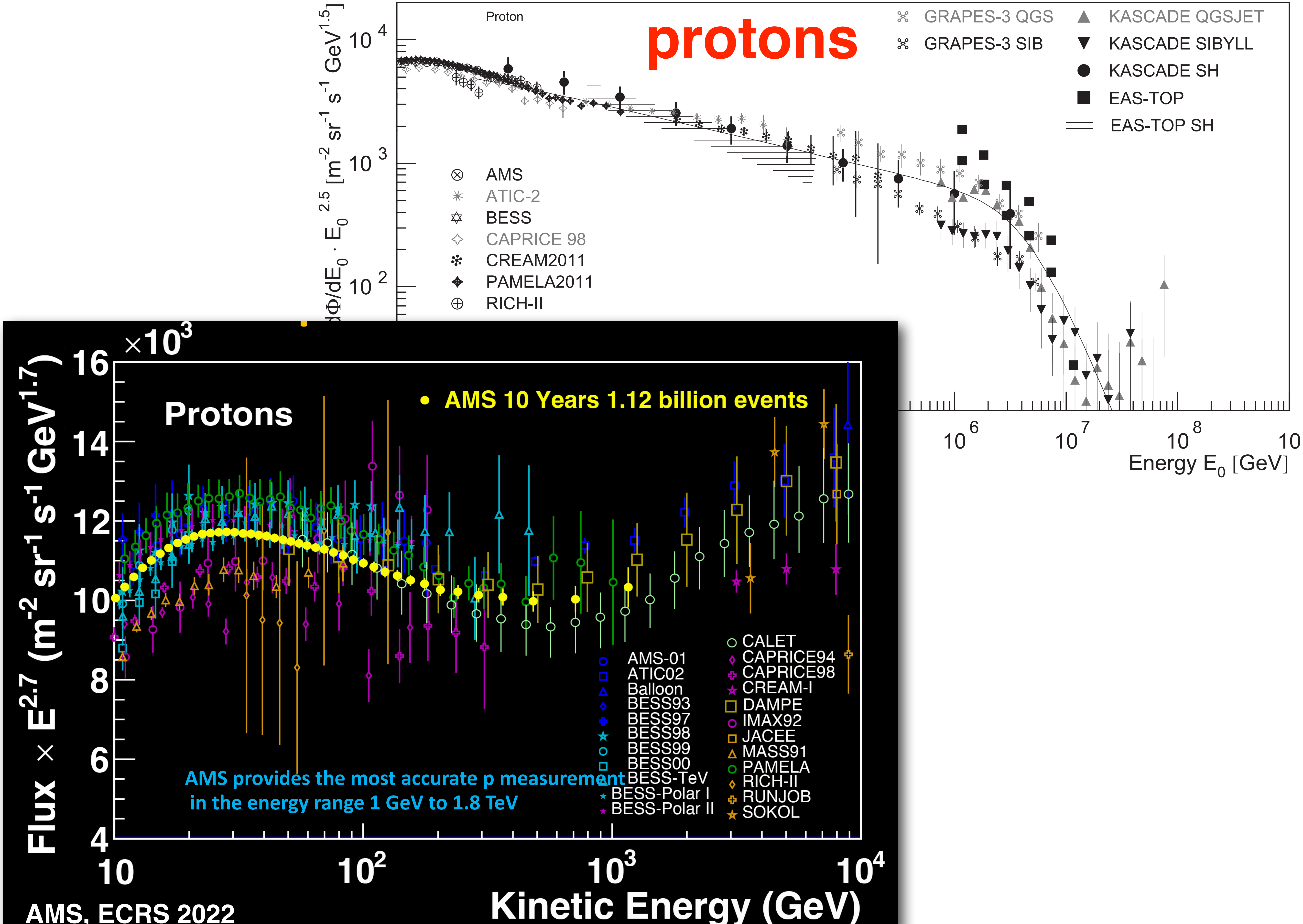

JRH, AIP Conf. Proc. 1516 (2013) 185

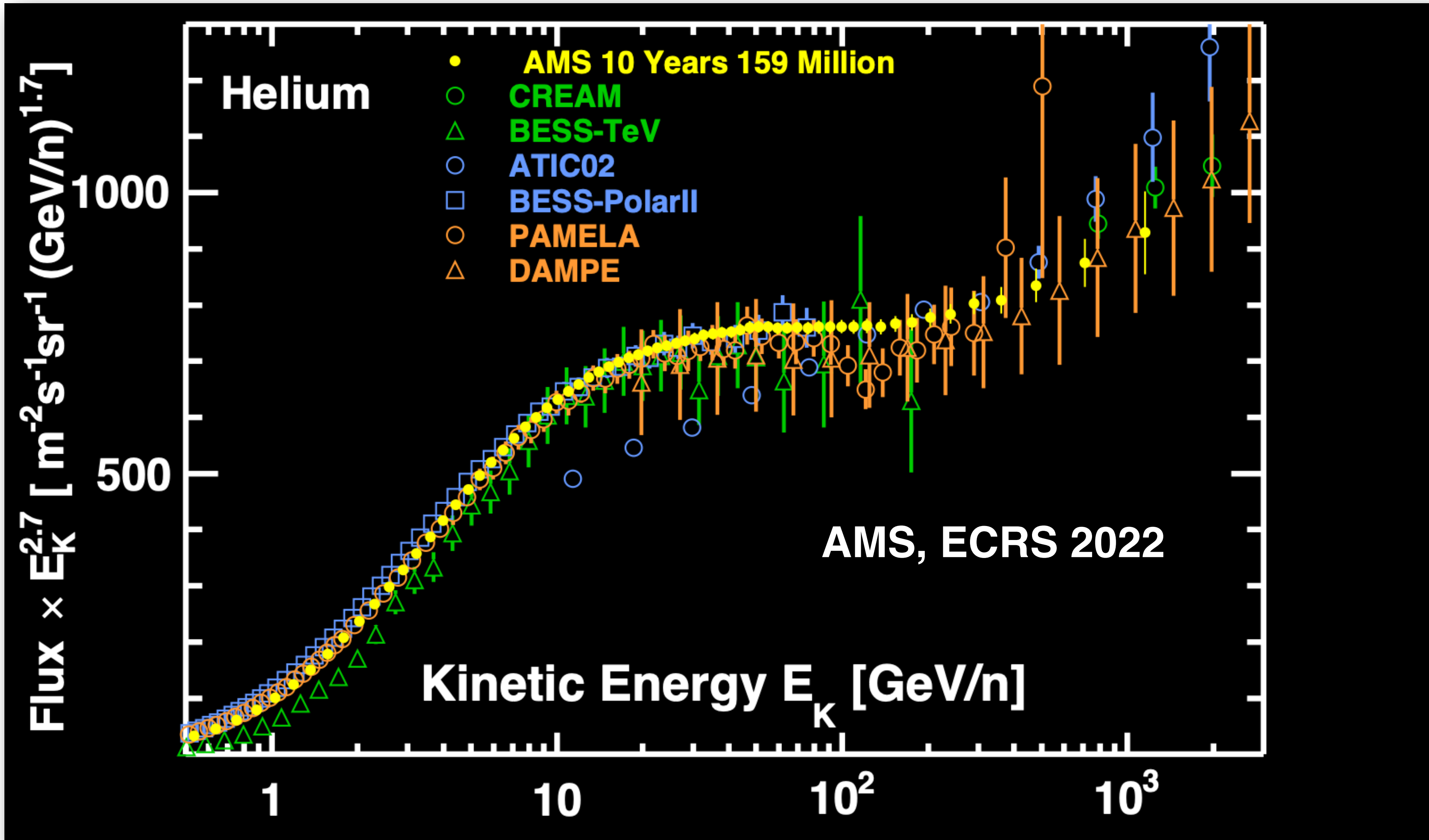

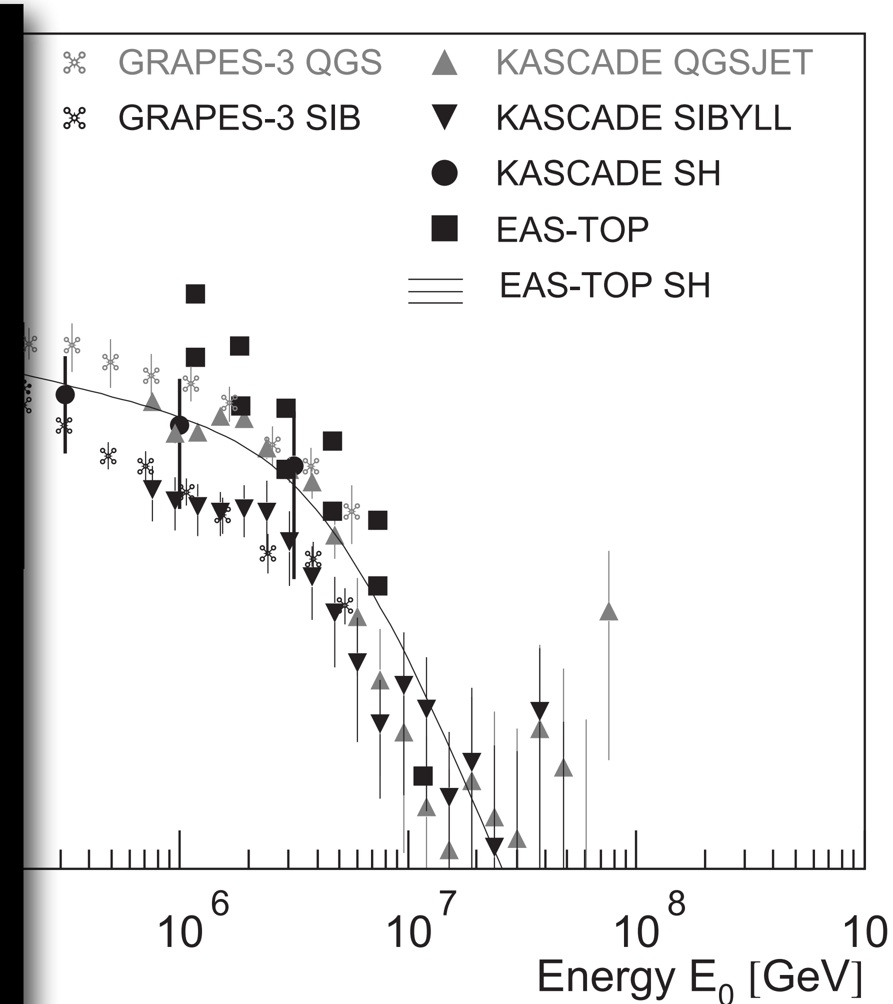

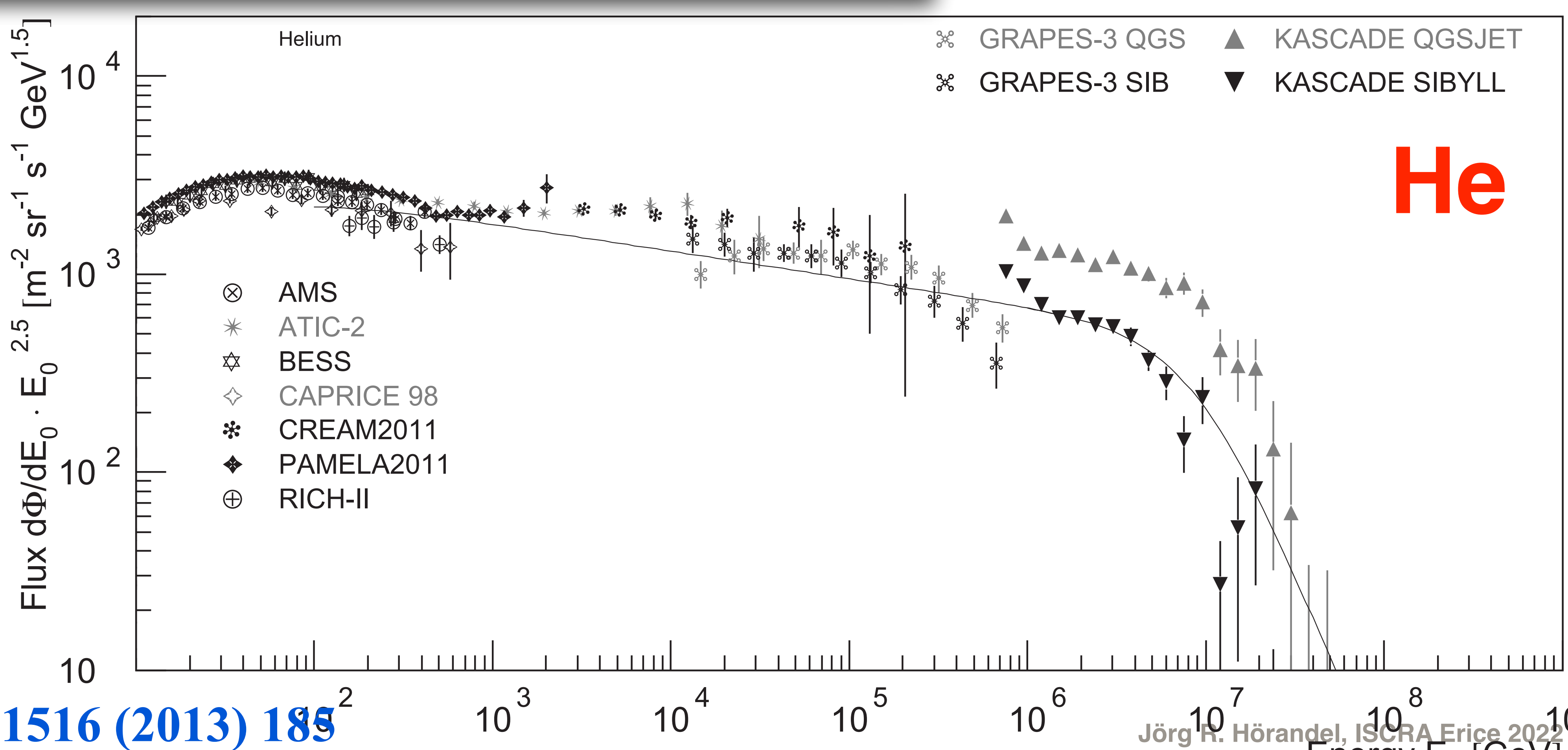

JRH, AIP Conf. Proc. 1516 (2013) 185

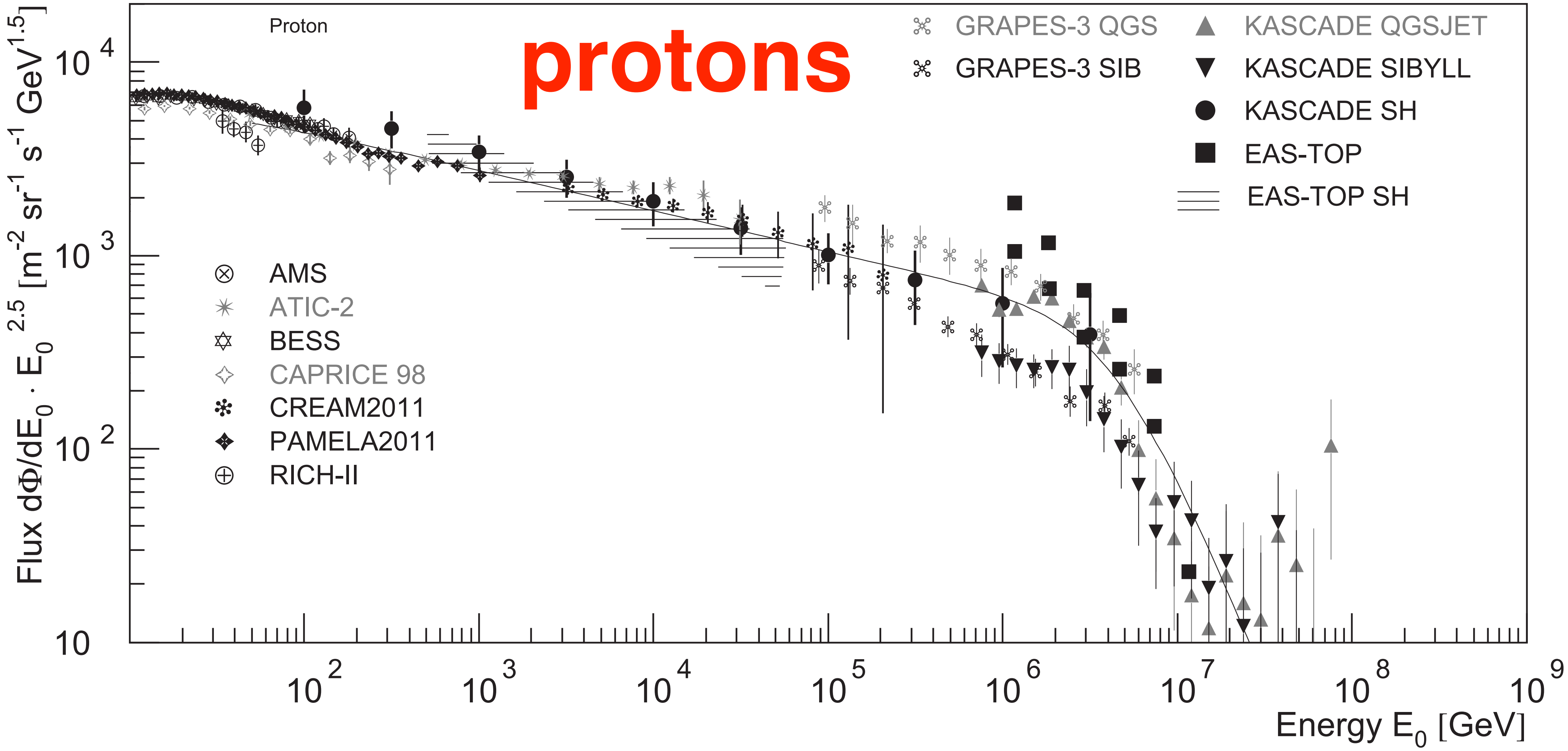

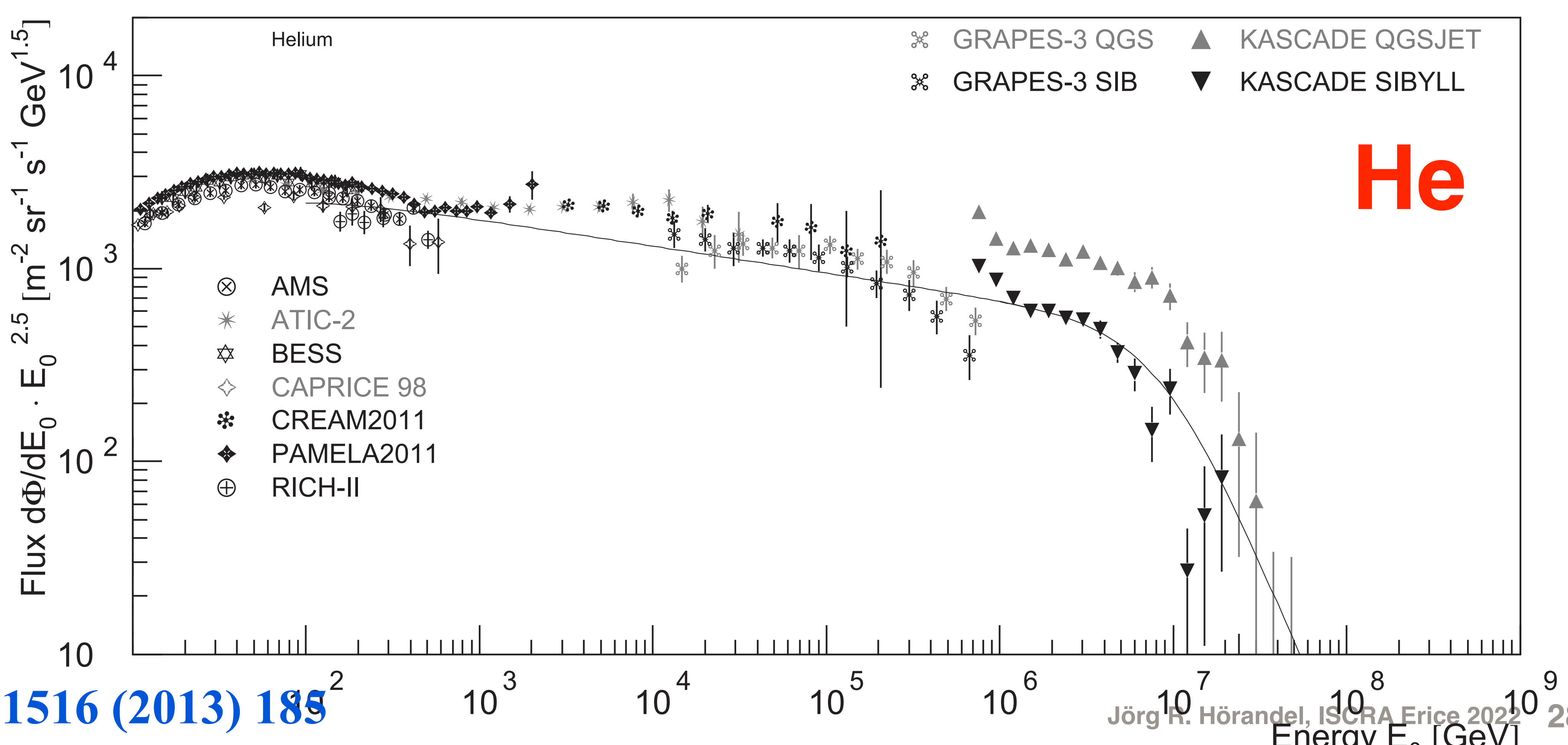

JRH, AIP Conf. Proc. 1516 (2013) 185

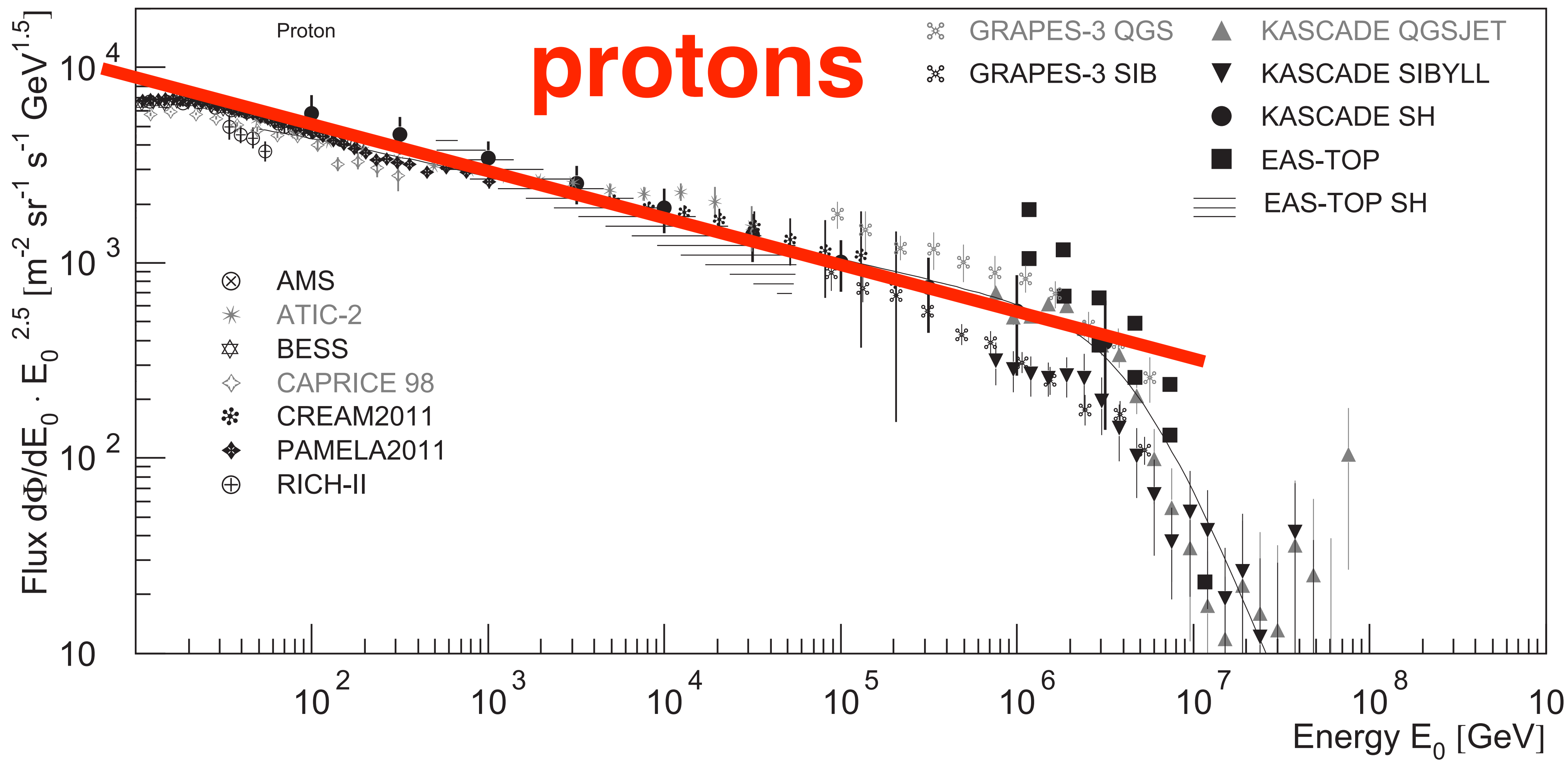

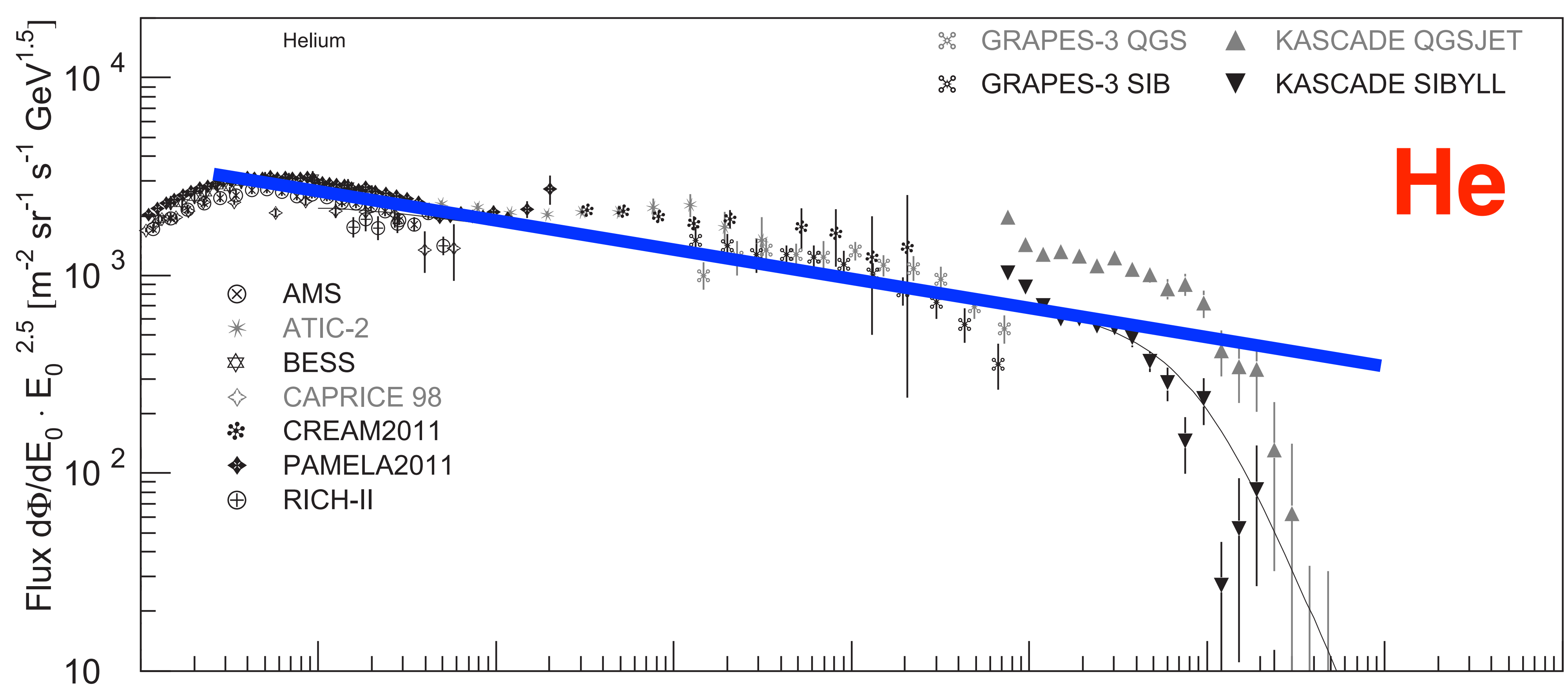

JRH, AIP Conf. Proc. 1516 (2013) 185

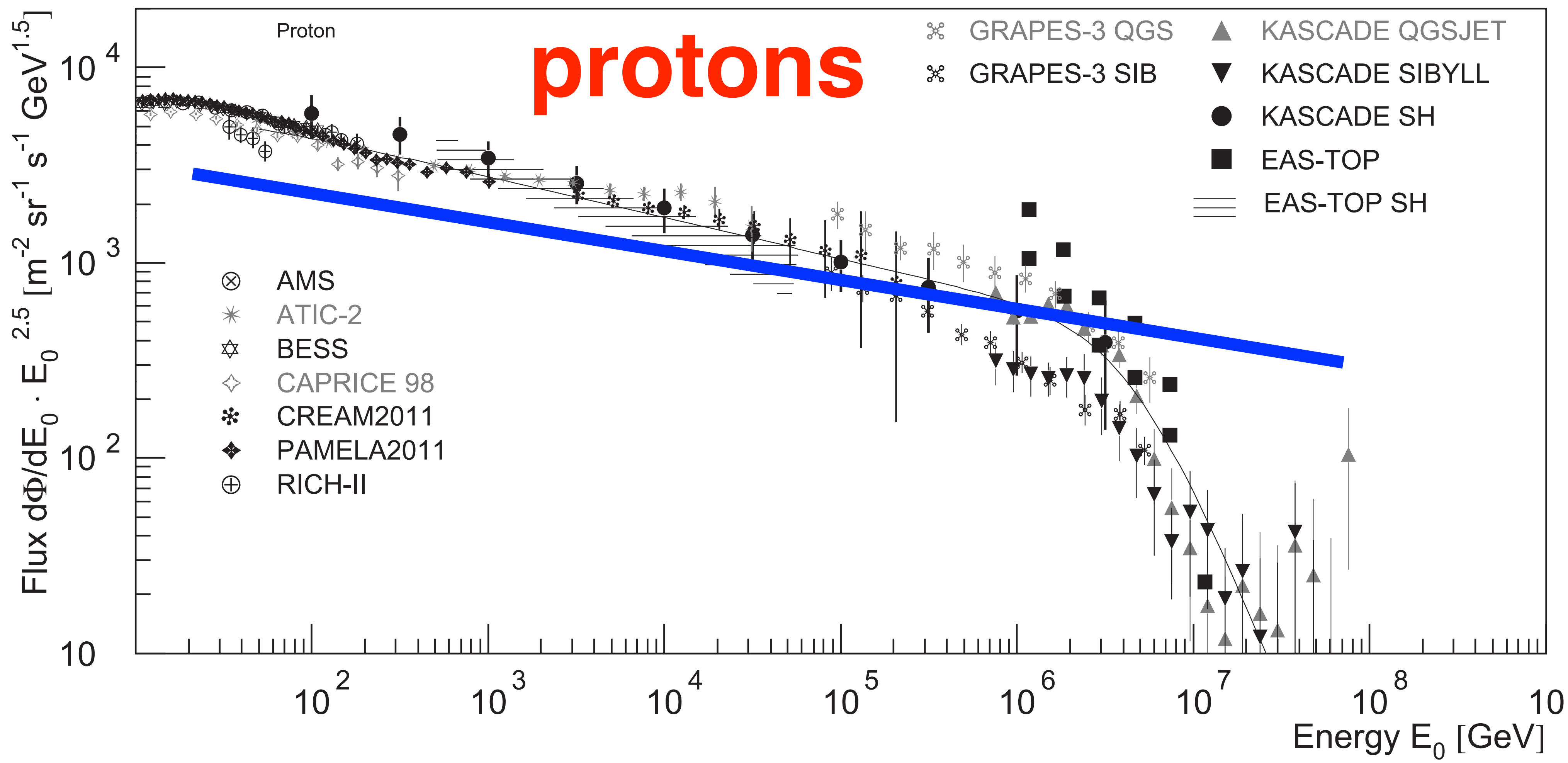

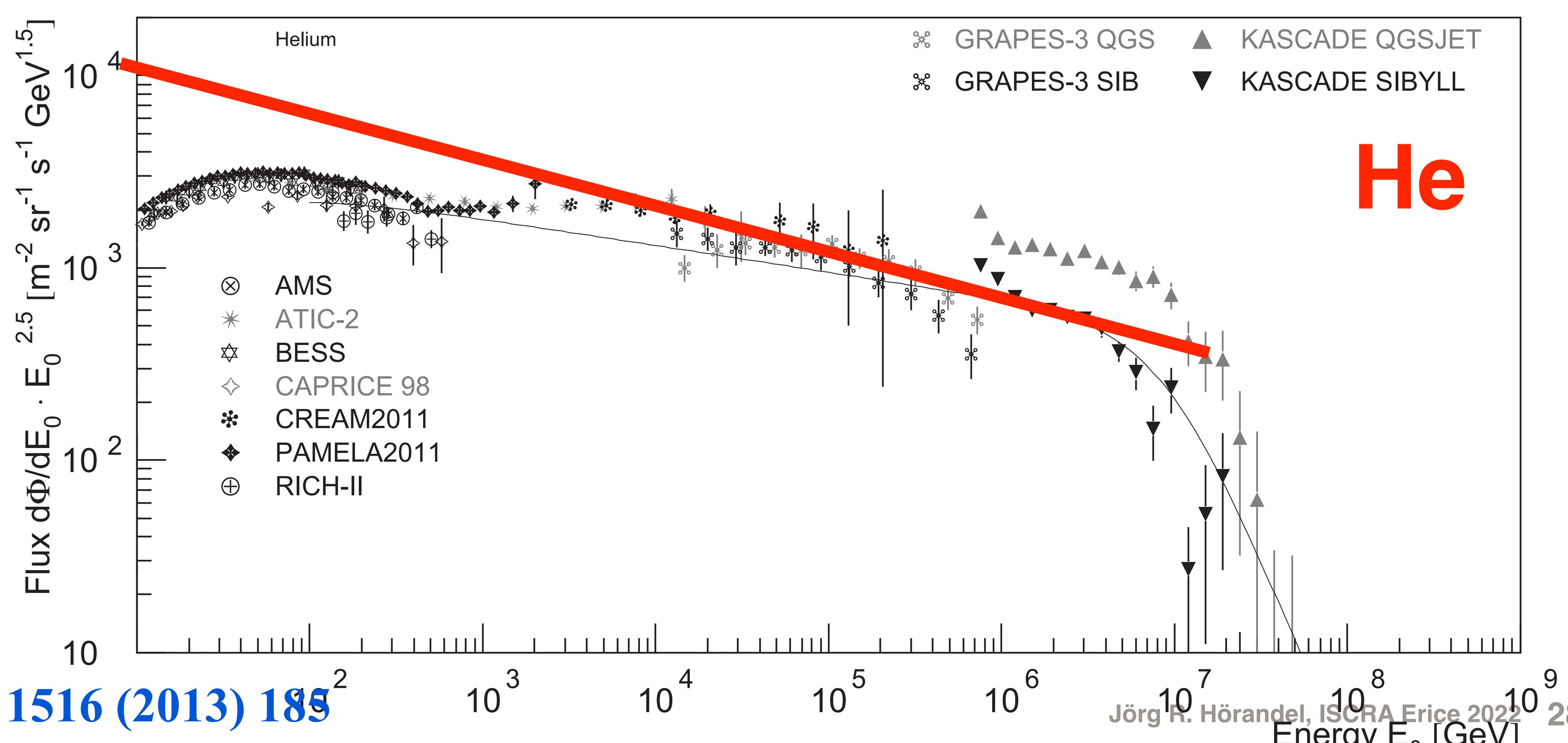

JRH, AIP Conf. Proc. 1516 (2013) 185

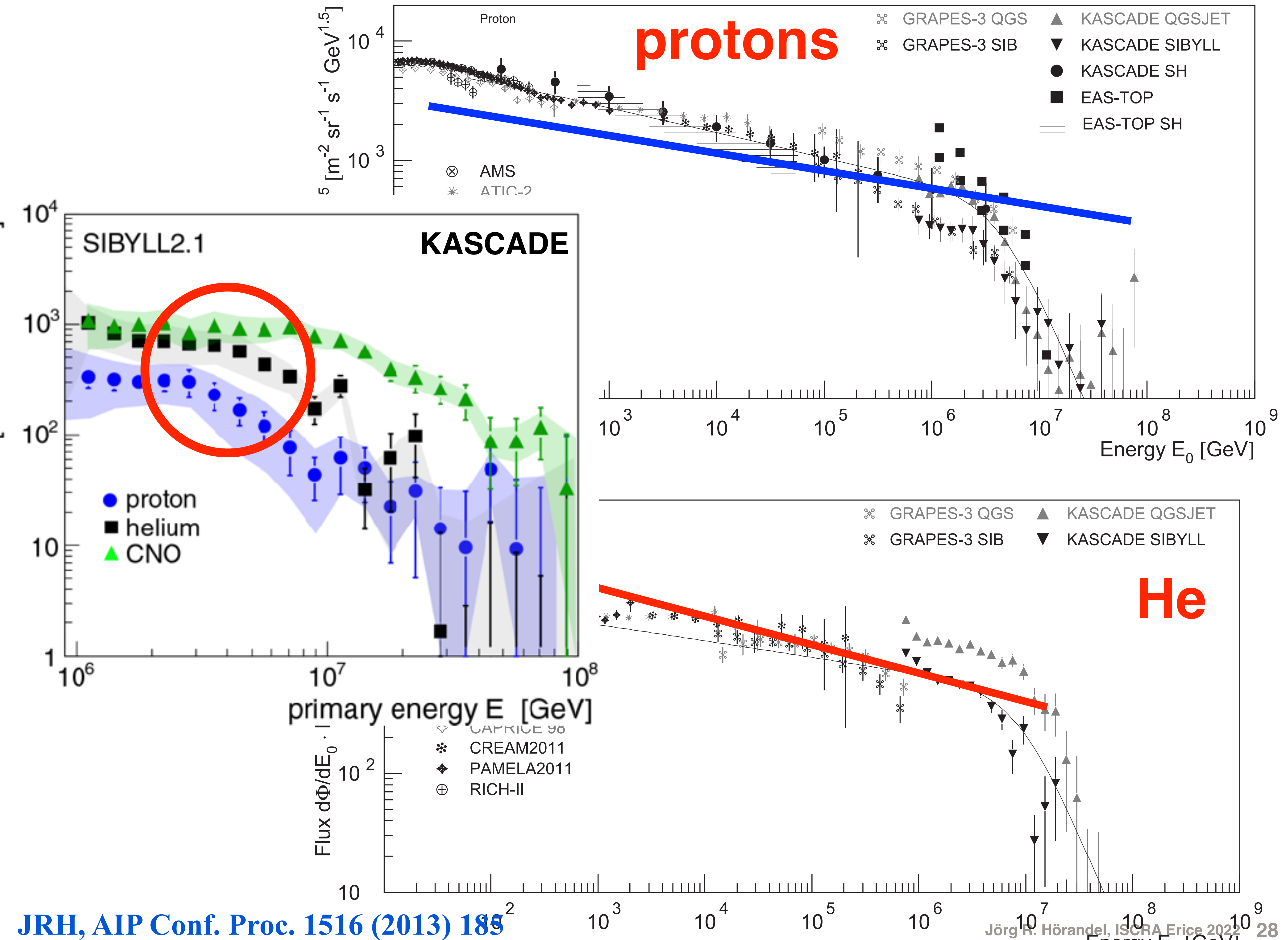

JRH, AIP Conf. Proc. 1516 (2013) 185

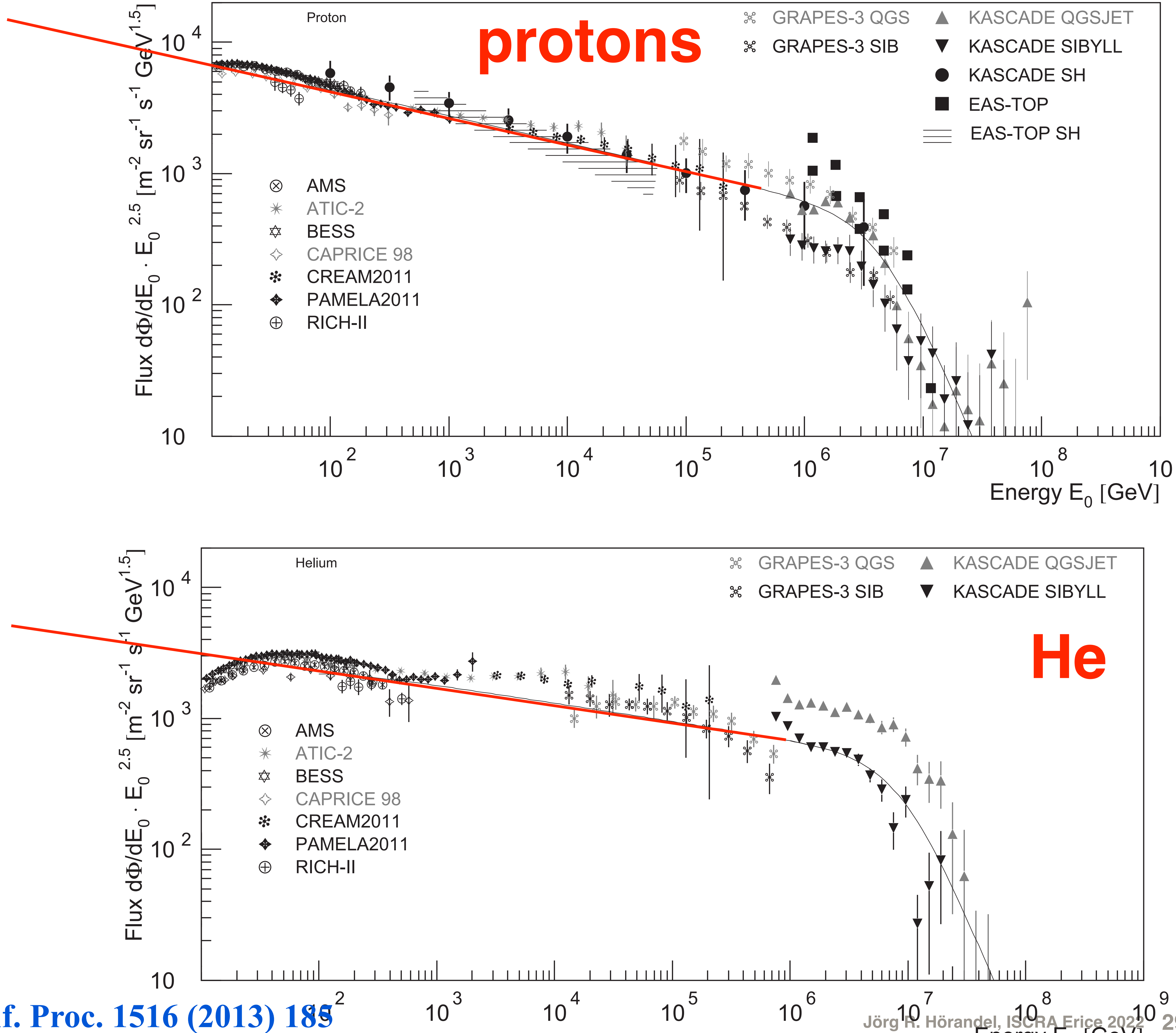

JRH, AIP Conf. Proc. 1516 (2013) 185

JRH, AIP Conf. Proc. 1516 (2013) 185

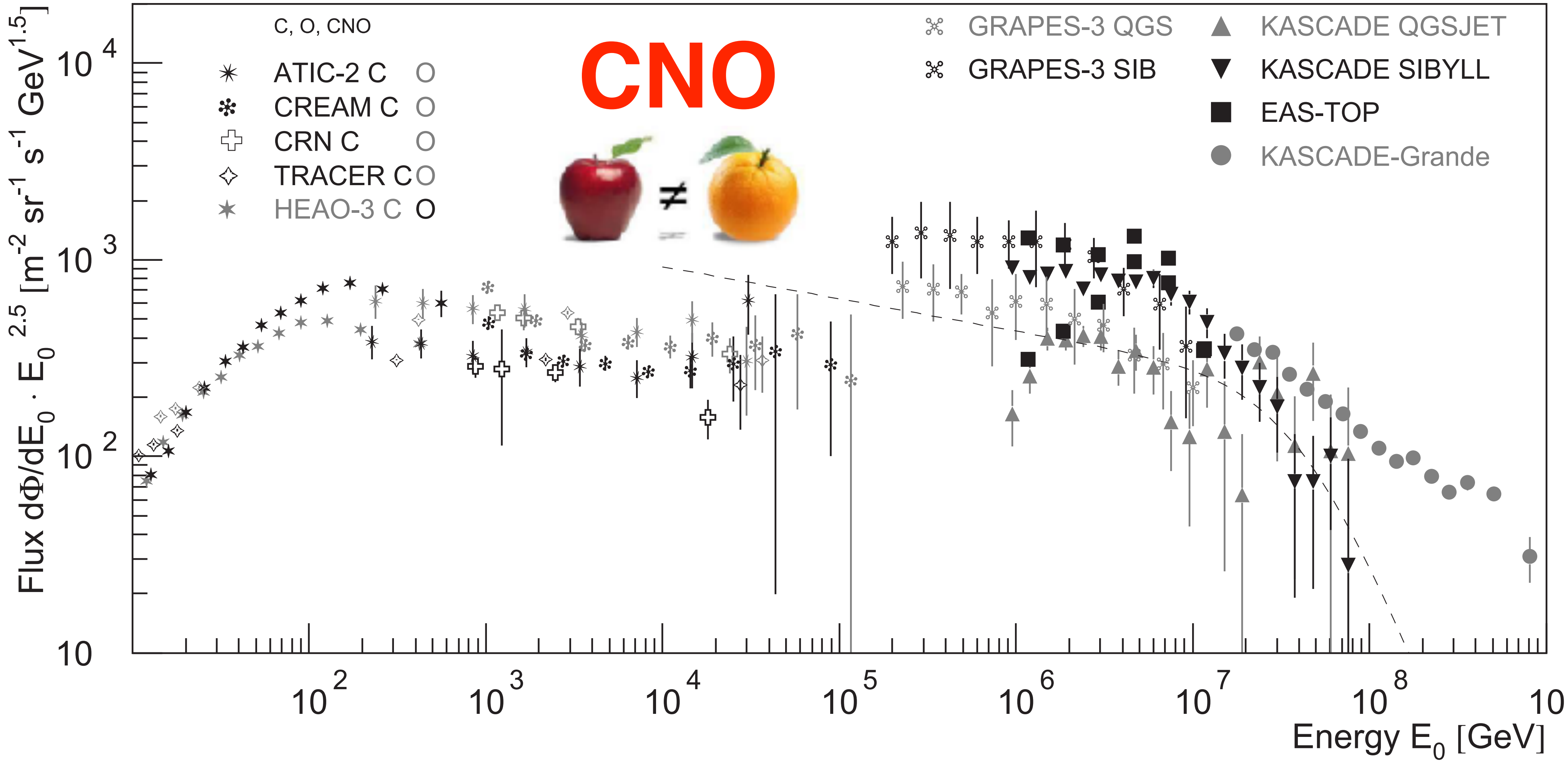

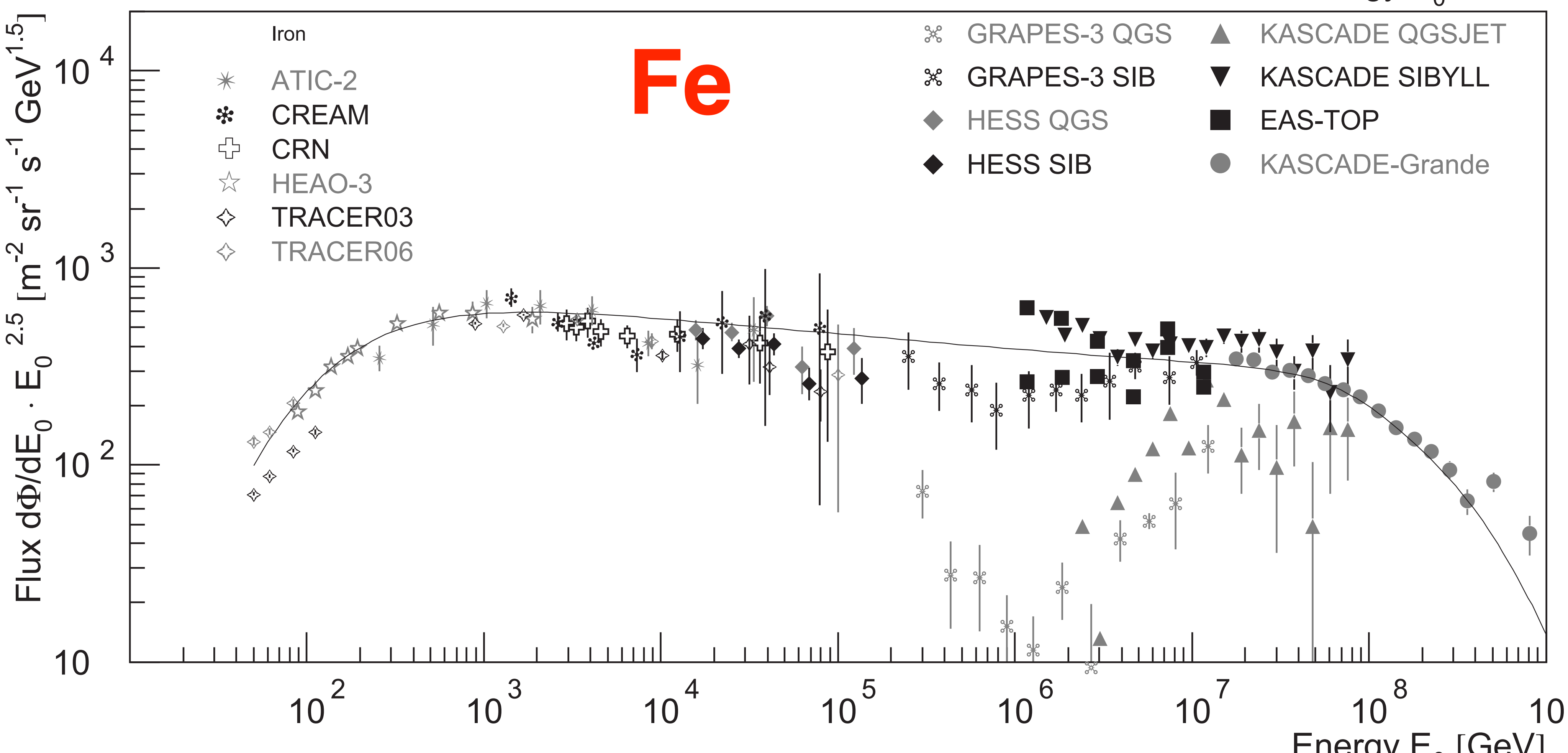

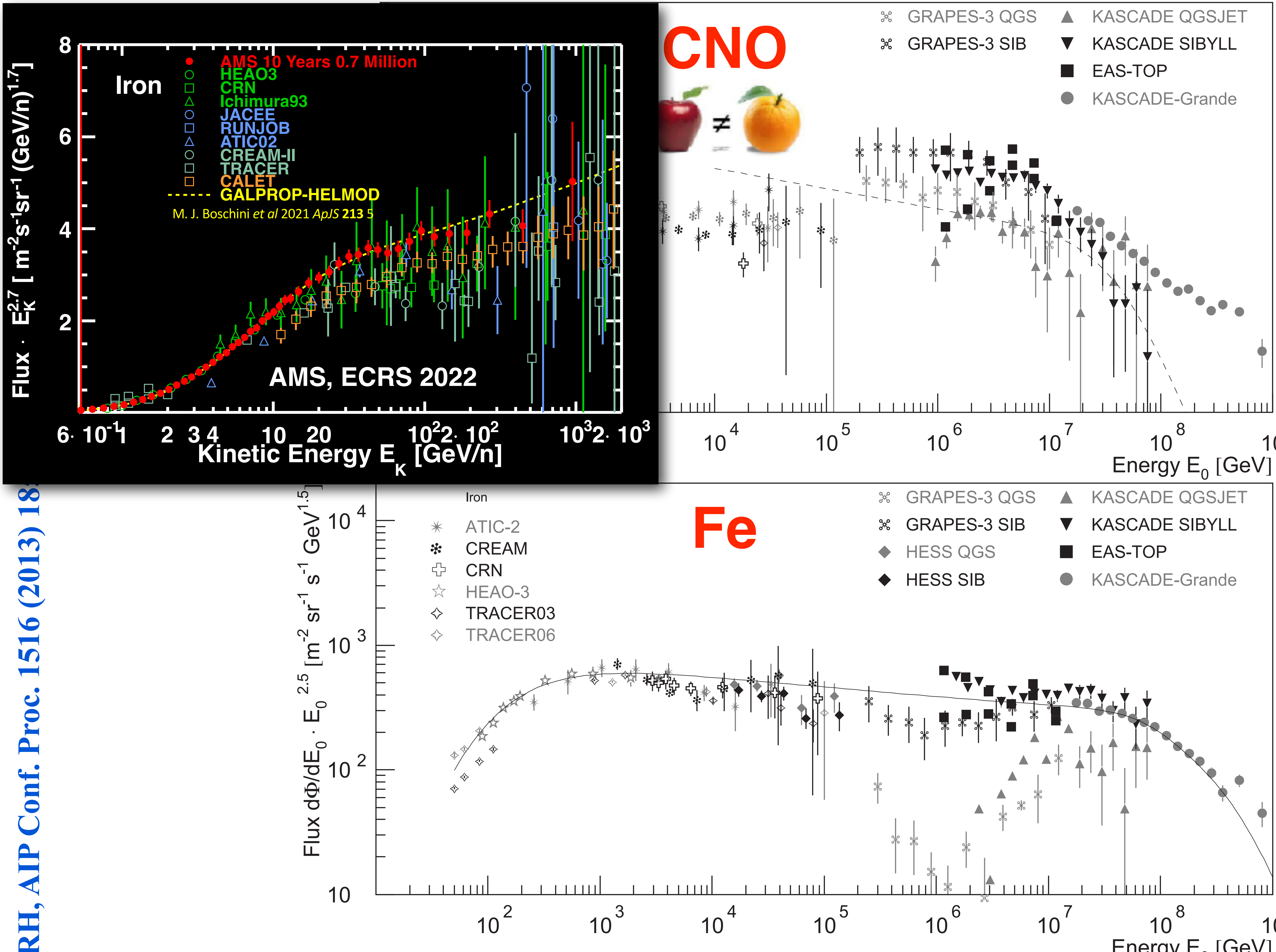

JRH, AIP Conf. Proc. 1516 (2013) 18

Transport equation for cosmic rays in the Galaxy

$$\frac{\partial N_i}{\partial t} = \nabla(D_i \nabla N_i) - \frac{\partial}{\partial E}(b_i N_i) - n\nu\sigma_i N_i - \frac{N_i}{\gamma\tau_i} + Q_i + \sum_{j>i} n\nu\sigma_{ij} N_j + \sum_{j>i} \frac{N_j}{\gamma_j \tau_{ij}}$$

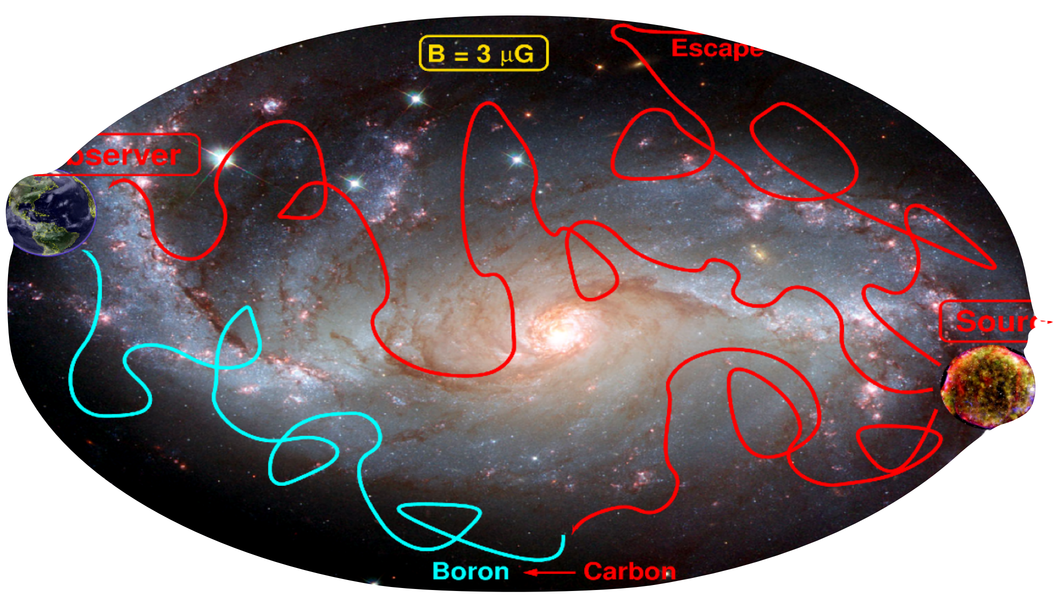

Transport equation for cosmic rays in the Galaxy

diffusion

$$\frac{\partial N_i}{\partial t} = \nabla(D_i \nabla N_i) - \frac{\partial}{\partial E}(b_i N_i) - n\nu\sigma_i N_i - \frac{N_i}{\gamma\tau_i} + Q_i + \sum_{j>i} n\nu\sigma_{ij} N_j + \sum_{j>i} \frac{N_j}{\gamma_j \tau_{ij}}$$

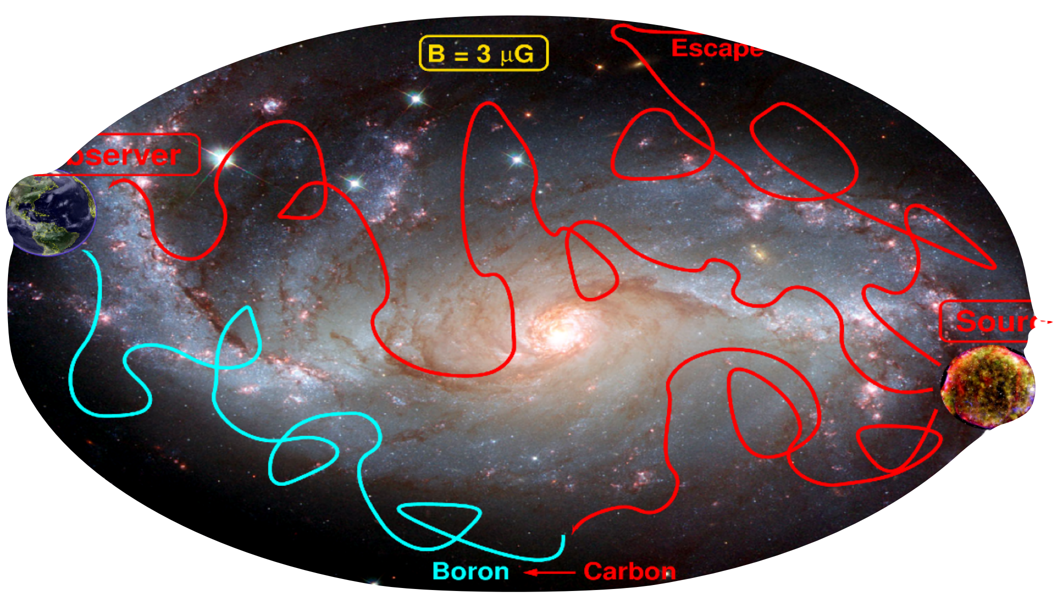

Transport equation for cosmic rays in the Galaxy

diffusion

energy loss (Bethe Bloch)

$$\frac{\partial N_i}{\partial t} = \nabla(D_i \nabla N_i) - \frac{\partial}{\partial E}(b_i N_i) - n\nu\sigma_i N_i - \frac{N_i}{\gamma\tau_i} + Q_i + \sum_{j>i} n\nu\sigma_{ij} N_j + \sum_{j>i} \frac{N_j}{\gamma_j \tau_{ij}}$$

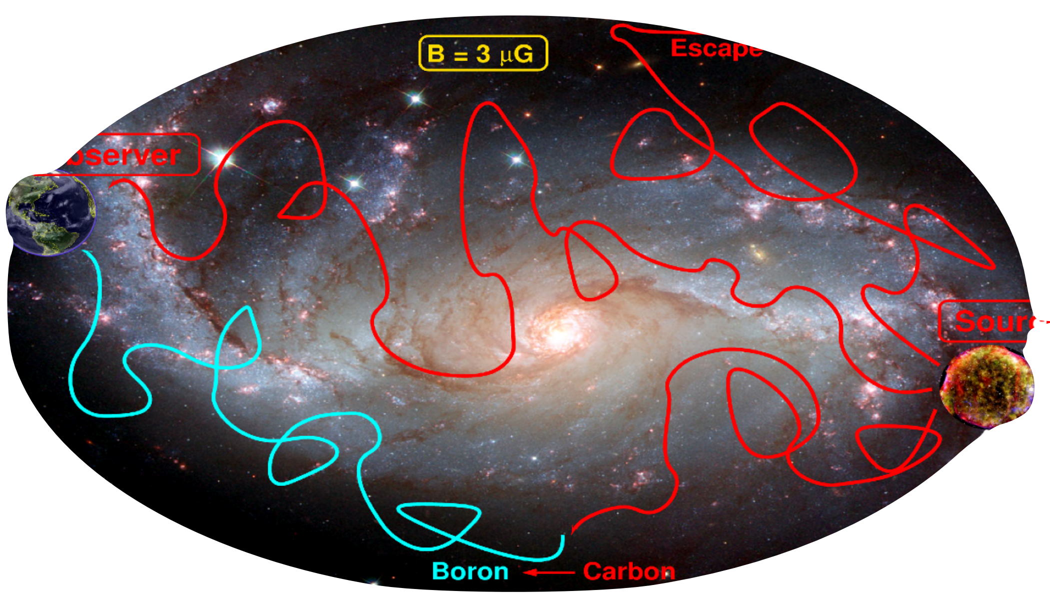

Transport equation for cosmic rays in the Galaxy

diffusion

energy loss (Bethe Bloch)

loss through interactions with ISM (spallation)

$$\frac{\partial N_i}{\partial t} = \nabla(D_i \nabla N_i) - \frac{\partial}{\partial E}(b_i N_i) - n\nu\sigma_i N_i - \frac{N_i}{\gamma\tau_i} + Q_i + \sum_{j>i} n\nu\sigma_{ij} N_j + \sum_{j>i} \frac{N_j}{\gamma_j \tau_{ij}}$$

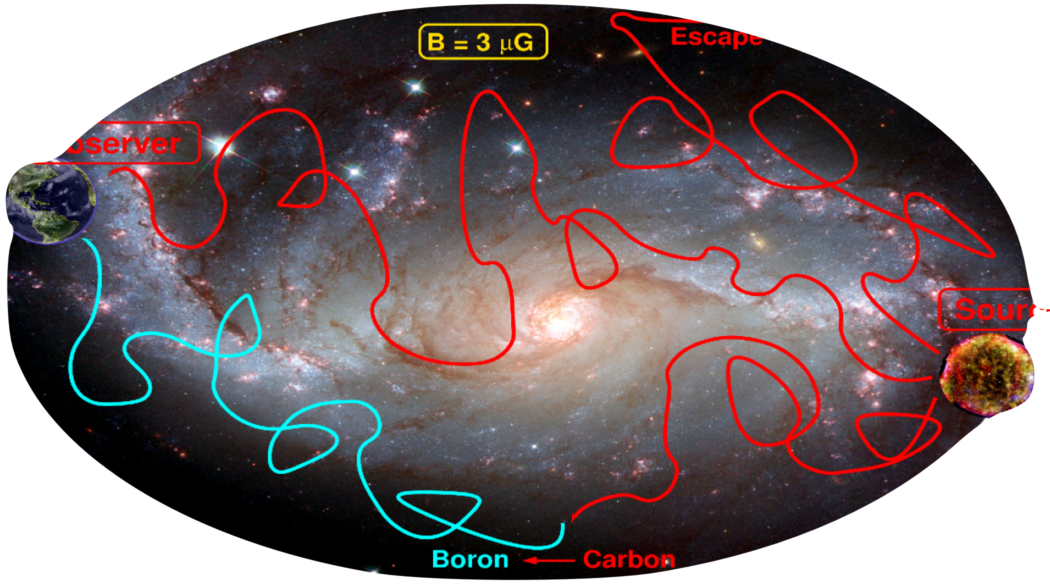

Transport equation for cosmic rays in the Galaxy

diffusion

energy loss (Bethe Bloch)

loss through interactions
with ISM (spallation)

loss through radioactive decay

$$\frac{\partial N_i}{\partial t} = \nabla(D_i \nabla N_i) - \frac{\partial}{\partial E}(b_i N_i) - n v \sigma_i N_i - \frac{N_i}{\gamma \tau_i} + Q_i + \sum_{j>i} n v \sigma_{ij} N_j + \sum_{j>i} \frac{N_j}{\gamma_j \tau_{ij}}$$

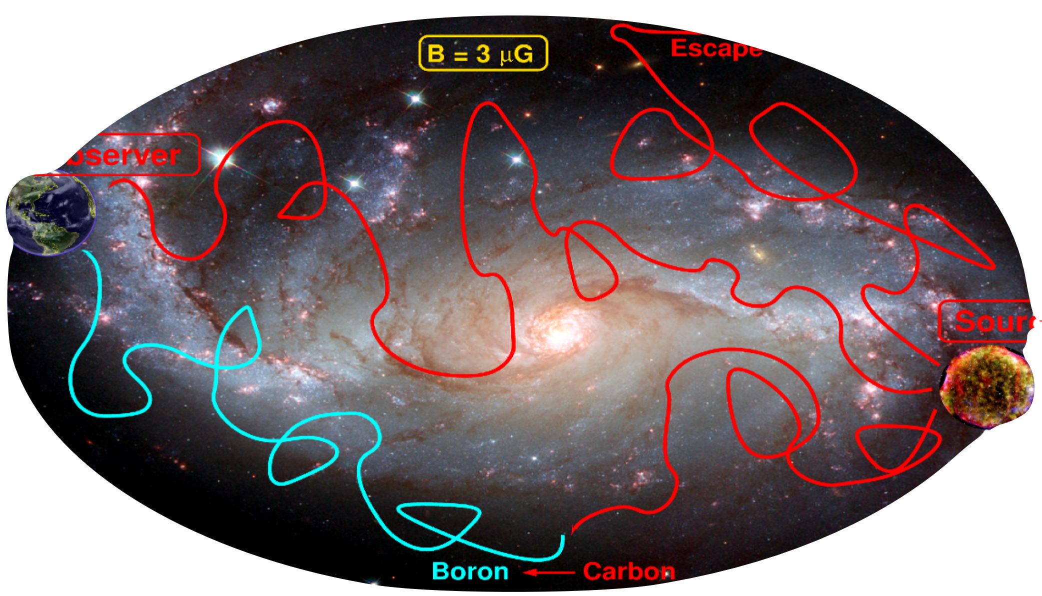

Transport equation for cosmic rays in the Galaxy

diffusion

energy loss (Bethe Bloch)

loss through interactions
with ISM (spallation)

loss through radioactive decay

$$\frac{\partial N_i}{\partial t} = \nabla(D_i \nabla N_i) - \frac{\partial}{\partial E}(b_i N_i) - n\nu\sigma_i N_i - \frac{N_i}{\gamma\tau_i} + Q_i + \sum_{j>i} n\nu\sigma_{ij} N_j + \sum_{j>i} \frac{N_j}{\gamma_j \tau_{ij}}$$

source term

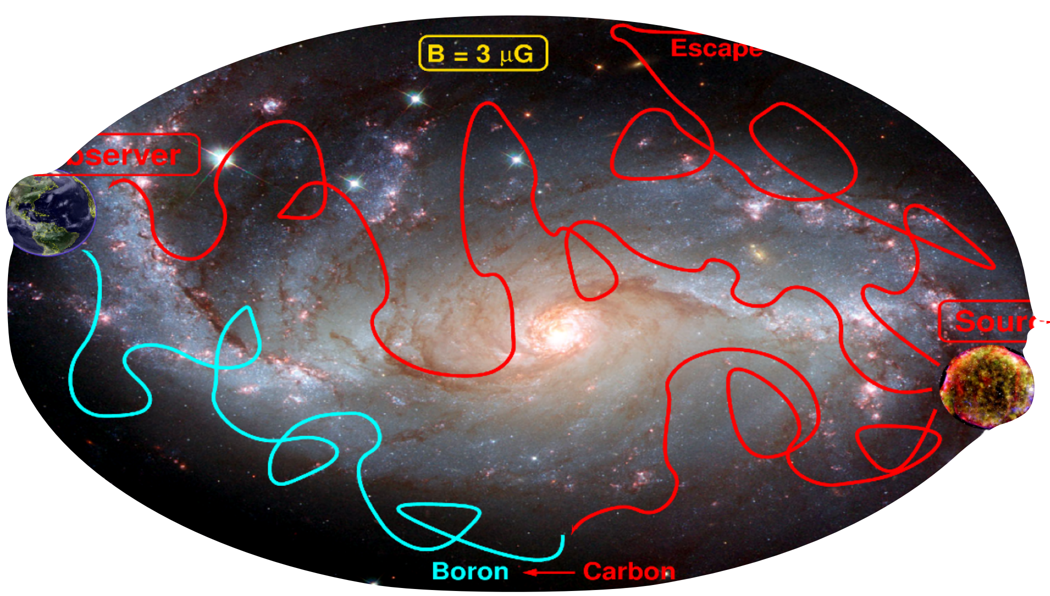

Transport equation for cosmic rays in the Galaxy

diffusion

energy loss (Bethe Bloch)

loss through interactions with ISM (spallation)

loss through radioactive decay

$$\frac{\partial N_i}{\partial t} = \nabla(D_i \nabla N_i) - \frac{\partial}{\partial E}(b_i N_i) - n\nu\sigma_i N_i - \frac{N_i}{\gamma\tau_i} + Q_i + \sum_{j>i} n\nu\sigma_{ij} N_j + \sum_{j>i} \frac{N_j}{\gamma_j \tau_{ij}}$$

source term

production through spallation of heavy nuclei

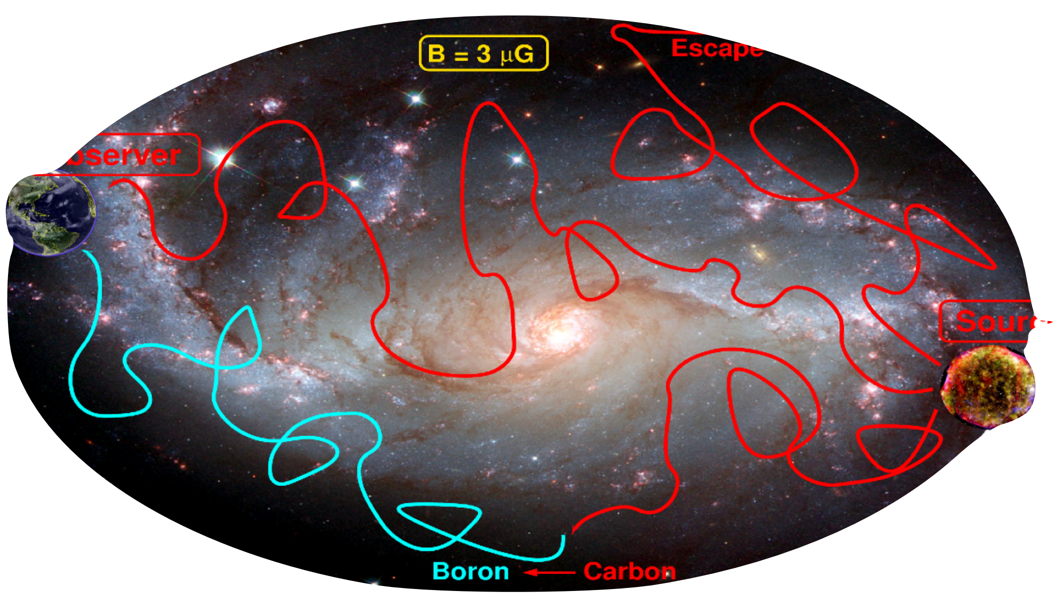

Transport equation for cosmic rays in the Galaxy

diffusion

energy loss (Bethe Bloch)

loss through interactions with ISM (spallation)

loss through radioactive decay

$$\frac{\partial N_i}{\partial t} = \nabla(D_i \nabla N_i) - \frac{\partial}{\partial E}(b_i N_i) - n\nu\sigma_i N_i - \frac{N_i}{\gamma\tau_i} + Q_i + \sum_{j>i} n\nu\sigma_{ij} N_j + \sum_{j>i} \frac{N_j}{\gamma_j \tau_{ij}}$$

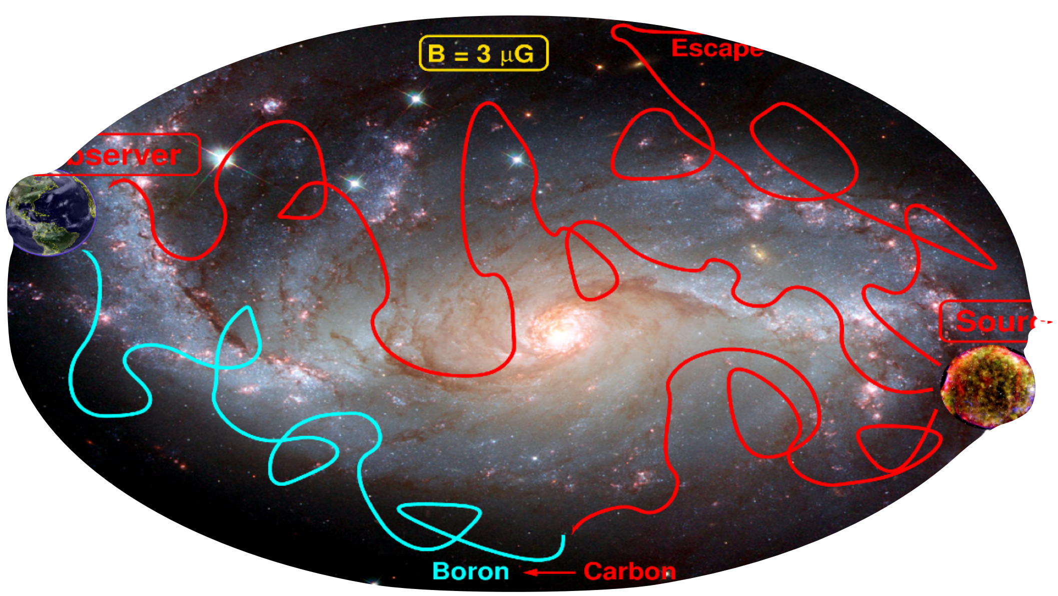

source term

production through spallation of heavy nuclei

production through decay of heavy nuclei

Transport equation f
Ga

diffusion

energy loss (Bethe Bloc

loss through
with

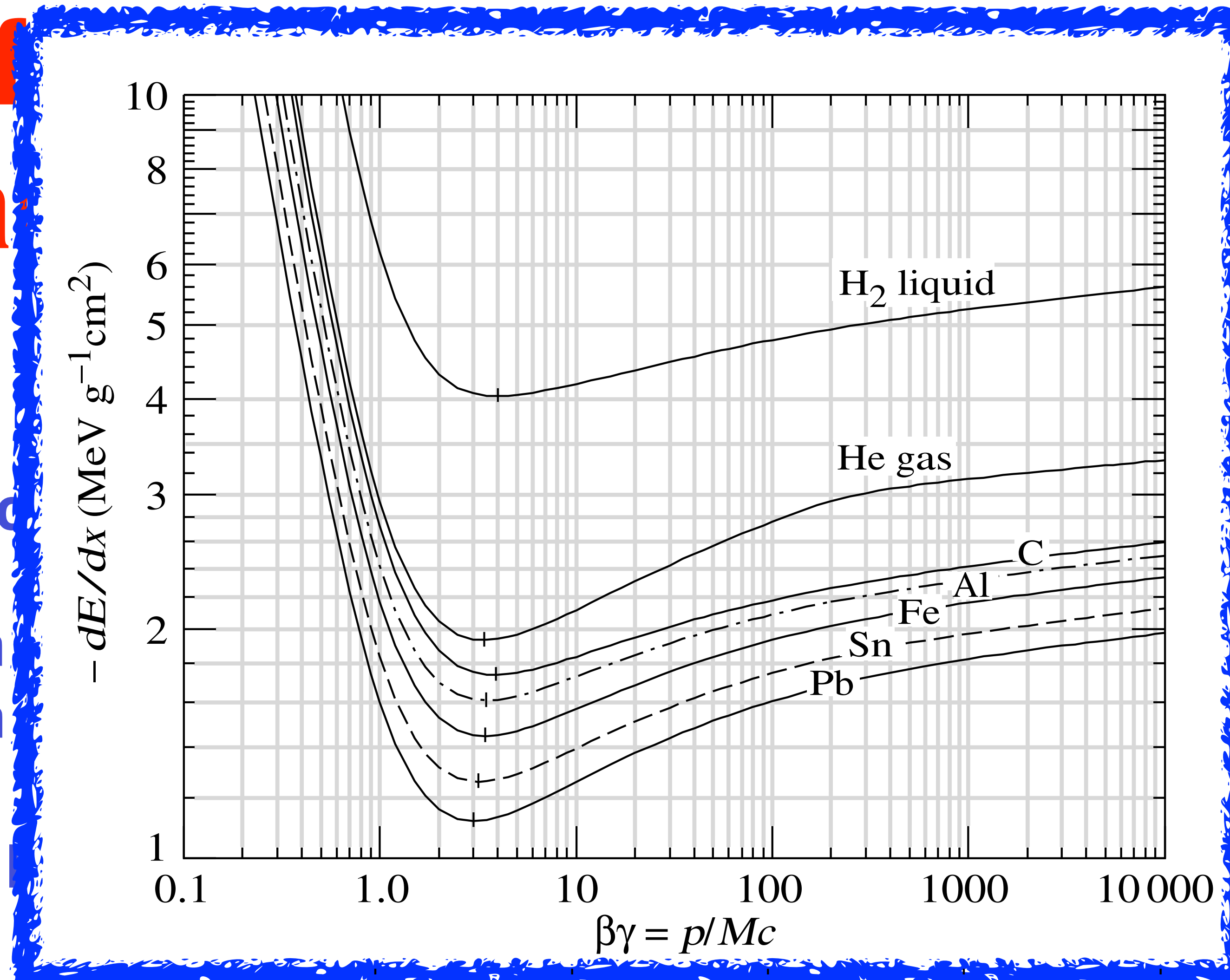

$$\frac{\partial N_i}{\partial t} = \nabla(D_i \nabla N_i) - \cancel{\frac{\partial}{\partial E}(b_i N_i)} - n\nu\sigma_i N_i - \frac{N_i}{\gamma\tau_i} + Q_i + \sum_{j>i} n\nu\sigma_{ij} N_j + \sum_{j>i} \frac{N_j}{\gamma_j \tau_{ij}}$$

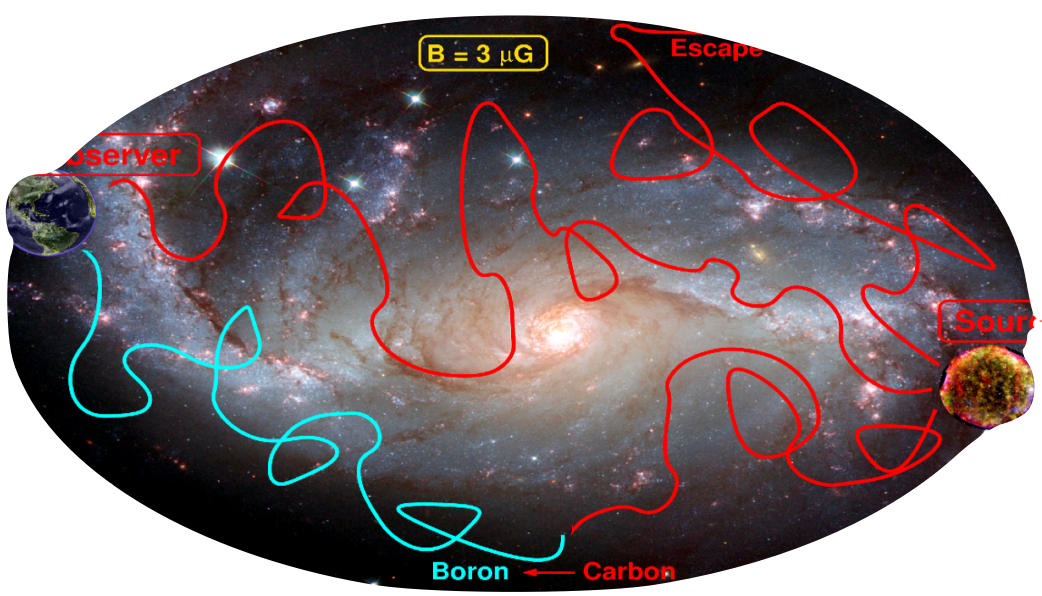

source term

production through spallation
of heavy nuclei

production through decay
of heavy nuclei

Transport equation for cosmic rays in the Galaxy

diffusion

energy loss (Bethe Bloch)

loss through interactions
with ISM (spallation)

loss through radioactive decay

$$\frac{\partial N_i}{\partial t} = \nabla(D_i \nabla N_i) - \cancel{\frac{\partial}{\partial E}(b_i N_i)} - n v \sigma_i N_i - \frac{N_i}{\gamma \tau_i} + Q_i + \sum_{j>i} n v \sigma_{ij} N_j + \sum_{j>i} \frac{N_j}{\gamma_j \tau_{ij}}$$

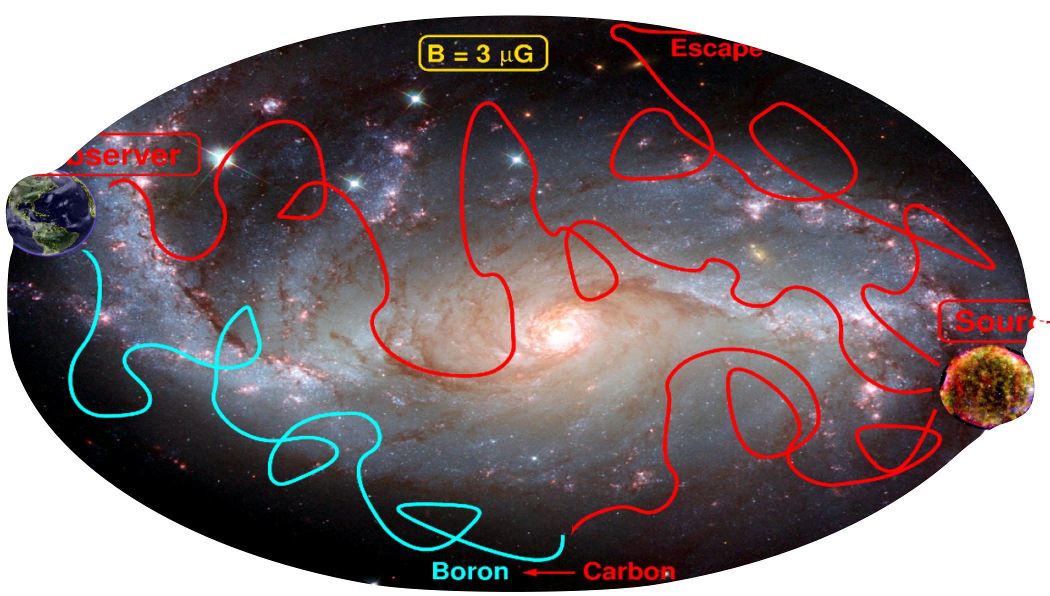

source term

production through spallation
of heavy nuclei

production through decay
of heavy nuclei

1st order Fermi acceleration at strong shock

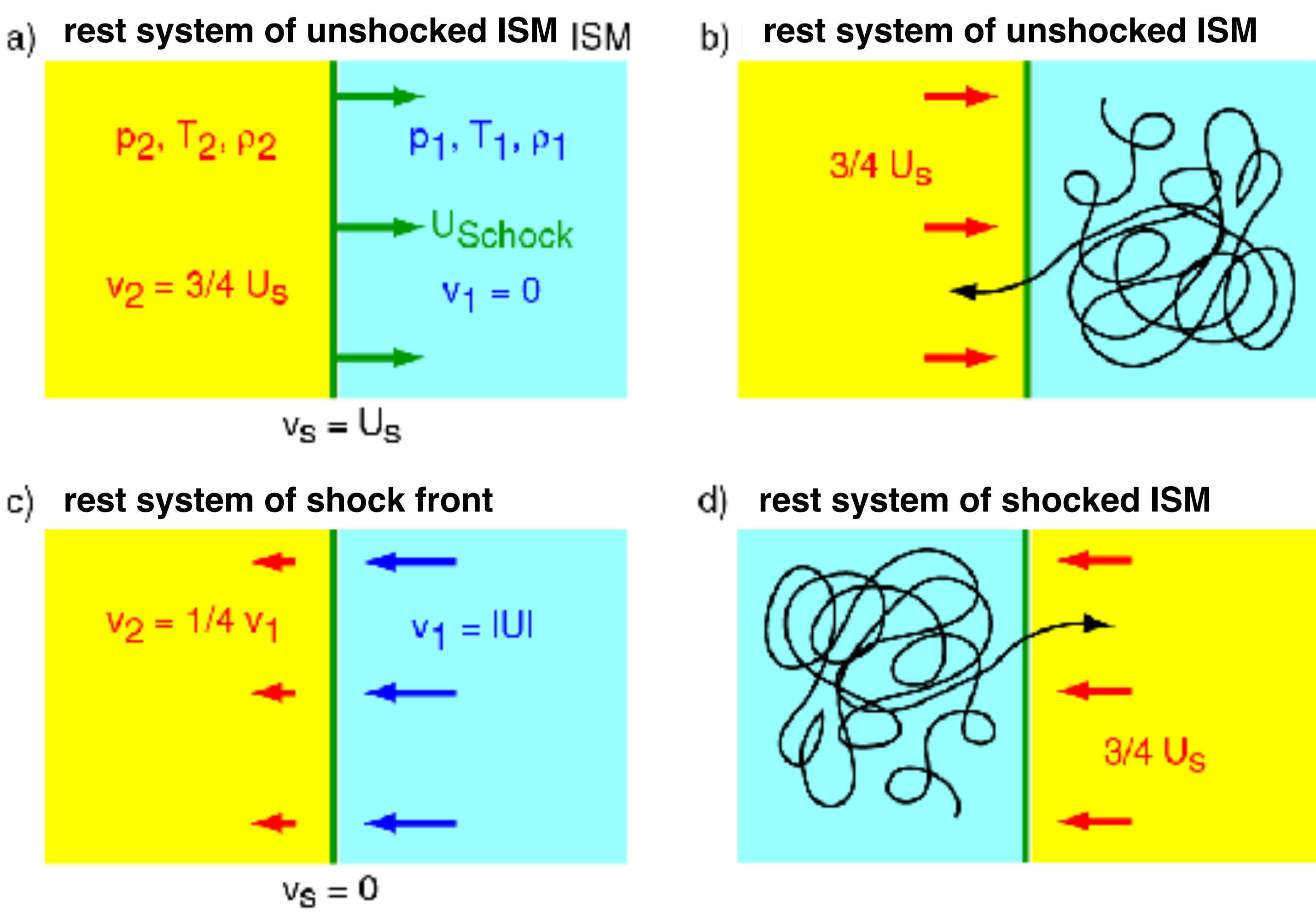

Bell, Blanford,Ostriker (1978)

energy gain $$\frac{\Delta E}{E} \propto \frac{U_s}{c}$$

$$N(E)\, dE \propto E^{-2}\, dE$$

power law with spectral index -2.0 ... -2.1

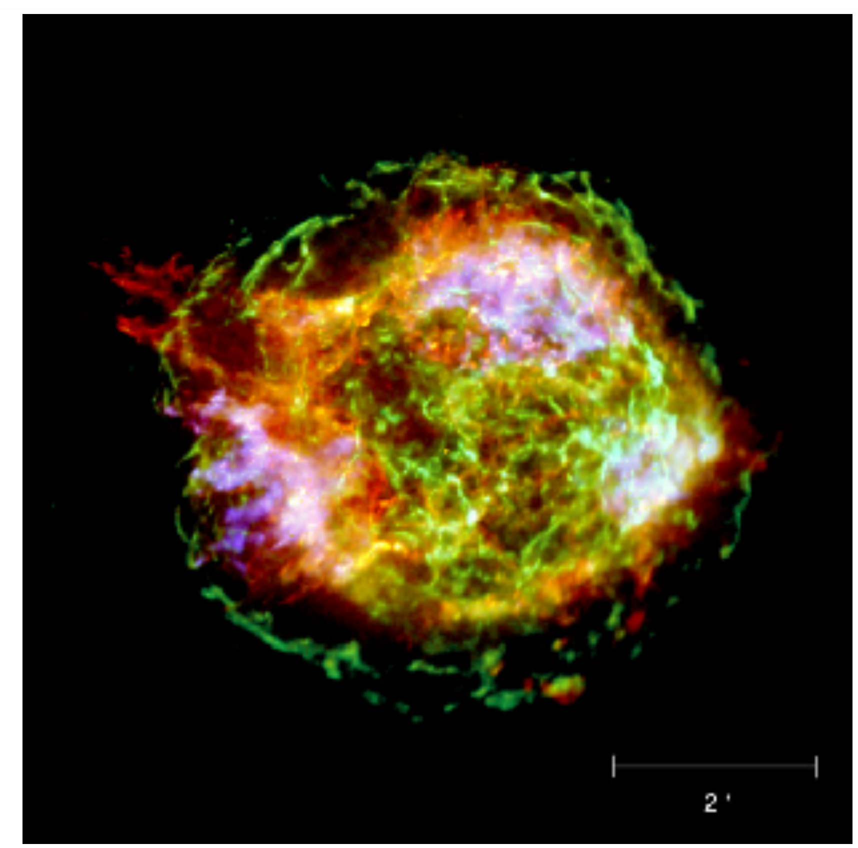

Supernova remnant (SNR) Cassiopeia A

H.E.S.S. supernova remnant RXJ 1713

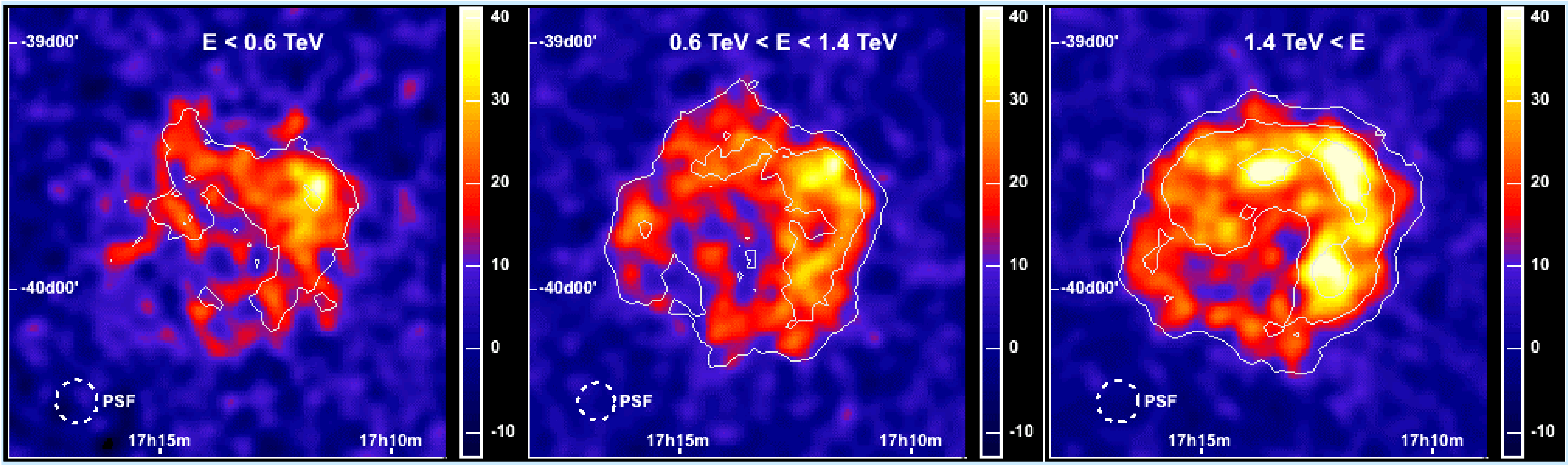

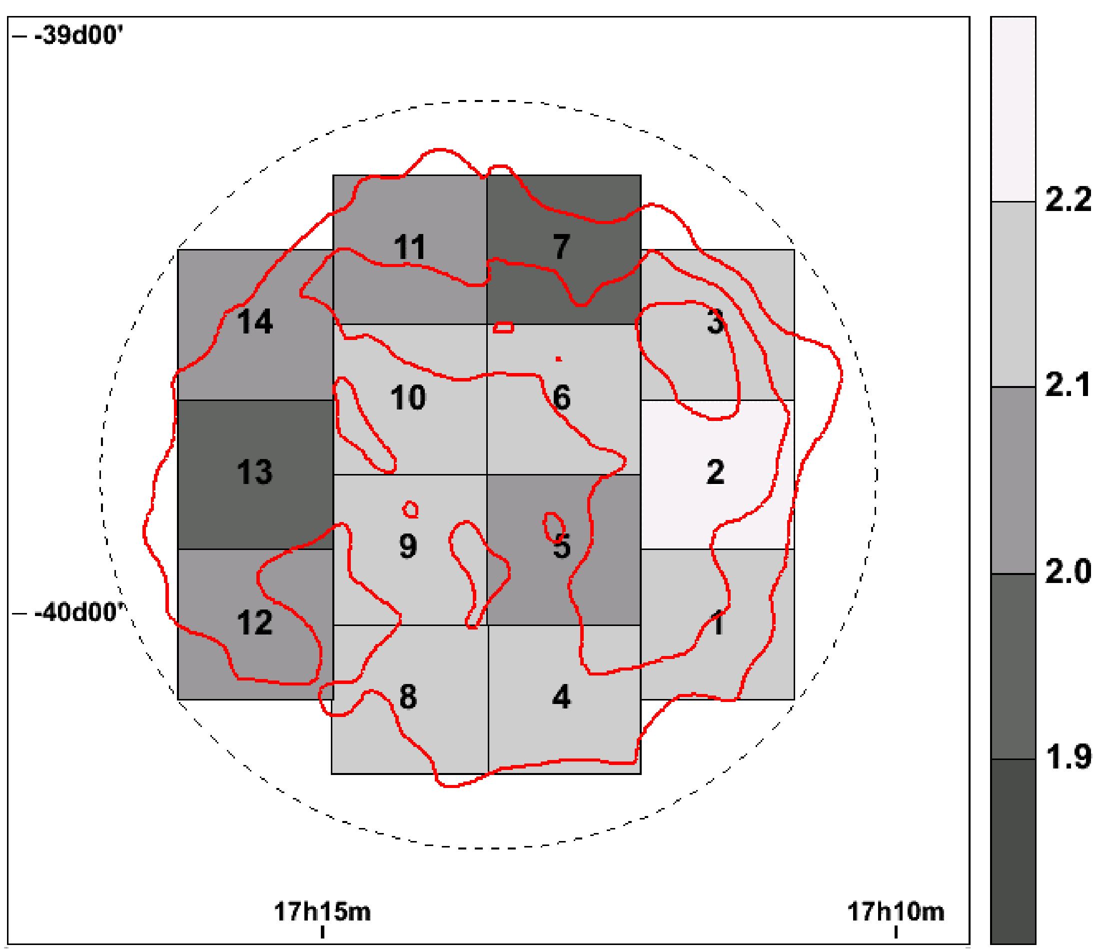

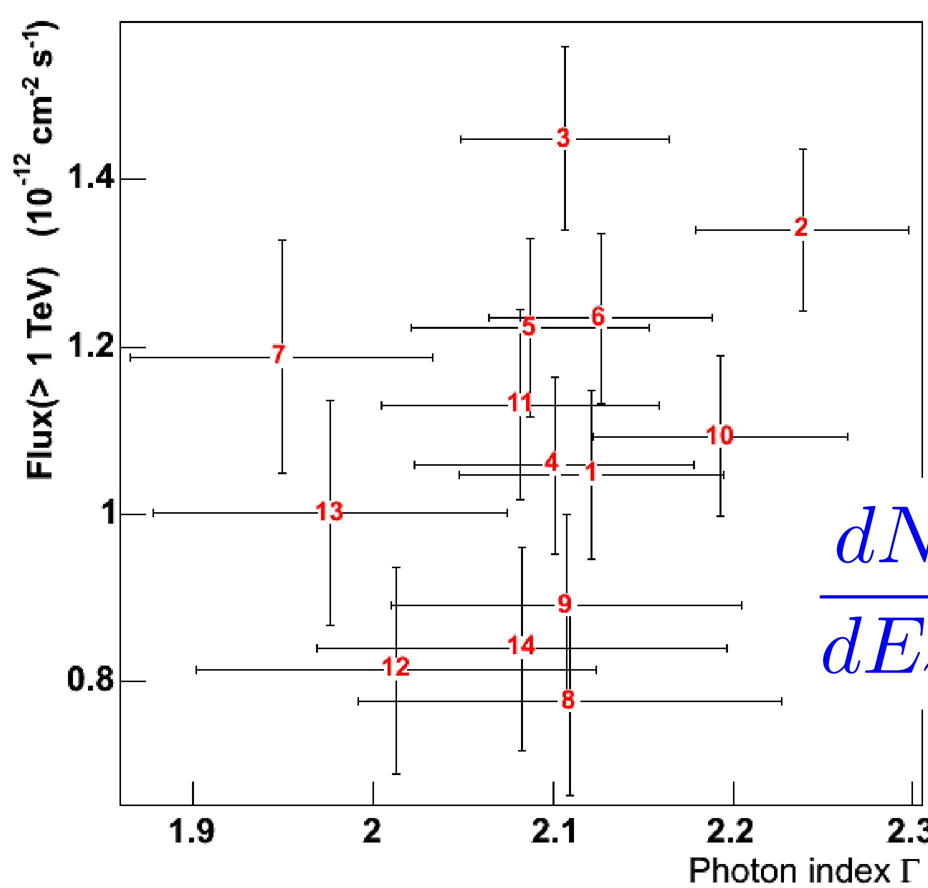

$$\frac{dN}{dE_\gamma} \propto E_\gamma^{-\Gamma}$$

Acceleration of cosmic rays at SNR

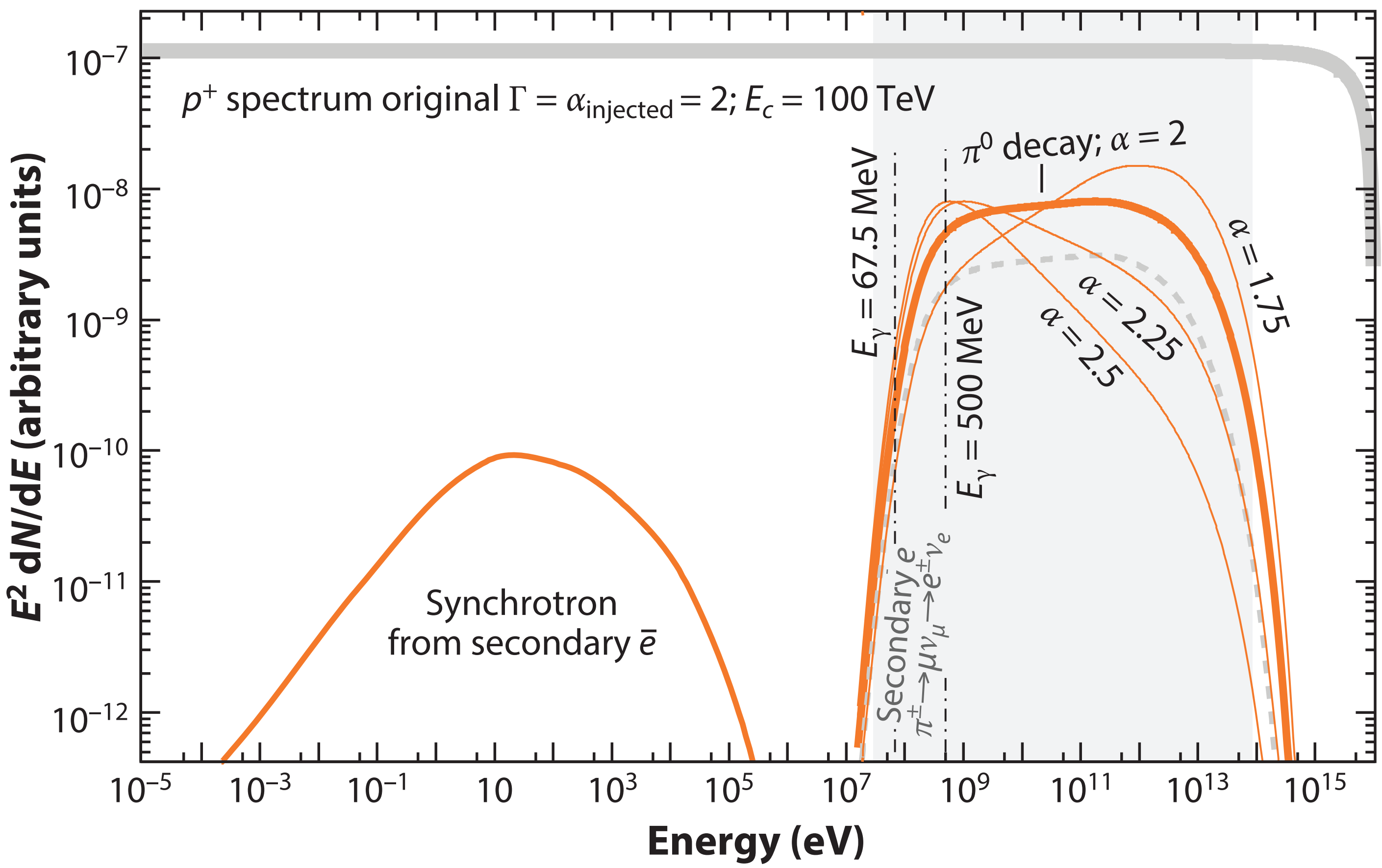

Figure 3

Spectral energy distribution of accelerated protons (power-law index $\alpha_{\mathrm{injected}} = 2.0$ and cutoff at 100 TeV) and γ-rays resulting from inelastic collisions with interstellar material. The dominant emission into photons occurs via the decay $\pi^0 \rightarrow \gamma\gamma$ (*solid orange curves*). The γ-ray spectrum follows the parent protons' spectrum rather closely in the midenergy range and in the high-energy cutoff region. For all proton indices, the low-energy turnover is a characteristic feature of the pion-decay emission. Also shown is the spectrum of electrons resulting from the inelastic proton–proton interactions via the decay chain $\pi^\pm \rightarrow \mu + \nu_\mu \rightarrow e^\pm \nu_e$ (*dashed gray curve*). For the synchrotron emission from these so-called secondary electrons, a source with age $t_{\mathrm{age}} = 1{,}000$ years and $B = 30\ \mu$G have been assumed. The shaded gray region shows the sensitive range of current γ-ray detectors (*Fermi*-LAT, imaging atmospheric Cherenkov detectors).

The emissivity can be turned into a flux at Earth by an astrophysical accelerator that puts a fraction ϵ_{CR} of its energy output E_{pr} into the acceleration of protons:

$$F_\gamma(>100\,\mathrm{MeV}) = 4.4 \times 10^{-7} \epsilon_{\mathrm{CR}} \frac{E_{\mathrm{pr}}}{10^{51}\,\mathrm{erg}} \frac{d}{\mathrm{kpc}}^{-2} \frac{n}{1\,\mathrm{cm}^{-3}} \mathrm{cm}^{-2}\,\mathrm{s}^{-1}. \qquad 3.$$

In other words, if the distance d and the density of the interaction region n are known, the amount of energy in protons E_{pr} at the interaction site can be directly inferred from the γ-ray flux F_γ.

S. Funk, Ann. Rev. Nucl. Part. Sci. 65 (2015) 245

Acceleration of cosmic rays at SNR

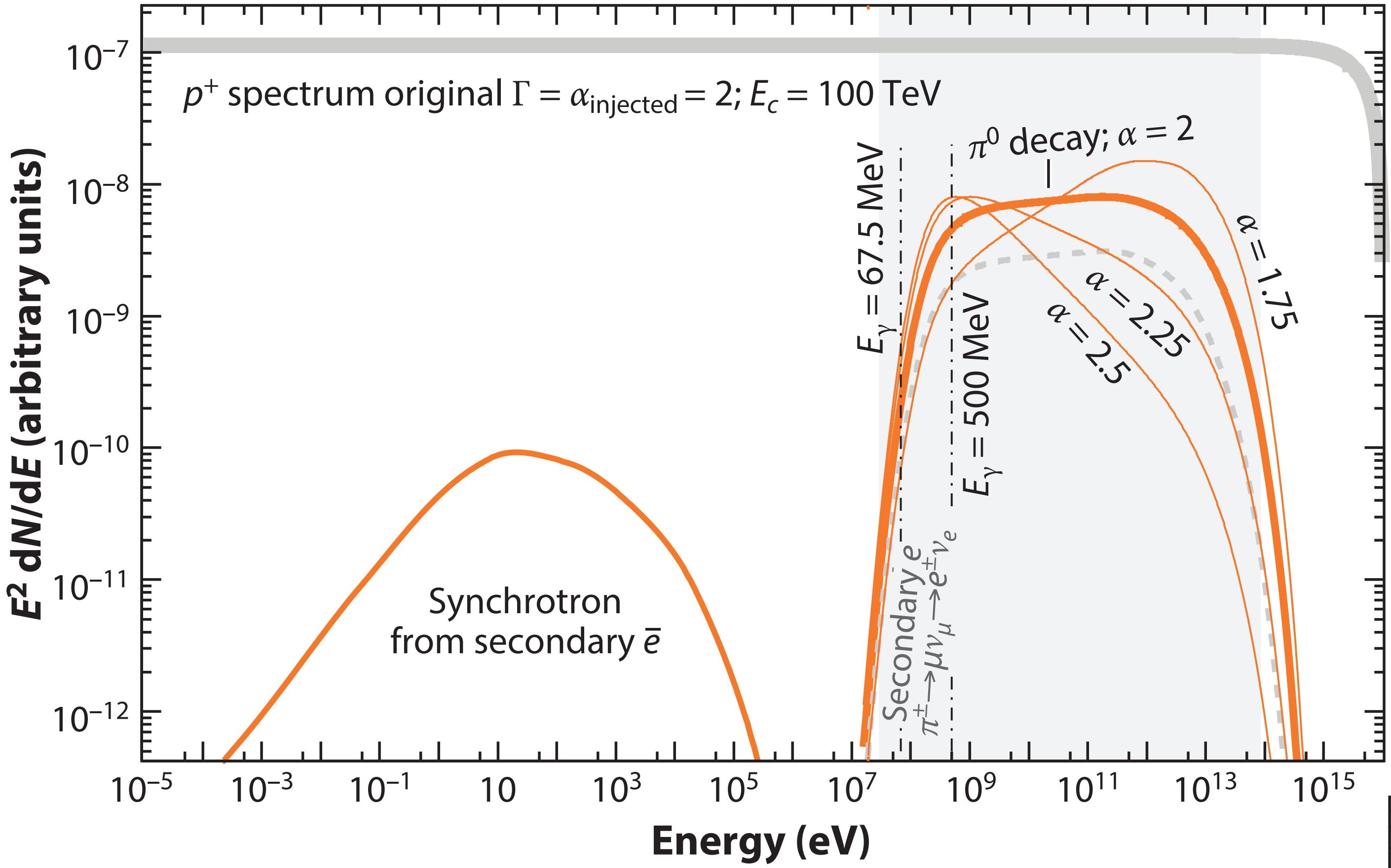

Figure 3

Spectral energy distribution of accelerated protons (power-law index $\alpha_{\rm injected} = 2.0$ and cutoff at 100 TeV) and γ-rays resulting from inelastic collisions with interstellar material. The dominant emission into photons occurs via the decay $\pi^0 \to \gamma\gamma$ (*solid orange curves*). The γ-ray spectrum follows the parent protons' spectrum rather closely in the midenergy range and in the high-energy cutoff region. For all proton indices, the low-energy turnover is a characteristic feature of the pion-decay emission. Also shown is the spectrum of electrons resulting from the inelastic proton–proton interactions via the decay chain $\pi^\pm \to \mu + \nu_\mu \to e^\pm \nu_e$ (*dashed gray curve*). For the synchrotron emission from these so-called secondary electrons, a source with age $t_{\rm age} = 1{,}000$ years and $B = 30\ \mu$G have been assumed. The shaded gray region shows the sensitive range of current γ-ray detectors (*Fermi*-LAT, imaging atmospheric Cherenkov detectors).

The emissivity can be turned into a flux at Earth by an astrophysical accelerator that puts a fraction $\epsilon_{\rm CR}$ of its energy output $E_{\rm pr}$ into the acceleration of protons:

$$F_\gamma(>100\,{\rm MeV}) = 4.4 \times 10^{-7} \epsilon_{\rm CR} \frac{E_{\rm pr}}{10^{51}\,{\rm erg}} \frac{d}{\rm kpc}^{-2} \frac{n}{1\,{\rm cm}^{-3}} {\rm cm}^{-2}\,{\rm s}^{-1}. \qquad 3.$$

In other words, if the distance d and the density of the interaction region n are known, the amount of energy in protons $E_{\rm pr}$ at the interaction site can be directly inferred from the γ-ray flux F_γ.

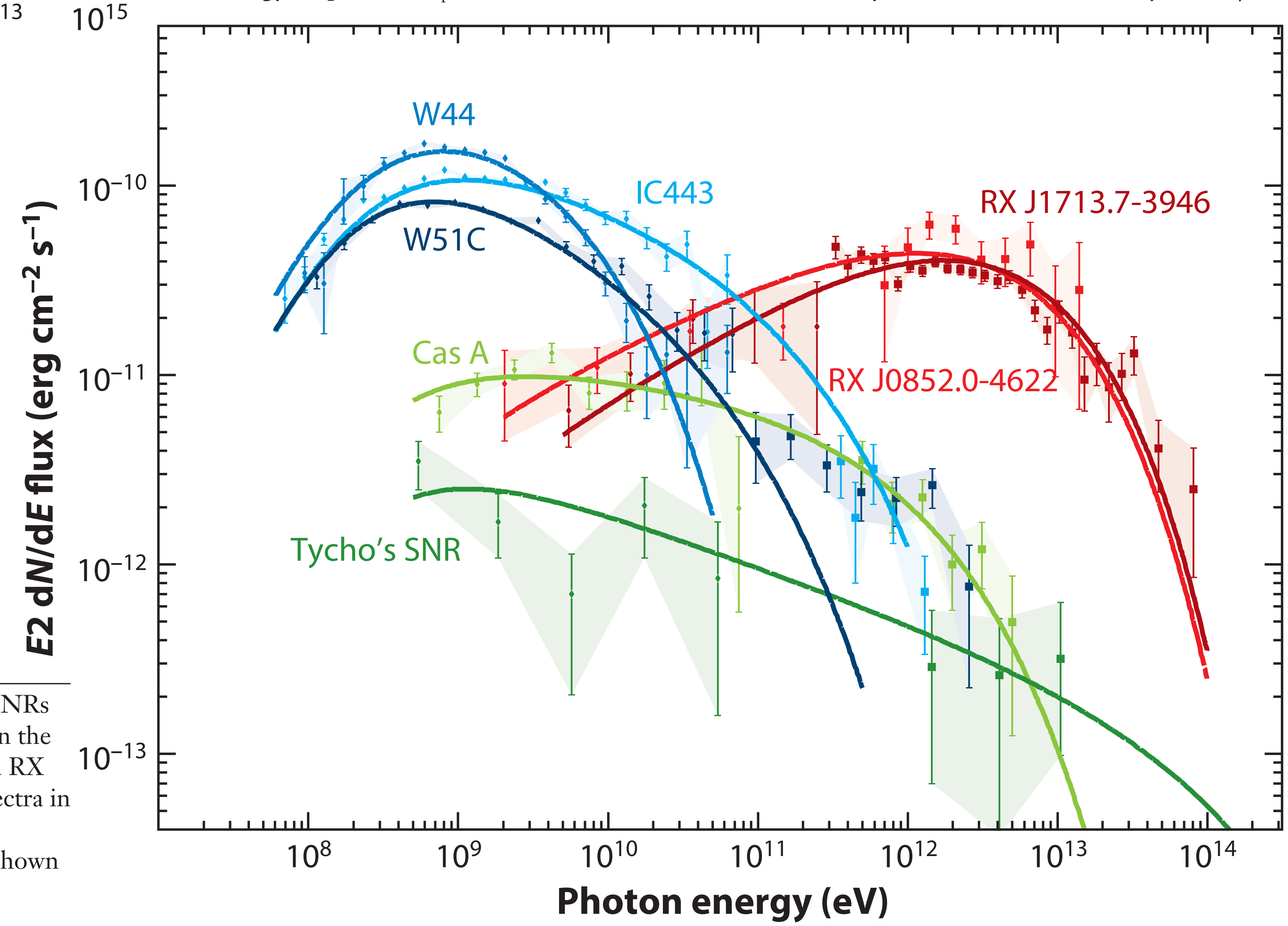

Figure 6

Typical γ-ray energy spectra for several of the most prominent supernova remnants (SNRs). Young SNRs (<1,000 years) are shown in green. These typically show smaller γ-ray fluxes but rather hard spectra in the GeV and TeV bands. The older (but still referred to as young) shell-type SNRs RX J1713.7-3946 and RX J0852.0-4622 (Vela Junior) of ages ~2,000 years are shown in shades of red. These show very hard spectra in the GeV band ($\Gamma = 1.5$) and a peak in the TeV band with an exponential cutoff beyond 10 TeV. The middle-aged SNRs (~20,000 years) interacting with molecular clouds (W44, W51C, and IC443) are shown in blue. Also shown are hadronic fits to the data (*solid lines*).

S. Funk, Ann. Rev. Nucl. Part. Sci. 65 (2015) 245

Article

Ultrahigh-energy photons up to 1.4 petaelectronvolts from 12 γ-ray Galactic sources

see Goodmann, ISCRA 2022

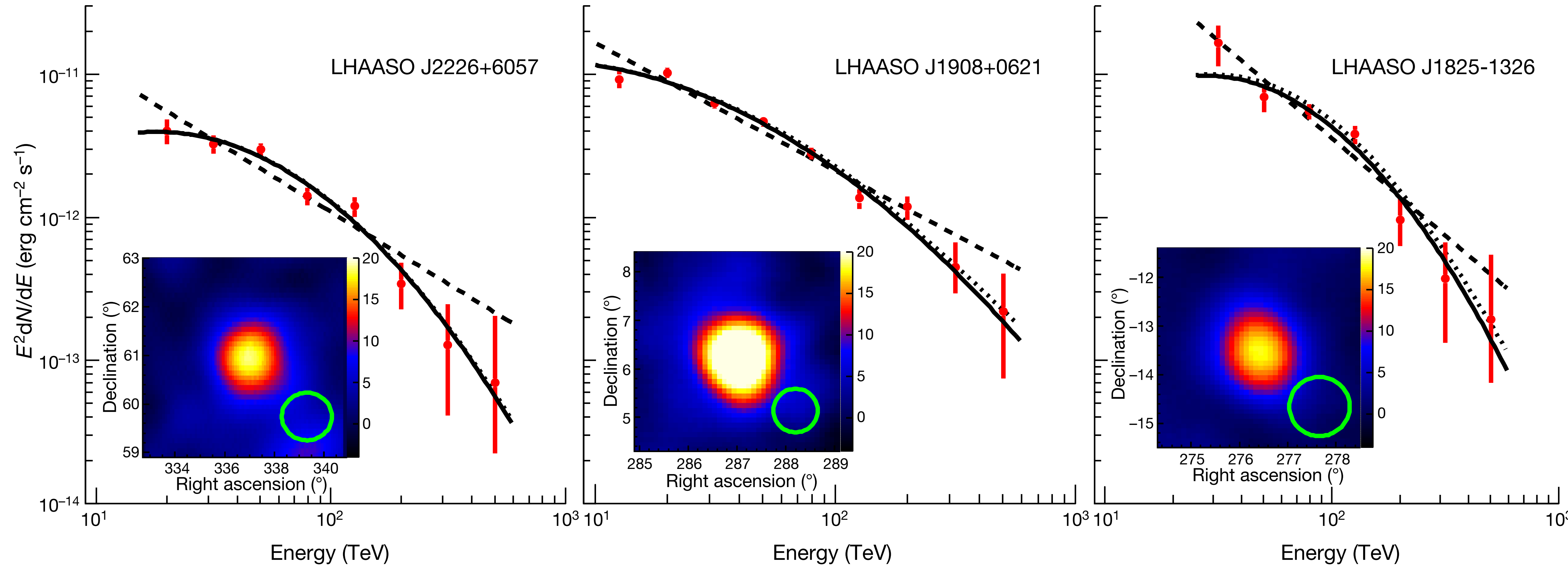

Fig. 1 | Spectral energy distributions and significance maps. a–c, Data are shown for LHAASO J2226+6057 (**a**), LHAASO J1908+0621 (**b**), and LHAASO J1825-1326 (**c**). Spectral fits with a log-parabola function (solid lines) in the form of $[E/(10\ \mathrm{TeV})]^{-a-b\log[E/(10\ \mathrm{TeV})]}$ are compared with the power-law fits $E^{-\Gamma}$ for: $a = 1.56$, $b = 0.88$ and $\Gamma = 3.01$ (**a**); $a = 2.27$, $b = 0.46$ and $\Gamma = 2.89$ (**b**); and $a = 0.92$, $b = 1.19$ and $\Gamma = 3.36$ (**c**). The dotted curves correspond to the log-parabola fits corrected for the interstellar γ–γ absorption (see Methods for the radiation fields and Extended Data Fig. 6 for the opacity curves). The comparison of the power-law (PL) model and the log-parabola (LOG) model with the Akaike Information Criterion[20] (AIC) gives: $AIC_{LOG} = 12.3$ and $AIC_{PL} = 24.4$ for LHAASO J2226+6057; $AIC_{LOG} = 15.1$ and $AIC_{PL} = 30.1$ for LHAASO J1908+0621; and $AIC_{LOG} = 11.6$ and $AIC_{PL} = 14.8$ for LHAASO J1825-1326. The insets show the significance maps of the three sources, obtained for γ-rays above 25 TeV. The colour bars show the square root of test statistics (TS), which is equivalent to the significance. The significance ($\sqrt{TS}$) maps are smoothed with the Gaussian-type point spread function (PSF) of each source. The size of PSFs (68% contamination regions) are shown at the bottom right of each map. We note that the PSFs of the three sources are slightly different owing to different inclination angles. Namely, the 68% contamination angles are 0.49° for LHAASO J2226+6057, 0.45° for LHAASO J1908+0621 and 0.62° for LHAASO J1825-1326. Error bars represent one standard deviation.

LHAASO, Nature 594 (2021) 33–36

general considerations about accelerators

trajectory of particle in B field

centripedal force = Lorentz force

$$m\frac{v^2}{r} = q \cdot v \cdot B \qquad\qquad m \cdot v = p$$ **momentum**

$$\frac{p}{r} = Z \cdot e \cdot B$$

$$r_L = \frac{p}{z \cdot e \cdot B}$$ **Larmor radius**

L **dimension of accelerator**

$L > 2\, r_L$

closer look (Hillas 1984): $L > \frac{2r_L}{\beta}$

velocity of scattering centers $\beta = \frac{v}{c}$

A.M. Hillas, Ann. Rev. Astron. Astrophys. 22 (1984) 425

$$L > \frac{2 \cdot p}{z \cdot e \cdot B \cdot \beta}$$

$$\boxed{B \cdot L > \frac{2 \cdot p}{z \cdot e \cdot \beta}}$$ **Hillas criterion**

in astrophyscial units

$$r_L = 1.08 \text{ pc} \frac{E_{15}}{Z \cdot B_{\mu G}}$$

$$\boxed{B_{\mu G} \cdot L_{pc} > \frac{2 \cdot E_{15}}{Z \cdot \beta}}$$ **necessary condition not sufficient**

$$E_{15} < Z \cdot B_{\mu G} \cdot L_{pc} \cdot \frac{\beta}{2}$$

A.M. Hillas, Ann. Rev. Astron. Astrophys. 22 (1984) 425

Contribution of (regular) SNR-CR

$$E_c = Z \cdot 4.5\ 10^6\ \text{GeV}$$

$$Q(p) = AQ_0(Ap)^{-q} \exp\left(-\frac{Ap}{Zp_c}\right),$$

Table 1. Source spectral indices, q, and energy injected per supernova, f, for the different species of cosmic rays used in the calculation of the SNR-CRs spectra shown in Figures 1 and 2.

Particle type	q	f $(\times 10^{49}$ ergs)
Proton	2.24	6.95
Helium	2.21	0.79
Carbon	2.21	2.42×10^{-2}
Oxygen	2.25	2.52×10^{-2}
Neon	2.25	3.78×10^{-3}
Magnesium	2.29	5.17×10^{-3}
Silicon	2.25	5.01×10^{-3}
Iron	2.25	4.95×10^{-3}

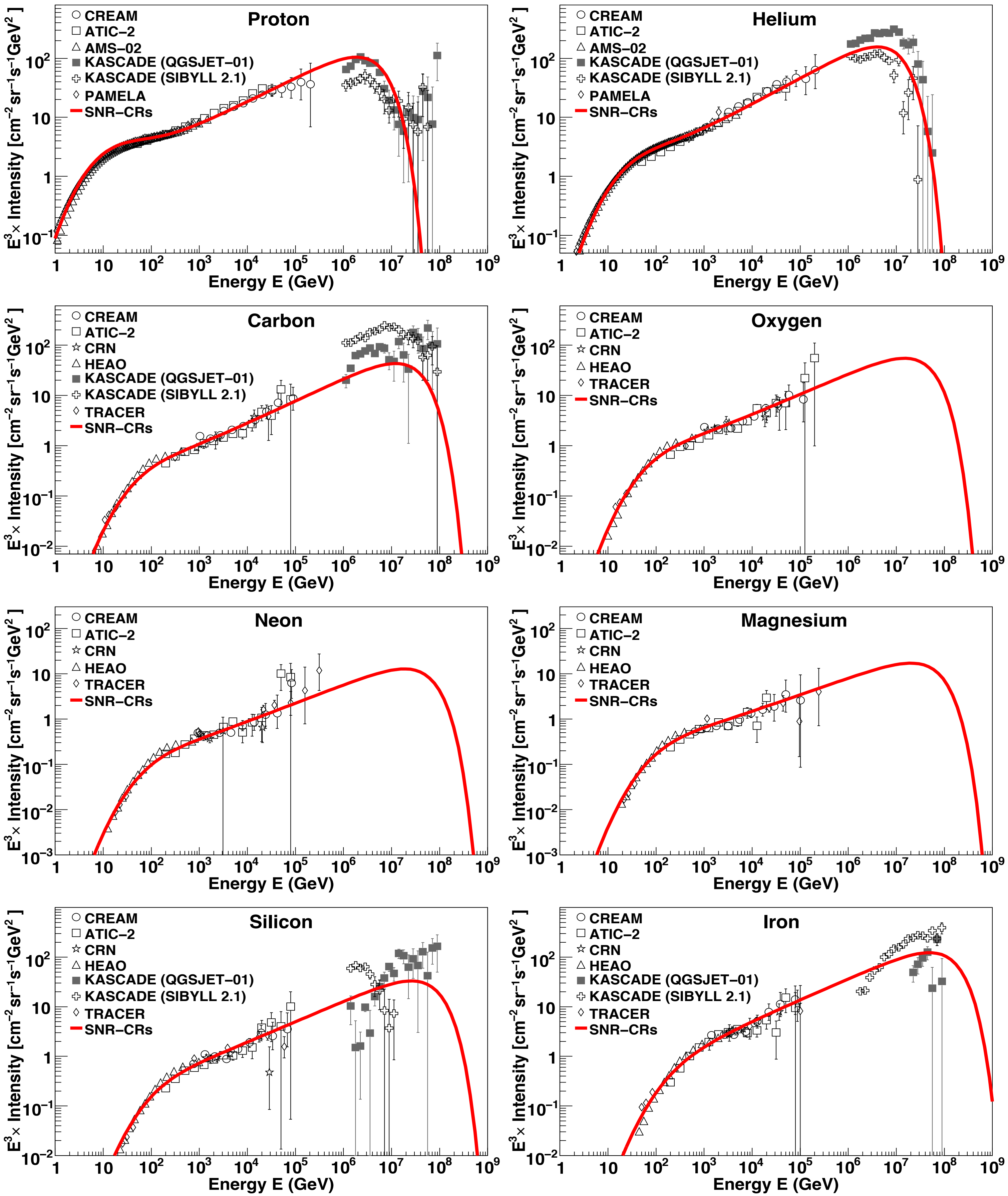

Fig. 1. Energy spectra for different cosmic-ray elements. *Solid line*: Model prediction for the SNR-CRs. *Data*: CREAM (Ahn et al. 2009; Yoon et al. 2011), ATIC-2 (Panov et al. 2007), AMS-02 (Aguilar et al. 2015a,b), PAMELA (Adriani et al. 2011), CRN (Müller et al. 1991; Swordy et al. 1990), HEAO (Engelmann et al. 1990), TRACER (Obermeier et al. 2011), and KASCADE (Antoni et al. 2005). Cosmic-ray source parameters (q, f) used in the calculation are given in Table 1. For the other model parameters (D_0, a, η, s), see text for details.

S. Thoudam et al., A&A 595 (2016) A33

Transport equation for cosmic rays in the Galaxy

diffusion

energy loss (Bethe Bloch)

loss through interactions with ISM (spallation)

loss through radioactive decay

$$\frac{\partial N_i}{\partial t} = \nabla(D_i \nabla N_i) - \cancel{\frac{\partial}{\partial E}(b_i N_i)} - n v \sigma_i N_i - \frac{N_i}{\gamma \tau_i} + Q_i + \sum_{j>i} n v \sigma_{ij} N_j + \sum_{j>i} \frac{N_j}{\gamma_j \tau_{ij}}$$

source term

production through spallation of heavy nuclei

production through decay of heavy nuclei

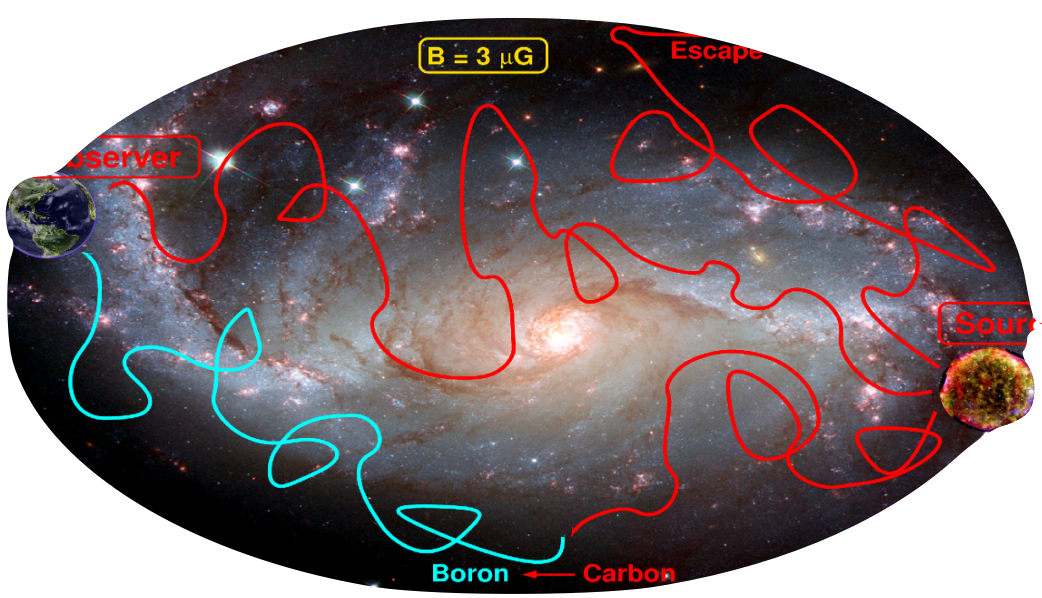

Pathlength of cosmic rays in Galaxy

TRACER balloon experiment

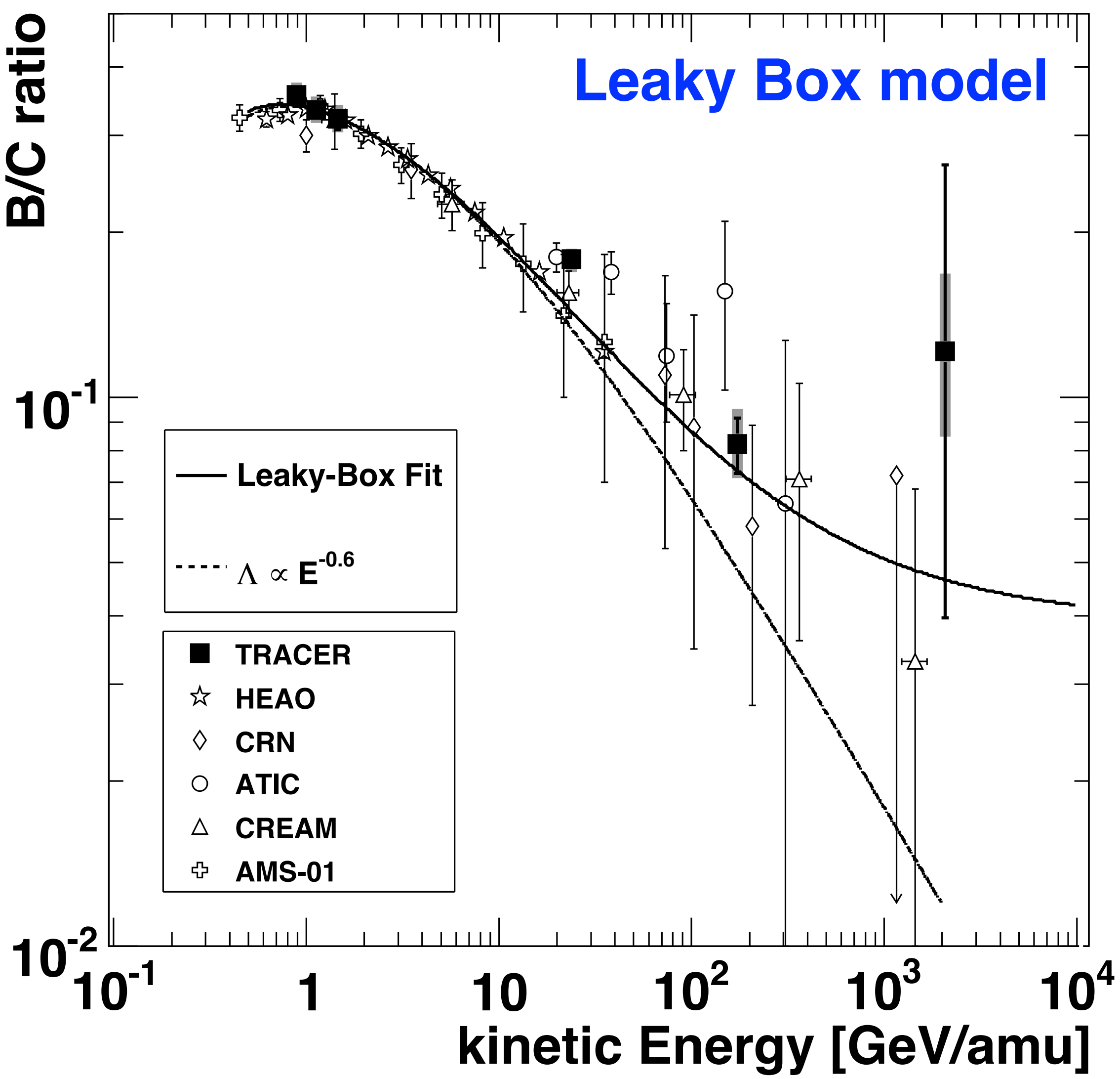

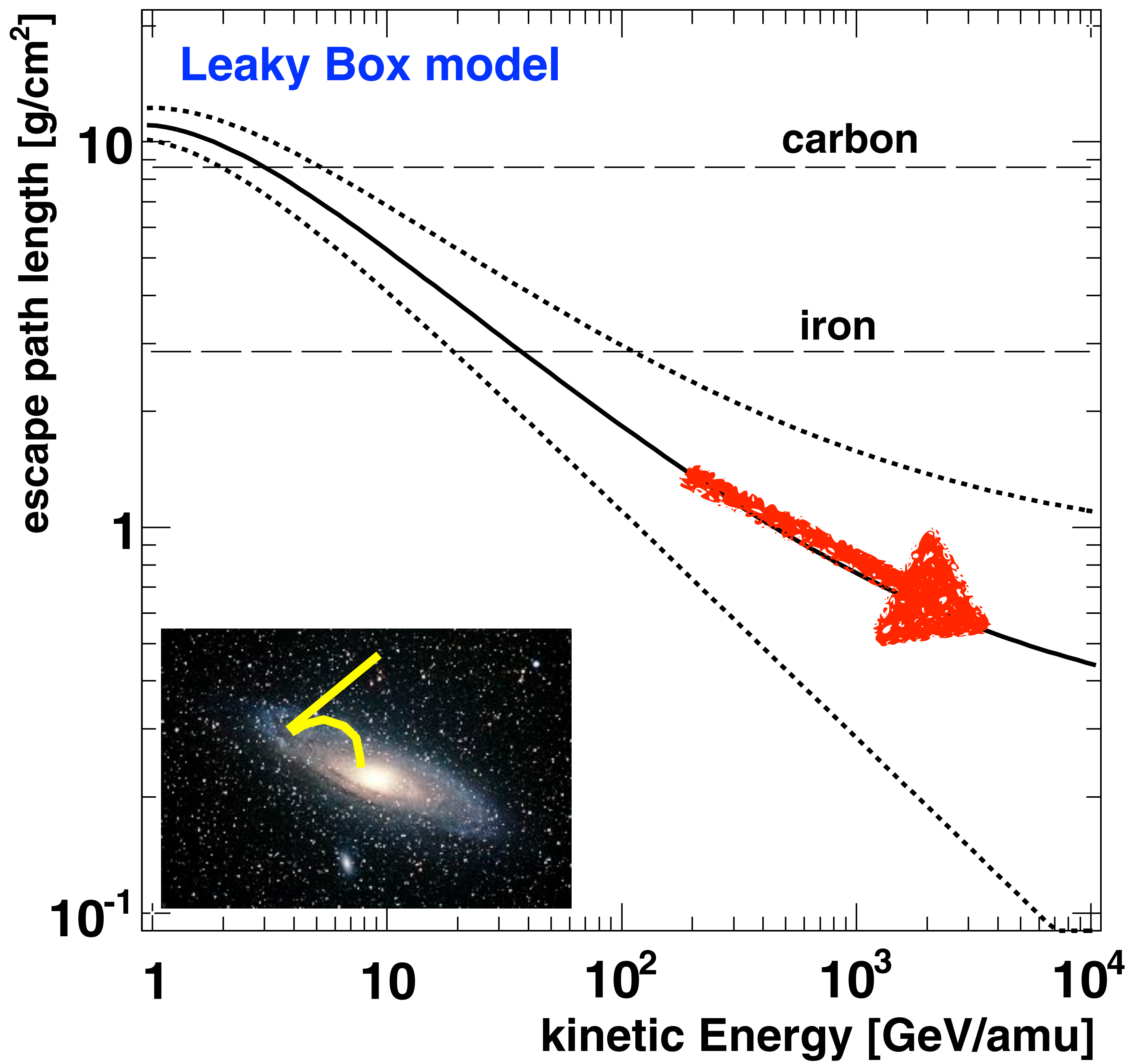

Escape Path Length:

$$\Lambda_{esc}(E) = CE^{-\delta} + \Lambda_0$$

- Propagation index: $\delta = 0.64 \pm 0.02$.
- Residual path length: $\Lambda_0 = 0.7 \pm 0.2$ g/cm^2.

$$\Lambda(R) = \frac{26.7\beta}{(\beta R)^{\delta} + (0.714 \cdot \beta R)^{-1.4}} + \Lambda_0 \text{ g/cm}^2,$$

A. Obermeier et al., ApJ 752 (2012) 69

Pathlength vs. interaction length

pathlength in Galaxy $\lambda_{esc} = 5 - 10 \text{ g/cm}^2$

interaction length

nuclear radius $r = r_0 A^{1/3} \qquad r_0 = 1.3 \cdot 10^{-13} \text{ cm}$

cross section $\sigma_{p-A} = \pi (r_p + r_0 A^{1/3})^2$

ISM: protons $n = 1/\text{cm}^3 \quad \rho = 1.67 \cdot 10^{-24} \text{ g/cm}^3$

interaction length $\lambda_{p-A} = \dfrac{\rho}{\sigma_{p-A} \cdot n}$

$$\lambda_{p-p} = 21 \text{ g/cm}^2 \qquad > \lambda_{esc}$$

$$\lambda_{p-Fe} = 1.6 \text{ g/cm}^2 \qquad < \lambda_{esc}$$

Shape of energy spectrum

$$\frac{dN}{dE} \propto E_0^{\gamma}$$

at source γ ~ -2.1

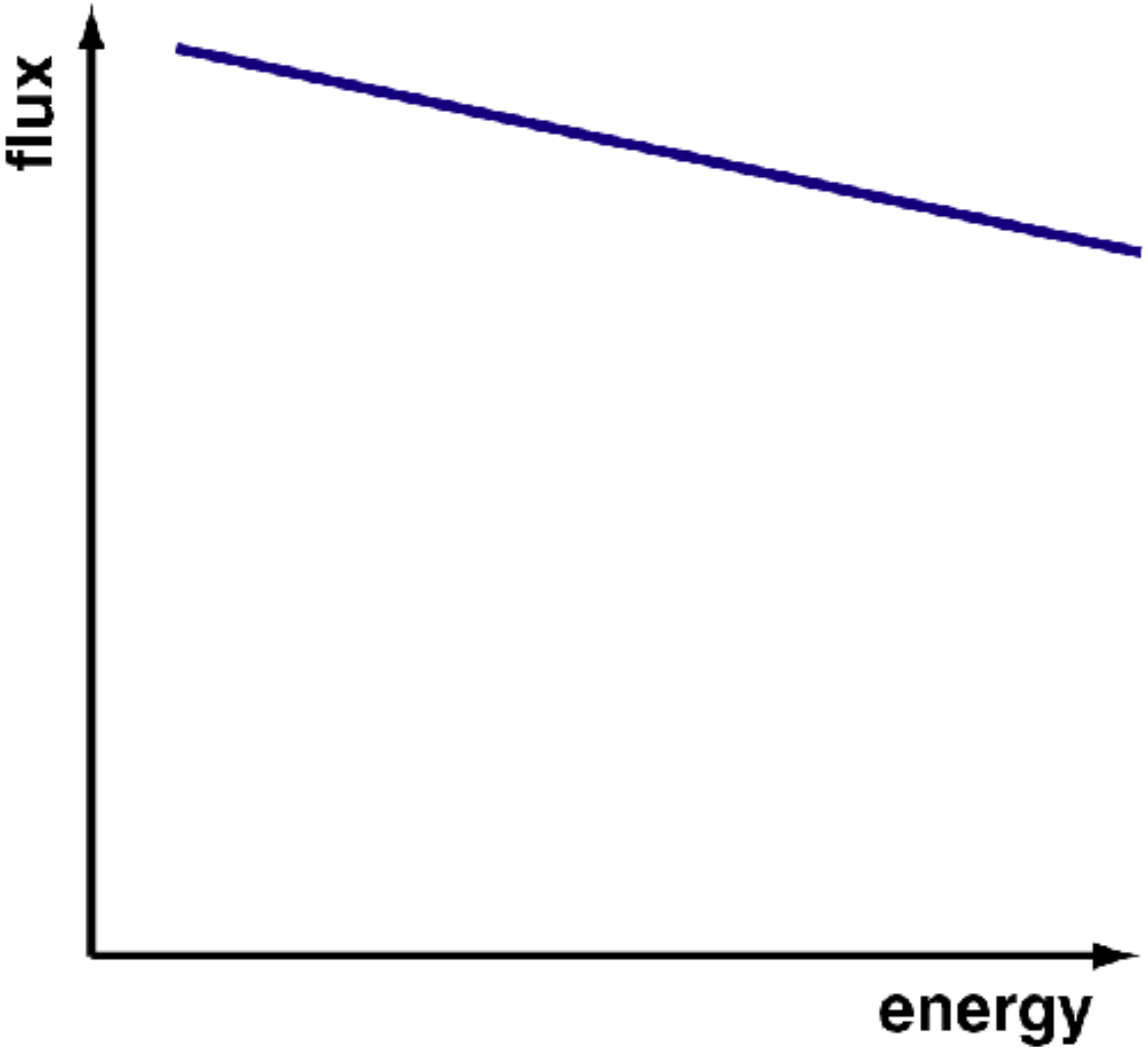

Shape of energy spectrum

$$\frac{dN}{dE} \propto E_0^{\gamma}$$

at source γ ~ -2.1

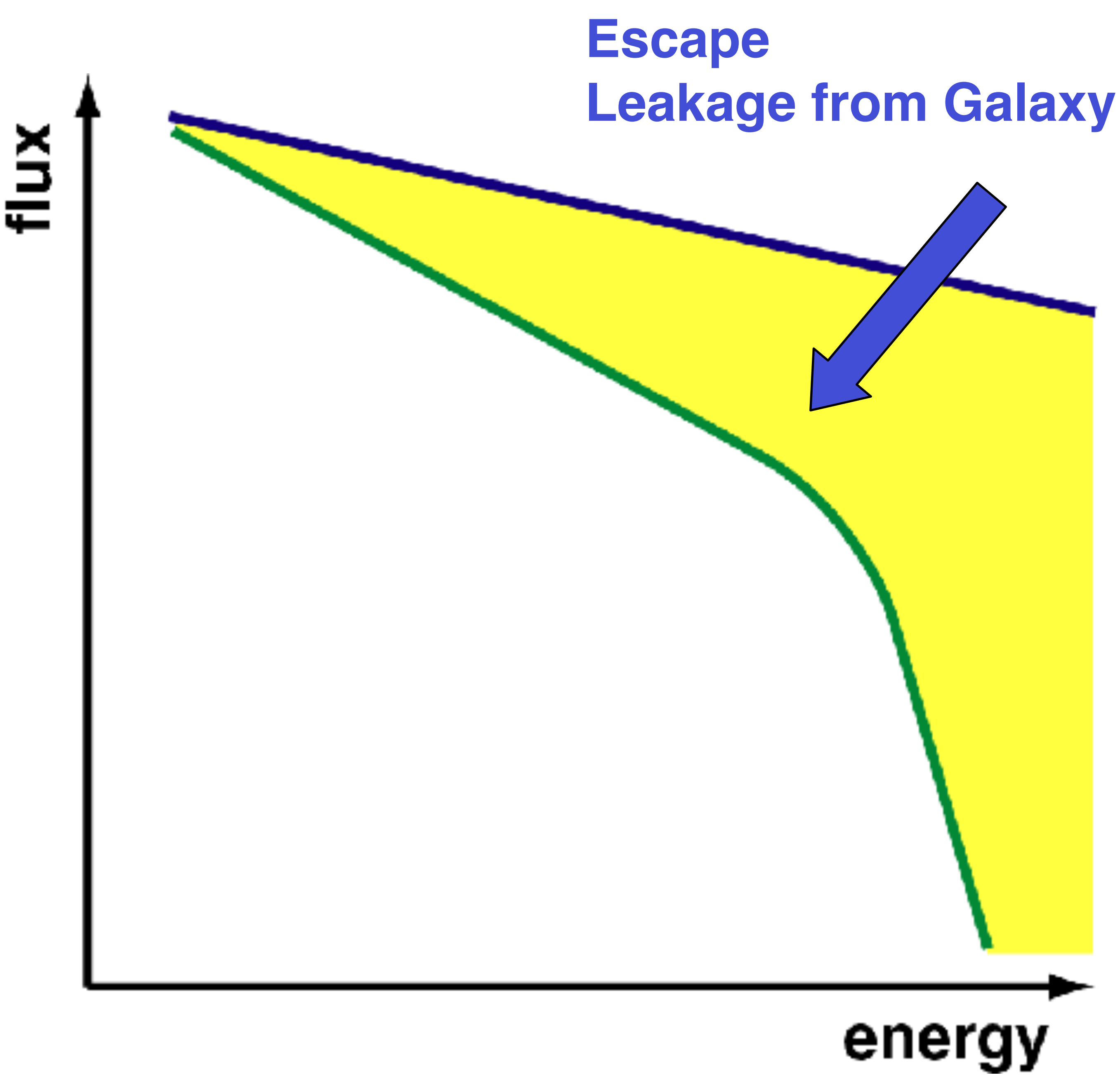

Shape of energy spectrum

$$\frac{dN}{dE} \propto E_0^{\gamma}$$

at source $\gamma \sim -2.1$

at Earth $\gamma \sim -2.6$ to -2.7

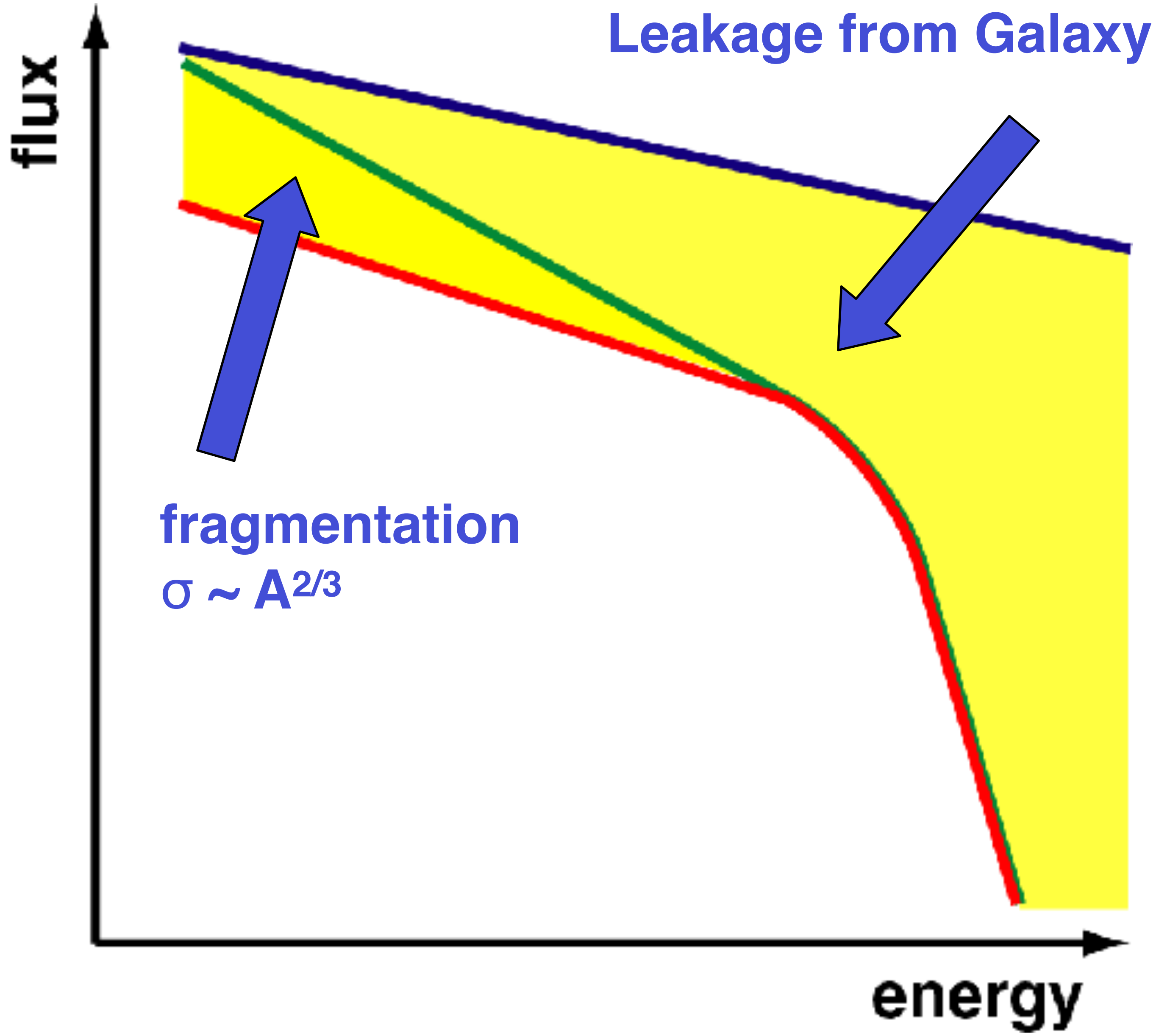

Shape of energy spectrum

$$\frac{dN}{dE} \propto E_0^{\gamma}$$

at source γ ~ -2.1

at Earth γ ~ -2.6 to -2.7

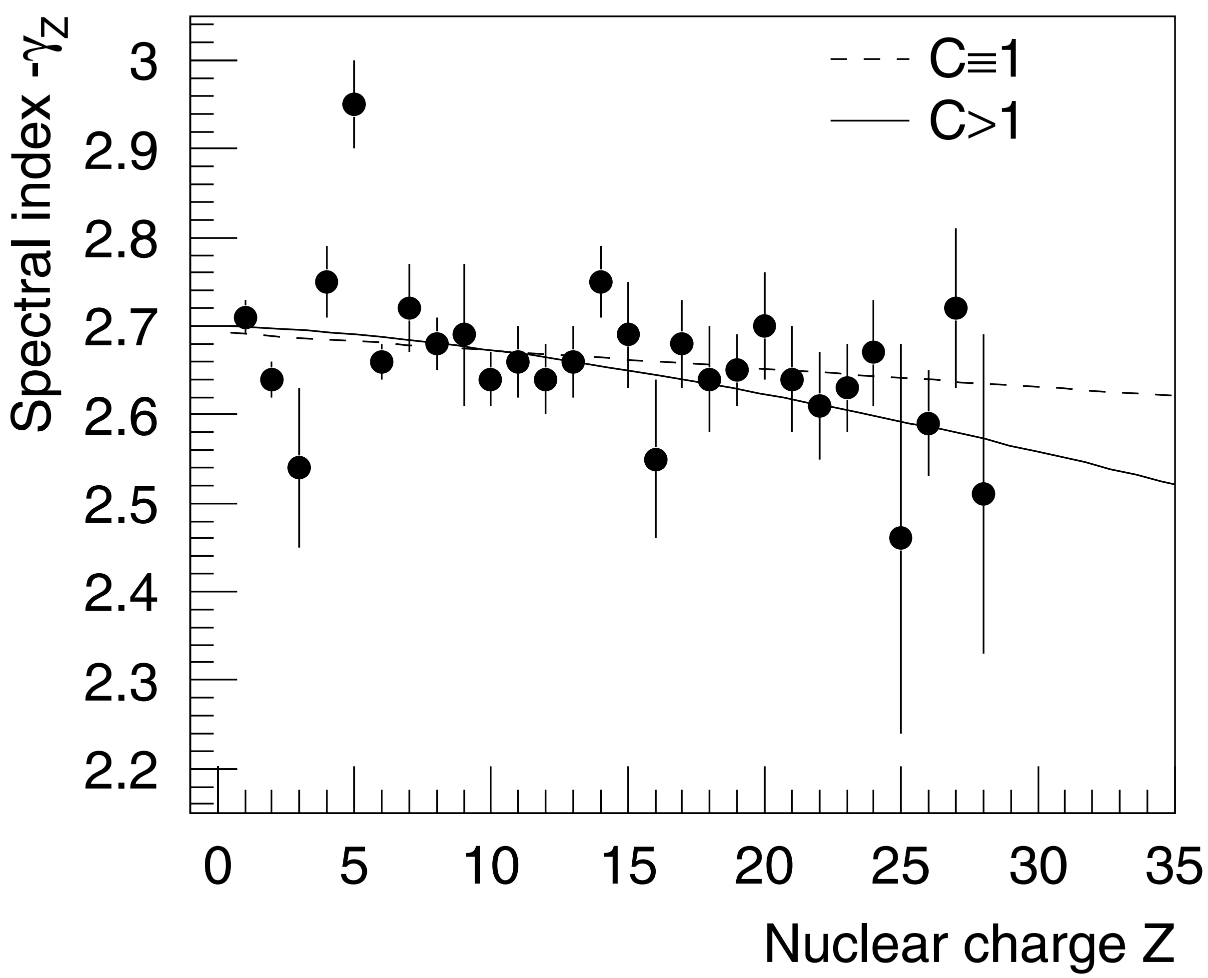

Fig. 5. Spectral index γ_Z versus nuclear charge Z (see Table 1). The solid line represents a three parameter fit according to Eq. (6), the dashed graph a linear fit.

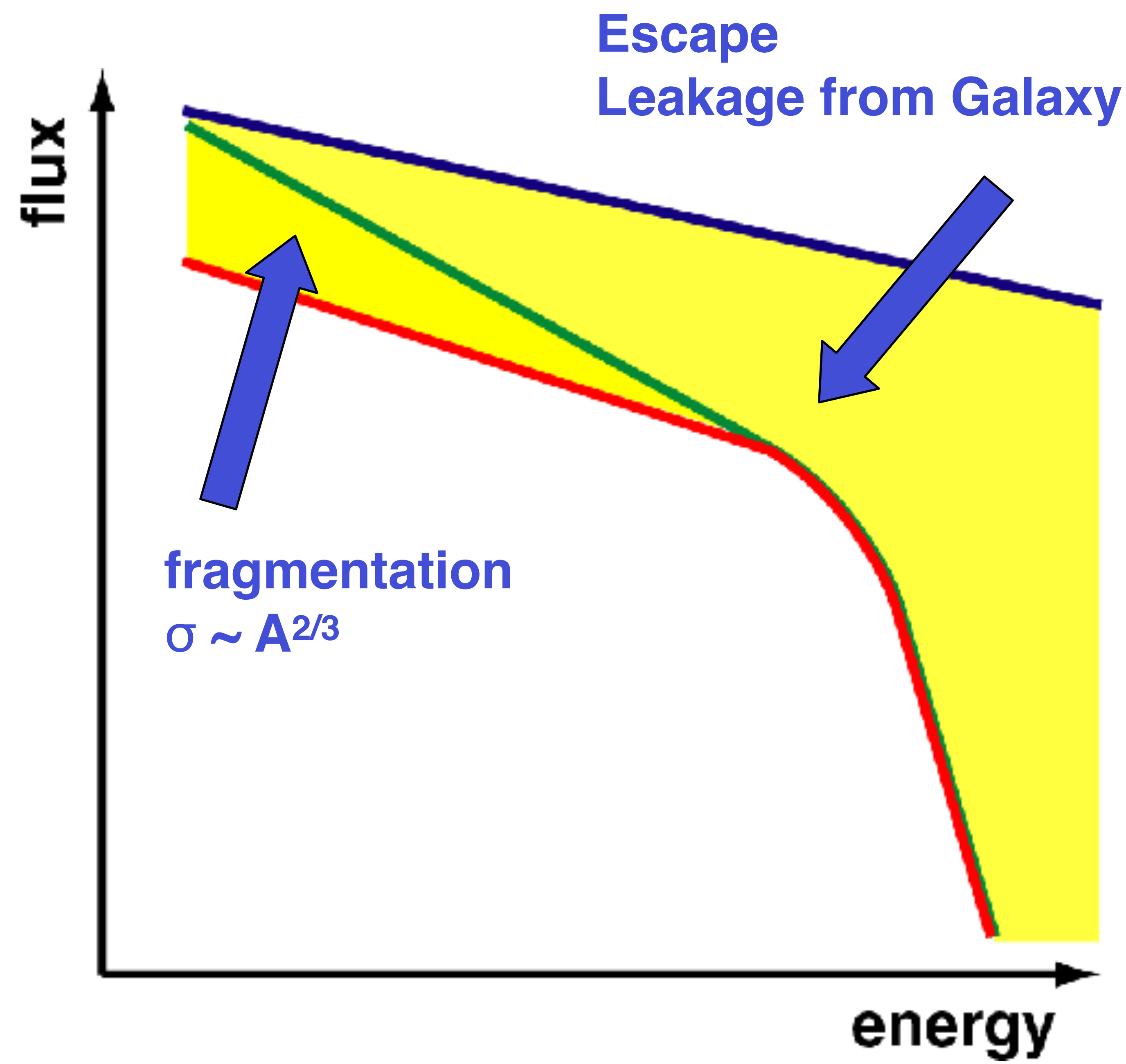

JRH, Astropart. Phys. 19 (2003) 193

Transport equation for cosmic rays in the Galaxy

diffusion *see Ahlers, ISCRA 2022* *also Cannady, ISCRA 2022*

energy loss (Bethe Bloch)

loss through interactions with ISM (spallation)

loss through radioactive decay

$$\frac{\partial N_i}{\partial t} = \nabla(D_i \nabla N_i) - \cancel{\frac{\partial}{\partial E}(b_i N_i)} - \cancel{n v \sigma_i N_i} - \cancel{\frac{N_i}{\gamma_i \tau_i}} + Q_i + \cancel{\sum_{j>i} n v \sigma_{ij} N_j} + \cancel{\sum_{j>i} \frac{N_j}{\gamma_j \tau_{ij}}}$$

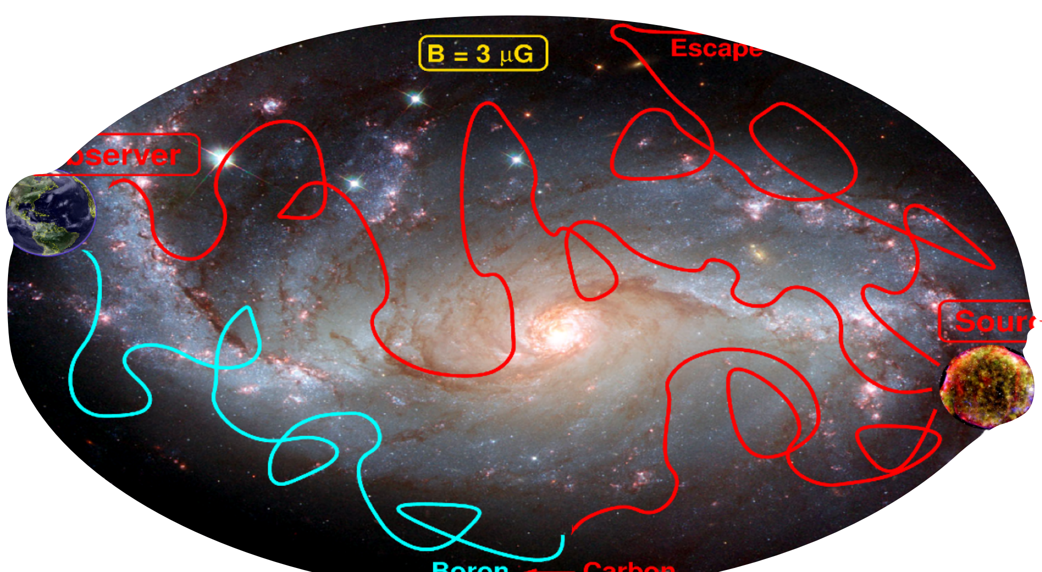

source term

production through spallation of heavy nuclei

production through decay of heavy nuclei

Available online at www.sciencedirect.com
ScienceDirect
Astroparticle Physics 27 (2007) 119–126
Astroparticle Physics
www.elsevier.com/locate/astropart

example of knee due to propagation/leakage from Galaxy

Propagation of super-high-energy cosmic rays in the Galaxy

Jörg R. Hörandel [a,*], Nikolai N. Kalmykov [b], Aleksei V. Timokhin [c]

The steady-state diffusion equation for the cosmic-ray density $N(r)$ is (neglecting nuclear interactions and energy losses)

$$\boxed{-\nabla_i D_{ij}(r)\nabla_j N(r) = Q(r).} \tag{1}$$

$Q(r)$ is the cosmic-ray source term and $D_{ij}(r)$ the diffusion tensor.

Available online at www.sciencedirect.com

ScienceDirect

Astroparticle Physics 27 (2007) 119–126

Astroparticle Physics

www.elsevier.com/locate/astropart

example of knee due to propagation/leakage from Galaxy

Propagation of super-high-energy cosmic rays in the Galaxy

Jörg R. Hörandel [a,*], Nikolai N. Kalmykov [b], Aleksei V. Timokhin [c]

The steady-state diffusion equation for the cosmic-ray density $N(r)$ is (neglecting nuclear interactions and energy losses)

$$\boxed{-\nabla_i D_{ij}(r)\nabla_j N(r) = Q(r).} \tag{1}$$

$Q(r)$ is the cosmic-ray source term and $D_{ij}(r)$ the diffusion tensor.

Under the assumption of azimuthal symmetry and taking into account the predominance of the toroidal component of the magnetic field, Eq. (1) is presented in cylindrical coordinates as

$$\boxed{\begin{aligned}&\left[-\frac{1}{r}\frac{\partial}{\partial r}rD_\perp\frac{\partial}{\partial r}-\frac{\partial}{\partial z}D_\perp\frac{\partial}{\partial z}-\frac{\partial}{\partial z}D_A\frac{\partial}{\partial r}\right.\\&\left.\quad+\frac{1}{r}\frac{\partial}{\partial r}rD_A\frac{\partial}{\partial z}\right]N(r,z)=Q(r,z),\end{aligned}} \tag{2}$$

where $N(r,z)$ is the cosmic-ray density averaged over the large-scale fluctuations with a characteristic scale $L \sim 100$ pc [3]. $D_\perp \propto E^m$ is the diffusion coefficient, where m is much less than one ($m \approx 0.2$), and $D_A \propto E$ the Hall diffusion coefficient. The influence of Hall diffusion becomes predominant at high energies ($>10^{15}$ eV). The sharp

Available online at www.sciencedirect.com
ScienceDirect
Astroparticle Physics 27 (2007) 119–126
Astroparticle Physics
www.elsevier.com/locate/astropart

example of knee due to propagation/leakage from Galaxy

Propagation of super-high-energy cosmic rays in the Galaxy

Jörg R. Hörandel [a,*], Nikolai N. Kalmykov [b], Aleksei V. Timokhin [c]

The steady-state diffusion equation for the cosmic-ray density $N(r)$ is (neglecting nuclear interactions and energy losses)

$$\boxed{-\nabla_i D_{ij}(r)\nabla_j N(r) = Q(r).} \tag{1}$$

$Q(r)$ is the cosmic-ray source term and $D_{ij}(r)$ the diffusion tensor.

Under the assumption of azimuthal symmetry and taking into account the predominance of the toroidal component of the magnetic field, Eq. (1) is presented in cylindrical coordinates as

$$\boxed{\begin{aligned}&\left[-\frac{1}{r}\frac{\partial}{\partial r}rD_\perp\frac{\partial}{\partial r}-\frac{\partial}{\partial z}D_\perp\frac{\partial}{\partial z}-\frac{\partial}{\partial z}D_A\frac{\partial}{\partial r}\right.\\&\left.\quad+\frac{1}{r}\frac{\partial}{\partial r}rD_A\frac{\partial}{\partial z}\right]N(r,z)=Q(r,z),\end{aligned}} \tag{2}$$

where $N(r,z)$ is the cosmic-ray density averaged over the large-scale fluctuations with a characteristic scale $L \sim 100$ pc [3]. $D_\perp \propto E^m$ is the diffusion coefficient, where m is much less than one ($m \approx 0.2$), and $D_A \propto E$ the Hall diffusion coefficient. The influence of Hall diffusion becomes predominant at high energies ($>10^{15}$ eV). The sharp

The magnetic field of the Galaxy consists of a large-scale regular and a chaotic, irregular component $\vec{B} = \vec{B}_{reg} + \vec{B}_{irr}$. A purely azimuthal magnetic field was assumed for the regular field

$$B_z = 0, \quad B_r = 0, \quad B_\phi = 1\ \mu\text{G}\exp\left(-\frac{z^2}{z_0^2}-\frac{r^2}{r_0^2}\right),$$

where $z_0 = 5$ kpc and $r_0 = 10$ kpc are constants [3].

ELSEVIER

Available online at www.sciencedirect.com
ScienceDirect

Astroparticle Physics 27 (2007) 119–126

Astroparticle Physics

www.elsevier.com/locate/astropart

example of knee due to propagation/leakage from Galaxy

Propagation of super-high-energy cosmic rays in the Galaxy

Jörg R. Hörandel [a,*], Nikolai N. Kalmykov [b], Aleksei V. Timokhin [c]

The steady-state diffusion equation for the cosmic-ray density $N(r)$ is (neglecting nuclear interactions and energy losses)

$$-\nabla_i D_{ij}(r)\nabla_j N(r) = Q(r). \tag{1}$$

$Q(r)$ is the cosmic-ray source term and $D_{ij}(r)$ the diffusion tensor.

Under the assumption of azimuthal symmetry and taking into account the predominance of the toroidal component of the magnetic field, Eq. (1) is presented in cylindrical coordinates as

$$\left[-\frac{1}{r}\frac{\partial}{\partial r}rD_{\perp}\frac{\partial}{\partial r}-\frac{\partial}{\partial z}D_{\perp}\frac{\partial}{\partial z}-\frac{\partial}{\partial z}D_{A}\frac{\partial}{\partial r}+\frac{1}{r}\frac{\partial}{\partial r}rD_{A}\frac{\partial}{\partial z}\right]N(r,z)=Q(r,z), \tag{2}$$

where $N(r,z)$ is the cosmic-ray density averaged over the large-scale fluctuations with a characteristic scale $L \sim 100$ pc [3]. $D_{\perp} \propto E^m$ is the diffusion coefficient, where m is much less than one ($m \approx 0.2$), and $D_A \propto E$ the Hall diffusion coefficient. The influence of Hall diffusion becomes predominant at high energies ($>10^{15}$ eV). The sharp

The magnetic field of the Galaxy consists of a large-scale regular and a chaotic, irregular component $\vec{B} = \vec{B}_{\mathrm{reg}} + \vec{B}_{\mathrm{irr}}$. A purely azimuthal magnetic field was assumed for the regular field

$$B_z = 0, \quad B_r = 0, \quad B_\phi = 1\ \mu\mathrm{G}\exp\left(-\frac{z^2}{z_0^2}-\frac{r^2}{r_0^2}\right),$$

where $z_0 = 5$ kpc and $r_0 = 10$ kpc are constants [3].

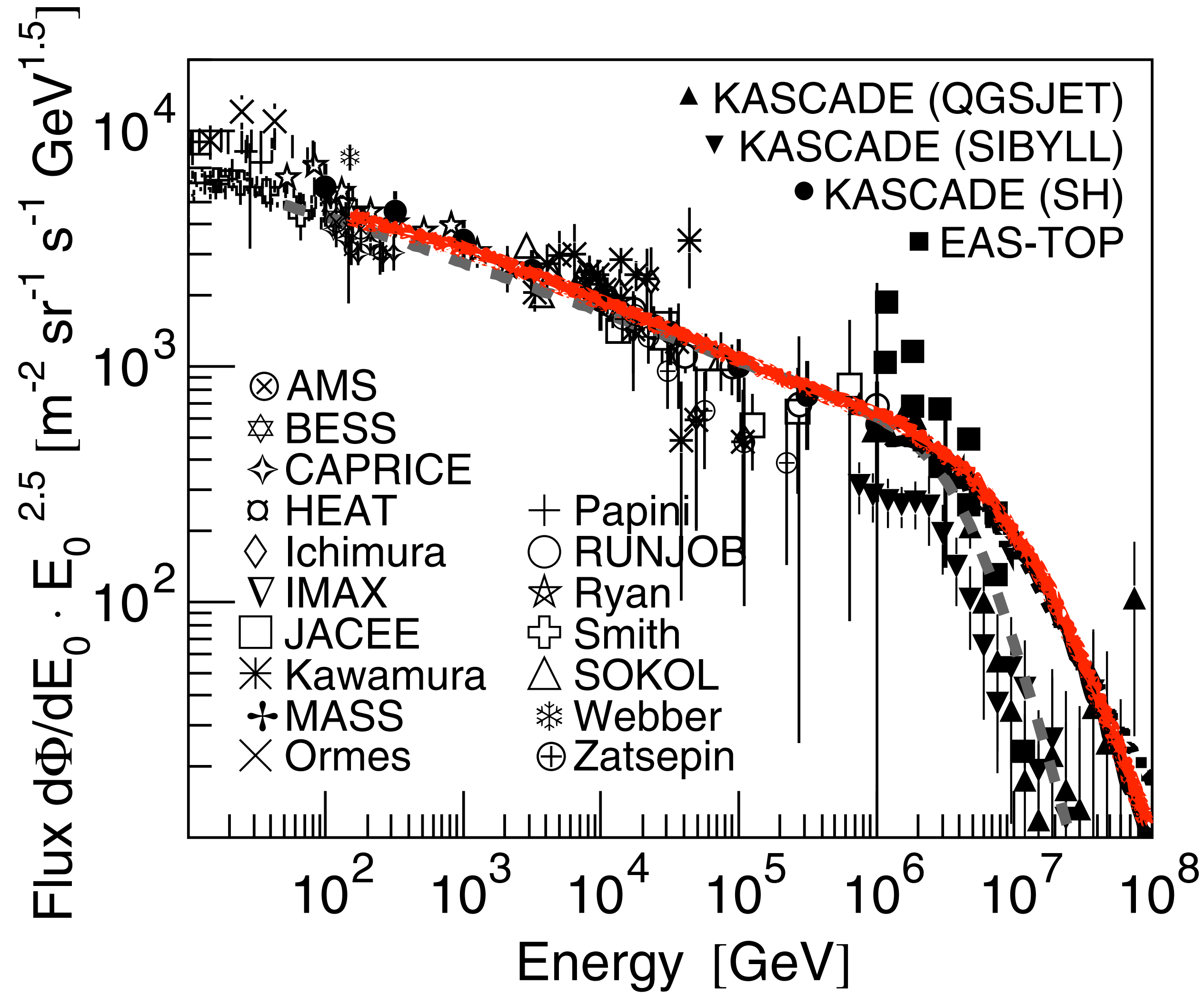

Fig. 7. Proton flux as obtained from various measurements, for references see [28], compared to the spectra shown in Fig. 6 (black lines) and the *polygonato* model [26] (grey, dashed line).

Origin of the knee?

JRH, Astropart. Phys. 21 (2004) 241 (updated)

Acceleration (SNR)

.. in SNR	Berezhko & Ksenofontov
.. in SNR + radio galaxies	Stanev ..
.. in oblique shocks	Kobayakawa ..
.. in variety of SNR	Sveshnikova
Single source model	Erlykin & Wolfendale
Reacceleration in galactic wind	Völk & Zirakashvili

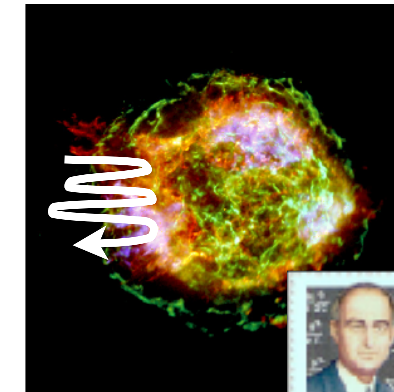

Origin of the knee?

JRH, Astropart. Phys. 21 (2004) 241 (updated)

Acceleration (SNR)

- .. in SNR — Berezhko & Ksenofontov
- .. in SNR + radio galaxies — Stanev ..
- .. in oblique shocks — Kobayakawa ..
- .. in variety of SNR — Sveshnikova
- Single source model — Erlykin & Wolfendale
- Reacceleration in galactic wind — Völk & Zirakashvili

Leakage from Galaxy

- Minimum pathlength model — Swordy
- Anomalous diffusion model — Lagutin ..
- Hall diffusion model — Ptuskin .., Kalmykov ..
- Diffusion in turbulent magnetic fields — Ogio & Kakimoto
- Diffusion and drift — Roulet ..

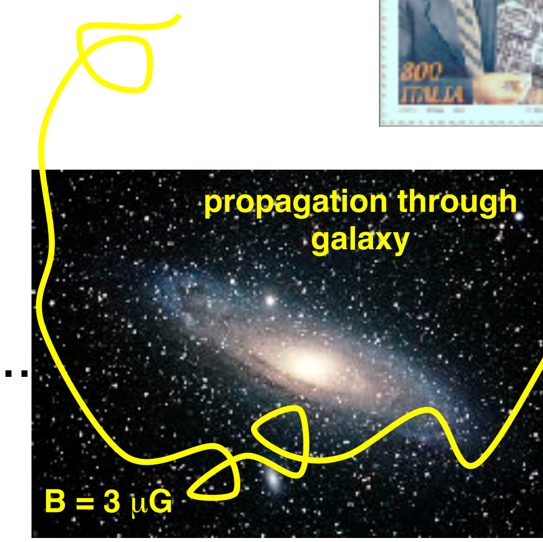

Origin of the knee?

JRH, Astropart. Phys. 21 (2004) 241 (updated)

Acceleration (SNR)

.. in SNR	Berezhko & Ksenofontov
.. in SNR + radio galaxies	Stanev ..
.. in oblique shocks	Kobayakawa ..
.. in variety of SNR	Sveshnikova
Single source model	Erlykin & Wolfendale
Reacceleration in galactic wind	Völk & Zirakashvili

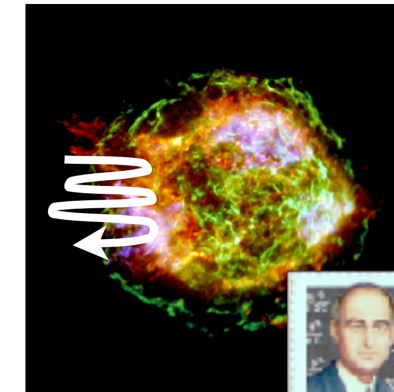

Leakage from Galaxy

Minimum pathlength model	Swordy
Anomalous diffusion model	Lagutin ..
Hall diffusion model	Ptuskin .., Kalmykov ..
Diffusion in turbulent magnetic fields	Ogio & Kakimoto
Diffusion and drift	Roulet ..

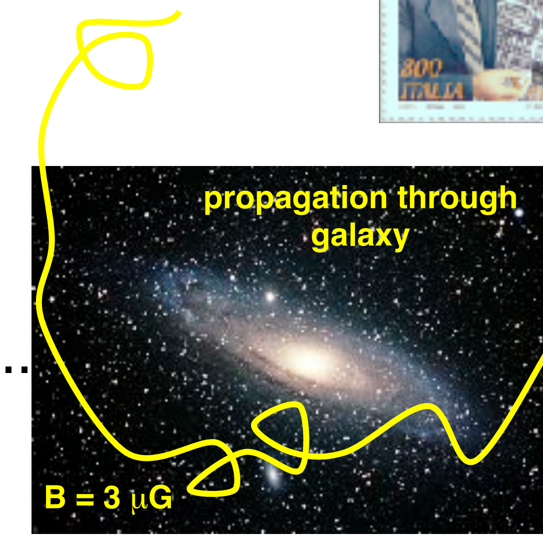

γ-ray bursts

Cannonball model	Plaga
Acceleration in GRB + diffusion	Wick ..
Acceleration in GRB E_{max} ~A	Dar ..

Origin of the knee?

JRH, Astropart. Phys. 21 (2004) 241 (updated)

Acceleration (SNR)

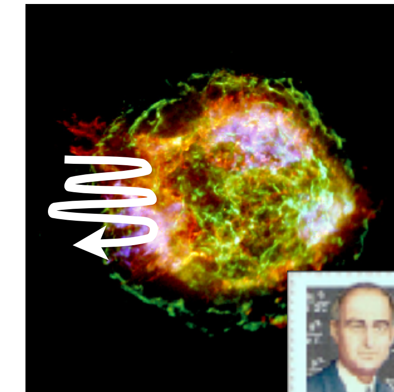

.. in SNR	Berezhko & Ksenofontov
.. in SNR + radio galaxies	Stanev ..
.. in oblique shocks	Kobayakawa ..
.. in variety of SNR	Sveshnikova
Single source model	Erlykin & Wolfendale
Reacceleration in galactic wind	Völk & Zirakashvili

Leakage from Galaxy

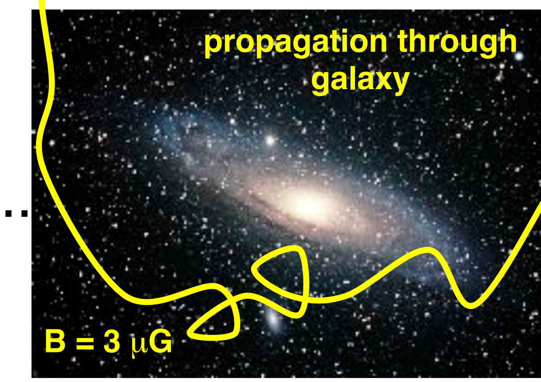

Minimum pathlength model	Swordy
Anomalous diffusion model	Lagutin ..
Hall diffusion model	Ptuskin .., Kalmykov ..
Diffusion in turbulent magnetic fields	Ogio & Kakimoto
Diffusion and drift	Roulet ..

γ-ray bursts

Cannonball model	Plaga
Acceleration in GRB + diffusion	Wick ..
Acceleration in GRB $E_{max} \sim A$	Dar ..

Interaction with background particles

Diffusion model + photo-disintegration	Tkaczyk
Interaction with neutrinos in galactic halo	Dova ..
Photo-disintegration (optical and UV photons)	Candia ..

Origin of the knee?

JRH, Astropart. Phys. 21 (2004) 241 (updated)

Acceleration (SNR)

.. in SNR	Berezhko & Ksenofontov
.. in SNR + radio galaxies	Stanev ..
.. in oblique shocks	Kobayakawa ..
.. in variety of SNR	Sveshnikova
Single source model	Erlykin & Wolfendale
Reacceleration in galactic wind	Völk & Zirakashvili

Leakage from Galaxy

Minimum pathlength model	Swordy
Anomalous diffusion model	Lagutin ..
Hall diffusion model	Ptuskin .., Kalmykov ..
Diffusion in turbulent magnetic fields	Ogio & Kakimoto
Diffusion and drift	Roulet ..

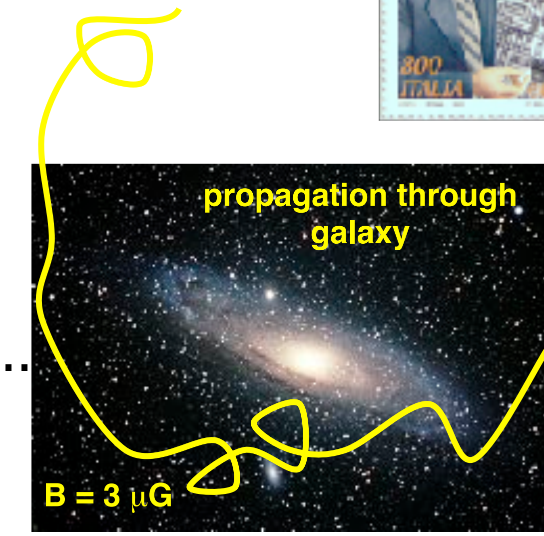

γ-ray bursts

Cannonball model	Plaga
Acceleration in GRB + diffusion	Wick ..
Acceleration in GRB E_{max} ~A	Dar ..

Interaction with background particles

Diffusion model + photo-disintegration	Tkaczyk
Interaction with neutrinos in galactic halo	Dova ..
Photo-disintegration (optical and UV photons)	Candia ..

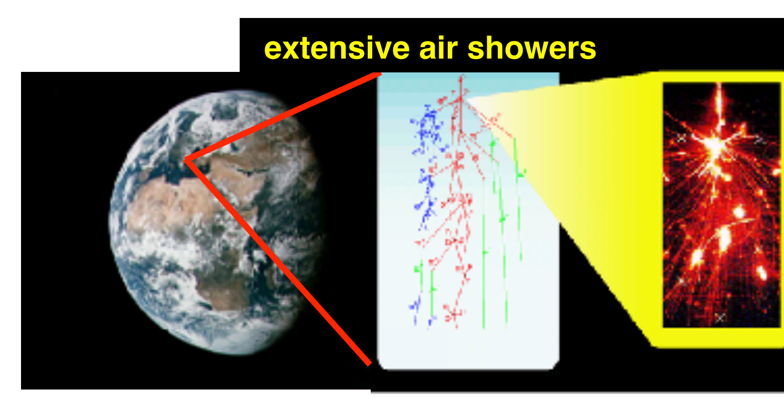

Particle physics in atmosphere

Gravitons, SUSY	Kazanas & Nicolaidis

Origin of the knee?

JRH, Astropart. Phys. 21 (2004) 241 (updated)

Acceleration (SNR)

.. in SNR	Berezhko & Ksenofontov
.. in SNR + radio galaxies	Stanev ..
.. in oblique shocks	Kobayakawa ..
.. in variety of SNR	Sveshnikova
Single source model	Erlykin & Wolfendale
Reacceleration in galactic wind	Völk & Zirakashvili

Leakage from Galaxy

Minimum pathlength model	Swordy
Anomalous diffusion model	Lagutin ..
Hall diffusion model	Ptuskin .., Kalmykov ..
Diffusion in turbulent magnetic fields	Ogio & Kakimoto
Diffusion and drift	Roulet ..

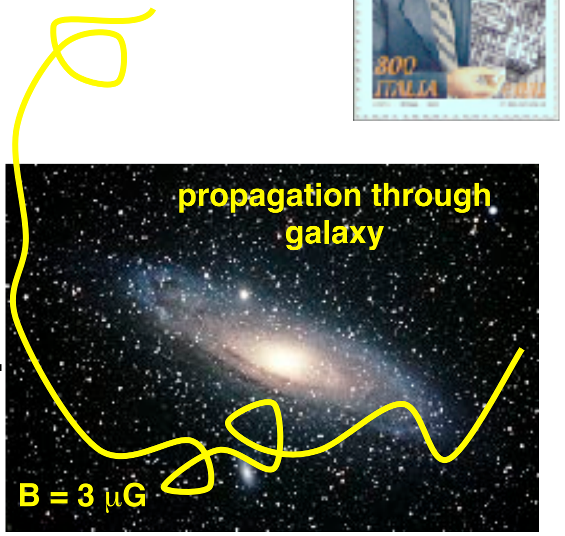

γ-ray bursts

Cannonball model	Plaga
Acceleration in GRB + diffusion	Wick ..
Acceleration in GRB E_{max} ~A	Dar ..

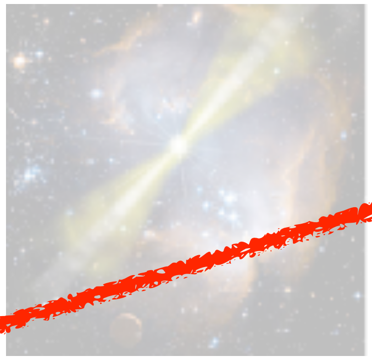

Interaction with background particles

Diffusion model + photo-disintegration	Tkaczyk
Interaction with neutrinos in galactic halo	Dova ..
Photo-disintegration (optical and UV photons)	Candia ..

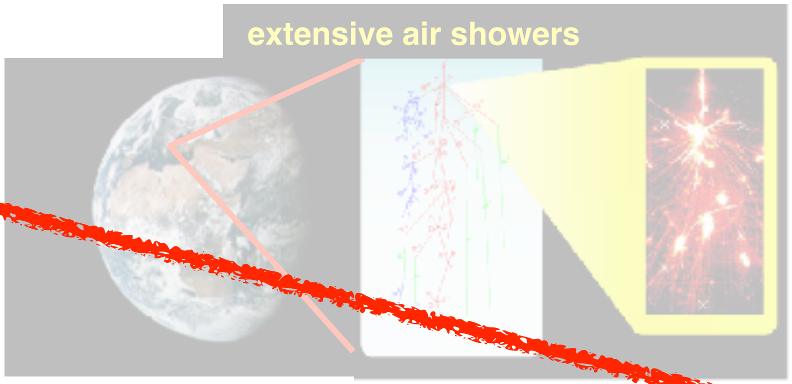

Particle physics in atmosphere

Gravitons, SUSY	Kazanas & Nicolaidis

J.R. Hörandel / Advances in Space Research 41 (2008) 442–463

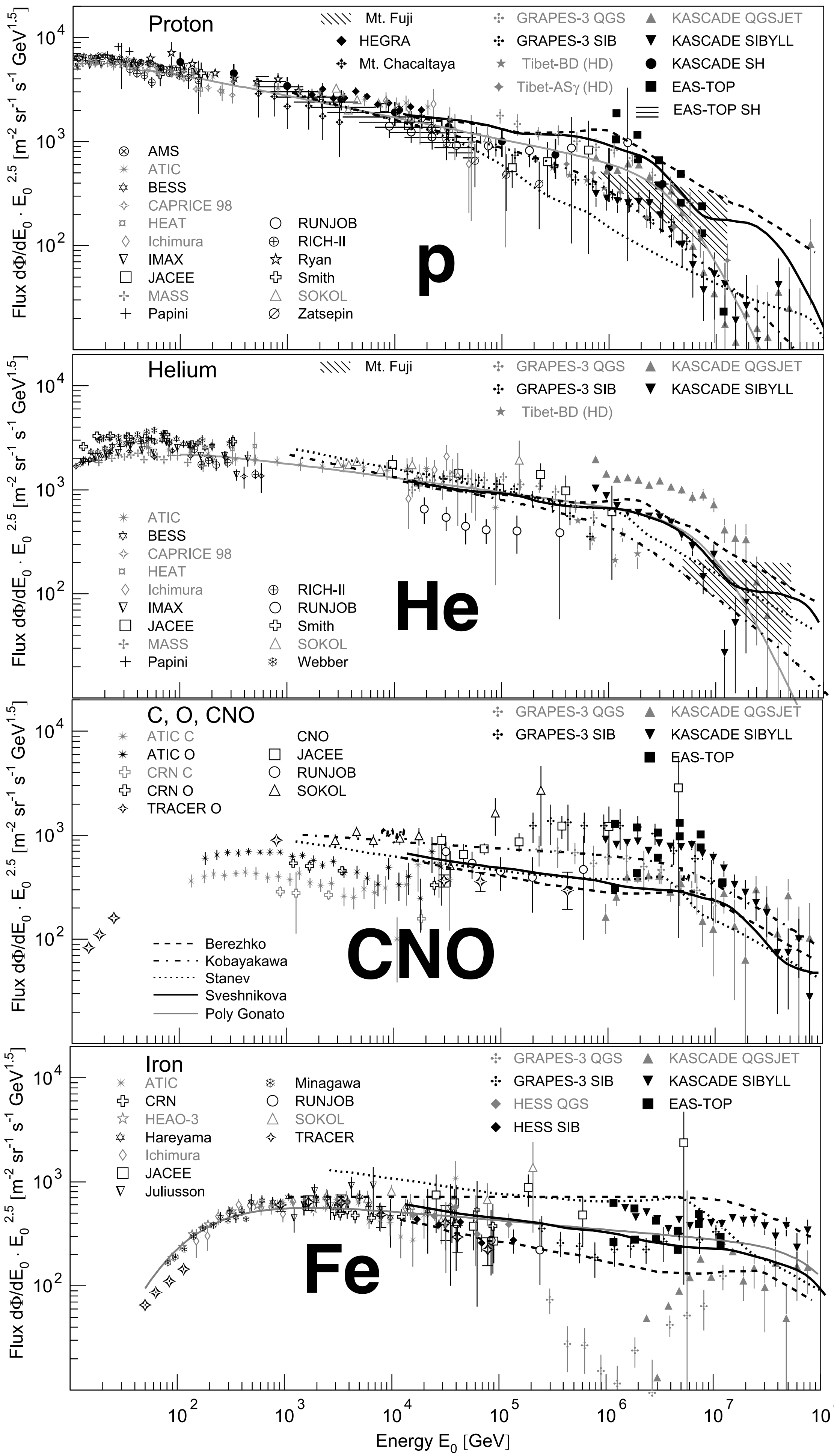

maximum energy

$$E_{max} \propto B \cdot Z$$

$$E_{max} \approx Z \cdot 100\ \text{TeV} \ldots Z \cdot 5\ \text{PeV}$$

JRH, Adv. Space Res. 41 (2008) 442

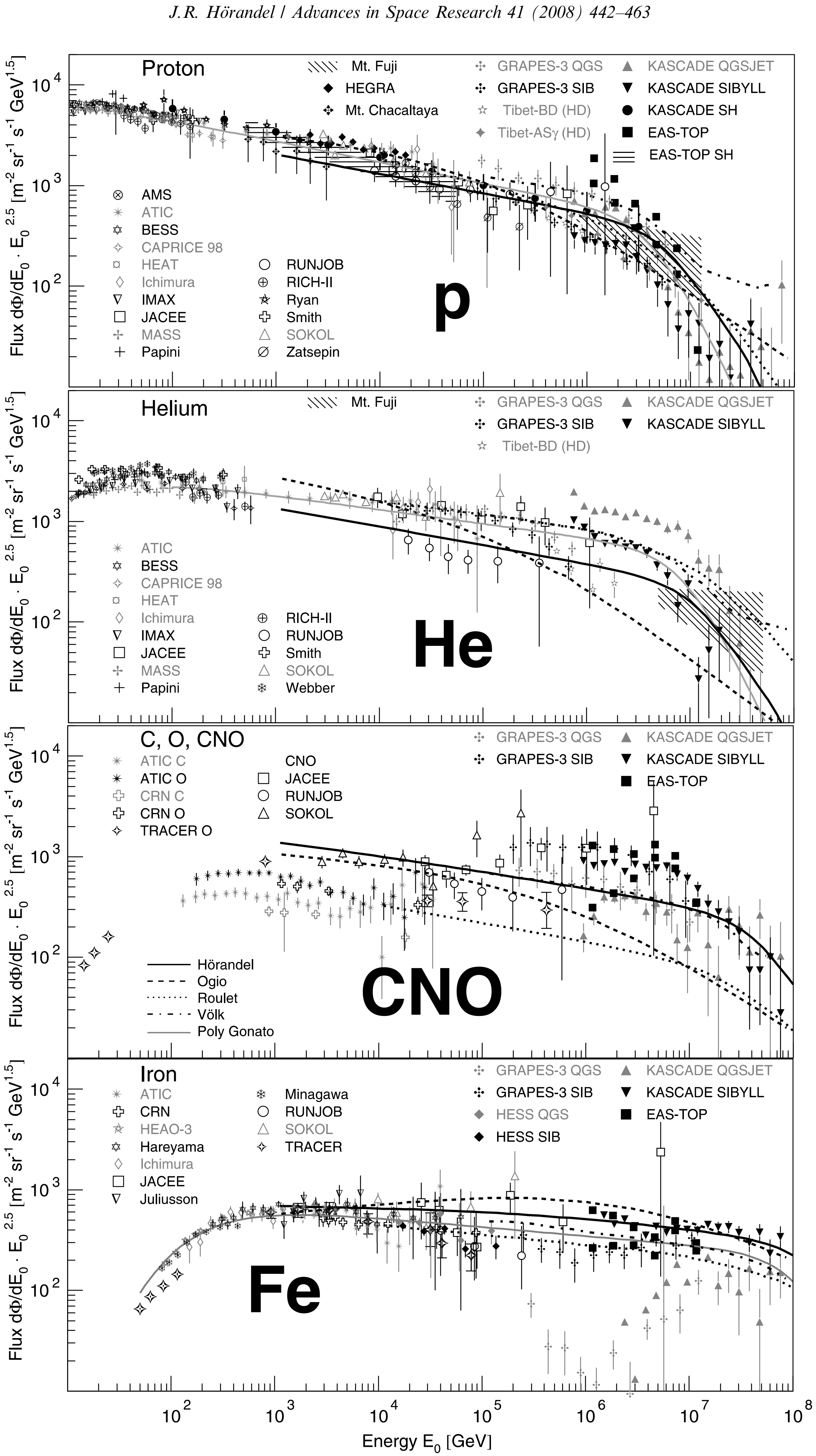

leakage from Galaxy

$$E_k \propto Z$$

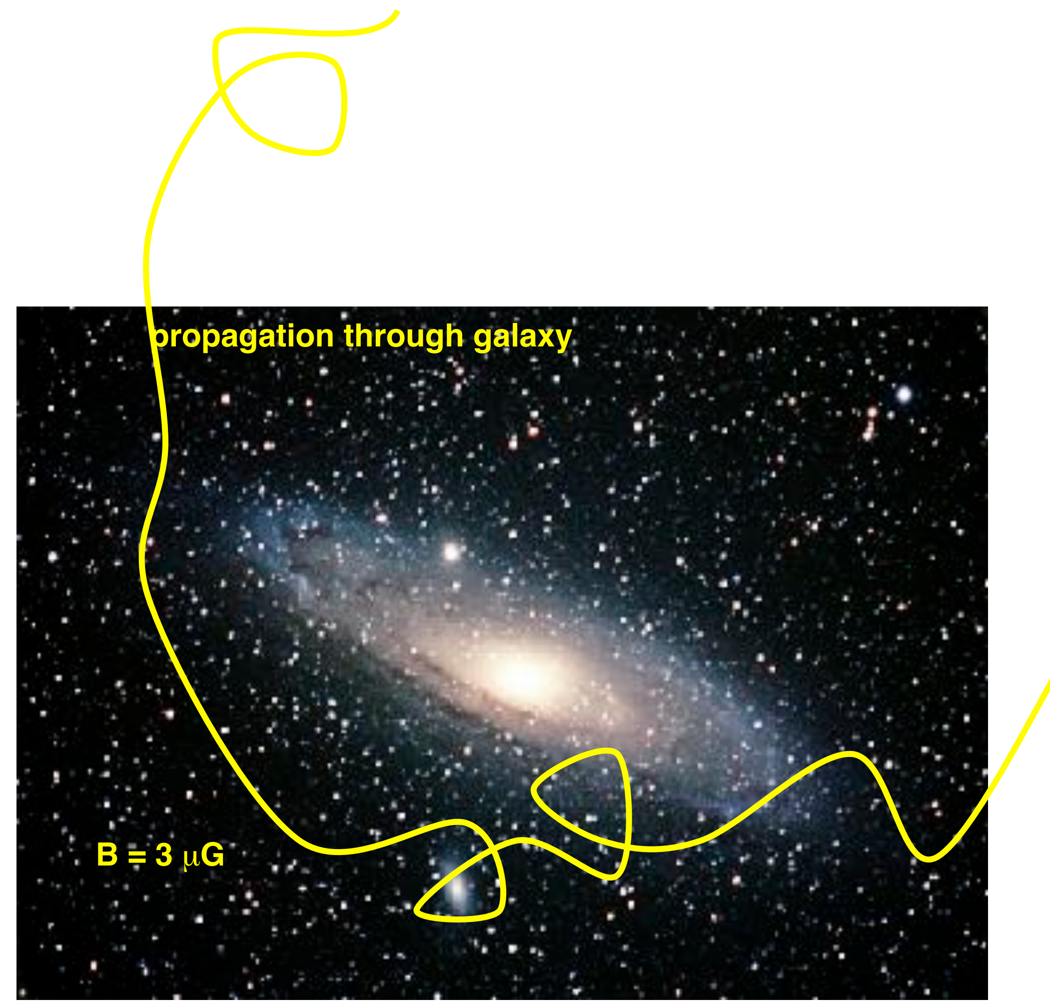

JRH, Adv. Space Res. 41 (2008) 442

Transition to extragalactic CR component

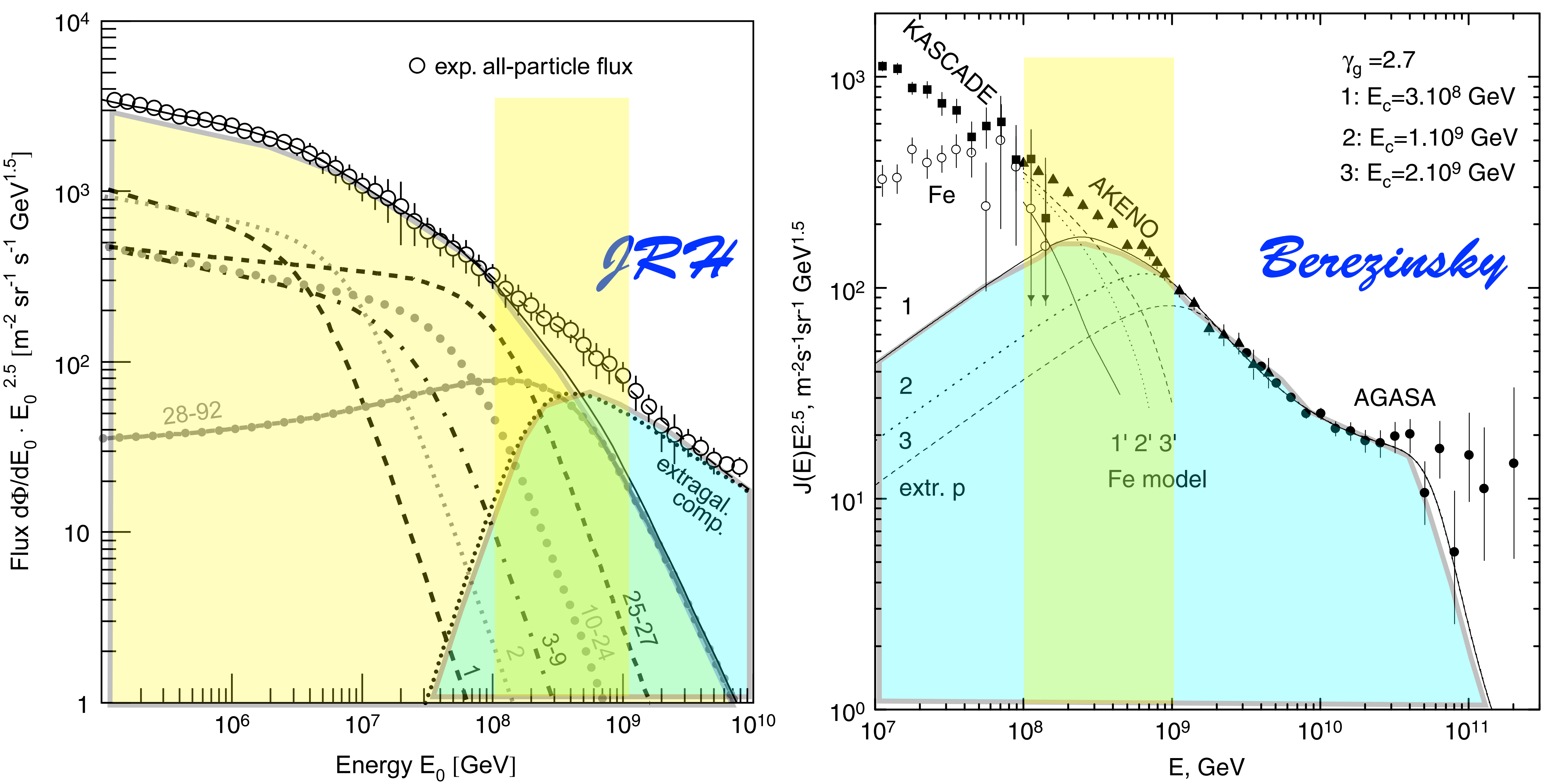

Fig. 26. *Left panel*: Cosmic-ray energy spectra according to the poly-gonato model [2]. The spectra for groups of elements are labeled by their respective nuclear charge numbers. The sum of all elements yields the galactic all-particle spectrum (—) which is compared to the average measured flux. In addition, a hypothetical extragalactic component is shown to account for the observed all-particle flux (- - -). *Right panel*: Transition from galactic to extragalactic cosmic rays according to Berezinsky et al. [451]. Calculated spectra of extragalactic protons (curves 1, 2, 3) and of galactic iron nuclei (curves 1′, 2′, 3′) are compared with the all-particle spectrum from the Akeno and AGASA experiments. KASCADE data are shown as filled squares for the all-particle flux and as open circles for the flux of iron nuclei.

Transition to extragalactic CR component

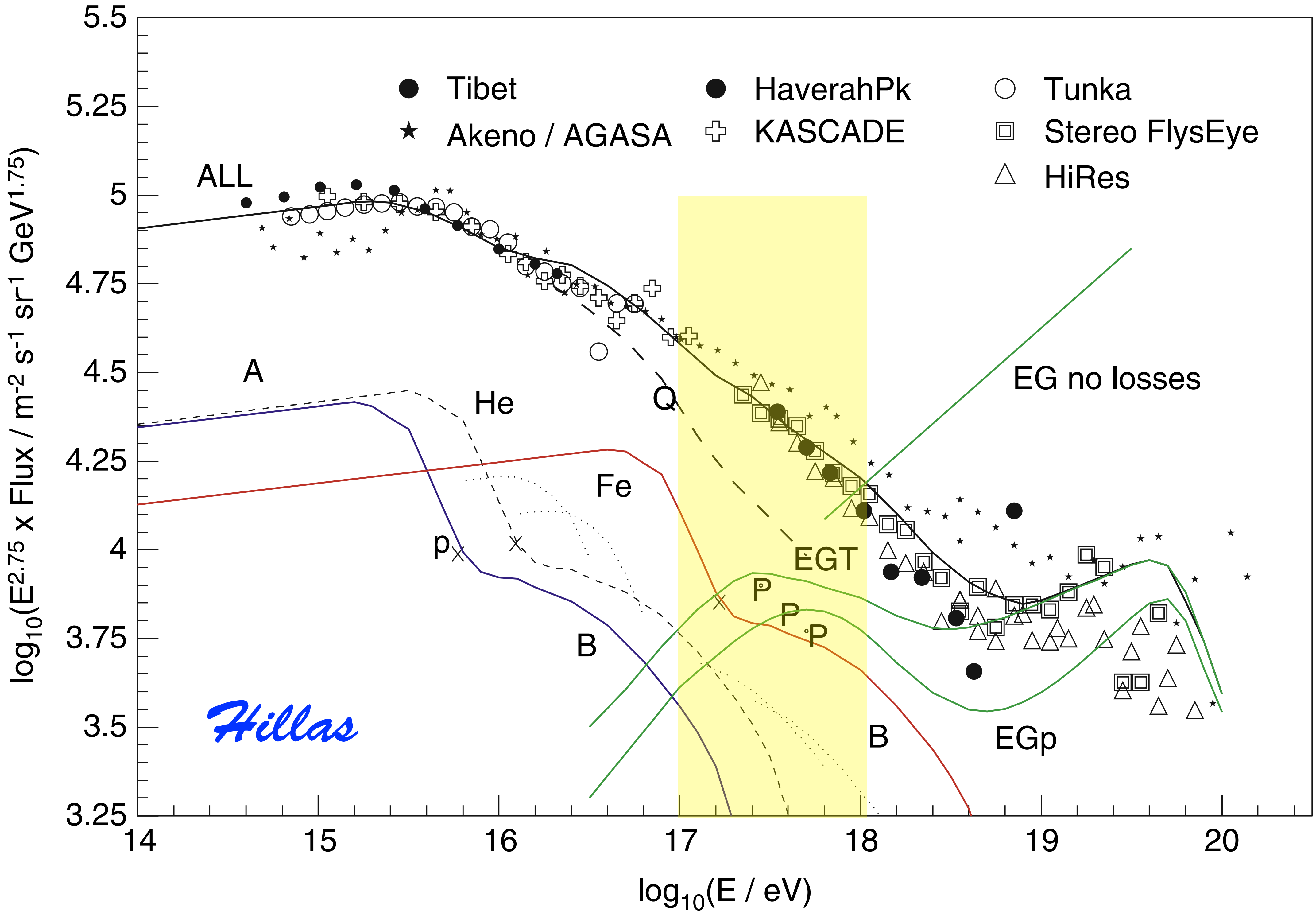

„classical" supernovae + additional component

M. Hillas, J. Phys. G 31 (2005) R95

Contribution of (regular) SNR-CR to all-particle spectrum

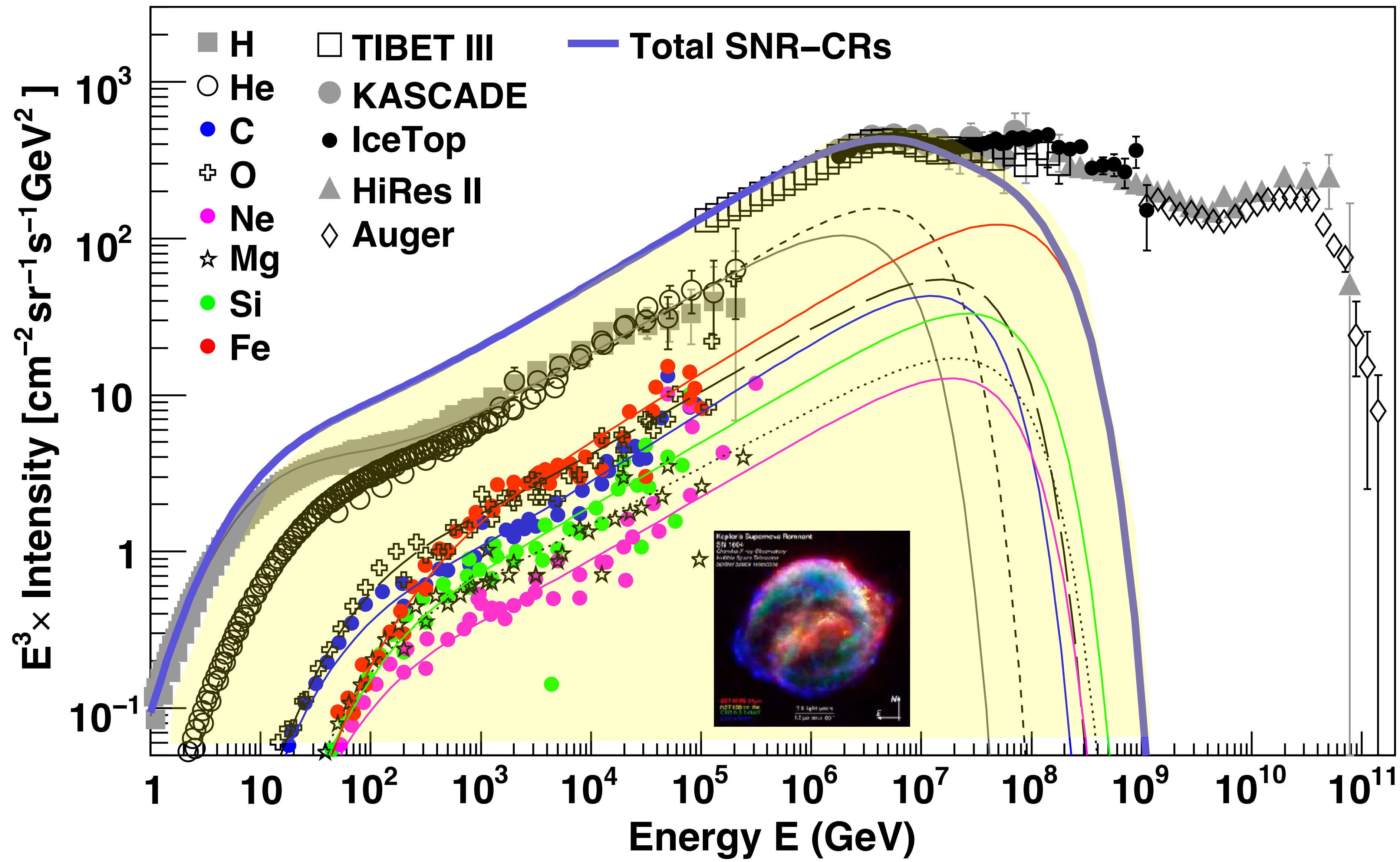

Fig. 2. Contribution of SNR-CRs to the all-particle cosmic-ray spectrum. The thin lines represent spectra for the individual elements, and the thick-solid line represents the total contribution. The calculation assumes an exponential cut-off energy for protons at $E_c = 4.5 \times 10^6$ GeV. Other model parameters, and the low-energy data are the same as in Figure 1. Error bars are shown only for the proton and helium data. High-energy data: KASCADE (Antoni et al. 2005), IceTop (Aartsen et al. 2013), Tibet III (Amenomori et al. 2008), the Pierre Auger Observatory (Schulz et al. 2013), and HiRes II (Abbasi et al. 2009).

S. Thoudam et al., A&A 595 (2016) A33

~8% of mechanical power of SN --> CRs

Contribution of (regular) SNR-CR to all-particle spectrum

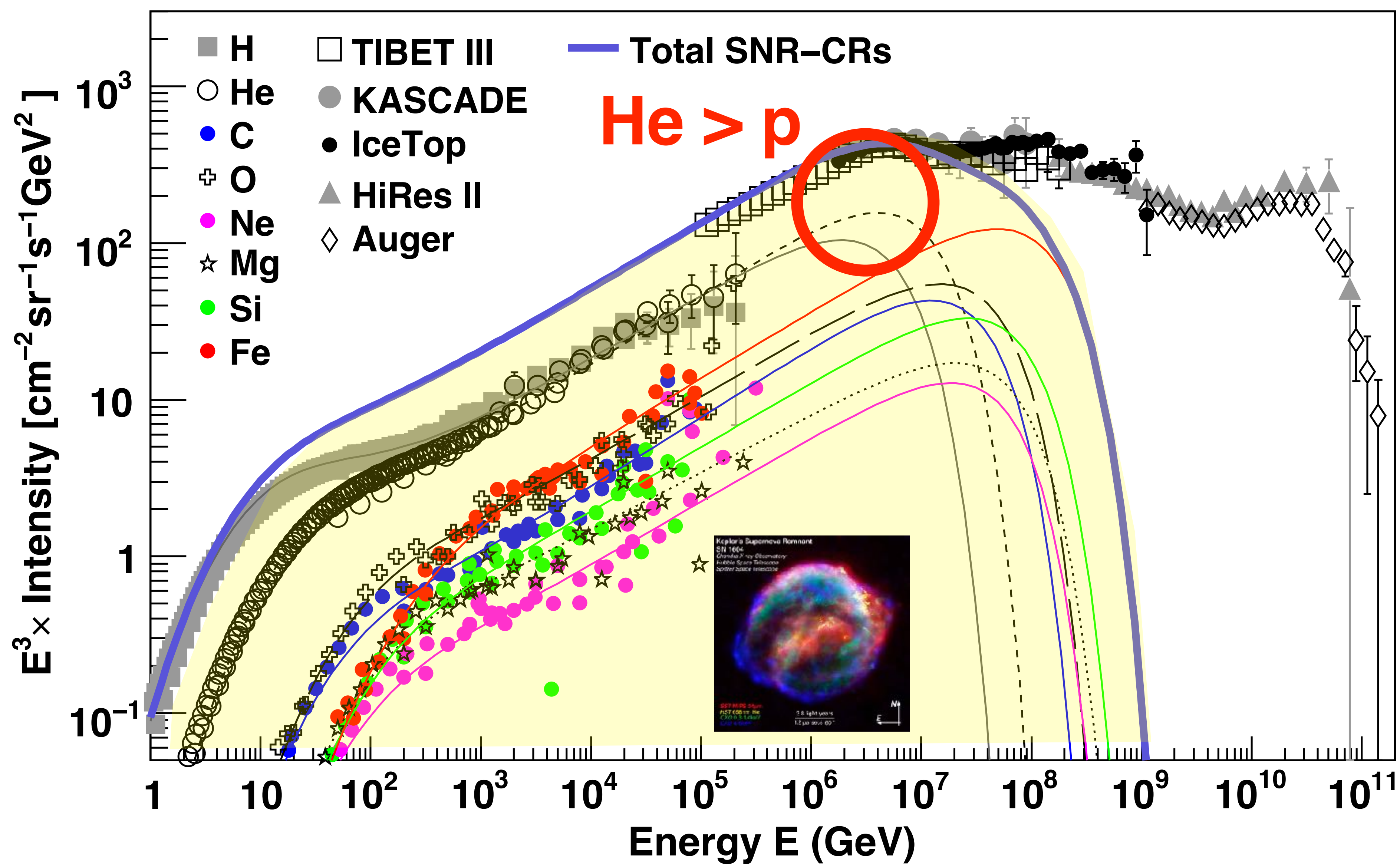

Fig. 2. Contribution of SNR-CRs to the all-particle cosmic-ray spectrum. The thin lines represent spectra for the individual elements, and the thick-solid line represents the total contribution. The calculation assumes an exponential cut-off energy for protons at $E_c = 4.5 \times 10^6$ GeV. Other model parameters, and the low-energy data are the same as in Figure 1. Error bars are shown only for the proton and helium data. High-energy data: KASCADE (Antoni et al. 2005), IceTop (Aartsen et al. 2013), Tibet III (Amenomori et al. 2008), the Pierre Auger Observatory (Schulz et al. 2013), and HiRes II (Abbasi et al. 2009).

~8% of mechanical power of SN --> CRs

S. Thoudam et al., A&A 595 (2016) A33

Contribution of (regular) SNR-CR to all-particle spectrum

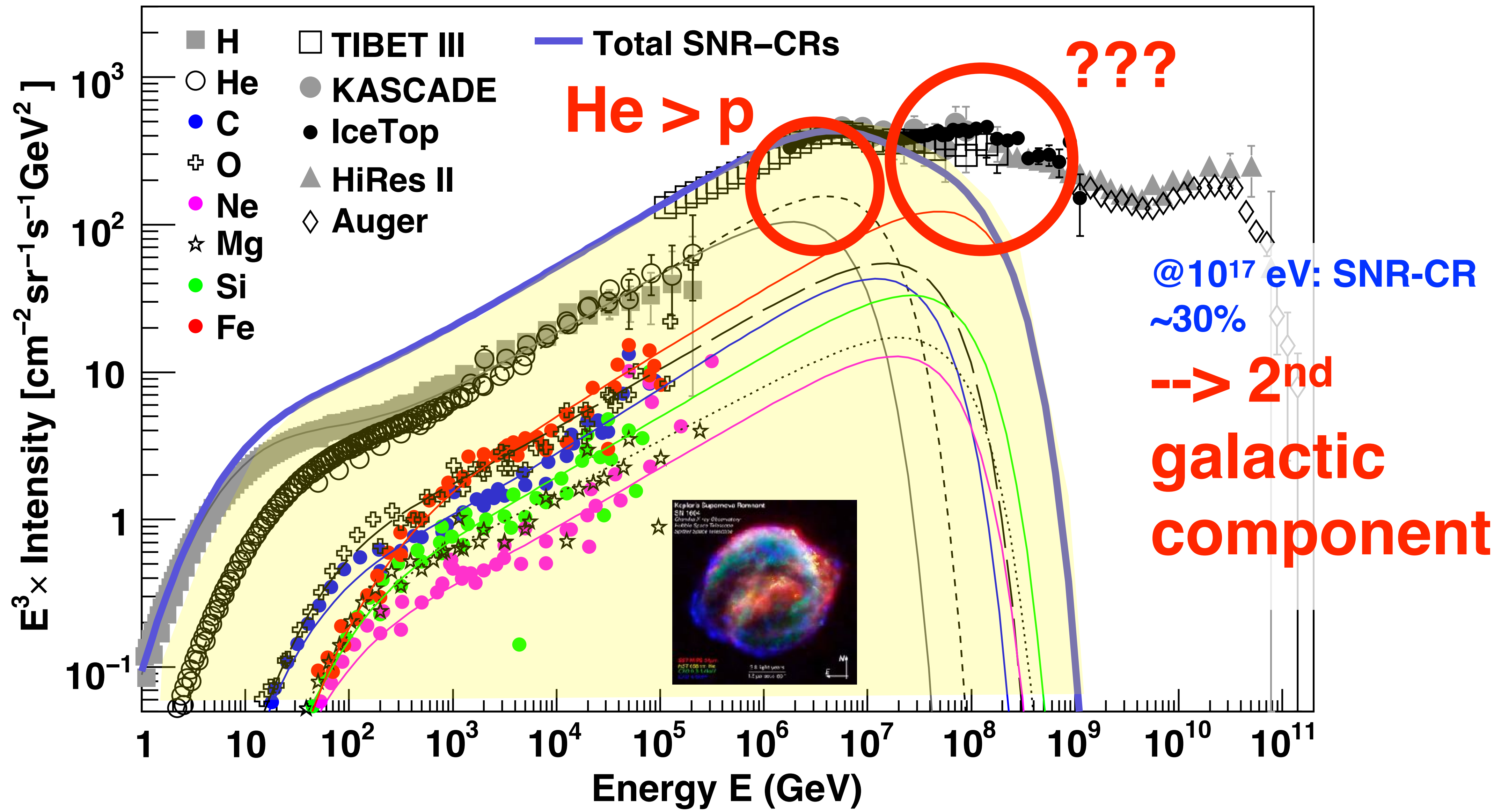

Fig. 2. Contribution of SNR-CRs to the all-particle cosmic-ray spectrum. The thin lines represent spectra for the individual elements, and the thick-solid line represents the total contribution. The calculation assumes an exponential cut-off energy for protons at $E_c = 4.5 \times 10^6$ GeV. Other model parameters, and the low-energy data are the same as in Figure 1. Error bars are shown only for the proton and helium data. High-energy data: KASCADE (Antoni et al. 2005), IceTop (Aartsen et al. 2013), Tibet III (Amenomori et al. 2008), the Pierre Auger Observatory (Schulz et al. 2013), and HiRes II (Abbasi et al. 2009).

S. Thoudam et al., A&A 595 (2016) A33

~8% of mechanical power of SN --> CRs

Combined fit of spectrum and composition data as measured by the Pierre Auger Observatory

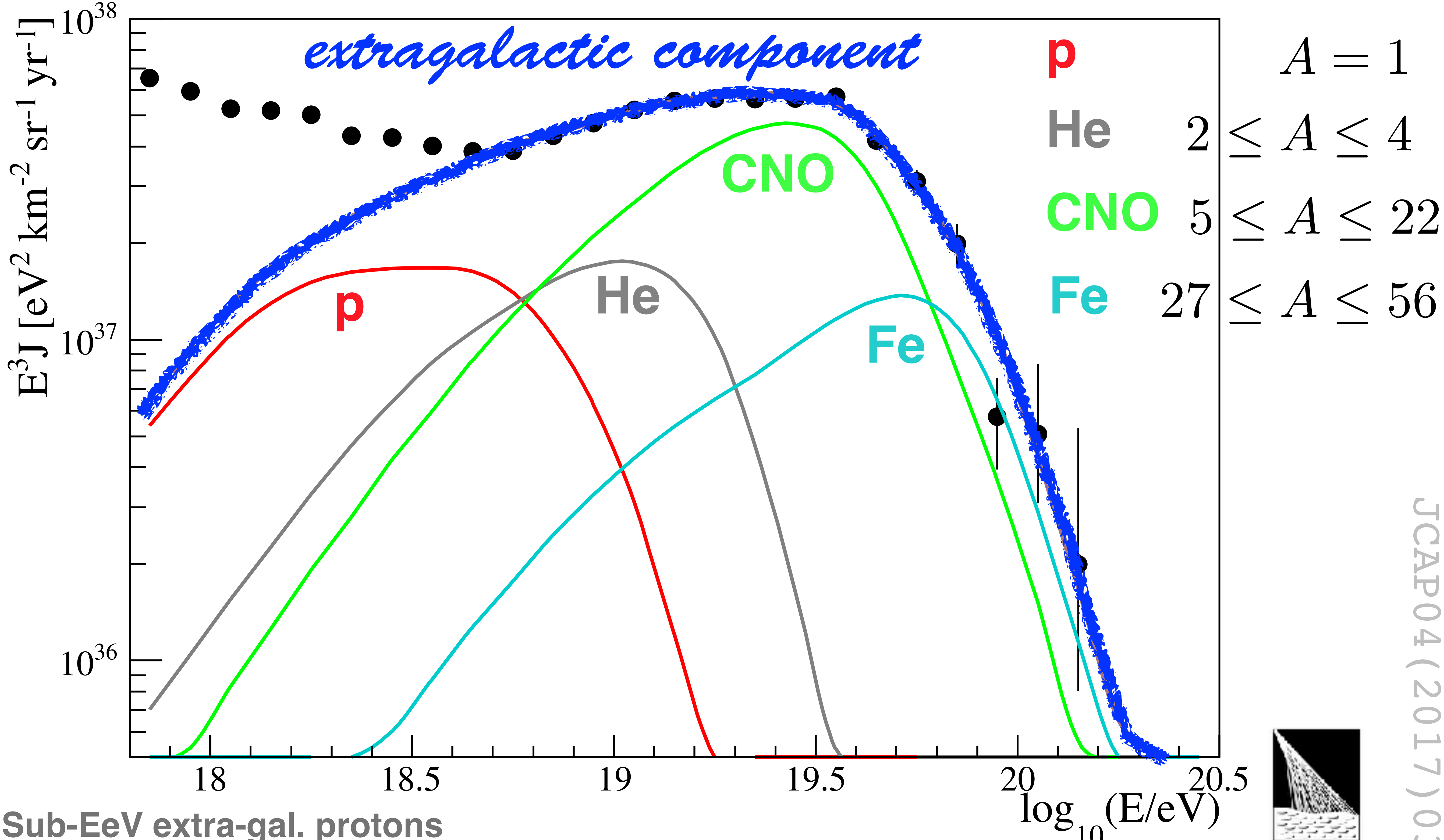

JCAP04(2017)038

Sub-EeV extra-gal. protons from interactions of heavier nuclei

see A. Castellina

PIERRE AUGER OBSERVATORY

all-particle spectra including 2nd galactic component

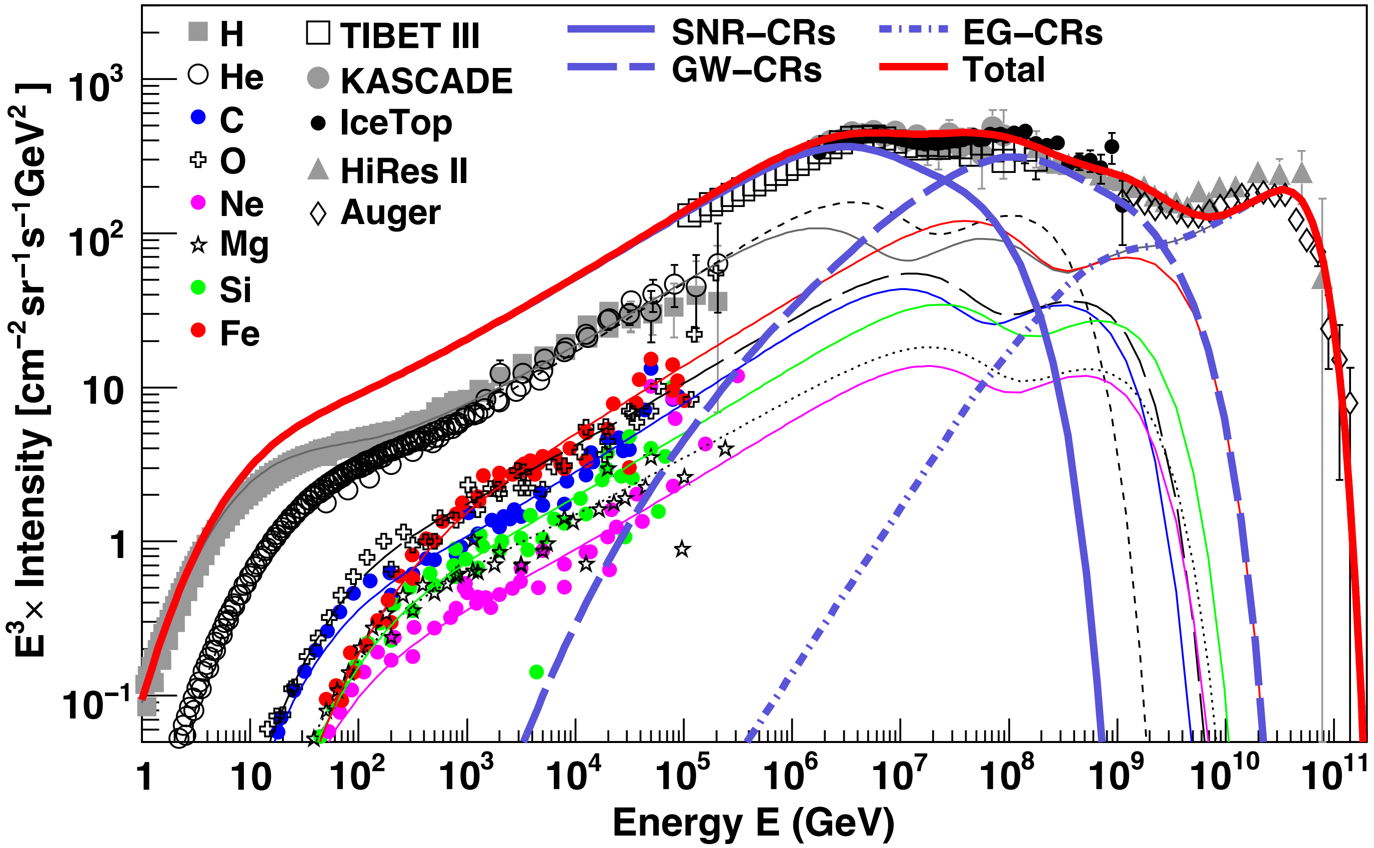

S. Thoudam et al., A&A 595 (2016) A33

all-particle spectra including 2nd galactic component

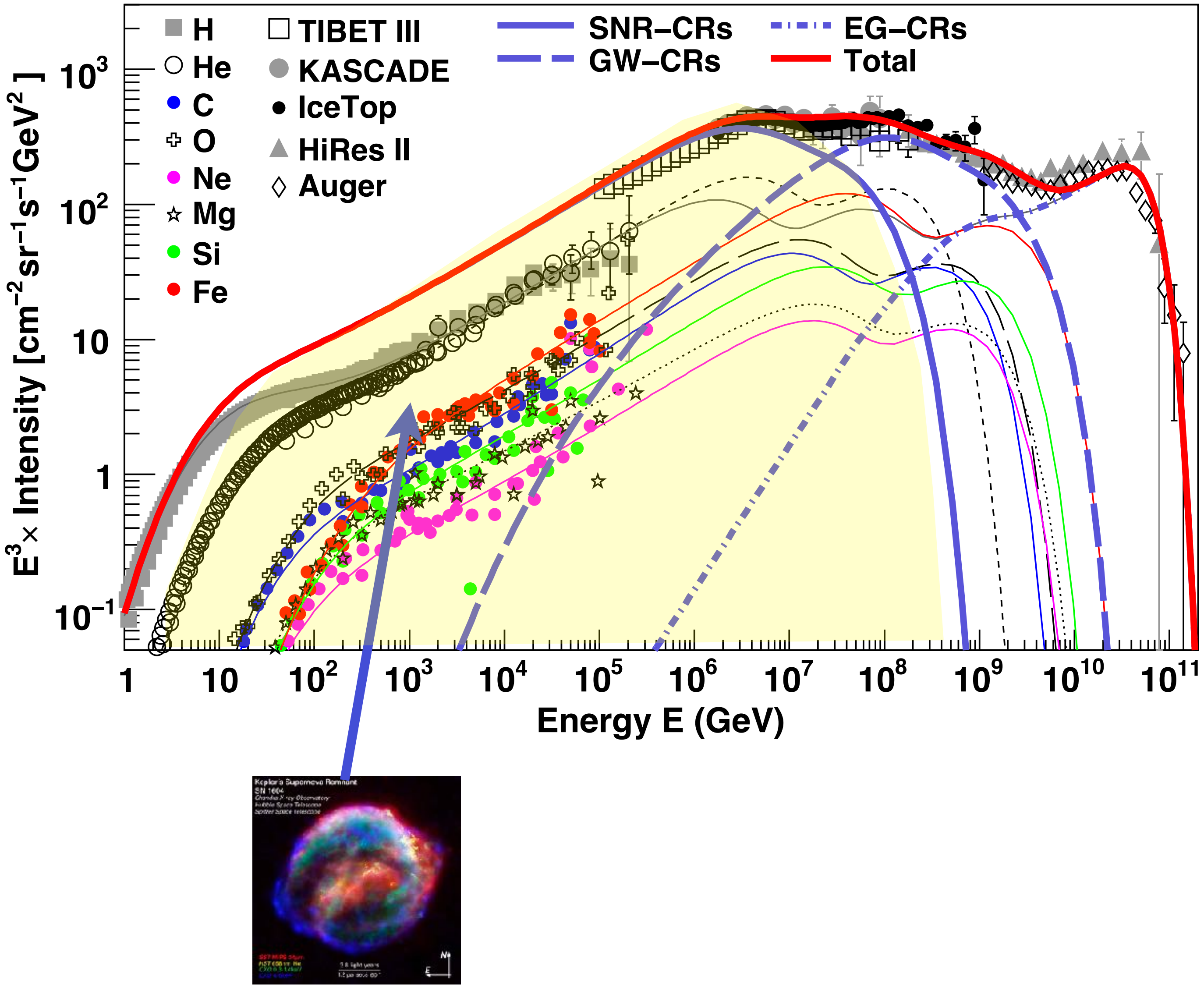

S. Thoudam et al., A&A 595 (2016) A33

all-particle spectra including 2nd galactic component

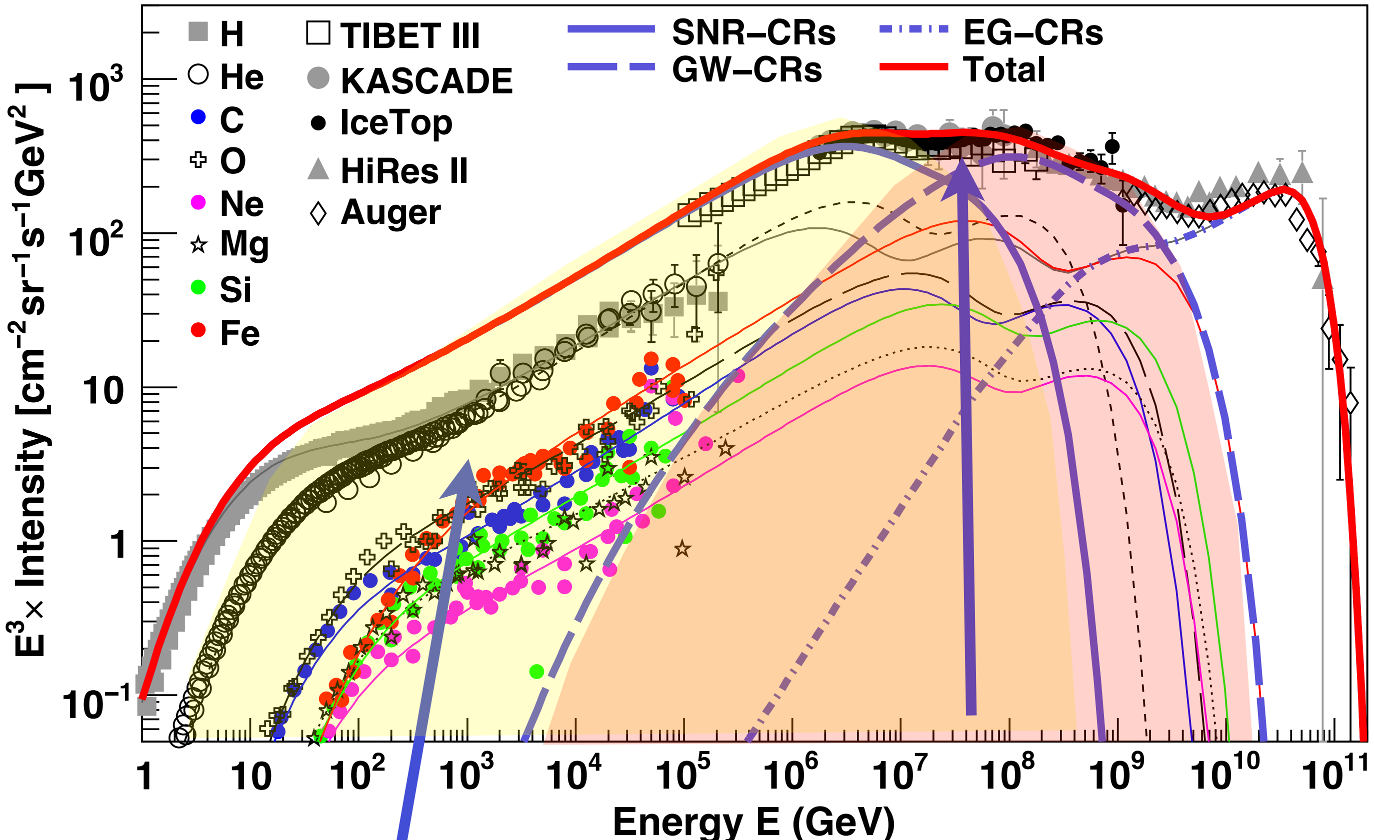

S. Thoudam et al., A&A 595 (2016) A33

all-particle spectra including 2nd galactic component

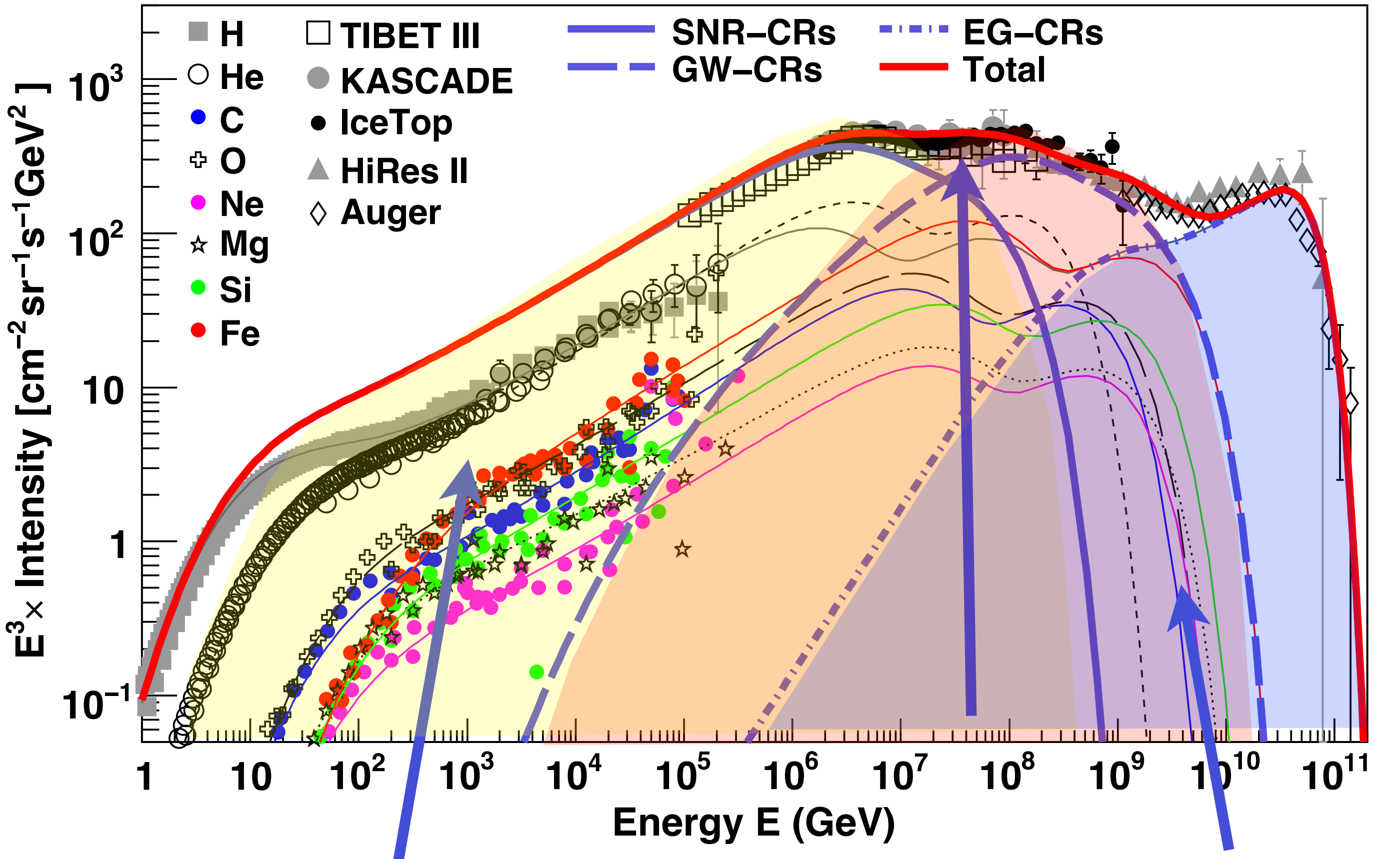

S. Thoudam et al., A&A 595 (2016) A33

all-particle spectra including 2nd galactic component

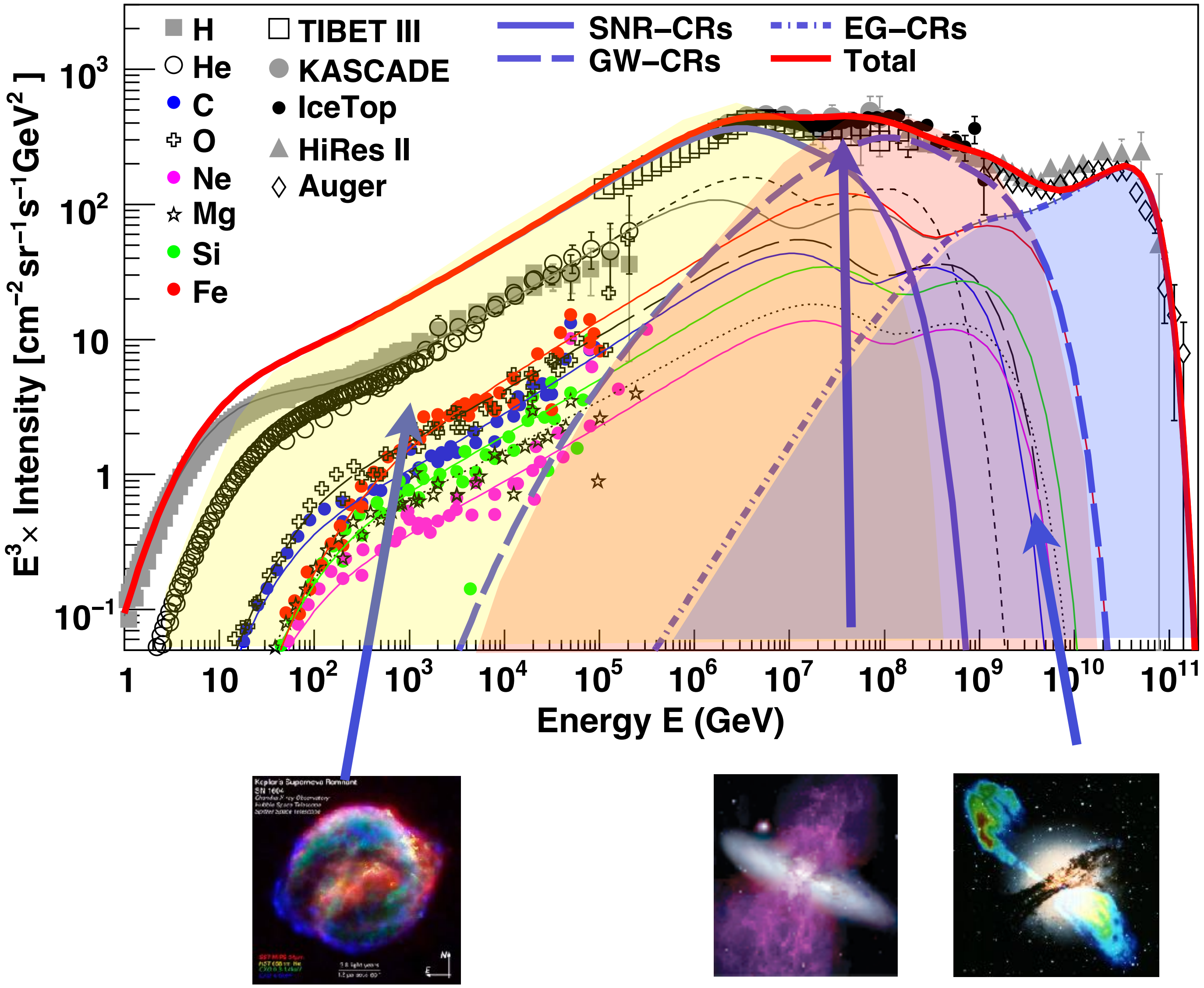

Table 3. Injection energy of SNR-CRs used in the calculation of all-particle spectrum in the WR-CR model (Figure 6).

Particle type	C/He = 0.1 $f(\times 10^{49}$ ergs)	C/He = 0.4 $f(\times 10^{49}$ ergs)
Proton	8.11	8.11
Helium	0.67	0.78
Carbon	2.11×10^{-2}	0.73×10^{-2}
Oxygen	2.94×10^{-2}	2.94×10^{-2}
Neon	4.41×10^{-3}	4.41×10^{-3}
Magnesium	6.03×10^{-3}	6.03×10^{-3}
Silicon	5.84×10^{-3}	5.84×10^{-3}
Iron	5.77×10^{-3}	5.77×10^{-3}

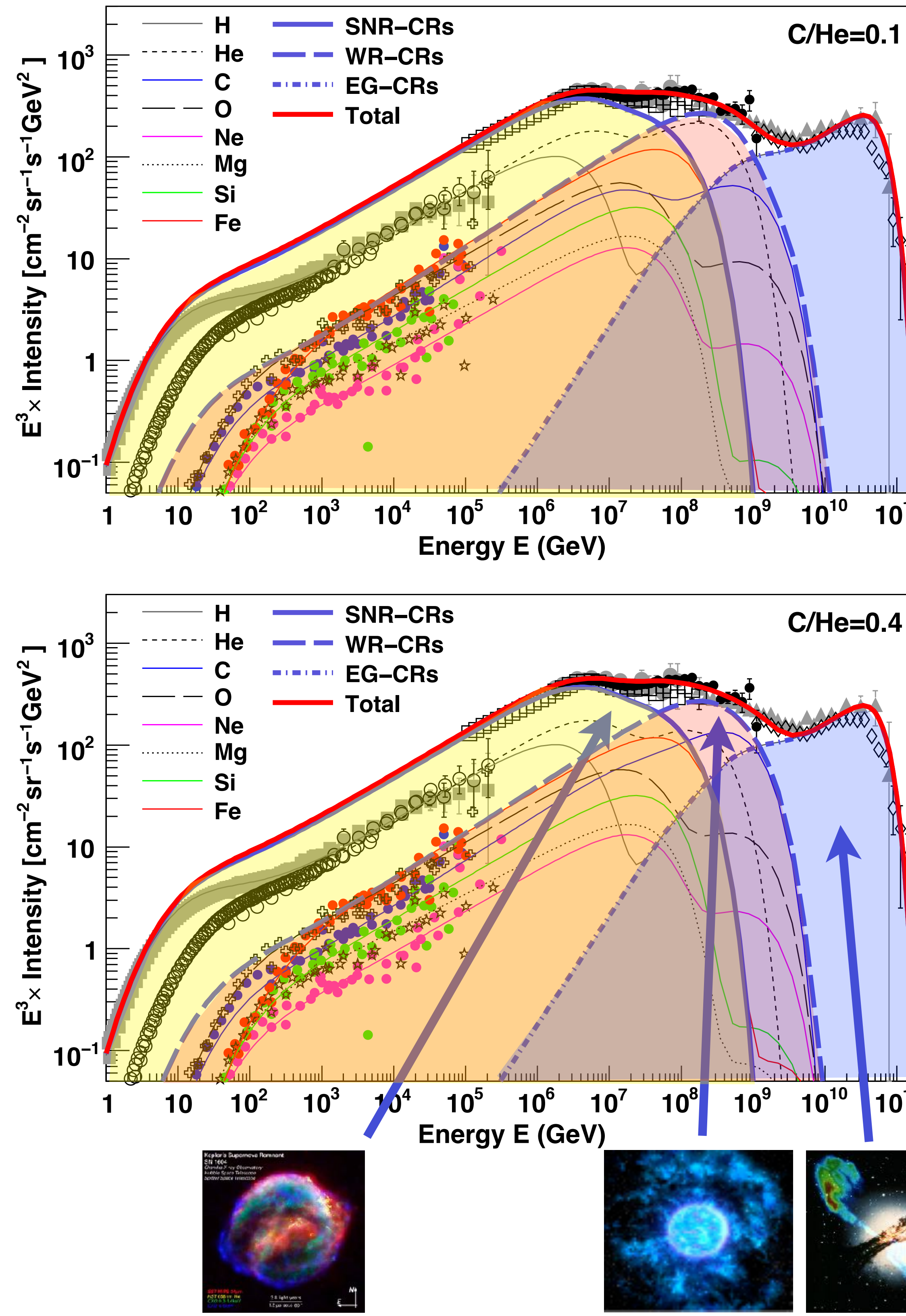

S. Thoudam et al., A&A 595 (2016) A33

all-particle spectra including 2nd galactic component

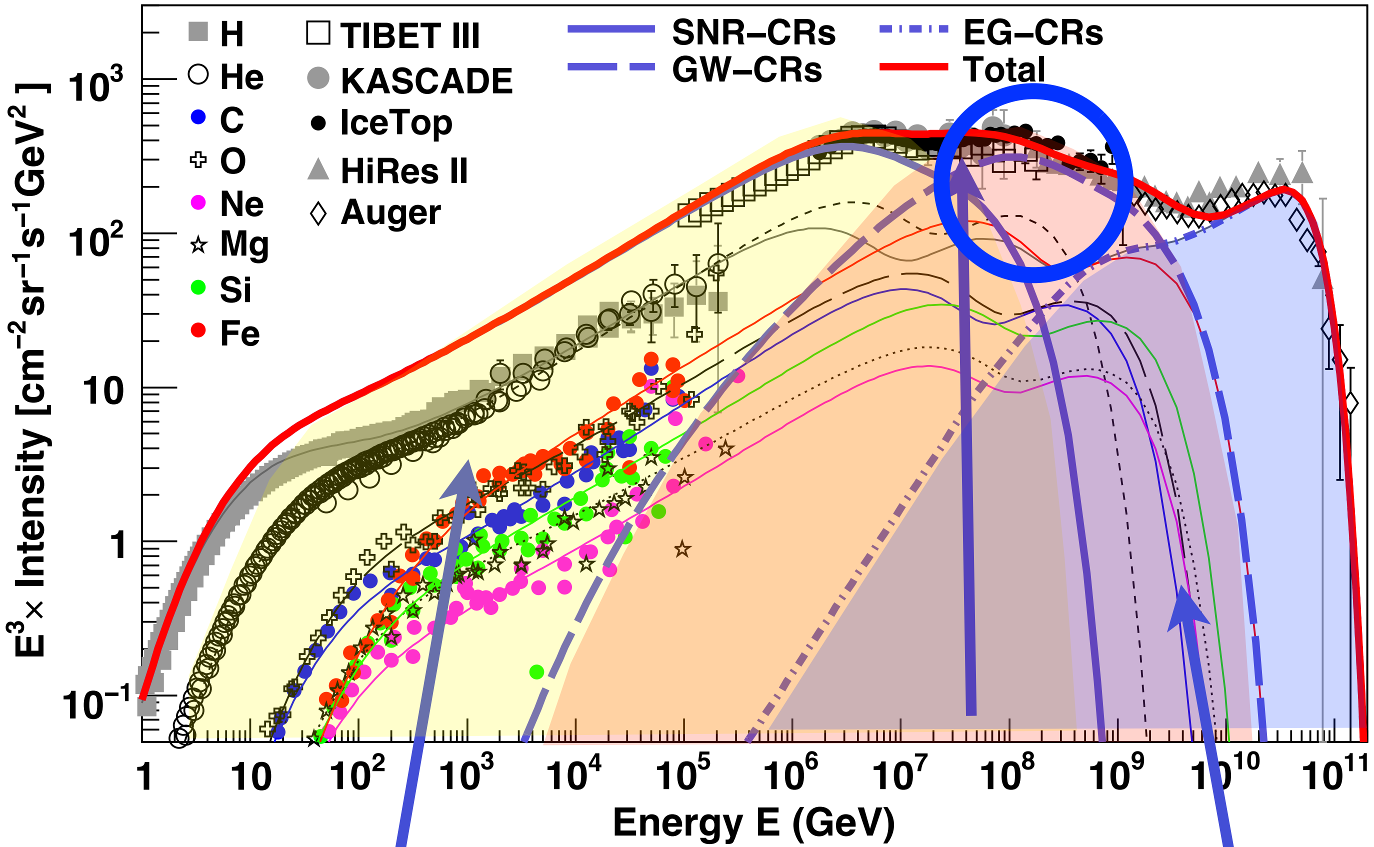

Table 3. Injection energy of SNR-CRs used in the calculation of all-particle spectrum in the WR-CR model (Figure 6).

Particle type	C/He = 0.1 $f(\times 10^{49}$ ergs)	C/He = 0.4 $f(\times 10^{49}$ ergs)
Proton	8.11	8.11
Helium	0.67	0.78
Carbon	2.11×10^{-2}	0.73×10^{-2}
Oxygen	2.94×10^{-2}	2.94×10^{-2}
Neon	4.41×10^{-3}	4.41×10^{-3}
Magnesium	6.03×10^{-3}	6.03×10^{-3}
Silicon	5.84×10^{-3}	5.84×10^{-3}
Iron	5.77×10^{-3}	5.77×10^{-3}

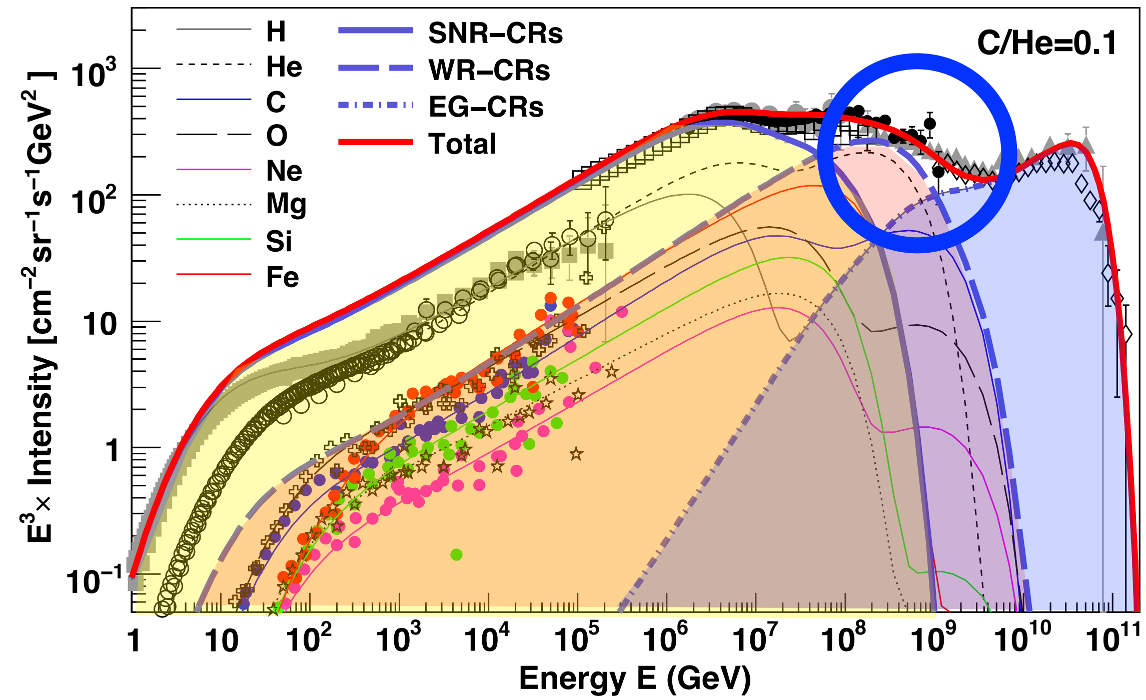

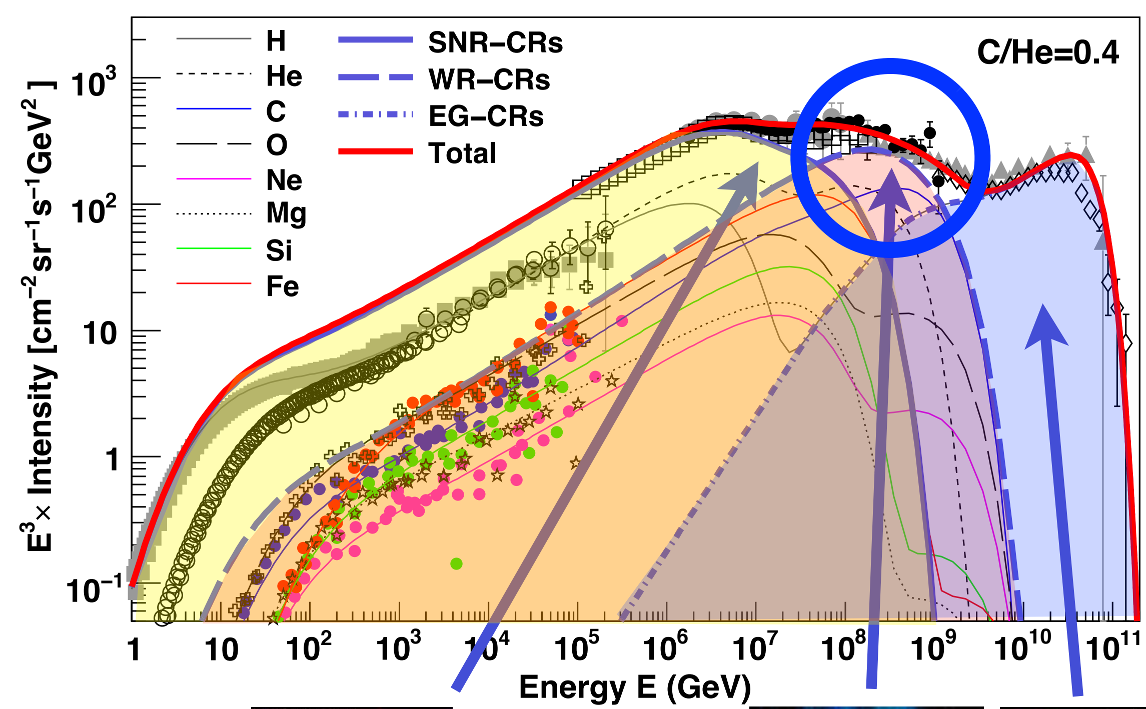

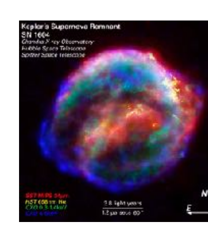

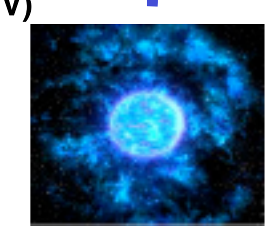

S. Thoudam et al., A&A 595 (2016) A33

Mean logarithmic mass (lnA)

WR-CR (C/He=0.4) + EG scenarios

$$\langle \ln A \rangle \equiv \sum_i r_i \ln A_i, \qquad \langle \ln A \rangle = \frac{X_{\max}^{\text{meas}} - X_{\max}^{\text{p}}}{X_{\max}^{\text{Fe}} - X_{\max}^{p}} \cdot \ln A_{\text{Fe}}.$$

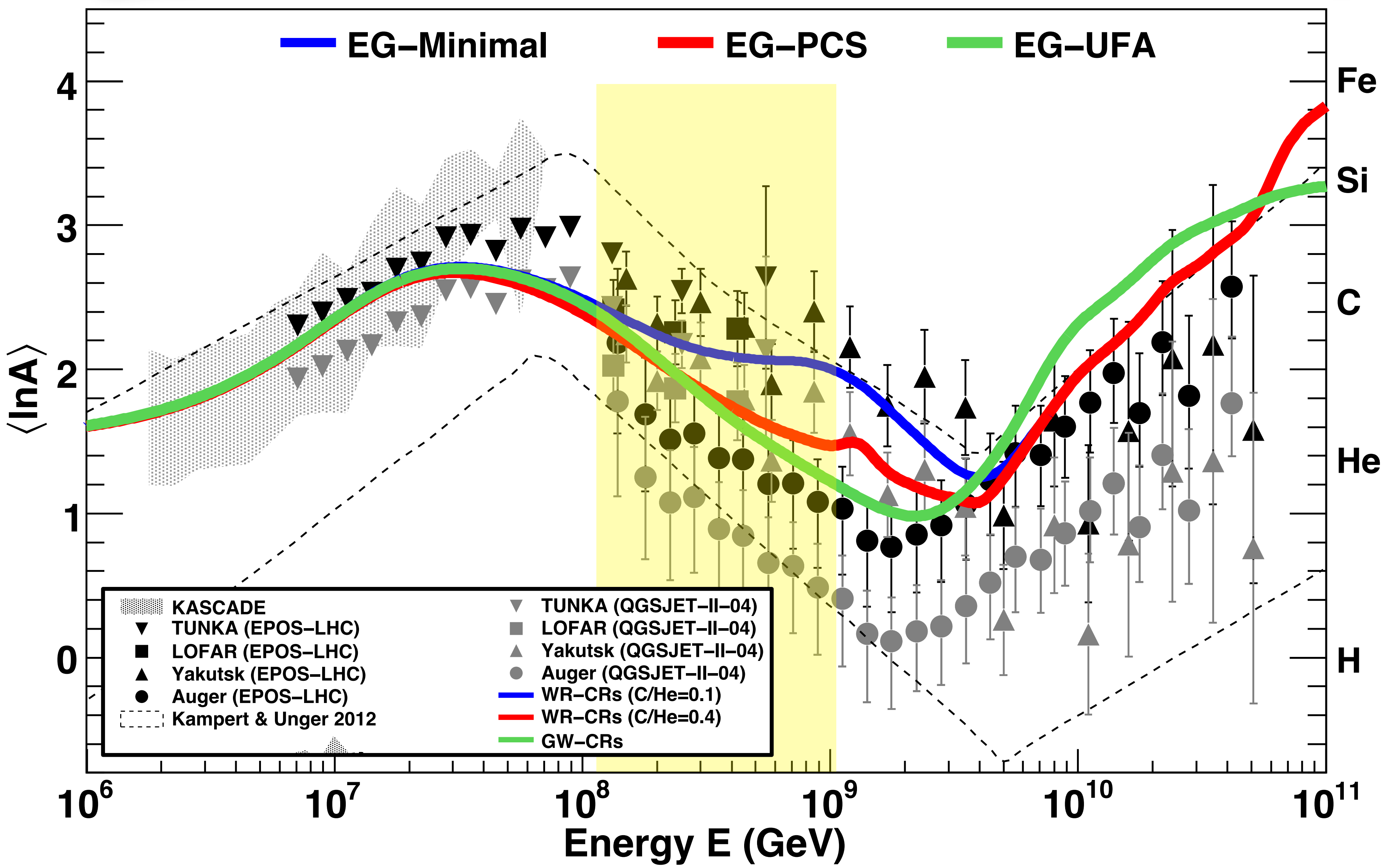

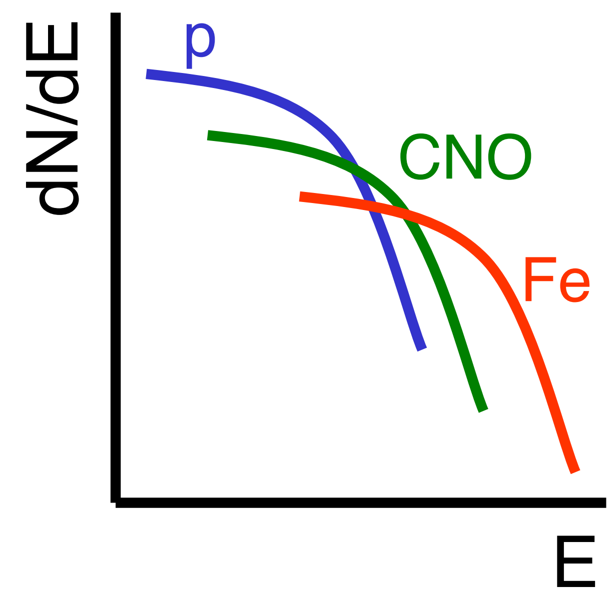

Fig. 11. Mean logarithmic mass for the three different EG-CR models combined with the WR-CR (C/He = 0.4) model. Data are the same as in Figure 8. Results obtained using WR-CR (C/He = 0.1) model are shown in Appendix B.

S. Thoudam et al., A&A 595 (2016) A33

Cosmic rays at the knee
Results and implications

- knee in all-particle spectrum at ~4.5 PeV caused by fall-off of light elements (p, He)
- experimental (world) data indicate rigidity-dependent fall-off of individual elements
  (in particular unfolding by KASCADE[-Grande] and IceCube/Top)
- spectrum above knee is superposition of individual spectra (elemental knees)
  —> fine structure in all-particle spectrum
  —> end of galactic CR component
- astrophysical origin of knee:
  combination of maximum energy attained in sources (Supernovae) (Hillas criterion)
  and leakage from Galaxy

- 2nd galactic component at ~10^{17} eV?
- extra-galactic origin >10^{18} eV

Jörg R. Hörandel RU Nijmegen, Nikhef, VU Brussel http://particle.astro.ru.nl